

AN ABSTRACT OF THE THESIS OF

Kathryn S. Pfretzschner for the degree of Master of Science in Wood Science and Civil Engineering presented on September 5, 2012

Title: Practical Modeling for Load Paths in a Realistic, Light-Frame Wood House

Abstract approved:

Rakesh Gupta

Thomas H. Miller

The objective of this study was to develop and validate practical modeling methods for investigating load paths and system behavior in a realistic, light-frame wood structure. The modeling methods were validated against full-scale tests on sub-assemblies and an L-shaped house. The model of the L-shaped house was then modified and used to investigate the effects of re-entrant corners, wall openings and gable-end retrofits on system behavior and load paths. Results from this study showed that the effects of adding re-entrant corners and wall openings on uplift load distributions were dependent on the orientation of the trusses with respect to the walls. Openings added to walls parallel to the trusses had the least effect on loads carried by the remaining walls in the building. Varying re-entrant corner dimensions of the L-shaped house under ASCE 7-05 (ASCE 2005) design wind loads caused increasing degrees of torsion throughout the house, depending on the relative location and stiffness of the in-plane walls (parallel to the applied wind loads) as well as the assumed direction of the wind loads. Balancing the stiffness of the walls on either side of the house with the largest re-entrant corner helped to decrease torsion in the structure somewhat. Finally, although previous full-scale tests on gable-end sections verified the effectiveness of the gable-end retrofit that was recently adopted into the 2010 Florida building code, questions remained about the effects of the retrofit on torsion in a full building. The current study found that adding the gable-end retrofits to the L-shaped house did not cause additional torsion.

©Copyright by Kathryn S. Pfretzschner
September 5, 2012
All Rights Reserved

Practical Modeling for Load Paths in a Realistic, Light-Frame Wood House

by
Kathryn S. Pfretzschner

A THESIS

submitted to

Oregon State University

in partial fulfillment of
the requirements for the
degree of

Master of Science

Presented: September 5, 2012
Commencement Date: June 2013

Master of Science thesis of Kathryn S. Pfretzschner presented on September 5, 2012.

APPROVED:

Co-Major Professor representing Wood Science and Engineering

Co-Major Professor representing Civil Engineering

Head of the Department of Wood Science and Engineering

Acting Head of the School of Civil and Construction Engineering

Dean of the Graduate School

I understand that my thesis will become part of the permanent collection of Oregon State University libraries. My signature below authorizes release of my thesis to any reader upon request.

Kathryn S. Pfretzschner, Author

ACKNOWLEDGMENTS

I would like to express my appreciation to the following people and organizations:

- My advisors, Dr. Rakesh Gupta and Dr. Thomas H. Miller, for their help, guidance and patience during the course of this project.
- Kenneth Martin, Dr. Phillip Paevere and Dr. Bohumil Kasal whose previous research and development made this project possible. I am especially thankful for Kenneth Martin, who proposed this project and instructed me in the design of wood structures.
- The Department of Wood Science & Engineering and the School of Civil & Construction Engineering at Oregon State University for providing the necessary resources and furthering my education.
- The Oregon State University Center for Wood Utilization Research for funding this project.

Finally, I would not have made it this far without my family. My parents, Janet and Richard Pfretzschner, provided the support and encouragement that kept me going throughout my undergraduate and graduate degrees. Also my older brother, Paul Pfretzschner, inspired me to pursue engineering through his own academic accomplishments in science and mathematics.

CONTRIBUTION OF AUTHORS

Dr. Rakesh Gupta and Dr. Thomas H. Miller provided technical guidance and support during the research stages. They also provided insight and editing for the final manuscript.

TABLE OF CONTENTS

	<u>Page</u>
INTRODUCTION	1
OBJECTIVES	1
RESEARCH APPROACH	2
MANUSCRIPT: PRACTICAL MODELING FOR LOAD PATHS IN A REALISTIC, LIGHT-FRAME WOOD HOUSE	4
ABSTRACT	5
INTRODUCTION	5
RESEARCH METHODS	7
Modeling Methods	7
Model Validation Procedure	10
RESULTS AND DISCUSSION	18
Model Validation	18
Uniform Uplift Investigation	20
Wind Load Investigation	23
CONCLUSIONS	27
ACKNOWLEDGMENTS	28
REFERENCES	29
CONCLUSIONS AND RECOMMENDATIONS	32
BIBLIOGRAPHY	34

LIST OF FIGURES

<u>Figure</u>	<u>Page</u>
Figure 1: (a) Floor Plan with Centerline Dimensions [m (ft-in)] and Wall Designation, (b) Wall framing (mm) (Paevere 2002)	11
Figure 2: Truss Orientation and Gable-End Framing	12
Figure 3: Plywood Sheathing on Exterior of Walls 5 and 9 (Paevere et al. 2003)	13
Figure 4: G_{12} vs. Wall Length for Plywood and GWB Wall Sheathing	14
Figure 5: Modified Gable-End Framing for Load Path Investigations.....	15
Figure 6: Wind Directions and ASCE 7-05 Load Cases.....	17
Figure 7: Example C-Shaped Gable-End Retrofit at Gable-End Stud.....	18
Figure 8: Load Distribution Plot for Paevere et al. (2003) Load Case 4	20
Figure 9: Uplift Reactions for Rectangular (Left) and L-shaped (Right) Index Buildings	21
Figure 10: Change in Uplift Reactions (Magnified 4x) due to Openings in Wall 2 (Left) and Wall 4 (Right)	22
Figure 11: Uplift Reactions in L-Shaped Index House.....	23
Figure 12: Lateral Load Distribution and Top Plate Deflected Shapes for Re-Entrant Corner Variations.....	26
Figure 13: Displaced Shape of Large Re-Entrant Corner Building with Increased Stiffness in Walls 1 and 2	27

LIST OF TABLES

<u>Table</u>	<u>Page</u>
Table 1: Sheathing Material Properties.....	13
Table 2: Material Densities used for Building Self-Weight	14

LIST OF APPENDICES

<u>Appendix</u>	<u>Page</u>
APPENDIX A: EXTENDED LITERATURE REVIEW	39
APPENDIX B: TWO-DIMENSIONAL TRUSS MODEL VALIDATION	54
APPENDIX C: THREE DIMENSIONAL ROOF ASSEMBLY MODEL VALIDATION	62
APPENDIX D: PLOTS FOR ROOF ASSEMBLY MODEL VALIDATION.....	71
APPENDIX E: TWO-DIMENSIONAL SHEAR WALL MODEL VALIDATION	95
APPENDIX F: SHEATHING G_{12} ADJUSTMENT PROCEDURE FOR EDGE NAIL SPACING...	106
APPENDIX G: DETAILS FOR FULL BUILDING MODEL OF PAEVERE ET AL. (2003) HOUSE	112
APPENDIX H: FULL BUILDING MODEL VALIDATION.....	123
APPENDIX I: MODEL VARIATIONS USED IN UPLIFT AND WIND LOAD INVESTIGATIONS	144
APPENDIX J: UNIFORM UPLIFT INVESTIGATION	152
APPENDIX K: ASCE 7-05 DESIGN LOADS USED FOR WIND LOAD INVESTIGATION	162
APPENDIX L: WIND LOAD INVESTIGATION	168

LIST OF APPENDIX FIGURES

<u>Figure</u>	<u>Page</u>
Figure B-1: 6:12 Truss Geometry	55
Figure B-2: 3:12 Truss Geometry	55
Figure B-3: Connectivity and Element Labels for 2D Truss Model	56
Figure C-1: Pattern of Truss Stiffness in Assemblies.....	62
Figure C-2: Local Coordinate Orientation of Thick Shell Elements for Sheathing	64
Figure C-3: Hooke's Law for Orthotropic Materials.....	65
Figure C-4: "Roller-Roller" Support Conditions	67
Figure C-5: Locations for Deflection Measurement on Each Truss	68
Figure D-1: Relative Reactions for 3:12 Truss Assembly When Truss 1 is Loaded	71
Figure D-2: Relative Reactions for 3:12 Truss Assembly When Truss 2 is Loaded	72
Figure D-3: Relative Reactions for 3:12 Truss Assembly When Truss 3 is Loaded	72
Figure D-4: Relative Reactions for 3:12 Truss Assembly When Truss 4 is Loaded	73
Figure D-5: Relative Reactions for 3:12 Truss Assembly When Truss 5 is Loaded	73
Figure D-6: Relative Reactions for 3:12 Truss Assembly When Truss 6 is Loaded	74
Figure D-7: Relative Reactions for 3:12 Truss Assembly When Truss 7 is Loaded	74
Figure D-8: Relative Reactions for 3:12 Truss Assembly When Truss 8 is Loaded	75
Figure D-9: Relative Reactions for 3:12 Truss Assembly When Truss 9 is Loaded	75
Figure D-10: Relative Reactions for 6:12 Truss Assembly When Truss 1 is Loaded	77
Figure D-11: Relative Reactions for 6:12 Truss Assembly When Truss 2 is Loaded	77
Figure D-12: Relative Reactions for 6:12 Truss Assembly When Truss 3 is Loaded	78
Figure D-13: Relative Reactions for 6:12 Truss Assembly When Truss 4 is Loaded	78
Figure D-14: Relative Reactions for 6:12 Truss Assembly When Truss 5 is Loaded	79
Figure D-15: Relative Reactions for 6:12 Truss Assembly When Truss 6 is Loaded	79

LIST OF APPENDIX FIGURES (Continued)

<u>Figure</u>	<u>Page</u>
Figure D-16: Relative Reactions for 6:12 Truss Assembly When Truss 7 is Loaded	80
Figure D-17: Relative Reactions for 6:12 Truss Assembly When Truss 8 is Loaded	80
Figure D-18: Relative Reactions for 6:12 Truss Assembly When Truss 9 is Loaded	81
Figure D-19: Relative Deflections for 3:12 Truss Assembly When Truss 1 is Loaded ...	83
Figure D-20: Relative Deflections for 3:12 Truss Assembly When Truss 2 is Loaded ...	83
Figure D-21: Relative Deflections for 3:12 Truss Assembly When Truss 3 is Loaded ...	84
Figure D-22: Relative Deflections for 3:12 Truss Assembly When Truss 4 is Loaded ...	84
Figure D-23: Relative Deflections for 3:12 Truss Assembly When Truss 5 is Loaded ...	85
Figure D-24: Relative Deflections for 3:12 Truss Assembly When Truss 6 is Loaded ...	85
Figure D-25: Relative Deflections for 3:12 Truss Assembly When Truss 7 is Loaded ...	86
Figure D-26: Relative Deflections for 3:12 Truss Assembly When Truss 8 is Loaded ...	86
Figure D-27: Relative Deflections for 3:12 Truss Assembly When Truss 9 is Loaded ...	87
Figure D-28: Relative Deflections for 6:12 Truss Assembly When Truss 1 is Loaded ...	89
Figure D-29: Relative Deflections for 6:12 Truss Assembly When Truss 2 is Loaded ...	89
Figure D-30: Relative Deflections for 6:12 Truss Assembly When Truss 3 is Loaded ...	90
Figure D-31: Relative Deflections for 6:12 Truss Assembly When Truss 4 is Loaded ...	90
Figure D-32: Relative Deflections for 6:12 Truss Assembly When Truss 5 is Loaded ...	91
Figure D-33: Relative Deflections for 6:12 Truss Assembly When Truss 6 is Loaded ...	91
Figure D-34: Relative Deflections for 6:12 Truss Assembly When Truss 7 is Loaded ...	92
Figure D-35: Relative Deflections for 6:12 Truss Assembly When Truss 8 is Loaded ...	92
Figure D-36: Relative Deflections for 6:12 Truss Assembly When Truss 9 is Loaded ...	93
Figure E-1: Testing Apparatus and Sensor Locations (Dolan and Johnson 1996).....	97

LIST OF APPENDIX FIGURES (Continued)

<u>Figure</u>	<u>Page</u>
Figure E-2: Example of Assumed Wall Framing with SAP2000 Wire Frame Overlay for Type D Shear Wall	99
Figure E-3: Example Frame Section Assignment for Type D Shear Wall	99
Figure E-4: Local Axes for Anchor Bolts and Hold-downs (Martin 2010).....	102
Figure E-5: Anchor Bolt and Hold-Down Placement in SAP2000 Model	102
Figure F-1: (Top) framing plan for example calibration (grey studs are single studs) and (Bottom) support and loading conditions for calibration model	107
Figure F-2: Sheathing G12 vs. Shear Wall Deflection in SAP2000 for Example Calibration Model	109
Figure F-3: AF&PA (2005b) Predicted Deflection and Required G12 in SAP2000 vs. Wall Length	111
Figure G-1: G12 vs. Wall Length for 9.5 mm Plywood and 13 mm GWB Sheathing ..	115
Figure G-2: Anchor Bolt and Load Sensor Placement (Paevere 2002).....	116
Figure G-3: Wall Locations Used in SAP2000 Model – m (ft-in)	116
Figure G-4: Wall Configurations (Paevere 2002)	117
Figure G-5: Wall 3 Configuration used for SAP2000 Model	118
Figure G-6: Wall Framing (Paevere 2002)	118
Figure G-7: Example of Assumed Framing with SAP2000 Wire Frame Overlay for Wall 2.....	119
Figure G-8: Example Frame Section Assignment for Wall 2	119
Figure G-9: Assumed Framing with SAP2000 Wire Frame Overlay for Type A Trusses	120
Figure G-10: Assumed Framing with SAP2000 Wire Frame Overlay for Type B Trusses	120
Figure G-11: Example Frame Section Assignment used for Trusses	120
Figure G-12: Truss Layout for Type A and Type B Trusses	121

LIST OF APPENDIX FIGURES (Continued)

<u>Figure</u>	<u>Page</u>
Figure G-13: 2-Joint Links used to Connect Wall 3 to Truss Bottom Chords	121
Figure G-14: Gable-End Overhang Framing used in SAP2000 Model	122
Figure G-15: Gable-End Sheathing Placement used in SAP2000 Model	122
Figure H-1: Load Case 2 – 2.78 kN Applied to Top-Plate at Wall 1	124
Figure H-2: Lateral Load Distribution to E-W Walls (Load Case 2)	124
Figure H-3: Load Case 3 – 4.79 kN Applied to Top-Plate at Wall 2	125
Figure H-4: Lateral Load Distribution to E-W Walls (Load Case 3)	125
Figure H-5: Load Case 4 – 4.92 kN Applied to Top-Plate at Wall 3	126
Figure H-6: Lateral Load Distribution to E-W Walls (Load Case 4)	126
Figure H-7: Load Case 5 – 4.92 kN Applied to Top-Plate at Wall 4	127
Figure H-8: Lateral Load Distribution to E-W Walls (Load Case 5)	127
Figure H-9: Load Case 6 – 5.18 kN Applied to Top-Plate at Wall 8	128
Figure H-10: Lateral Load Distribution to N-S Walls (Load Case 6)	128
Figure H-11: Load Case 7 – 5.07 kN Applied to Top-Plate at Wall 2 and 5.13 kN Applied to Top-Plate at Wall 8	129
Figure H-12: Lateral Load Distribution to E-W Walls (Load Case 7)	129
Figure H-13: Lateral Load Distribution to N-S Walls (Load Case 7)	130
Figure H-14: Load Case 8 – 5.16 kN Applied to Top-Plate at Wall 5	131
Figure H-15: Lateral Load Distribution to N-S Walls (Load Case 8)	131
Figure H-16: Load Case 9 – 8.04 kN Applied to Top-Plate at Wall 4 and 5.17 kN Applied to Top-Plate at Wall 5	132
Figure H-17: Lateral Load Distribution to E-W Walls (Load Case 9)	132
Figure H-18: Lateral Load Distribution to N-S Walls (Load Case 9)	133

LIST OF APPENDIX FIGURES (Continued)

<u>Figure</u>	<u>Page</u>
Figure H-19: Load Case 10 – 5.12 kN Applied to Top-Plate at Wall 2 and 3.18 kN Applied to Top-Plate at Wall 5	134
Figure H-20: Lateral Load Distribution to E-W Walls (Load Case 10)	134
Figure H-21: Lateral Load Distribution to N-S Walls (Load Case 10)	135
Figure H-22: Load Case 11 – 6.80 kN Applied to Top-Plate between Walls 2 and 3.....	136
Figure H-23: Lateral Load Distribution to E-W Walls (Load Case 11)	136
Figure H-24: Load Case 12 – 1.10 kN, 5.43 kN, 15.0 kN and 6.50 kN Applied to Top-Plate at Walls 1, 2, 3 and 4, respectively	137
Figure H-25: Lateral Load Distribution to E-W Walls (Load Case 12)	137
Figure H-26: Load Case 13 – 5.09 kN Applied to Roof Ridge of East Gable-End (at -5 degrees)	138
Figure H-27: Lateral Load Distribution to E-W Walls (Load Case 13)	138
Figure H-28: Lateral Load Distribution to N-S Walls (Load Case 13)	139
Figure H-29: Load Case 14 – 5.21 kN Applied to Roof Ridge of East Gable-End (at -10 degrees).....	140
Figure H-30: Lateral Load Distribution to E-W Walls (Load Case 14)	140
Figure H-31: Lateral Load Distribution to N-S Walls (Load Case 14)	141
Figure H-32: Load Case 15 – 2.80 kN Applied to Roof Ridge of East Gable-End (at 20 degrees).....	142
Figure H-33: Lateral Load Distribution to E-W Walls (Load Case 15)	142
Figure H-34: Lateral Load Distribution to N-S Walls (Load Case 15)	143
Figure I-1: Gable End-Framing and Sheathing Modifications for Uplift and Wind Load Investigations	145
Figure I-2: Progression of Building Variations Used in Uplift Investigation	145
Figure I-3: Rectangular Index Building for Uplift Investigation	146
Figure I-4: L-Shaped Index Building for Uplift Investigation	146

LIST OF APPENDIX FIGURES (Continued)

<u>Figure</u>	<u>Page</u>
Figure I-5: Framing Detail for Openings used in Uplift Investigation	147
Figure I-6: Locations of Openings Used for Uplift Investigation	147
Figure I-7: Progression of Building Variations Used in Wind Load Investigation	148
Figure I-8: L-Shaped Index House for Wind Load Investigation	148
Figure I-9: Gable-End Retrofit Detail from 2010 Florida Building Code (ICC 2011)...	149
Figure I-10: Gable-End Studs + Retrofit Studs Modeled with L-Shaped Cross-Section	149
Figure I-11: Example of Gable-End Retrofit in the Model	150
Figure I-12: Re-Entrant Corner Variations Used in Wind Load Investigation	150
Figure I-13: Re-Entrant Corner Variation Dimensions for Wind Load Investigation	151
Figure J-1: Uplift Reactions for Rectangular Index Building under Uniform Uplift Pressure	153
Figure J-2: Uplift Reactions for L-Shaped Index Building under Uniform Uplift Pressure	153
Figure J-3: Difference in Uplift Reactions between Rectangular and L-Shaped Index Buildings under Uniform Uplift Pressure	154
Figure J-4: Uplift Reactions for L-Shaped Building with Opening in Wall 2 (under Uniform Uplift Pressure)	155
Figure J-5: Difference in Uplift Reactions due to Opening in Wall 2	155
Figure J-6: Uplift Reactions for L-Shaped Building with Opening in Wall 4 (under Uniform Uplift Pressure)	156
Figure J-7: Difference in Uplift Reactions due to Opening in Wall 4	156
Figure J-8: Uplift Reactions for L-Shaped Building with Opening in Wall 9, Centered Under Gable-End (under Uniform Uplift Pressure).....	157
Figure J-9: Difference in Uplift Reactions due to Opening in Wall 9, Centered Under Gable-End	157

LIST OF APPENDIX FIGURES (Continued)

<u>Figure</u>	<u>Page</u>
Figure J-10: Uplift Reactions for L-Shaped Building with Opening in Wall 9, Opposite Re-Entrant Corner (under Uniform Uplift Pressure	158
Figure J-11: Difference in Uplift Reactions due to Opening in Wall 9, Opposite Re-Entrant Corner	158
Figure J-12: Uplift Reactions for L-Shaped Building with GWB (under Uniform Uplift Pressure).....	159
Figure J-13: Difference in Uplift Reactions from L-Shaped Building due to addition of GWB	159
Figure J-14: Uplift Reactions for L-Shaped Building with Opening in Wall 2 and GWB (under Uniform Uplift Pressure).....	160
Figure J-15: Difference in Uplift Reactions in L-Shaped Building with Opening in Wall 2 Due to Addition of GWB	160
Figure J-16: Uplift Reactions for L-Shaped Building with Opening in Wall 9 and GWB (under Uniform Uplift Pressure).....	161
Figure J-17: Difference in Uplift Reactions in L-Shaped Building with Opening in Wall 9 Due to Addition of GWB	161
Figure K-1: Wind Directions Considered for Wind Load Investigation	162
Figure K-2: ASCE 7-05 Design Wind Load Cases for Main Wind Force Resisting System, Method 2 (ASCE 7-05 Figure 6-9)	163
Figure K-3: Surface Designations used for Wind Pressure Calculations	164
Figure L-1: Uplift Reactions for L-shaped index house under North-South Wind Loads	169
Figure L-2: Lateral Load Distribution to North-South walls under North-South Wind Loads.....	169
Figure L-3: Uplift Reactions for L-shaped index house under West-East Wind Loads .	170
Figure L-4: Lateral Load Distribution to East-West walls under West-East Wind Loads	170
Figure L-5: Uplift Reactions for L-shaped index house under Southeast-Northwest Wind Loads	171

LIST OF APPENDIX FIGURES (Continued)

<u>Figure</u>	<u>Page</u>
Figure L-6: Lateral Load Distribution to North-South walls under Southeast-Northwest Wind Loads	171
Figure L-7: Lateral Load Distribution to East-West walls under Southeast-Northwest Wind Loads	172
Figure L-8: Uplift Reactions for Building with Gable-End Retrofits under North-South Wind Loads	173
Figure L-9: Difference in Uplift Reactions between Building with Gable-End Retrofits and L-shaped index house under North-South Wind Loads	173
Figure L-10: Lateral Load Distribution to North-South walls under North-South Wind Loads	174
Figure L-11: Uplift Reactions for Building with Gable-End Retrofits under West-East Wind Loads	175
Figure L-12: Difference in Uplift Reactions between Building with Gable-End Retrofits and L-shaped index house under West-East Wind Loads	175
Figure L-13: Lateral Load Distribution to East-West walls under West-East Wind Loads	176
Figure L-14: Uplift Reactions for Building with Gable-End Retrofits under Southeast-Northwest Wind Loads	177
Figure L-15: Difference in Uplift Reactions between Building with Gable-End Retrofits and L-shaped index house under Southeast-Northwest Wind Loads	177
Figure L-16: Lateral Load Distribution to East-West walls under Southeast-Northwest Wind Loads	178
Figure L-17: Lateral Load Distribution to North-South walls under Southeast-Northwest Wind Loads	178
Figure L-18: Uplift Reactions for Building with Small Re-Entrant Corner under North-South Wind Loads	179
Figure L-19: Difference in Uplift Reactions between Building with Small Re-Entrant Corner and L-shaped index house under North-South Wind Loads	179
Figure L-20: Uplift Reactions for Building with Medium Re-Entrant Corner under North-South Wind Loads	180

LIST OF APPENDIX FIGURES (Continued)

<u>Figure</u>	<u>Page</u>
Figure L-21: Difference in Uplift Reactions between Building with Medium Re-Entrant Corner and L-shaped index house under North-South Wind	180
Figure L-22: Uplift Reactions for Building with Large Re-Entrant Corner under North-South Wind Loads	181
Figure L-23: Difference in Uplift Reactions between Building with Large Re-Entrant Corner and L-shaped index house under North-South Wind Loads	181
Figure L-24: Lateral Load Distribution to North-South walls under North-South Wind Loads	182
Figure L-25: Unit Shear in North-South walls under North-South Wind Loads	182
Figure L-26: Uplift Reactions for Building with Small Re-Entrant Corner under West-East Wind Loads	183
Figure L-27: Difference in Uplift Reactions between Building with Small Re-Entrant Corner and L-shaped index house under West-East Wind Loads	183
Figure L-28: Uplift Reactions for Building with Medium Re-Entrant Corner under West-East Wind Loads	184
Figure L-29: Difference in Uplift Reactions between Building with Medium Re-Entrant Corner and L-shaped index house under West-East Wind Loads	184
Figure L-30: Uplift Reactions for Building with Large Re-Entrant Corner under West-East Wind Loads	185
Figure L-31: Difference in Uplift Reactions between Building with Large Re-Entrant Corner and L-shaped index house under West-East Wind Loads	185
Figure L-32: Lateral Load Distribution to East-West walls under West-East Wind Loads	186
Figure L-33: Uplift Reactions for Building with Small Re-Entrant Corner under Southeast-Northwest Wind Loads	187
Figure L-34: Difference in Uplift Reactions between Building with Small Re-Entrant Corner and L-shaped index house under Southeast-Northwest Wind Loads (with Self Weight)	187
Figure L-35: Uplift Reactions for Building with Medium Re-Entrant Corner under Southeast-Northwest Wind Loads	188

LIST OF APPENDIX FIGURES (Continued)

<u>Figure</u>	<u>Page</u>
Figure L-36: Difference in Uplift Reactions between Building with Medium Re-Entrant Corner and L-shaped index house under Southeast-Northwest Wind Loads	188
Figure L-37: Uplift Reactions for Building with Large Re-Entrant Corner under Southeast-Northwest Wind Loads	189
Figure L-38: Difference in Uplift Reactions between Building with Large Re-Entrant Corner and L-shaped index house under Southeast-Northwest Wind Loads	189
Figure L-39: Lateral Load Distribution to East-West walls under Southeast-Northwest Wind Loads	190
Figure L-40: Lateral Load Distribution to North-South walls under Southeast-Northwest Wind Loads	190
Figure L-41: Unit Shear in North-South walls under Southeast-Northwest Wind Loads	191

LIST OF APPENDIX TABLES

<u>Table</u>	<u>Page</u>
Table B-1: Modulus of Elasticity Assignments	57
Table B-2: Average MOEs Used for Individual 6:12 Trusses	57
Table B-3: Comparison of Experimental and Model Displacements	59
Table B-4: Comparison of Average Displacements for Simplified 6:12 Trusses using Average MOE Values	59
Table B-5: Comparison of Average Displacements for 3:12 Trusses using Average MOE Values	60
Table B-6: Comparison of Average Displacements for trusses with AF&PA (2005a) design MOE	60
Table C-1: Average MOE's used for Trusses in 3:12 Truss Assembly	63
Table C-2: Average MOE's used for Trusses in 6:12 Truss Assembly	63
Table C-3: Engineering Properties in Bending for 3-Ply Panel Generated by OSU Laminates and scaled to Wolfe and McCarthy (1989)	66
Table C-4: Absolute Error in Predicted Relative Reactions at Loaded Trusses in Each Assembly	69
Table C-5: Absolute Error in Predicted Relative Deflections at Loaded Trusses in Each Assembly	69
Table D-1: Relative Reactions of Trusses in 3:12 Assembly from Wolfe and McCarthy (1989).....	76
Table D-2: Relative Reactions of Trusses in 3:12 Assembly from Current Study	76
Table D-3: Difference in Relative Reactions for 3:12 Assembly	76
Table D-4: Reactions of Trusses in 6:12 Assembly from Wolfe and McCarthy (1989) ...	82
Table D-5: Reactions of Trusses in 6:12 Assembly from Current Study	82
Table D-6: Difference in Relative Reactions for 6:12 Assembly	82
Table D-7: Relative Deflections of Trusses in 3:12 Assembly from Wolfe and McCarthy (1989).....	88

LIST OF APPENDIX TABLES (Continued)

<u>Table</u>	<u>Page</u>
Table D-8: Relative Deflections of Trusses in 3:12 Assembly from Current Study	88
Table D-9: Difference in Relative Deflections for 3:12 Assembly	88
Table D-10: Relative Deflections of Trusses in 6:12 Assembly from Wolfe and McCarthy (1989).....	94
Table D-11: Relative Deflections of Trusses in 6:12 Assembly from Current Study	94
Table D-12: Difference in Relative Deflections for 3:12 Assembly	94
Table E-1: Description of Shear Wall Configurations (Dolan and Johnson 1996)	95
Table E-2: Description of Materials and Construction Methods (Dolan and Johnson 1996)	96
Table E-3: Description of Connections used in Construction (Dolan and Johnson 1996)	96
Table E-4: Frame Sections Used for Modeling in SAP2000	98
Table E-5: Layered Shell Element Used for Modeling Sheathing in SAP2000	100
Table E-6: Material Properties Used for Modeling in SAP2000.....	101
Table E-7: Properties for Wall Anchorage used for Modeling in SAP2000	103
Table E-8: Stiffness Comparison between the SAP2000 Models from the Current Study and Tests from Dolan and Johnson (1996)	104
Table F-1: Example of Shear Wall Deflections vs. Sheathing Shear Modulus, G_{12} in SAP2000	108
Table F-2: Example Shear Wall Deflection Calculation using Equation F-1 (AF&PA 2005b Equation C4.3.2-2).....	110
Table G-1: Construction Details from Paevere (2002).....	113
Table G-2: Frame Sections Used in SAP2000 Model	114
Table G-3: Sheathing Material Properties used in SAP2000 Model	114
Table G-4: Properties for Wall Anchorage used for SAP2000 Model	115
Table G-5: Material Densities used for Building Self-Weight	115

LIST OF APPENDIX TABLES (Continued)

<u>Table</u>	<u>Page</u>
Table K-1: Parameters used for ASCE 7-05 MWFRS Design Wind Loads Method 2	.164
Table K-2: Design Pressures for Index House under North-South Wind	165
Table K-3: Design Pressures for Index House under West-East Wind	165
Table K-4: ASCE 7-05 Design Pressures for Index House under South-North Wind ..	166
Table K-5: ASCE 7-05 Design Pressures for Index House under East-West Wind	166
Table K-6: Design Pressures for Index Building under Southeast-Northwest Wind	167

INTRODUCTION

Light-frame, wood residential structures are indeterminate structural systems that rely on complex interactions between structural members and connections to transfer loads through the structure and into the foundation. The majority of light-frame wood structures are comprised of *sub-assemblies* including vertical shear walls spanned by horizontal floor and roof diaphragms. Sub-assemblies share and transmit forces through inter-component connections comprised of nails, bolts, and other mechanical connectors. The sequence in which the loads are transferred from their source to components and cladding, then to the main-load carrying systems, and finally to the foundation and supporting ground is referred to as the load path (Taly 2003). Load paths are dependent on the relative stiffness of individual components and sub-assemblies within the structure as well as the direction of loading. Gravity loads act vertically downward and are created by the self-weight of the structure as well as possible snow accumulation on the roof. Additional uplift and lateral loads can be created by pressures from strong wind events (tornadoes and hurricanes) and ground acceleration during earthquakes. Due to their light weight, wood frame houses are particularly vulnerable to uplift pressures created by strong winds.

The damage caused by Hurricane Andrew in 1992, demonstrated this weakness. In the wake of Hurricane Andrew, building codes for high wind events were developed in Florida and adopted in hurricane prone areas of the United States (van de Lindt et al. 2007). However, since more than 80 percent of single-family homes in the US were constructed before these updated codes, wind damage to residential structures is still a pressing concern (Prevatt et al. 2009). Structural investigations performed by van de Lindt et al. (2007) after the 2005 hurricane Katrina, showed that the prevalent source of structural damage in light-frame houses was an overall lack of design for uplift load paths. Failures were seen in roof-to-wall connections and wall-to-foundation connections, where mechanical connectors were of insufficient strength and spacing to transfer the required uplift loads. Loss of sheathing on roof and gable-end trusses was another common issue, which was attributed to improper edge nail spacing used to

connect the sheathing to the wood framing (van de Lindt et al. 2007). Structural investigations performed after the 2011 Joplin and Tuscaloosa tornadoes showed similar damage along the outskirts of the tornado paths where lower wind speeds occurred (Prevatt et al. 2012a). In light of this, it was suggested that high wind codes and retrofits developed for coastal communities could also help to reduce damages in tornado-prone areas (Prevatt et al. 2012a).

Due to the complex and indeterminate nature of light-frame wood structures, developing economic yet effective building codes and retrofits requires a detailed understanding of full building system behavior. Unfortunately, full-scale testing of complete structures is costly and limited by the size of existing testing facilities. In light of this, a considerable amount of research has focused on developing accurate and practical methods for modeling full building systems using computer software programs. A detailed review of previous full-scale testing and modeling is included in Appendix A of this thesis.

OBJECTIVES

The two main objectives of the current study were to: (1) develop and validate practical modeling methods and (2) analyze the effects of plan geometry, wall openings and gable-end retrofits on lateral and uplift wind load paths through a realistic house with complex geometry.

RESEARCH APPROACH

The modeling methods used in this study were based on the work of Martin et al. (2011) and intended to represent practical methods that could be easily applied in industry. All models were developed using commercially available software, SAP2000 Version 14 (Computers and Structures 2009). Inter-component connections were modeled with linear springs, or as simple pinned or rigid connections. Additionally, industry standards and specifications were used to select the material properties used in the model.

A four-step validation procedure was used to validate load sharing and system behavior in the model:

1. Two-dimensional trusses were modeled and validated against full-scale tests from Wolfe et al. (1986) – (Appendix B)
2. Three-dimensional roof assemblies were modeled and validated against full-scale tests from Wolfe and McCarthy (1989) – (Appendices C and D)
3. Two-dimensional shear-walls were modeled and validated against full-scale tests from Dolan and Johnson (1996) – (Appendices E and F)
4. A three dimensional, L-shaped house was modeled and validated against full-scale tests from Paevere et al. (2003) – (Appendices G and H)

Results from the validation procedure are briefly discussed in the journal manuscript and fully detailed in the appendices listed above. Once validated, the modeling methods were used to create various models for two load path investigations:

1. ***Uniform Uplift Investigation:*** The effects of large wall openings and a re-entrant corner on uplift load paths were investigated in models of simple buildings with no interior walls. The models were loaded with a uniform uplift pressure applied normal to the roof. – (Appendix J)
2. ***Wind Load Investigation:*** The effects of gable-end retrofits and re-entrant corner dimensions on lateral and uplift load paths were investigated in a realistic, L-shaped house. Models of the house were loaded with ASCE 7-05 Main Force Resisting System (MWFRS) design wind loads (ASCE 2005). – (Appendices K and L)

Details for the models used in the load path investigations are included in Appendix I. Results from the investigations are included in the appendices listed above, and discussed in the manuscript.

MANUSCRIPT:

**PRACTICAL MODELING FOR LOAD PATHS IN A REALISTIC, LIGHT-
FRAME WOOD HOUSE**

Kathryn S. Pfretzschner, Rakesh Gupta, and Thomas H. Miller

American Society of Civil Engineers
Journal of Performance of Constructed Facilities

ASCE Journal Services
1801 Alexander Bell Drive
Reston, VA 20191

Submitted 2012

ABSTRACT

The objective of this study was to develop and validate practical modeling methods for investigating load paths and system behavior in a realistic, light-frame wood structure. The modeling methods were validated against full-scale tests on sub-assemblies and an L-shaped house. The model of the L-shaped house was then modified and used to investigate the effects of re-entrant corners, wall openings and gable-end retrofits on system behavior and load paths. Results from this study showed that the effects of adding re-entrant corners and wall openings on uplift load distributions were dependent on the orientation of the trusses with respect to the walls. Openings added to walls parallel to the trusses had the least effect on loads carried by the remaining walls in the building. Varying re-entrant corner dimensions under ASCE 7-05 (ASCE 2005) design wind loads caused increasing degrees of torsion throughout the house, depending on the relative location and stiffness of the in-plane walls (parallel to the wind loads) as well as the assumed direction of the wind loads. Balancing the stiffness of the walls on either side of the house with the largest re-entrant corner helped to decrease torsion in the structure under lateral loads. Finally, although previous full-scale tests on gable-end sections verified the effectiveness of the gable-end retrofit that was recently adopted into the 2010 Florida building code, questions remained about the effects of the retrofit on torsion in a full building. The current study found that adding the gable-end retrofits to the L-shaped house did not cause additional torsion.

INTRODUCTION

In the United States wind damage accounted for approximately 70 percent of insured losses from 1970 to 1999 (Holmes 2001). Wood-frame residential structures are particularly vulnerable to damage from wind due to their light weight. Additionally, the majority of existing single-family houses in the United States were constructed before building codes were updated after Hurricane Andrew in 1992. More recent wind storms in the United States, including the 2005 hurricane Katrina and the 2011 Joplin, Missouri, and Tuscaloosa, Alabama, tornadoes have shown that structural damage from wind is still

a prevalent issue, especially for wood-framed residential structures. Structural investigations from these hurricane and tornado events showed that the main source of damage in houses was an overall lack of design for uplift load paths (van de Lindt et al. 2007 and Prevatt et al. 2012a). Additionally, gable-end failures were reported as an area of concern (van de Lindt et al. 2007 and Prevatt et al. 2012a). In order to develop retrofitting options and improve building codes for residential structures, it is necessary to gain a better understanding of system behavior and load paths in light-frame structures.

Analyzing system behavior in complex structures requires the development of practical and accurate analytical models validated against full-scale tests. Phillips et al. (1993) and Paevere et al. (2003) performed full-scale tests on realistic, rectangular and L-shaped residential structures. Results from these studies showed that light-frame roof diaphragms act relatively stiff compared to shear walls. Additionally, in-plane walls (parallel to applied lateral loads) are capable of sharing approximately 20 to 80 percent of their loads with other walls in the structure depending on the relative location and stiffness of the surrounding walls (Paevere et al. 2003). Data from these tests have also been used by a number of researchers to develop practical models for load path analysis.

Doudak (2005) developed a non-linear model of the Paevere et al. (2003) house, using a rigid element for the roof diaphragm. Individual sheathing nail connections were modeled using non-linear spring elements. The model was capable of predicting lateral load distributions to the walls, however, the level of detailing in the walls proved time consuming. Kasal (1992) and Collins et al. (2005) developed non-linear models of the Phillips et al. (1993) and Paevere et al. (2003) houses, respectively, also using rigid elements for the roof diaphragm. Unlike Doudak (2005), the in-plane stiffness of the shear walls was controlled using diagonal non-linear springs. This reduced the amount of time required for modeling; however, full-scale tests were necessary to determine the non-linear stiffness of the springs and material properties for the structure. None of these models were used to examine uplift load paths. Shivarudrappa and Nielson (2011) modeled uplift load paths in light-frame roof systems. For increased accuracy, the models incorporated individual trusses, sheets of sheathing (modeled with individual nail connections) and semi-rigid roof-to-wall connections. Results from the model showed

that the load distribution was affected by the location of gaps in the sheathing as well as the stiffness of the sheathing and connections.

Martin et al. (2011) developed a simple, linear model of a rectangular structure tested at one-third scale at the University of Florida. The model relied on material properties and wall stiffness properties readily available in industry standards. The in-plane stiffness of the walls was controlled by adjusting the shear modulus of the wall sheathing. The roof diaphragm was modeled as semi-rigid with individual trusses and sheathing, although gaps between individual sheets of sheathing were not included. Martin et al. (2011) found that the linear modeling methods were sufficient for predicting lateral load paths as well as uplift load paths through the structure when loaded within the elastic range. Additionally, the distribution of uplift loads was highly dependent on the orientation of the roof trusses. The modeling methods developed by Martin et al. (2011) were used in the current study to analyze lateral and uplift load paths in a more realistic light-frame house. A more detailed review of previous full-scale testing and modeling can be found in Pfretzschner (2012).

RESEARCH METHODS

The two main objectives of this study were to: (1) further develop and validate the practical, linear modeling methods of Martin et al. (2011) for a rectangular building, and (2) apply the modeling methods towards investigating uplift and lateral load paths in a realistic light-frame structure with complex geometry (L-shaped house). The modeling methods were developed using SAP2000 software (Computers and Structures, Inc. 2009). Additional details about the research methods can be found in Pfretzschner (2012).

Modeling Methods

Framing Members

Framing members, including wall studs, truss chords, etc., were modeled using SAP2000's frame element. The frame element was assigned the actual cross-section of each framing member. Multiple framing members located side by side, such as a "double

stud” or “double top-plate,” were modeled using a single frame element with a cross section equal to the sum of the individual cross sections of the framing members.

Isotropic material properties for the framing members were determined using longitudinal design properties listed in the AF&PA (2005a) *National Design Specification for Wood Construction* (NDS) based on wood species and grade. Adjustment factors for moisture content, incising, etc, were applied to the design properties as specified by the NDS (AF&PA 2005a).

Sheathing

Wall sheathing in the current study was modeled using SAP2000’s layered shell element with plywood and gypsum wallboard (GWB) assigned as individual layers. Each shell element was modeled through the center of the wall studs with the sheathing layers displaced to either side of the wall. Roof and ceiling sheathing were also represented using the layered shell element; modeled through the centerline of the truss chords, with one layer of either plywood or GWB displaced accordingly.

Plywood layers were assigned orthotropic properties calculated using Nairn (2007) OSULaminates software. Plywood sheathing layers for the walls and roof were assigned in-plane and out-of-plane properties, respectively, based on their general behavior within the full building. GWB layers were assigned isotropic material properties listed by the Gypsum Association (2010).

In accordance with Martin et al. (2011), individual sheets of plywood and GWB were not modeled as separate elements. Instead, one continuous shell element was applied to each wall, ceiling and roof surface, and meshed into smaller elements for analysis. Although the effects of “gaps” between individual sheathing members were neglected, validation studies against full-scale tests showed that these methods were sufficient for portraying system behavior and load distribution.

Framing Connectivity

All framing connections were modeled as either simple “pinned” or “rigid” connections. Trusses were modeled with pinned connections at the ends of the webs and at the ridge. Rigid connections were used at the truss heels, and top and bottom chords

were modeled as continuous members through the web connections. Truss-to-wall connections were modeled as rigid connections and were not coincident with the heel connections (Martin et al. 2011). Gable-end trusses were also rigidly connected to the gable-end walls.

All framing connections in the walls were modeled as pinned connections. This allowed for the stiffness of the walls to be controlled entirely by the sheathing properties. Shear wall stiffness is highly dependent on the spacing of the nail connections between the sheathing and framing members. As in Martin et al. (2011), the effects of edge nail spacing on wall stiffness were incorporated by adjusting the shear modulus, G_{12} , of the wall sheathing.

Sheathing G_{12} Adjustment Procedure

To account for the effects of sheathing edge nail spacing, the shear modulus, G_{12} of the sheathing was adjusted using a procedure similar to the “correlation procedure” used by Martin et al. (2011). The procedure in the current study was performed using a simple “*calibration model*” of a wall in SAP2000; with a specific length, rigid supports, no openings, and sheathed on one side only. Material properties were assigned to the sheathing using previously described methods. G_{12} , of the sheathing was then altered until the deflection of the calibration model matched a predicted deflection calculated using Equation C4.3.2-2 from AF&PA (2005b) for a specific edge nail spacing and wall length.

Equation C4.3.2-2 is a three-term, linear equation used to predict deflections of wood-framed shear walls based on “framing bending deflection, panel shear deflection, deflection from nail slip, and deflection due to tie-down slip” (AF&PA 2005b). The effects of panel shear and nail slip are incorporated into an apparent stiffness term, G_a . Values for G_a are tabulated in AF&PA (2005b) based on sheathing material, framing layout and edge-nail spacing. Since rigid supports were used in the calibration model, the deflection due to tie-down slip was negated from the three-term equation. The purpose of the calibration model was to determine the required stiffness of the sheathing element. The effects of the anchor bolts and hold downs were incorporated later on, into the actual wall models, by using linear springs with realistic stiffness properties.

Repeating this method for shear walls of various lengths revealed that the required G_{12} for a specific edge nail spacing changed approximately linearly with wall length. Thus, for a building with multiple wall lengths and uniform edge nail spacing, this procedure is only necessary for the shortest and longest walls in the building. Additionally, G_{12} for the plywood sheathing and GWB sheathing can be determined separately using the procedure above for a wall sheathed on one side and applied to the respective sides of a wall sheathed on two sides. This method is supported by Patton-Mallory et al. (1984), who found that the stiffness of a wall sheathed on two sides is equal to the sum of the stiffnesses of two walls sheathed on one side with the same materials.

Wall Anchorage

Anchor bolts and hold-downs were modeled using directional linear spring elements. Three springs were used for the anchor bolts: one oriented in the vertical, Z-direction (representing the axial stiffness of each bolt connection), and two oriented in the lateral, X- and Y- directions (representing the shear stiffness of each bolt connection). Hold-down devices were represented with only one spring oriented in the Z-direction.

The axial stiffness of the anchor bolts was assigned in accordance with Martin et al. (2011) based on full-scale tests performed by Seaders (2004). The full-scale tests incorporated the effects of bolt slip and wood crushing under the washers. The lateral stiffness of the anchor bolts was calculated using equations for the load slip modulus, γ , for dowel type connections in Section 10.3.6 of the NDS (AF&PA 2005a). Finally, the axial stiffness of the hold-down devices was determined from properties published by the manufacturer, Simpson Strong-Tie.

Model Validation Procedure

Similar to Martin et al. (2011), the modeling methods in this study were validated against full-scale tests. Sub-assembly models, including two-dimensional trusses, three-dimensional roof assemblies and two-dimensional shear walls, were validated against tests performed by Wolfe et al. (1986), Wolfe and McCarthy (1989) and Dolan and

Johnson (1996), respectively. Shear walls from Dolan and Johnson (1996) were anchored with both anchor bolts and hold-downs allowing for the simultaneous validation of anchorage and shear wall modeling methods. Details for the sub-assembly models are included in Pfretzschner (2012). The final validation study was performed using full-scale tests on a realistic L-shaped house from Paevere et al. (2003).

Paevere et al. (2003) House

Paevere et al. (2003) performed static, cyclic and destructive load tests on a full-scale, L-shaped house. The house was designed to reflect a typical, North American “stick frame” house with a gable-style roof. Construction details for the L-shaped house can be found in Paevere et al. (2003) and Paevere (2002). Results from the static load tests were used to validate a model of the house.

Figure 1 shows the layout and framing used for the walls in the house, including six exterior shear walls (W1, W2, W4, W5, W7 and W9) and three interior non-load bearing walls (W3, W6 and W8). The exterior walls were 2.4 m (7.9 ft) tall. The interior walls were modeled 25 mm (1 in.) shorter than the exterior walls so that the trusses spanned the exterior walls only (Dr. Phillip Paevere, personal communication, June 25, 2012). W3 was connected to the trusses using non-structural slip connections to restrain the trusses laterally (Paevere 2002). These connections were modeled in SAP2000 using two-joint link elements, “fixed” in the direction parallel to the wall. Interior walls 6 and 8 were not connected to the trusses.

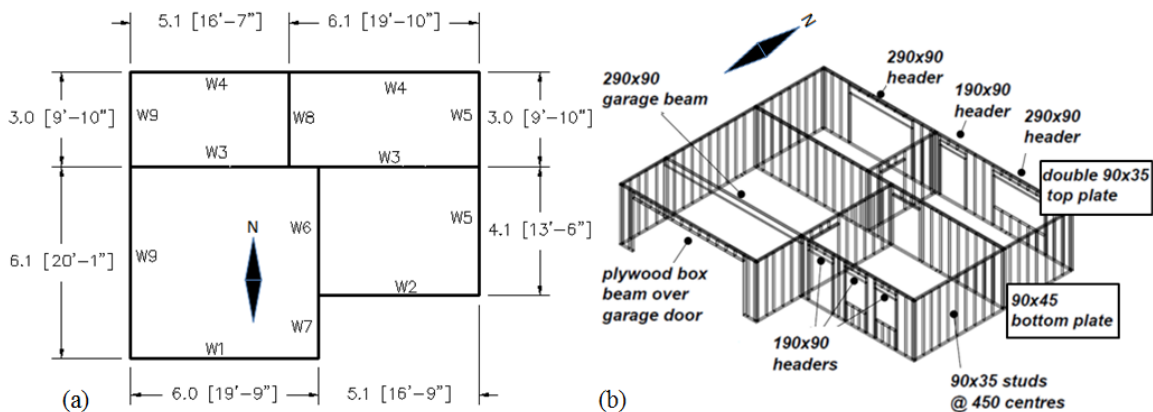


Figure 1: (a) Floor Plan with Centerline Dimensions [m (ft-in)] and Wall Designation, (b) Wall framing (mm) (Paevere 2002)

The gable roof was modeled as a semi-rigid diaphragm with 1.6-m- (5.2-ft-) tall, Fink trusses, spaced 0.6 m (2 ft) on center and oriented as shown in Figure 2, and plywood sheathing. Unsheathed Fink trusses were also used for the gable-end trusses. Framing members used for the truss chords and webs were 35x90 mm (1.4x3.5 in.) and 35x70 mm (1.4x2.8 in.), respectively. Details for the roof over-framing, where the two legs of the “L” meet above the garage, were not included in Paevere (2002) or Paevere et al. (2003). Therefore, over-framing in the model was assumed based on typical, North-American residential construction methods as shown in Figure 2.

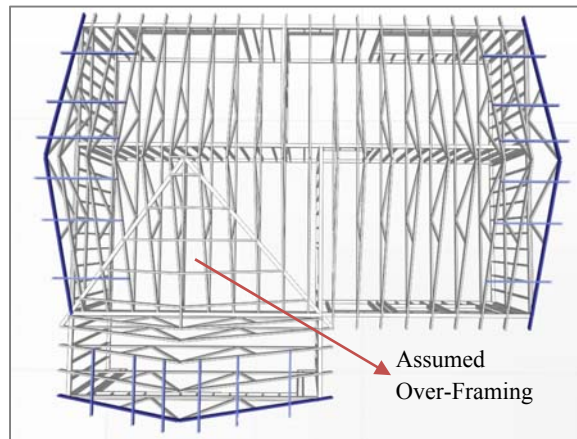


Figure 2: Truss Orientation and Gable-End Framing

All framing members in the house were Australian radiata pine sawn lumber. Since radiata pine is not included in AF&PA (2005a), the MOE reported by Paevere (2002) of 10000 MPa (1450 ksi) was used for the frame elements in SAP2000. Sheathing consisted of 9.5-mm- (0.375-in.-) and 12.5-mm- (0.492-in.-) thick plywood on the walls and roof respectively, with 13-mm- (0.5-in.-) thick GWB interior lining on the walls and ceiling. All walls were fully sheathed on the interior with GWB. Exterior walls were fully sheathed on the outside with plywood with the exception of walls 5 and 9. The partial exterior sheathing used for walls 5 and 9 is shown in Figure 3.

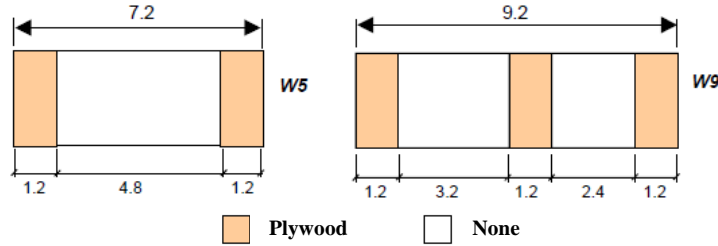


Figure 3: Plywood Sheathing on Exterior of Walls 5 and 9 (Paevere et al. 2003)

Table 1 provides the material properties used to model the sheathing elements. Figure 4 shows the required G_{12} versus wall length for the plywood and GWB wall sheathing based on edge fastener spacing. The fasteners used for the plywood sheathing were equivalent to 6d common nails spaced at 152 mm (6 in.) along the edges. The GWB fasteners were equivalent to No. 6 drywall screws spaced 305 mm (12 in.) along the edges. The maximum fastener spacing listed in AF&PA (2005b) of 203 mm (8 in.) for GWB sheathing was used to determine values of G_{12} for the GWB in the model.

Table 1: Sheathing Material Properties

Material	Properties	Source
Plywood Sheathing (Roof)	$E_1 = 8280 \text{ MPa (1201 ksi)}$ $E_2 = 2393 \text{ MPa (347 ksi)}$ $U_{12} = 0.011$ $G_{12} = 482 \text{ MPa (70 ksi)}$	<i>OSULaminates (Nairn 2007)</i> <i>(Flexural Properties)</i>
Plywood Sheathing (Walls)	$E_1 = 7017 \text{ MPa (1018 ksi)}$ $E_2 = 3657 \text{ MPa (530 ksi)}$ $U_{12} = 0.016$	<i>OSULaminates (Nairn 2007)</i> <i>(In-Plane Properties)</i>
Gypsum Wallboard (Walls and Ceiling)	$E_1 = 1820 \text{ MPa (264 ksi)}$ $E_1 = 1820 \text{ MPa (264 ksi)}$ $U_{12} = 0.3$	<i>Gypsum Association (2010)</i>

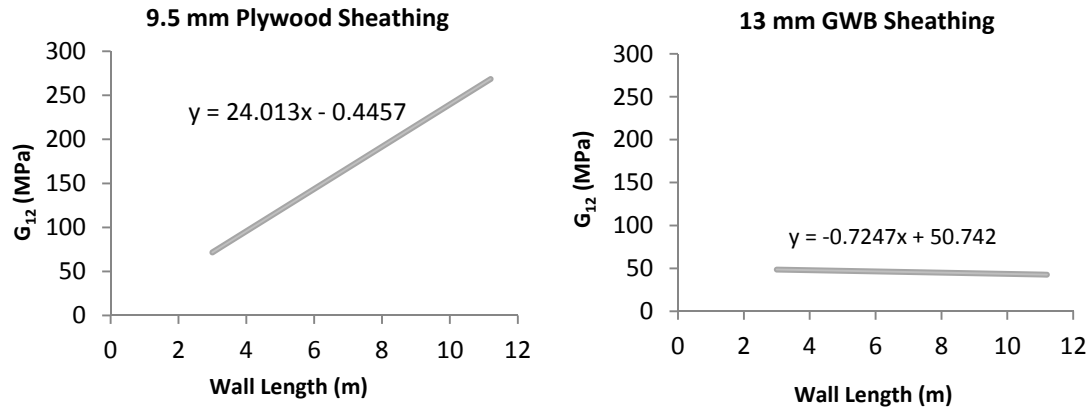


Figure 4: G_{12} vs. Wall Length for Plywood and GWB Wall Sheathing

The walls were anchored with 12.7 mm (0.5 in.) diameter anchor bolts, only (no hold-downs were used). Vertical and lateral springs used to represent the axial and shear behavior of the bolt connections were assigned a stiffness of 6.1 kN/mm (35 kip/in) and 16.7 kN/mm (95.5 kip/in), respectively. Stiffness properties were determined from Seaders (2004) and AF&PA (2005a) as explained in the modeling methods. Each anchor bolt in the full-scale house was connected to a load cell capable of measuring lateral and vertical reactions. Reactions at the anchor bolts in the model were validated against reactions from Paevere et al. (2003) for 15 static load tests consisting of one gravity load test and 14 lateral, concentrated load tests. Table 2 lists the material densities used to model the self weight (gravity loads) of the house. A complete list of lateral load cases can be found in either Paevere (2002) or Pfretzschner (2012).

Table 2: Material Densities used for Building Self-Weight

Material	Density kg/m ³ (pcf)	Source
Framing Members	550 (1.07)	<i>Paevere (2002)</i>
Plywood	600 (1.16)	<i>EWPA (2009)</i>
GWB	772 (1.50)	<i>Gypsum Association (2010)</i>

Load Path Investigations

After the modeling methods were validated, variations of the Paevere et al. (2003) house were created and used to perform load path investigations for uniform uplift

pressures and ASCE 7-05 design wind loads. All structures used in the investigations were modeled based on the materials and construction methods used by Paevere et al. (2003) with the following exceptions: (1) Gable-end overhang framing was changed to “out-looker” or “out-rigger” style framing commonly used in North America (Martin et al. 2011). (2) Gable-end trusses were changed from Fink trusses to more common, non-structural gable-end trusses. Modified gable-end framing is shown in Figure 5. (3) The exterior was fully sheathed with plywood, including the gable-end trusses. The shell element used to model the sheathing on the gable-end truss was not connected to the shell element used for sheathing on the gable-end wall. (4) Simpson Strong-Tie HDU2 hold-downs, modeled with an axial stiffness of 6.1 kN/mm (35 kip/in), were added to the exterior walls at the ends and at either side of door openings.

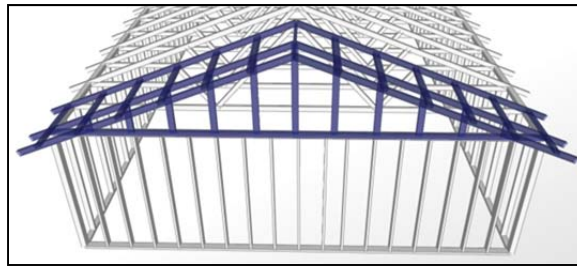


Figure 5: Modified Gable-End Framing for Load Path Investigations

For each load path investigation, index buildings were created as a baseline for load path comparisons. The index buildings were then altered systematically to analyze the effects of geometric variations (wall openings and re-entrant corners) and gable-end retrofits on uplift and lateral load paths. Detailed descriptions of the structures used in the load path investigations can be found in Pfretzschner (2012).

Uniform Uplift Investigation

As an extension of Martin et al. (2011), the effects of re-entrant corners and large wall openings were explored under a uniform uplift pressure of 2.4 kPa (50 psf) acting normal to the surface of the roof.

Two simple index buildings were used for the uplift investigation: a *rectangular index building* and an *L-shaped index building*. The L-shaped index building had the same plan geometry as the Paevere et al. (2003) house; with the modifications described

previously, no interior walls, no wall openings and no GWB lining. The rectangular index building was then created by removing the short leg of the “L” and extending wall 2. Note that the wall designations used by Paevere et al. (2003) (shown in Figure 1) were maintained throughout both load path investigations. Similar to Martin et al (2011), the self-weight of the buildings was not included in order to analyze load paths due to uplift pressures, only. Reactions at the anchor bolts and hold-downs of the L-shaped index building were compared to the rectangular building to analyze the effects of the re-entrant corner.

The redistribution of load paths due to large wall openings was also explored in this investigation. Martin et al. (2011) analyzed the effects of wall openings on uplift load paths in a simple rectangular building. In the current study, the effects of large, 3.2-m- (10.5-ft-) long, wall openings in the L-shaped index building were explored. Wall openings were added to the building one at a time in the following locations, representing scenarios that were not previously explored by Martin et al. (2011): wall 2 adjacent to the re-entrant corner, wall 4 opposite the re-entrant corner, wall 9 centered under the gable end, and wall 9 opposite the re-entrant corner. Due to the configuration of the roof, wall 9 represents both a gable-end wall and a side wall, with trusses running both parallel and perpendicular to the wall.

Wind Load Investigation

The second load path investigation explored load paths in a more realistic house with applied ASCE 7-05 design wind loads. Design loads were calculated using the Main Wind Force Resisting System, MWFRS, method 2 (ASCE 2005). Although ASCE 7-05 MWFRS codified pressures are intended for buildings with regular plan geometry, a method for adapting the pressures to buildings with re-entrant corners is given in Mehta and Coulbourne (2010). This methodology was adopted for the current study. Additional methods of determining design wind loads for irregular buildings are discussed in Pfretzschner (2012).

Three wind directions were considered with design loads calculated based on ASCE 7-05 Load Cases 1 and 3 as shown in Figure 6. Load Case 1 includes all windward, leeward, sidewall and “roof parallel to wind” pressures indicated by ASCE 7-

05 Figure 6-6. Load Case 3 is meant to simulate diagonal winds by combining leeward and windward pressures for X and Y winds acting simultaneously at 75% of their full design value (Mehta and Coulbourne 2010). Parameters for the design wind loads were selected in accordance with Martin et al. (2011) including: a basic wind speed of 209 km/h (130 mph), a topographic factor, K_{zt} , of 1.0 and exposure category, B. The building was assumed to be a low-rise, enclosed building with occupancy category II, and an importance factor of 1.0. Positive internal pressure was used to produce “worst-case” uplift scenarios.

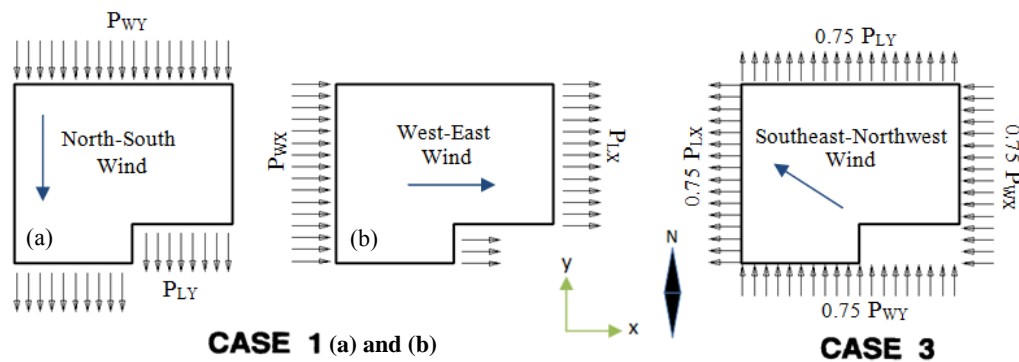


Figure 6: Wind Directions and ASCE 7-05 Load Cases

The index structure for this investigation was a realistic *L-shaped index house*, different from the L-shaped index building, representing the Paevere et al. (2003) house with the gable-end framing, sheathing and hold-down modifications described previously. The L-shaped index house was then altered to investigate the effects of (1) the addition of gable-end retrofits at every gable-end stud, and (2) the effects of increasing the size of the re-entrant corner. The gable end retrofits were modeled based on the C-shaped, gable-end retrofit recently adopted into the 2010 Florida Building Code (ICC 2011). An additional stud was added at each vertical web in the gable-end trusses, with the strong axis oriented perpendicular to the wall (forming an “L”) to reinforce the webs against out-of-plane winds. Additionally, horizontal braces were added to help transfer load from the gable-end wall into the roof and ceiling diaphragm. Additional details about the retrofit can be found in ICC (2011). Figure 7 shows one of the C-shaped retrofits in the model, added at every gable-end stud. Connections between the retrofit

studs and horizontal braces were accomplished with steel L-straps and compression blocks, and modeled as rigid connections.

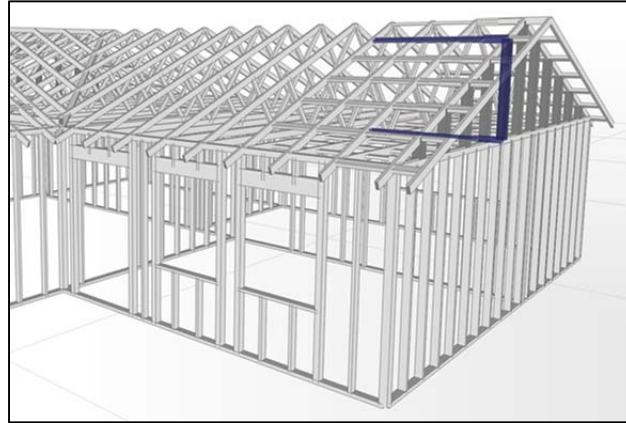


Figure 7: Example C-Shaped Gable-End Retrofit at Gable-End Stud

The effects of the re-entrant corner were explored by altering the short leg of the *L*-shaped index house to create three different sized re-entrant corners: *small*, *medium*, and *large*. For the small and medium re-entrant corners, the leg was shortened and lengthened by 2.4 m (7.9 ft) respectively. The large re-entrant corner was created by extending the leg so that the dimensions of the re-entrant corner had a 1:1 ratio. Wind loads for the re-entrant corner variations were adjusted accordingly based on the dimensions of the house.

RESULTS AND DISCUSSION

Model Validation

Sub-Assemblies

Sub-assembly models were used to validate the applicability of previously described modeling methods in predicting two- and three-dimensional system behavior. Two-dimensional models of individual trusses validated the use of ideal pinned and rigid connections between truss chords and webs. Three-dimensional models of roof assemblies validated the use of the layered shell element for modeling plywood sheathing. The roof assembly models were capable of predicting load sharing and

relative truss deflection in roofs with variable truss stiffness. Finally, models of two-dimensional shear walls validated methods for incorporating the effects of sheathing edge-nail spacing, wall openings and wall anchorage on shear wall stiffness. Full details and results for the sub-assembly validation studies are included in Pfretzschner (2012).

Paevere et al. (2003) House

The full-scale L-shaped house, tested by Paever et al. (2003), was used to validate the ability of the model to predict load sharing between walls connected by the roof diaphragm in a realistic house. Reactions at the anchor bolts in the model were compared against reactions in the full-scale house for 15 static load cases. The first static load case included gravity loads only to determine the self-weight of the house. Paevere et al. (2003) measured a self-weight of 50.8 kN (11.4 kips), which was 9% smaller than the self-weight of the model: 55.7 kN (12.5 kips). Paevere (2002) reported uplift reactions at some of the load cells during the gravity load test, which were attributed to possible residual stresses from construction. This could account for the smaller self-weight seen in the test house. The error could also stem from differences in the framing methods used to represent roof over-framing.

The remaining 14 load cases consisted of concentrated lateral loads applied at various locations along the top chords of walls 4 and 5, and at various angles at the roof ridge directly above wall 5. The distribution of lateral loads to the in-plane walls of the model was compared to reactions from Paevere et al. (2003). Figure 8, for example, compares the load distributions from the test house and the model for Load Case 4. Results from all 14 lateral load cases can be found in Pfretzschner (2012). Overall, the model proved capable of predicting the overall trends in load distributions (Figure 8) to the in-plane walls. Reactions at the walls carrying the maximum in-plane load were predicted within 20% error on average. For example, the largest load in Figure 8 occurred at wall 3 and was accurate to about 17%. This is similar to the level of accuracy reported by Doudak (2005) for static loading and elastic behavior of the structure.

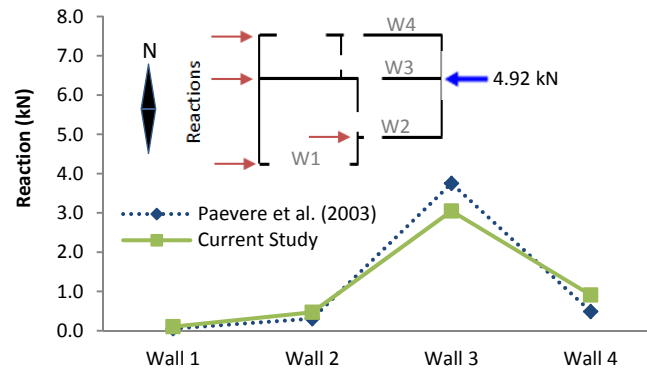


Figure 8: Load Distribution Plot for Paevere et al. (2003) Load Case 4

Uniform Uplift Investigation

The vertical reactions and changes in reaction at the anchor bolts and hold-downs of the models used in the uplift investigation were recorded and plotted in “bubble” plots. Each bubble represented an anchor bolt or hold-down while the size of the bubble represented the magnitude of either the uplift reaction or change in reaction at that anchorage device. The locations of the hold-downs were designated with an x. Detailed reaction plots for all model variations can be found in Pfretzschner (2012).

Rectangular vs. L-Shaped Buildings

To analyze the effects of re-entrant corners, the uplift reactions for the rectangular and L-shaped index buildings were plotted in Figure 9. Uplift reactions in the rectangular building were symmetrical with a maximum reaction of 11.0 kN (2.5 kips), occurring at the anchor bolts at the center of the side walls (walls 2 and 4). Since the roof trusses spanned between the side walls, the majority of the load applied to the roof was directed into the side walls rather than the gable-end walls. The maximum uplift reaction in the L-shaped index building, on the other hand, was 14.7 kN (3.3 kips), occurring at the hold-down directly under the re-entrant corner. In this case, the uplift loads that would have been transferred to the west side of wall 2 in the rectangular building, were instead transferred to the garage beam in the L-shaped building (shown in Figure 1b). The garage beam then directed the loads to the re-entrant corner and wall 9 opposite the re-entrant corner, causing load concentrations at these locations. Uplift load concentrations also occurred at anchor bolts under wall 4, directly opposite the re-entrant corner. The

flow of loads in the L-shaped index building is illustrated by the arrows in Figure 9. Note that trusses span perpendicularly from the re-entrant corner to wall 4 at this location. The load distribution to wall 5, parallel to the trusses, was not affected by the addition of the re-entrant corner. This suggests that the re-distribution of uplift loads due to a re-entrant corner is dependent on the orientation of the roof trusses with respect to the walls. A similar observation was noted by Martin et al. (2011) when investigating the effects of wall openings. Future research should examine the effects of re-entrant corners in buildings with different truss orientations.

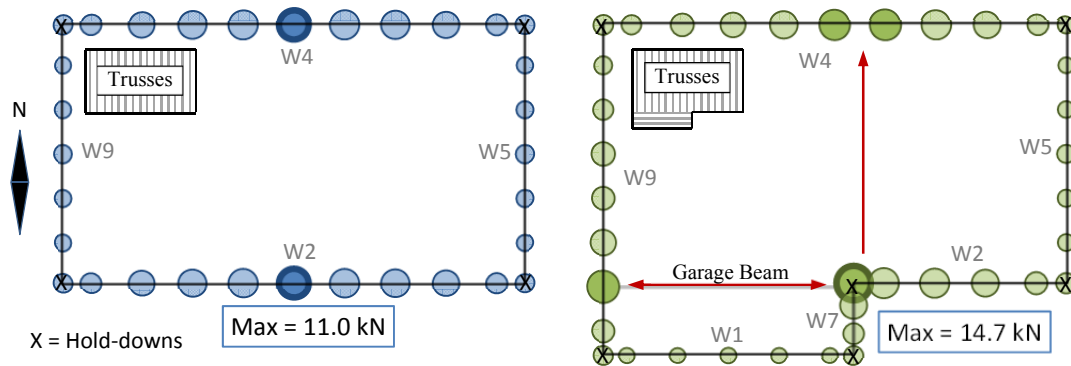


Figure 9: Uplift Reactions for Rectangular (Left) and L-shaped (Right) Index Buildings

Effects of Wall Openings

Martin et al. (2011) explored the effects of large wall openings placed in the gable-end walls and side walls of a rectangular building under uniform uplift pressure. The current study examined openings in an L-shaped building with a re-entrant corner and trusses oriented in two orthogonal directions. Similar to Martin et al. (2011), the opening centered under the gable-end portion (North end) of wall 9 caused relatively localized effects, increasing uplift loads in the side wall portion (South end) of wall 9, and having negligible effects on walls on the opposite side of the building. The openings placed in the side walls, on the other hand, had more global effects on uplift reactions throughout the building. Figure 10 shows the change in uplift reactions due to openings in the two different side walls: wall 4 (opposite the re-entrant corner) and wall 2 (adjacent to the re-entrant corner). As expected, uplift loads at the location of the openings were re-directed through the headers to either side of the doors, causing load concentrations at

the hold-downs directly under the door jams. The largest load concentrations were seen on the side of the opening in wall 2, closest to the re-entrant corner. Uplift reactions at this point increased by 60 percent over the reactions seen in the building without openings. Comparatively, the opening in wall 4 caused less than a 30 percent increase in uplift loads at either side of the opening. The larger load concentration at the opening in wall 2 was likely due to the uplift load concentrations in wall 2 from the re-entrant corner itself.

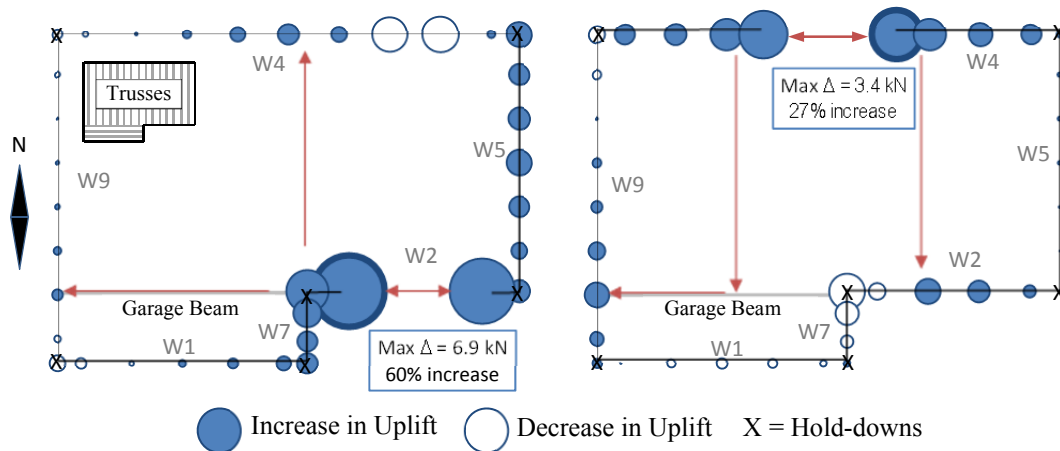


Figure 10: Change in Uplift Reactions (Magnified 4x) due to Openings in Wall 2 (Left) and Wall 4 (Right) – arrows represent load paths

As in Martin et al. (2011), openings placed in the side walls in this investigation also caused uplift load concentrations in the remaining side walls. Examining the truss orientation in the building shows that uplift loads at these points of concentration were clearly transferred from either side of the wall opening by the roof trusses. In the case of the opening in wall 4, for example, uplift loads were transferred from the east side of the wall opening, through the north-south trusses, to the opposite side wall (wall 2). Uplift loads were also transferred from the west side of the opening, through the north-south trusses to the garage beam shown in Figure 1(b), and redirected through the garage beam and the east-west trusses to wall 9 (adjacent to wall 4). Similar system behavior was seen for the opening in wall 2 as shown in Figure 10, and for other side wall openings included in Pfretschner (2012). This strongly supports findings from Martin et al. (2011) that the effects of openings on uplift load distribution are dependent on the relative truss orientation with respect to the walls. The effects of openings in walls perpendicular to

the trusses were shared by other walls in the building spanned by the same trusses, while the effects of openings in walls parallel to the trusses were more isolated.

Finally, Martin et al. (2011) reported that the addition of an opening to any wall resulted in a decrease in the total load carried by the wall. In the current study, the opening in wall 2 also caused a decrease in the total load carried by the wall of up to 20 percent. The opening placed in wall 4, however, caused a 0.2 percent increase in the amount of total uplift load carried by the wall. It is likely that this small increase was due to the effects of the re-entrant corner.

Wind Load Investigation

Uplift reactions for each of the model variations in the wind load investigation were also plotted in bubble graphs and included in Pfretzschner (2012). Figure 11 shows the uplift reactions at the anchor bolts and hold-downs in the L-shaped index house for each wind load case. In all cases, uplift load concentrations were seen at the hold-downs located under the corners of the house, as well as on either side of the door openings. In addition, to determine whether the large uplift reactions at the west gable-end were due to the geometry of the building or the selected load cases, a fourth load case for east to west winds was added. This demonstrated that uplift reactions at the east gable end under the east to west wind loads were of similar magnitude to the reactions at the west gable-end under west to east wind loads.

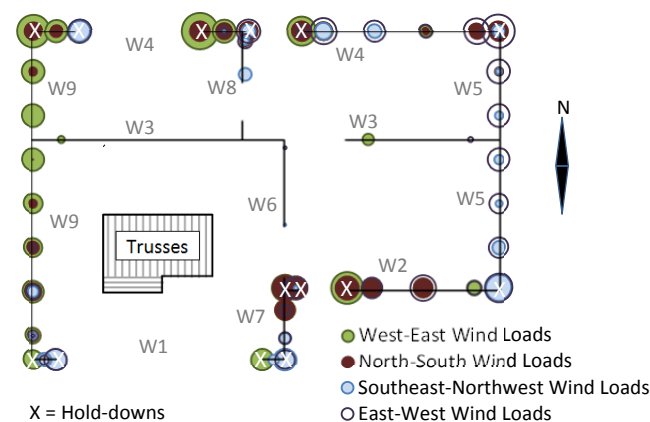


Figure 11: Uplift Reactions in L-Shaped Index House

Lateral load distributions to the walls parallel to the wind loads, for each model, were also plotted (Figure 12) and used to support the findings described below. For the southeast-northwest load case, lateral load distributions to both the N-S and E-W walls were plotted. Note that walls 6, 7 and 8 (shown individually in Figure 1) were grouped together here to simplify data presentation.

Addition of Gable-End Retrofits

Due to the number of gable-end failures seen in the aftermath of hurricanes, the 2010 Florida Building Code recently adopted a C-shaped gable-end retrofit for existing buildings (ICC 2011). Full-scale tests performed on gable-end sections (comprised of four Fink trusses and a gable-end wall) by Suksawang and Mirmiran (2009) showed that the retrofit sufficiently increased the strength of the gable-ends. However, questions remained about whether load redistribution due to the retrofit could cause additional torsion within a full building (beyond the original design). To address this question, C-shaped retrofits were modeled at every gable-end stud within the L-shaped index house used in this investigation.

The distribution of lateral loads and top plate deflections of the walls were then analyzed under ASCE 7-05 design wind loads for signs of torsion. For all wind load cases, the addition of the gable-end retrofits to the L-shaped index house caused negligible changes in lateral reactions under the walls parallel to the wind loads. Changes in deflections were equally small, within 0.1 mm (0.004 in), and showed no signs of additional torsion. These results were based on the three ASCE 7-05 load cases shown in Figure 6 only. Additionally, alternative retrofits recommended by the 2010 Florida Building Code for buildings with pre-existing obstacles were not explored in this investigation.

Effects of Re-Entrant Corner Dimensions

Figure 12 shows the lateral load distributions to the walls parallel to the wind loads and displaced shapes of the exterior wall top-plates for each wind load case. For north to south (N-S) design wind loads, the displaced shape of the top-chords for each model variation showed little to no torsion due to the increasing size of the re-entrant

corner. As walls 7 and 9 were extended, lateral loads carried by the outer walls running N-S (walls 5 and 9) were re-distributed to the inner N-S walls 6, 7 and 8. The percent of N-S loads carried by these central walls increased by 14 percent; while the percent of N-S loads carried by the outer walls, walls 5 and 9, decreased by 7 and 3 percent, respectively.

In the case of west to east (W-E) wind loads, the displaced shape of the top chords clearly showed increasing degrees of torsion as the size of the re-entrant corner increased. Although the relative distribution of these loads to each of the W-E walls changed by less than 5 percent, increasing the length of the southern end of wall 9 (perpendicular to the wind) increased the total amount of W-E wind load on the house. As a result, the relative in-plane deflections of southern walls 1 and 2 as compared to northern walls 3 and 4 increased dramatically. This can be attributed to the fact that walls 1 and 2 were significantly less stiff than walls 3 and 4, due to the shorter lengths and relatively large opening to surface-area ratios of walls 1 and 2. This asymmetry in relative stiffness between the north and south sides of the house caused torsion to occur with increasing loads in the W-E direction. Wind loads applied diagonally, southeast to northwest (SE-NW), into the re-entrant corner also caused increasing amounts of torsion as the size of the re-entrant corner increased. For all load cases, the effects of increasing the size of the re-entrant corner were dependent on the relative stiffness and location of the walls, as well as the orientation of the wind loads. Additionally, the displaced shapes of the top plates in Figure 12 show a combination of torsional behavior and in-plane displacements characteristic of a semi-rigid diaphragm.

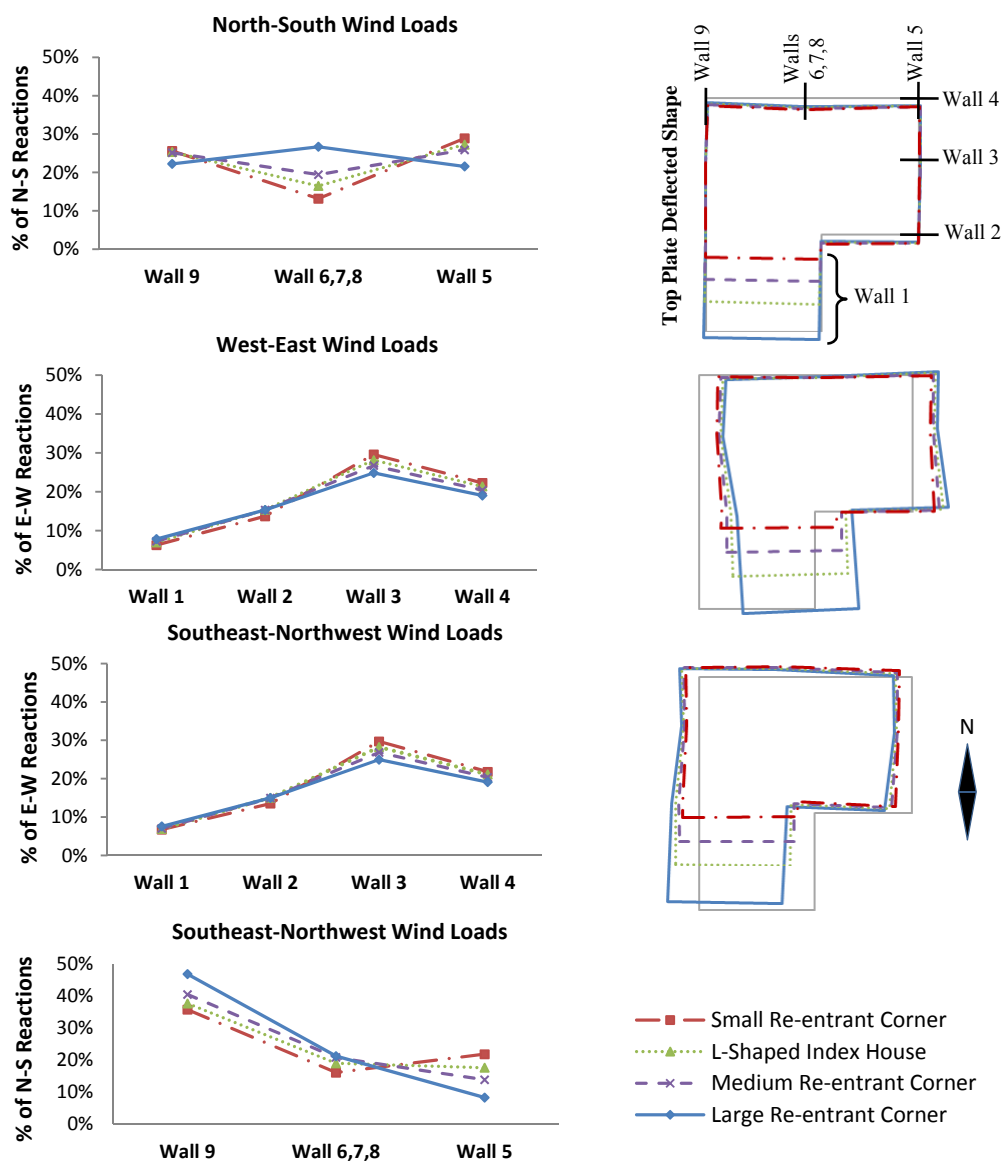


Figure 12: Lateral Load Distribution and Top Plate Deflected Shapes for Re-Entrant Corner Variations

The results of this study imply that balancing the stiffness of the walls along each of the major axes of the house may reduce torsion due to large re-entrant corners. In an effort to reduce torsion in the model with the largest re-entrant corner, the stiffnesses of walls 1 and 2 were increased by assuming realistic changes in the construction of the walls: (1) blocking was added to the walls, (2) the edge fastener spacing for the GWB was decreased to 102mm (4 in), (3) the nails used for the plywood were upgraded from 6d to 8d common nails and (4) the edge nail spacing for the plywood was decreased to 51

mm (2 in). Based on these assumptions, new values of G_{12} for the GWB and plywood sheathing on walls 1 and 2 were calculated using the adjustment procedure described in the modeling methods section. Figure 13 shows the deflected shapes of the original model and the model with increased stiffnesses in walls 1 and 2 for the W-E and SE-NW wind loads. In both cases, increasing the stiffnesses of walls on the south side of the house slightly decreased the amount of torsion seen in the deflected shape of the top chords.

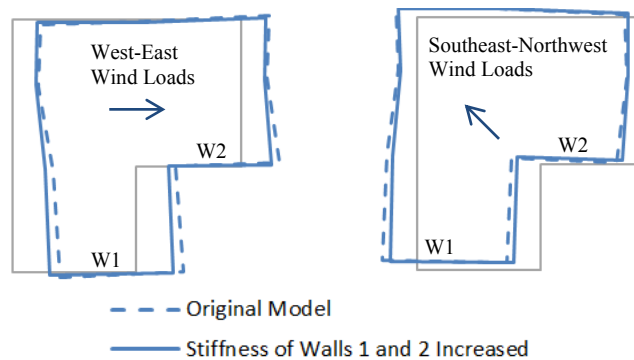


Figure 13: Displaced Shape of Large Re-entrant Corner Building with Increased Stiffness in Walls 1 and 2

CONCLUSIONS

Based on the validation studies, the simplified linear modeling methods created by Martin et al. (2011), and further developed in this study, were capable of predicting uplift and lateral load paths in a light-frame, wood residential structure with complex, realistic plan geometry. This conclusion is strictly for loading conditions within the elastic range of the structure. The modeling methods used in this study cannot be applied for inelastic or failure analysis.

Using the validated modeling methods, two different load path investigations were performed using uniform uplift pressures and ASCE 7-05 design wind loads. The following conclusions were drawn based on results from the load path investigations:

1. The addition of a re-entrant corner in a low-rise structure, under uniform uplift pressure, caused load concentrations at the re-entrant corner as well as in either wall directly opposite the re-entrant corner; depending on the truss orientation.

2. The addition of wall openings in a low-rise structure under uniform uplift pressure caused load concentrations on either side of the openings. Uplift loads at these points of concentration were further distributed to the remaining walls by the roof trusses. The largest load concentrations occurred when an opening was placed in a side wall, directly adjacent to the re-entrant corner. Openings in walls parallel to the trusses had the least effect on uplift reactions in the remaining walls.
3. ASCE 7-05 Main Wind Force Resisting System (MWFRS) design wind loads caused uplift load concentrations at the hold-downs placed under the door jams and the corners of the L-shaped house.
4. There was no evidence that the gable-end retrofit adopted by the 2010 Florida Building Code caused additional torsion in the L-shaped house when loaded with ASCE 7-05 MWFRS design wind loads.
5. The effects of increasing the size of the re-entrant corner in an L-shaped house, under ASCE 7-05 MWFRS design wind loads, were dependent on the location and relative stiffness of the in-plane walls, as well as the assumed direction of the wind.

ACKNOWLEDGMENTS

Previous research contributions from Kenneth Martin, Dr. Phillip Paevere and Dr. Bohumil Kasal were greatly appreciated, as well as funding from the Oregon State University Center for Wood Utilization Research.

REFERENCES

- AF&PA (2005a). *National Design Specification for Wood Construction (NDS)*. ANSI/AF&PA NDS-2005. Washington, DC.
- AF&PA (2005b). *Special Design Provisions for Wind and Seismic*. ANSI/AF&PA NDS-2005. Washington, DC.
- ASCE – American Society of Civil Engineers. (2005). *ASCE/SEI 7-05 Minimum Design Loads for Buildings and Other Structures*. New York, NY.
- Computers and Structures, Inc. (2009). *CSI Analysis Reference Manual: For SAP2000, ETABS and SAFE*. Berkeley, CA.
- Collins, M., Kasal, B., Paevere, P. and Foliente, G. C. (2005). “Three-Dimensional Model of Light Frame Wood Buildings. II: Experimental Investigation and Validation of Analytical Model.” *Journal of Structural Engineering*, 131(4), 676-683.
- Dolan, J.D. and Johnson, A.C. (1996) “Monotonic Tests of Long Shear Walls with Openings.” Virginia Polytechnic Institute and State University Timber Engineering Report TE-1996-001, Blacksburg, VA.
- Doudak, G. (2005). “Field Determination and Modeling of Load Paths in Wood Light-Frame Structures.” PhD. Thesis, McGill University, Montreal, Quebec.
- EWPPA - Engineered Wood Products Association of Australia (2009). “Structural Plywood and LVL Design Manual.” *EWPPA Design Guides*, <http://www.ed.ewp.asn.au:85/Library/document_List.aspx?type=Design> (July 19, 2012).
- Gypsum Association (2010). “Gypsum Board Typical Mechanical and Physical Properties.” Gypsum Association (GA 235-10), Hyattsville, MD.
- Holmes, J.D., (2001). *Wind Loading of Structures*. Spon Press, New York, NY.
- ICC (2011). *Florida Building Code 2010 – Residential*. International Code Council, Inc. Country Club Hills, IL.
- Kasal, B. (1992) “A Nonlinear Three-Dimensional Finite-Element Model of a Light-Frame Wood Structure.” Ph.D. Diss., Oregon State University, Corvallis, Oregon.
- Martin, K. (2010). “Evaluation of System Effects and Structural Load Paths in a Wood Framed Structure.” M.S. Thesis, Oregon State University, Corvallis, OR.
- Martin, K.G., Gupta, R., Prevatt, D.O., Datin, P.L., van de Lindt, G.W., (2011). “Modeling System Effects and Structural Load Paths in a Wood-Framed Structure.” *Journal of Architectural Engineering*. 17, 134-143.

- Mehta, K.C. and Coulbourne, W.L. (2010). *Wind Loads: Guide to the Wind Load Provisions of ASCE 7-05*. ASCE Press, Reston, VA.
- Nairn, J. (2007). *OSULaminates – Java Application for Laminated Theory Analysis, Version 2.1*. Available at: < <http://www.cof.orst.edu/cof/wse/faculty/Nairn/OSULaminates.html>> (July 31 2012).
- Paevere, P. (2002). “Full-Scale Testing, Modeling and Analysis of Light-Frame Structures Under Lateral Loading.” Ph.D. Diss., The University of Melbourne, Victoria, Australia.
- Paevere, P., Foliente, A.M., and Kasal, B. (2003). “Load-Sharing and Redistribution in a One-Story Woodframe Building.” *Journal of Structural Engineering*, 129 (9), 1275-1284.
- Patton-Mallory, M., Gutkowski, R.M., and Solstis, L.A. (1984). “Racking Performance of Light-Frame Walls Sheathed on Two Sides.” FPL-448. Forest Products Laboratory, Madison, WI.
- Pfretzschner, K.S. (2012). “Practical Modeling for Load Paths in a Realistic, Light-Frame Wood House.” M.S Thesis, Oregon State University, Corvallis, OR.
- Phillips, T., Itani, R., and McLean, D. (1993). “Lateral Load Sharing by Diaphragms in Wood-Framed Buildings.” *Journal of Structural Engineering*, 119(5), 1556-1571.
- Prevatt, D.O., Roueche, D.B., van de Lindt, J.W., Pei, S., Dao, T., Coulbourne, W., Graettinger, A.J., Gupta, R., and Grau, D. (2012). “Building Damage Observations and EF Classifications from the Tuscaloosa, AL and Joplin, MO Tornadoes.” Structures Congress 2012, ASCE 2012, 999-1010.
- Seaders, P. (2004). “Performance of Partially and Fully Anchored Wood Frame Shear Walls Under Monotonic, Cyclic and Earthquake Loads.” M.S. Thesis, Oregon State University, Corvallis, OR.
- Shivarudrappa, R., Nielson, B.G. (2011) “Sensitivity of load distribution in light-framed wood roof systems due to typical modeling parameters.” *Journal of Performance of Constructed Facilities*, Accepted Manuscript.
- Suksawang, N. and Mirmiran, A., “Hurricane Loss Reduction for Housing in Florida: Performance of Gable End Wall Bracing Retrofit for Hurricane Protection, Phase II” Florida International University < http://www.ihrc.fiu.edu/lwer/docs/Year%209_Section4_GableEndBracing_RCMP08-09.pdf> (July 22, 2012).
- van de Lindt, J.W., Graettinger, A., Gupta, R., Skaggs, T., Pryor, S., and Fridley, K.J., (2007). “Performance of Wood-Frame Structures during Hurricane Katrina.” *Journal of Performance of Constructed Facilities*, 21(2), 108-116.

- Wolfe, R.W., and McCarthy, M. (1989). "Structural Performance of Light Frame Roof Assemblies – I. Truss Assemblies with High Truss Stiffness Variability" FPL-RP-492. Forest Products Laboratory, Madison, WI.
- Wolfe, R.W., Percival, D.H., and Moody, R.C. (1986). "Strength and Stiffness of Light Framed Sloped Trusses." FPL-RP-471. Forest Products Laboratory, Madison, WI.

CONCLUSIONS AND RECOMMENDATIONS

In order to establish effective building codes and retrofit options for houses in high wind zones, it is important to fully understand the system behavior and propagation of load paths through these structures. In this study, practical, linear modeling methods were developed for analyzing load paths in light-frame wood structures. The methods were validated against full-scale tests and found to be sufficient for predicting load paths and system behavior when loaded within the elastic range. Once validated, the methods were used in two load path investigations to analyze the effects of geometric variations and gable-end retrofits in light-frame wood structures.

The first investigation considered uniform uplift pressures applied to simple rectangular and L-shaped buildings with no interior walls, no gypsum wall board (GWB) and no wall openings. Uplift reactions at the anchor bolts and hold-downs in the two structures were compared to examine the effects of adding a re-entrant corner. In the L-shaped building, uplift concentrations appeared under the re-entrant corner and under walls opposite the re-entrant corner. These concentrations occurred in locations where trusses spanned directly between the re-entrant corner and the opposite walls. Similar behavior was observed when large openings were systematically added to walls in the L-shaped building. All openings added to the building caused uplift load concentrations at either side of the opening. Openings placed in the side-walls caused additional uplift load concentrations under opposite walls spanned by perpendicular trusses, while openings placed in gable-end walls (parallel to roof trusses) had little effect on the remaining walls in the building. This suggested that geometric variations in a structure can have global effects on uplift loads throughout the structure depending on the orientation of the roof trusses. Effects of large openings can be contained to local areas of the building by placing them in gable-end walls, parallel to the trusses.

The second load path investigation evaluated lateral and uplift load paths in a realistic L-shaped house (with interior walls, GWB and realistic door and window openings) under ASCE 7-05 MWFRS design wind loads. During the investigation, the house was modified to determine the effects of gable-end retrofits and varying re-entrant

corner dimensions on the distribution of loads. Uplift reactions at anchor bolts and hold-downs in the original L-shaped house showed load concentrations at either side of door openings and at the corners of the structure (including the re-entrant corner). Gable-end retrofits recommended by the 2010 Florida building Code were added to investigate effects on lateral load distributions (ICC 2011). Although the retrofits have proved effective in previous full-scale tests, questions remained about the possible effects on load paths and torsion within a full building. Lateral load distributions and displaced shapes of the retrofitted, L-shaped house in this study showed no signs of additional torsion due to the gable-end retrofits. The effects of re-entrant corner dimensions were analyzed by altering the length of one leg of the “L” in the original house. Lateral load distributions and displaced shapes of the models with various re-entrant corner dimensions showed that the effects of large re-entrant corners were dependent on the relative stiffness of the walls and the direction of loading. Balancing the stiffness of walls on either side of the building may help reduce the amount of torsion caused by the re-entrant corner.

Results from this study were limited to an L-shaped building. Future research should consider buildings with T, Y, X and U-shaped plan geometries, as well as alternate truss orientations. Furthermore, additional emphasis should be placed on using models to develop and verify retrofitting options for residential structures. This task may require a combination of the simplified modeling methods described in the current study and more detailed models of sub-assemblies. Finally, there was a considerable amount of debate concerning methods for calculating wind loads on buildings with irregular geometry and very little published information on the subject. Combining full building models with wind tunnel tests on scaled structures could help to verify current methods for calculating wind loads on structures with re-entrant corners.

BIBLIOGRAPHY

- AF&PA (2005a). *National Design Specification for Wood Construction (NDS)*. ANSI/AF&PA NDS-2005. Washington, DC.
- AF&PA (2005b). *Special Design Provisions for Wind and Seismic*. ANSI/AF&PA NDS-2005. Washington, DC.
- Amini, M.O. (2012). "Determination of Rational Tornado Design Wind Speed for Residential Woodframe Structures." M.S. Thesis, University of Alabama, Tuscaloosa, AL.
- APA – The Engineered Wood Association (2008). *Panel Design Specification*. The Engineered Wood Association. Tacoma, Washington.
- ASCE – American Society of Civil Engineers. (2005). *ASCE/SEI 7-05 Minimum Design Loads for Buildings and Other Structures*. ASCE, New York, NY.
- Collins, M., Kasal, B., Paevere, P. and Foliente, G. C. (2005a). "Three-Dimensional Model of Light Frame Wood Buildings. II: Experimental Investigation and Validation of Analytical Model." *ASCE Journal of Structural Engineering*, 131(4), 676-683.
- Collins, M., Kasal, B., Paevere, P. and Foliente, G. C. (2005b). "Three-Dimensional Model of Light Frame Wood Buildings. I: Model Description." *ASCE Journal of Structural Engineering*, 131(4), 684-692.
- Computers and Structures, Inc. (2009). *CSI Analysis Reference Manual: For SAP2000, ETABS and SAFE*. Berkeley, CA.
- Cramer, S. M., and Wolfe, R. W. (1989). "Load-Distribution Model for Light-Frame Wood Roof Assemblies." *ASCE Journal of Structural Engineering*, 115(10), 2603-2615.
- Cramer, S.M., Drozdek, J.M., and Wolfe, R.W. (2000) "Load Sharing Effects in Light-Frame Wood-Truss Assemblies" *ASCE Journal of Structural Engineering*, 115(10), 2602-2616.
- Dolan, J.D. and Johnson, A.C. (1996) "Monotonic Tests of Long Shear Walls with Openings." Virginia Polytechnic Institute and State University Timber Engineering Report TE-1996-001.
- Doudak, G. (2005). "Field Determination and Modeling of Load Paths in Wood Light-Frame Structures." PhD. Thesis, McGill University, Montreal, Quebec.

- Doudak, G., McClure, G., and Smith, I. (2012). "Experimental Evaluation of Load Paths in Light-Light Frame Wood Structure." *ASCE Journal of Structural Engineering*, 138(2), 258-265.
- Dung, D. (1999). "A practical approach to analyze the system effects of metal-plate-connected wood truss assembly." MS thesis, Oregon State University, Corvallis, Oregon.
- EWPPA - Engineered Wood Products Association of Australia (2009). "Structural Plywood and LVL Design Manual." *EWPPA Design Guides*, <http://www.ed.ewp.asn.au:85/Library/document_List.aspx?type=Design> (July 19, 2012).
- Fanella, D.A. (2008). *Structural Load Determination Under 2006 IBC and ASCE/WEI 7-05*. International Code Council, Springfield, IL.
- Gupta, R. (2005). "System Behaviour of Wood Truss Assemblies." *Prog. Struct. Engng. Mater.*, 7: 183-193.
- Gupta, R., and Limkatanyoo, P. (2008). "Practical Approach to Designing Wood Roof Truss Assemblies." *Practice Periodical on Structural Design and Construction*, 13(3), 183-193.
- Gupta, R., Miller, T. H., and Dung, D. (2004). "Practical solution to wood truss assembly design problems." *Practice Periodical on Structural Design and Construction*, 9(1), 54-60.
- Gypsum Association (2010) "Gypsum Board Typical Mechanical and Physical Properties" Gypsum Association (GA 235-10)
- Holmes, J.D., (2001). *Wind Loading of Structures*. Spon Press, New York, NY.
- ICC (2011). *Florida Building Code 2010 – Residential*. International Code Council, Inc. Country Club Hills, IL.
- Kasal, B. (1992) "A Nonlinear Three-Dimensional Finite-Element Model of a Light-Frame Wood Structure." Ph.D. Diss., Oregon State University, Corvallis, Oregon.
- Kasal, B., Collins, M. S., Paevere, P. and Foliente, G. C. (2004). "Design Models of Light Frame Wood Buildings under Lateral Loads." *ASCE Journal of Structural Engineering*, 130(8), 1263-1271.
- Kasal, B., and Leichti, R. J. (1992). "Nonlinear Finite-Element Model for Light-Frame Stud Walls," *ASCE Journal of Structural Engineering*, 118 (11), 3122-3135.
- Kasal, B., Leichti, R. J. and Itani, R. (1994). "Nonlinear Finite Element Model of Complete Light-Frame Structures." *ASCE Journal of Structural Engineering*, 120(1), 100-119.

- LaFave, K. and Itani, R. Y. (1992). "Comprehensive Load Distribution Model for Wood Truss Roof Assemblies." *Wood and Fiber Science*, 24(1), 79-88.
- Langlois, J.D. (2002). "Effects of Reference Displacement and Damage Accumulation in Wood Shear Walls Subjected to the CUREE Protocol." M.S. Thesis, Oregon State University, Corvallis, OR.
- Langlois, J., Gupta, R., and Miller, T.H. (2004). "Effects of reference displacement and damage accumulation in wood shear walls." *ASCE Journal of Structural Engineering*, 130(3), 470-479.
- Lebeda, D.J. (2002). "Behavior of Wood Shear Walls with Misplaced Holdowns." M.S. Thesis, Oregon State University, Corvallis, Oregon.
- Lebeda, D., Gupta, R., Rosowsky, D. and Dolan, J.D. (2005). "The effect of hold-down misplacement on the strength and stiffness of wood shear walls." *Practice Periodical on Structural Design and Construction*, 10(2), 79-87.
- Li, Z. (1996). "A Practical Approach to Model the Behavior of a Metal-Plate-Connected Wood Truss System." M.S. thesis, Oregon State University, Corvallis, Oregon.
- Li, Z., Gypta, R., and Miller, T.H. (1998). "Practical approach to modeling of wood truss roof assemblies." *Practice Periodical on Structural Design and Construction*, 3(3): 119-124.
- Limkatanyoo, P. (2003). "System Behavior of Three-Dimensional Wood Truss Assemblies." M.S. Thesis, Oregon State University, Corvallis, Oregon.
- Martin, K. (2010). "Evaluation of System Effects and Structural Load Paths in a Wood Framed Structure." M.S. Thesis, Oregon State University, Corvallis, OR.
- Martin, K.G., Gupta, R., Prevatt, D.O., Datin, P.L., van de Lindt, G.W., (2011). "Modeling System Effects and Structural Load Paths in a Wood-Framed Structure." *ASCE Journal of Architectural Engineering*. 17, Special Issue: Residential Construction, 134-143.
- Mehta, K.C. and Coulbourne, W.L. (2010). *Wind Loads: Guide to the Wind Load Provisions of ASCE 7-05*. American Society of Civil Engineers - ASCE Press, Reston, VA.
- Mensah A.F., et al. (2010) "Database-assisted design methodology to predict wind-induced structural behavior of a light-framed wood building." *Engineering Structures* (2010), doi: 10.1016/j.engstruct.2010.11.028.
- Mtenga, P. (1991). "Reliability Performance of Light-Frame Wood Roof Systems." PhD. Thesis, University of Wisconsin-Madison, Madison, Wisconsin.

- Nairn, J. (2007). *OSULaminates – Java Application for Laminated Theory Analysis, Version 2.1*. Available at: <<http://www.cof.orst.edu/cof/wse/faculty/Nairn/Software.htm>>. Oregon State University, Corvallis, Oregon.
- Paevere, P. (2002). “Full-Scale Testing, Modeling and Analysis of Light-Frame Structures Under Lateral Loading.” Ph.D. Diss., The University of Melbourne, Victoria, Australia.
- Paevere, P., Foliente, A.M., Kasal, B. (2003). “Load-Sharing and Redistribution in a One-Story Woodframe Building.” *ASCE Journal of Structural Engineering*, 129(9), 1275-1284.
- Patton-Mallory, M., Gutkowski, R.M., Solstis, L.A. (1984). “Racking Performance of Light-Frame Walls Sheathed on Two Sides.” FPL-448. Forest Products Laboratory, Madison, WI.
- Phillips, T. L. 1990. "Load Sharing Characteristics of Three-Dimensional Wood Diaphragms." M.S. Thesis, Washington State University, Pullman, WA.
- Phillips, T., Itani, R., and McLean, D. (1993). “Lateral Load Sharing by Diaphragms in Wood-Framed Buildings.” *ASCE Journal of Structural Engineering*, 119(5), 1556-1571.
- Prevatt, D.O., Datin, P.L. and Mensah, A. (2009) “Performance Based Wind Engineering (PBWE): Interaction of Hurricanes with Residential Structures” *Proc. 2009 NSF Engineering Research and Innovation Conference*, National Science Foundation, Honolulu, HI.
- Prevatt, D.O., Roueche, D.B., van de Lindt, J.W., Pei, S., Dao, T., Coulbourne, W., Graettinger, A.J., Gupta, R., Grau, D., (2012a). “Building Damage Observations and EF Classifications from the Tuscaloosa, AL and Joplin, MO Tornadoes.” Structures Congress 2012, ASCE 2012, 999-1010.
- Prevatt, D.O., Beata, P.A., Roueche, D.B., Consolazio, G.R., and Datin, P.L. (2012b) “Database-assisted Design and Finite Element Analysis of Residential Light-Framed Wood Structures.” 1st International Conference on Performance Based and Life Cycle Structural Engineering, Hong Kong, China.
- Rocha, D., Eamon, C.D., Murphy, J.F. (2010). “Reliability analysis of roof sheathing panels exposed to a hurricane wind” *Elsevier Journal of Structural Safety*, 33(2011), 74-81.
- Seaders, P. (2004). “Performance of Partially and Fully Anchored Wood Frame Shear Walls Under Monotonic, Cyclic and Earthquake Loads.” M.S. Thesis, Oregon State University, Corvallis, OR.

- Shanmugam, B., Nielson, B.G., Prevatt, D.O. (2008). "Probabilistic descriptions of in-situ roof to top plate connections in light frame wood structures." *ASCE Structures Congress 2008: Crossing Borders*.
- Shivarudrappa, R., Nielson, B.G. (2011) "Sensitivity of load distribution in light-framed wood roof systems due to typical modeling parameters." *Journal of Performance of Constructed Facilities*, Accepted Manuscript.
- Simpson Strong-Tie (2012a) "Discontinued Products." *Simpson Strong-Tie*, <<http://strongtie.com/obsolete.html>> (July 7, 2012).
- Simpson Strong-Tie (2012b) "LTT/HTT Tension Ties." *Simpson Strong-Tie*, <<http://strongtie.com/products/connectors/LTT-HTT.asp>> (July 7, 2012)
- Sinha, A. (2007). "Strain Distribution in OSB and GWB in Wood Frame Shear Walls." M.S. Thesis, Oregon State University, Corvallis, OR.
- Songlai, C., Chengmou, F., and Jinglong, P. (2010). "Experimental Study on Full-Scale Light-Frame Wood House under Lateral Load." *ASCE Journal of Structural Engineering*, 136(7), 805-812.
- Suksawang, N., Mirmiran, A., "Hurricane Loss Reduction for Housing in Florida: Performance of Gable End Wall Bracing Retrofit for Hurricane Protection, Phase II" Florida International University <http://www.ihrc.fiu.edu/lwer/docs/Year%209_Section4_GableEndBracing_RCMP08-09.pdf> (July 22, 2012).
- Taly, N., "Loads and Load Paths in Buildings: Principles of Structural Design," International Code Council, ICC Publishing, Country Club Hills, IL.
- van de Lindt, J.W., Graettinger, A., Gupta, R., Skaggs, T., Pryor, S., and Fridley, K.J., (2007). "Performance of Wood-Frame Structures during Hurricane Katrina." *Journal of Performance of Constructed Facilities*, 21(2), 108-116.
- Wolfe, R.W., and LaBissoniere, T. (1991). "Structural Performance of Light Frame Roof Assemblies – II. Conventional Truss Assemblies" FPL-RP-499. Forest Products Laboratory, Madison, WI.
- Wolfe, R.W., and McCarthy, M. (1989). "Structural Performance of Light Frame Roof Assemblies – I. Truss Assemblies with High Truss Stiffness Variability" FPL-RP-492. Forest Products Laboratory, Madison, WI.
- Wolfe, R.W., Percival, D.H., and Moody, R.C. (1986). "Strength and Stiffness of Light Framed Sloped Trusses." FPL-RP-471. Forest Products Laboratory, Madison, WI.

APPENDIX A

EXTENDED LITERATURE REVIEW

System Behavior and Modeling

Full Building

Light-frame wood structures are highly indeterminate structural systems composed of vertical (shear walls) and horizontal (roof and floor) subassemblies, joined by inter-component connections (including nails, screws and other mechanical connectors). Lateral and vertical external forces are transferred through out-of-plane walls, to the horizontal roof and floor diaphragms, to the shear walls and finally into the foundation. Consequently, load paths through the structure as a whole are dependent on both the behavior of the individual subassemblies, as well as the interaction between subassemblies. Current design methods often consider each subassembly separately, which can possibly lead to unsafe or inefficient designs. In order to accurately predict load paths, the full system must be considered.

Testing and Behavior

Due to the high costs associated with the construction and testing of complete structures, as well as the limited number of facilities capable of performing such tests, very few full-scale tests on light-frame wood structures have been performed. Until recently, the majority of full-scale testing has focused on individual roof and wall assemblies (discussed in later sections of this review).

Phillips et al. (1993) performed full-scale static tests on a single-story, light-frame wood structure at Washington State University. The structure was rectangular in plan, with two interior walls and door and window openings. Doors, windows and other architectural finishes were not installed in the building. Sheathing edge nail spacing was varied for each wall to create variable wall stiffness. The structure was cyclically loaded in three stages with hydraulic cylinders, and reaction forces under each shear wall were measured. The objective of the project was to provide data for an analytical model

created by Kasal (1992). Therefore, materials and subassemblies were also tested during construction in order to assemble adequate data for model validation.

Similarly, Paevere et al. (2003) performed full-scale testing on a North American style L-shaped light-frame wood house at the Commonwealth Scientific & Industrial Research Organization (CSIRO) Division of Building, Construction and Engineering in Melbourne, Australia. Plans and specifications for the test structure were developed by the National Association of Home Builders (NAHB) Research Center, CSIRO, and North Carolina State University. As in Phillips (1990), the objective was to provide data for finite element modeling. Architectural finishes were not included in the test structure, and various tests were performed on the materials and subassemblies during construction. The full structure was tested in multiple stages including: elastic tests, non-destructive dynamic tests and destructive tests. Reaction forces were measured by tri-axial load cells spaced evenly under all walls, and deflections were also measured at various locations. This structure was used to validate multiple finite element models that are discussed further in the next section.

Doudak (2005) and Doudak et al. (2012) established a real time monitoring program on a wood-frame house located on the campus of the University of New Brunswick in Canada. The structure has a simple rectangular plan and rests on a series of load cells around its perimeter. The structure was first tested under a series of static point loads to validate an analytical model developed by Doudak (2005) as discussed in the next section. The structure was then instrumented for continuous in-situ monitoring to measure the structure's response to actual dynamic and static environmental loads.

Among the observations noted by Phillips et al. (1993), Paevere et al. (2003) and Doudak et al. (2012), the following behavioral aspects of structures are important to the research at hand:

1. Despite its overall flexible behavior, the roof diaphragm acts relatively rigid when compared to the shear walls (Phillips et al. 1993, Paevere et al. 2003 and Doudak et al. 2012).
2. In-plane shear walls can transfer approximately 20 to 80 percent of their load to the rest of the structure when loaded individually (Paevere et al. 2003 and Doudak

et al. 2012). Additionally, the amount of load sharing is dependent on the relative location and stiffness of the loaded wall compared to the surrounding walls in the structure (Phillips et al. 1993 and Paevere et al. 2003).

3. The transverse shear walls can carry approximately 5 to 25 percent of the load depending on the type of loading (Phillips et al. 1993 and Paevere et al. 2003). This percentage decreased with increasing magnitude of applied load (Phillips et al. 1993).

Finally, Songlai et al. (2010) performed full-scale tests on a single-story, L-shaped, light-frame wood house under uniform lateral loads. The house was constructed with a floor diaphragm rather than a roof diaphragm, representing the first story of a structure. Results of the study showed that gypsum sheathing had significant effects on the strength and stiffness of shear walls (Songlai et al. 2010). Additionally, the floor diaphragm acted as a semi-rigid diaphragm in transferring lateral loads to the shear walls (Songlai et al. 2010).

Analytical Modeling

As a result of the intrinsic level of complexity of light-frame wood structures, a number of simplifying assumptions must be made to develop a practical analytical model. The most debated assumptions for system models are those concerning the behavior of inter-component connections, which are semi-rigid and behave non-linearly. Additional assumptions include representation of subassemblies, which can either be modeled using individual construction materials or idealized to various levels based on results from full-scale tests. Material properties can also be modeled based on recommended values from engineering design specifications, or can be entered as actual values given sufficient testing data.

Kasal (1992) used ANSYS finite-element software to develop an analytical model of the structure tested by Phillips (1990). The roof and floor were modeled as relatively rigid, linear “superelements” incorporating only the degrees of freedom along the boundaries of the element. Individual trusses and joists were not included. The walls were modeled as simplified nonlinear systems based on full-scale tests as discussed

further in the shear wall section of this review. Finally, inter-component connections were modeled using one-dimensional, nonlinear springs. Nonlinear spring properties were based on load-displacement relationships developed through experimental tests performed at Oregon State University. The model was accurate in predicting boundary reaction forces and deformations, but was relatively inaccurate when small loads were applied. Similar methods were also employed by Collins et al. (2005a,b) in developing ANSYS models of the more realistic CSIRO house from Paevere et al. (2003).

The models discussed thus far present a few limitations. For example, the level of simplification of the shear wall assemblies in the three-dimensional model requires that the boundary forces be taken from the original model and applied to separate, more detailed models of the individual walls in order to determine individual nail forces. Doudak (2005) addressed this problem in a model of the New Brunswick House and the Paevere et al. (2003) house created in SAP2000. Sheathing nail connections were individually detailed within each wall using spring elements. The finite element model was able to accurately predict the three-dimensional behavior of the building under various loads, the interactions between the roof and walls, as well as the interactions within the individual walls without the need for additional models. Unfortunately, the amount of time that was required for this level of detailing proved impractical for use in modeling for industry design.

Another limitation to these models is the element used to represent the roof, which may not be applicable to more complex structures. Like Kasal (1992) and Collins (2005a,b), Doudak (2005) also modeled the roof as a single linear element, neglecting the individual trusses. The load distribution in roof assemblies, however, is dependent on the relative stiffness of individual trusses. In roofs with complex geometries, different sizes and types of trusses lead to large variations in stiffness that would not be accounted for in the simplified models described above.

Martin (2010) incorporated individual trusses into an analytical model of a simple rectangular building. Similar to Kasal (1992), individual nails in the shear walls were not detailed. Instead, the directional shear modulus in the sheathing was adjusted to incorporate the effects of nail spacing as explained in the shear wall section of this report.

The model was simplified even further than in earlier models by assuming linear behavior in the inter-component connections based on properties provided by the connection manufacturer. Martin (2010) validated the full model against wind tunnel experiments performed on a scaled version of the building at the University of Florida with good results. It is important to note that unlike the previous models, the methods used by Martin (2010) relied on properties found readily available in industry specifications rather than properties determined from tests performed on materials and connections for the particular building being modeled.

The objective of the current project is to develop a practical means for exploring load paths through light-frame wood buildings with realistic, complex geometry. For this purpose, the methods used by Martin (2010) are ideal. The modeling of individual roof trusses allows for accurate representations of complex roofs. Additionally, the model relies on properties that are easily found in specifications rather than properties measured from experimental tests. This is ideal for industry since buildings are designed well before construction begins. While Martin (2010) and other previous studies modeled structures with simple plans, the current model accounts for the growing geometric complexity in actual residential structures.

Roof Assemblies

Light-framed wood roof assemblies typically consist of a series of trusses spaced approximately 0.6 m (2 ft) on center and sheathed with plywood or OSB to produce a system capable of complex load transfer mechanisms. Conventionally, trusses are designed individually by incorporating a tributary area approach for calculating design loads. Under this methodology, system behavior within the full assembly is accounted for by a repetitive system factor. Although roofs designed in this manner have performed favorably in the past, the increasingly complicated geometries of modern roof systems over the past few decades have created a need for a better understanding of load transfer through complex truss assemblies (Gupta 2005).

Testing and Behavior

In the 1980's, the Forest Products Laboratory in Wisconsin began a series of full-scale tests on light-frame wood truss assemblies to compile a database of information on system behavior for use in developing structural models. Wolfe et al. (1986) began the series by testing 42 full-sized Fink trusses using 38 x 89 mm (1.5 x 3.5 in), referred to as nominal 2x4, wood framing members with variable stiffness properties and metal plate connections. Wolfe and McCarthy (1989) and Wolfe and LaBissoniere (1991) continued the study by testing four 9-truss roof assemblies: two with highly variable truss stiffness properties, and two with more uniform, conventional construction. Based on the roof assembly tests, Wolfe and McCarthy (1989) and Wolfe and LaBissoniere (1991) concluded that:

1. Individual trusses and trusses within the assembly behaved approximately linearly when loaded up to twice their design loads.
2. Deflections of the individual trusses within the assembly were 50% lower than trusses outside the assembly under similar loading.
3. Composite action between the sheathing and the top chords effectively increased the stiffness of the top chords by up to 20%.
4. 40 – 70% of loads applied to trusses within the assembly were transferred through the sheathing to adjacent trusses.
5. Stiffer trusses tended to attract and carry a larger percentage of the applied loads.
6. Assemblies acted as parallel systems, in which loads are carried in proportion to truss stiffness rather than being uniformly distributed across tributary areas as commonly assumed by conventional design practices.

Lafave and Itani (1992) also performed tests on 9-truss gable roof assemblies constructed using conventional construction and tested on pinned and roller supports. The end trusses were placed on wooden blocks to simulate stiffer gable end trusses that were not considered in previous studies. The results of these tests showed that the stiffer gable end trusses attracted a large amount of the load away from adjacent trusses up to two trusses away from the ends.

Shanmugam et al. (2008) performed in-situ tests on existing roof to wall toe-nail connections to analyze differences between as-built connections and laboratory tests. Results showed that the average capacity of the as-built connections was lower than previous laboratory tests, with a higher variability. Additionally, there was a strong correlation between the uplift capacity and stiffness of the connections.

Analytical Modeling

Using information collected by the Forest Products Laboratory, several different analytical models were developed by various researchers. Cramer and Wolfe (1989) used a matrix analysis program called ROOFSYS to model four nine-truss roof assemblies (two with high degrees of stiffness variation) similar to those tested by the Forest Products Laboratory. Individual trusses were modeled with simple pinned connections throughout. Sheathing was modeled using continuous beam elements on either side of the truss ridge to incorporate the effects of load transfer. Composite effects from the addition of roof sheathing were modeled by adjusting the moment of inertia of the top chords for each truss. The model portrayed similar load sharing behavior as the full-scale assembly tests, showing that approximately 50% of loads applied to a single truss within the assembly were transferred to adjacent trusses. Cramer and Wolfe (1989) recognized that although the model performed well for the nine-truss assemblies that were studied, it would be difficult and time consuming to apply to more complex roof systems.

LaFave and Itani (1992) developed and validated a comprehensive finite element model of a simple gable roof assembly. The finite element model included more realistic semi-rigid spring elements for the metal plate connections, and successfully predicted the load distributions seen in the actual assembly. The model validated that the stiffer gable end trusses attracted load away from adjacent trusses up to two trusses away from the ends. While this model attempted to simulate a more realistic gable roof, however, its applicability to more complex geometries was still questionable.

Mtenga (1991) and Cramer et al. (2000) used computer modeling to derive system (or load sharing) factors for application to roof design. Mtenga (1991) developed a 9-truss, simple gable roof model in a non-linear modeling program called NARSYS.

Composite and load sharing effects were included in the same manner as Cramer and Wolfe (1989), and non-linear, semi-rigid connections were used to incorporate the behavior of plate connections. Mtenga (1991) found that the repetitive system factor of 1.15, recommended by the National Design Specification (AF&PA 2005a), was relatively conservative. A sensitivity study was also performed, demonstrating that sheathing thickness had little effect on the system factors. Changes in configuration or slope of the assembly, on the other hand, could affect the factors dramatically.

Cramer et al. (2000) used a non-linear modeling program called SAWFTR. Unlike the model by Mtenga (1991), Cramer et al. (2000) modeled six different truss assemblies and a joist floor assembly. Composite action was neglected, and only load sharing behavior was explored. Cramer et al. (2000) agreed that the NDS repetitive system factor of 1.15 was conservative for floor assemblies, and some roof trusses, however, the roof truss system factors ranged from 1.06 to 1.24, depending largely on the stiffness and strength of the truss in question, and those of adjacent trusses.

With the development of commercialized software for modeling, researchers including Li (1996), Dung (1999) and Limkatanyoo (2003) began creating models for more practical applications. Li (1996) modeled simple gable style truss assemblies similar to those tested by the Forest Products Laboratory using a commercial program called ETABS. Linear, semi-rigid connections were modeled at the heels of the trusses only, while all other joints were modeled with simple rigid or pinned connections. Composite action was incorporated by adjusting the moment of inertia of the top chords, and sheathing was modeled using the program's beam elements, which were assigned the same thickness and stiffness properties as structural grade plywood. Sheathing was connected to the top chords using rigid connections where sheathing joints were flush, and pinned connections where gaps were present. The model accurately depicted the three-dimensional system behavior of tests performed in the literature, and demonstrated that simplified joint connections could still provide accurate results.

Dung (1999) and Limkatanyoo (2003) took commercial program modeling one step further, by incorporating more complex, realistic geometries. Both studies were performed in SAP2000 and validated against the Forest Products Laboratory full-scale

tests. Dung (1999) modeled an L-shaped hip roof assembly, as well as a T-shaped assembly with two gable end trusses. Individual trusses were simulated with semi-rigid connections at heel and peak joints in accordance with material properties provided by truss-plate manufacturers. All other joints were modeled as either rigid or pinned as in Li (1996). Roof sheathing was also modeled with beam elements having the same thickness, stiffness, and width of actual plywood. Gaps between sheathing elements and composite action were not considered based on sensitivity studies performed by previous researchers. Limkatanyoo (2003) simplified the modeling methods of Dung (1999) even further and validated that the use of rigid connections to represent plate connections produced reasonably accurate results compared to semi-rigid modeling. This more practical approach was used to model and compare assemblies with the same geometries used by Dung (1999) in addition to creating and exploring a complex hip roof system.

Dung (1999) and Limkatanyoo (2003) determined combined stress indices (CSI's) for trusses within the complex assemblies, and compared them to CSI values recommended by truss manufacturers. While most CSI values determined within the assemblies were smaller than recommended values due to system effects; a few trusses surpassed a CSI of 1.0 suggesting potentially unsafe conditions. Such conditions occurred where trusses with more flexible supports (trusses supported by other trusses) transferred significantly large loads to supporting and neighboring trusses. Most surprisingly, Limkatanyoo (2003) noted that compression within bottom chords was observed in some areas of the complex hip roof system. Conventional design assumes that the bottom chords of trusses experience tension forces, and does not consider compression.

Limkatanyoo (2003) highlighted an issue with using beam elements for sheathing, as the behavior was highly dependent on the orientation of the elements. This issue was addressed by Martin (2010), who substituted the beam elements with SAP2000's thick shell element. This substitution was applied to the same pinned and rigid modeling techniques employed by Limkatanyoo (2003) in order to model the gable roof assembly tested by Wolfe and McCarthy (1989). The model showed that the use of the shell element surpassed the beam elements as a representation in sheathing in both practicality

as well as accuracy. The current project uses the same practical modeling techniques as Martin (2010), but applies them to a roof assembly with a more complex geometry, similar to Limkatanyoo (2003).

Rocha et al. (2010) analyzed the reliability of roof sheathing panels under realistic hurricane wind loads using detailed modeling methods. Individual sheets of sheathing were depicted using plate elements, disconnected along the edges to form gaps. Frame elements were used to represent individual sheathing nail connections. When compared to more simplified models, the detailed model showed significant differences concerning the reliability of sheathing panels, suggesting that detailed models should be used for analysis beyond the elastic range of a structure.

Shear Walls

Shear walls serve as one of the main force resisting systems in structures exposed to wind, seismic and other lateral loads. Until recently, analysis and design for these substructures was simple and straight forward. With the growing complexity of geometry and the increasing number and size of openings for doors and windows in residential structures, however, traditional methods of analysis are no longer viable (Doudak 2005).

Testing and Behavior

Doudak (2005) performed full-scale tests on seven different 2.4 m x 2.4 m (8 ft x 8 ft) shear wall configurations, containing various openings and tie-down patterns. The walls were constructed using conventional Canadian construction methods and tested under a combination of gravity and racking loads. Doudak (2005) observed the following behavior during testing:

1. The main modes of deformation were racking and in-plane rigid body rotation.
2. Openings caused significant decreases in both the ultimate capacity and stiffness of the walls. For example, a wall with an opening that was 28% of the total surface area of the wall showed decreases in ultimate capacity and stiffness of 55% and 44%, respectively, when compared to a wall with no openings.

3. The presence of tie-downs effectively decreased the loss of ultimate capacity and stiffness due to openings, and nearly eliminated in-plane rigid body rotation.

Additional full scale shear wall tests were performed by Sinha (2007), Langois (2002) and Lebeda (2002). The 2.4 x 2.4 m (8 x 8 ft) shear walls tested in these studies include unsheathed walls, walls with oriented strand board (OSB) sheathing only, walls with both OSB and gypsum board sheathing, as well as walls containing door or window openings. These tests are useful for validating finite element models, but will not be discussed further in this section.

Patton-Mallory et al. (1984) performed a series of tests on shear walls with aspect ratios ranging from 1 to 3; and sheathed on one or both sides with plywood, gypsum wallboard (GWB) or a combination of the two. Tests of one and two-sided walls showed that the stiffness of a wall sheathed on two sides is equal to the sum of two walls sheathed on one side only. Additionally, Mallory et al. (1984) noted that the stiffness per foot of wall length for a wall with an aspect ratio of 1 could be used to reasonably predict the stiffness of a wall with an aspect ratio of 3.

Finally, Dolan and Johnson (1996) performed full scale tests on 12.2 m (40 ft) long shear walls with various opening configurations. Each shear wall was sheathed with plywood on one side and GWB on the other. Results from Dolan and Johnson were used to validate the methods used in this thesis for modeling two-sided shear walls with wall openings.

Analytical Modeling

When modeling sheathing for shear walls, both in-plane shear and out-of-plane behavior must be considered. Doudak (2005) accomplished this through a complex and detailed finite element model using SAP2000. Studs and lintels were represented by beam-like framing elements. Sheathing was modeled using an orthotropic shell element, which incorporated both in-plane and out-of-plane effects. Finally, individual nail connections were detailed using non-linear spring elements. Although the model proved accurate when validated against full-scale tests, the level of detailing required for the nail connections was overly time consuming.

Alternatively, Kasal and Leichti (1992) developed a simplified finite element approach using an equivalent energy method. Out-of-plane stiffness was modeled with an orthotropic plate element (having zero membrane stiffness), and a diagonally oriented, non-linear spring was used to simulate in-plane shear strength. The equivalent energy model was validated against results in the literature, and proved accurate in predicting shear wall behavior (both with and without openings). Similar modeling techniques were later implemented by Collins et al. (2005a). Finally, Martin (2010) performed a correlation study on in-plane shear with respect to various nail schedules using a 3-term equation for shear walls from the AF&PA Special Design Provisions for Wind and Seismic (2005b). This information was used to determine directional shear modulus values that could be applied to orthotropic shell elements to incorporate the effects of nail spacing in shear walls without meticulous detailing. The algorithm proved accurate in predicting shear wall behavior when validated against full-scale tests performed by Sinha (2007), Langlois (2002) and Lebeda (2002).

Of the previous research, the modeling procedures developed by Martin (2010) prove the most practical for the project at hand. However, Martin (2010) did not model gypsum wall board sheathing on the shear walls. Since the current model contains interior walls with gypsum board as sheathing, a correlation procedure was necessary to determine directional shear modulus values to apply to the gypsum board in addition to the plywood sheathing.

Wind Effects and Engineering

Wind Storms and Structural Damage

According to Holmes (2001), strong winds are created and driven by a variety of forces, the largest of which are atmospheric pressure differences due to differential heating of the earth's surface and ground movement due to the rotation of the earth. Wind storms capable of generating large wind loads can manifest in several different forms and locations across the globe. Among such wind storms are gales created by depressions (areas of low atmospheric pressure), downslope winds in areas near large mountain ranges, and downbursts caused by the cooling effects of thunderstorms. The

strongest wind loads generally come from cyclone-type storms including tornadoes (created by strong thunderstorms known as “supercells”) and tropical cyclones also known as hurricanes or typhoons (Holmes 2001). Strong wind loads from these types of storms are capable of causing extensive damage to structures. In the United States, alone, wind damage accounted for approximately 70 percent of insured losses from 1970 to 1999 (Holmes 2001).

More recent wind storms in the United States, including Hurricane Katrina (2005) and the Joplin and Tuscaloosa Tornadoes (2011), have shown that structural damage from wind is still a prevalent issue, especially for wood-framed residential structures. Van de Lindt et al. (2007) investigated damage to residential structures in non-flooded areas affected by Hurricane Katrina. The main cause of structural damage seen in these areas was a lack of design and construction for uplift load paths at both wall-to-foundation and roof-to-wall connections (van de Lindt et al. 2007). Loss of sheathing on gable-end walls was also noted as an area of concern. Similar issues with uplift load paths and gable-end failure were seen in houses located on the outskirts of the Joplin and Tuscaloosa Tornado paths where lower wind speeds occurred (Prevatt et al. 2012a). Although it is not considered economical to design for tornado wind loads, fragility models developed by Amini (2012) showed that current high-wind design methods could be beneficial during tornadoes with wind speeds up to 177 km/hr (110 mph). Prevatt et al. (2012a) reported that most of the houses with significant structural damage during the 2011 Tuscaloosa, AL and Joplin, MO tornadoes were not constructed to meet current wind codes.

Gable-End Retrofitting

Since the majority of single-family residential structures in the United States were built before updated building codes following Hurricane Andrew in 1992, the development and implementation of retrofitting options for these structures is important. Weaknesses in non-structural gable-end walls have become an area of particular concern. According to Reynolds (2008), three common gable-end failures can occur during high-wind events:

1. Loss of support along the top edge of the gable-end wall due to loss of sheathing.
2. Hinging action at the connection between the triangular gable-end truss and rectangular wall under suction pressures.
3. Collapse of gable-end framing members due to bending stress under positive wind pressures.

In light of these vulnerabilities, the Florida Building Commission adopted a gable-end retrofitting option into the 2010 Florida Building Code as detailed in ICC (2012). The gable-end retrofit (shown in Appendix I of this paper) was tested in full-scale tests performed by Suksawang and Mirmiran (2009) at Florida International University. Based on the tests, it was concluded that the retrofit was capable of increasing gable-end strength to meet current building codes. However, Suksawang and Mirmiran (2009) expressed concern about possible load path alteration and unforeseen torsional effects due to the addition of the general retrofit and variations of the retrofit used for pre-existing obstacles. In light of this concern, the effects of the general gable-end retrofit on load path redistribution in a realistic L-shaped house were explored in the current study.

Design Wind Loads for Buildings with Irregular Plan Geometry

Mensah et al. (2010) discussed the development and validation of a database-assisted design (DAD) methodology for simulating realistic, spatiotemporal wind loads on building components. Prevatt et al. (2012b) used DAD methods to determine uplift loads on a light-frame wood structure tested at 1/3rd scale. Uplift reactions calculated using ASCE (2005) design loads and tributary analysis underestimated reactions under the building loaded with DAD wind loads by up to 50 percent. While DAD methods may be preferable to codified wind pressures, they are still under development and require specific software for implementation. As far as codified pressures are concerned, there are few provisions addressing irregular buildings. ASCE 7-05, for example, contains design provisions for calculating wind pressures on buildings with regular geometry only, and recommends wind tunnel simulation for all other structures (ASCE 2005).

Mehta and Coulbourne (2010), *Wind Loads: Guide to the Wind Load Provisions of 7-05*, provides examples for adapting ASCE 7-05 codified pressures to buildings with

re-entrant corners. Under this methodology, each surface of the structure is designated as windward, leeward, etc., based on wind exposure (regardless of its proximity to the re-entrant corner). Wind pressures for each surface are then calculated using ASCE 7-05 Main Wind Force Resisting System (MWFRS) Method 2. This same methodology was recommended by Fanella (2008). Cook (1985), on the other hand, argued that in the case of wind blowing at a skew angle into a re-entrant corner, a “region of stagnant air” becomes trapped in the corner, increasing the pressure in this area. In order to account for this, Cook (1985) outlined a method of calculating the local area within a re-entrant corner for which higher pressure should be considered. For consistency in the current study, ASCE recommended methods outlined by Mehta and Coulbourne (2010) were selected for calculating ASCE 7-05 MWFRS wind loads as outlined in Appendix K.

APPENDIX B

TWO-DIMENSIONAL TRUSS MODEL VALIDATION

Introduction

Modeling methods for two dimensional trusses were validated against full- scale tests performed by Wolfe et al. (1986). Wolfe et al. (1986) tested forty-two 12.8-meter (28-foot) span Fink trusses spaced 61 cm (24 in) on center in a residential roof. Half of the trusses had a slope of 3:12 and the other half had a slope of 6:12. Truss members were comprised of No. 2 southern pine lumber, divided into three Modulus of Elasticity (MOE) categories: high, medium and low. Each truss was constructed with 38x89 mm (1.5x3.5 in) lumber from one of the MOE categories and labeled with a three-part identification including its slope (3 or 6), MOE category (H, M, or L) and a sequence number (1-7). From the original 42 trusses, four 6:12 sloped trusses from each MOE category and four 3:12 sloped trusses from each MOE category were selected for individual truss tests. The remaining trusses were tested by Wolfe and McCarthy (1989) in three dimensional roof assemblies.

The individual trusses were loaded in a horizontal position with 3.5-inch supports located at either end of the truss. The 3:12 trusses were tested with a live load of 0.84 kPa (17.5 psf), the 6:12 trusses were tested with a live load of 1.10 kPa (23 psf), and both were tested with a dead load of 0.48 kPa (10 psf). All loads were applied along the top chords of the trusses. Deflections were measured at the ridge and at the ends of each web, and averaged to determine the total deflection of each truss.

Modeling Methods

The chords and webs of each truss were modeled using SAP2000's frame elements. The geometry for the trusses was determined using the centerlines of the top and bottom chords as shown in Figures B-1 and B-2.

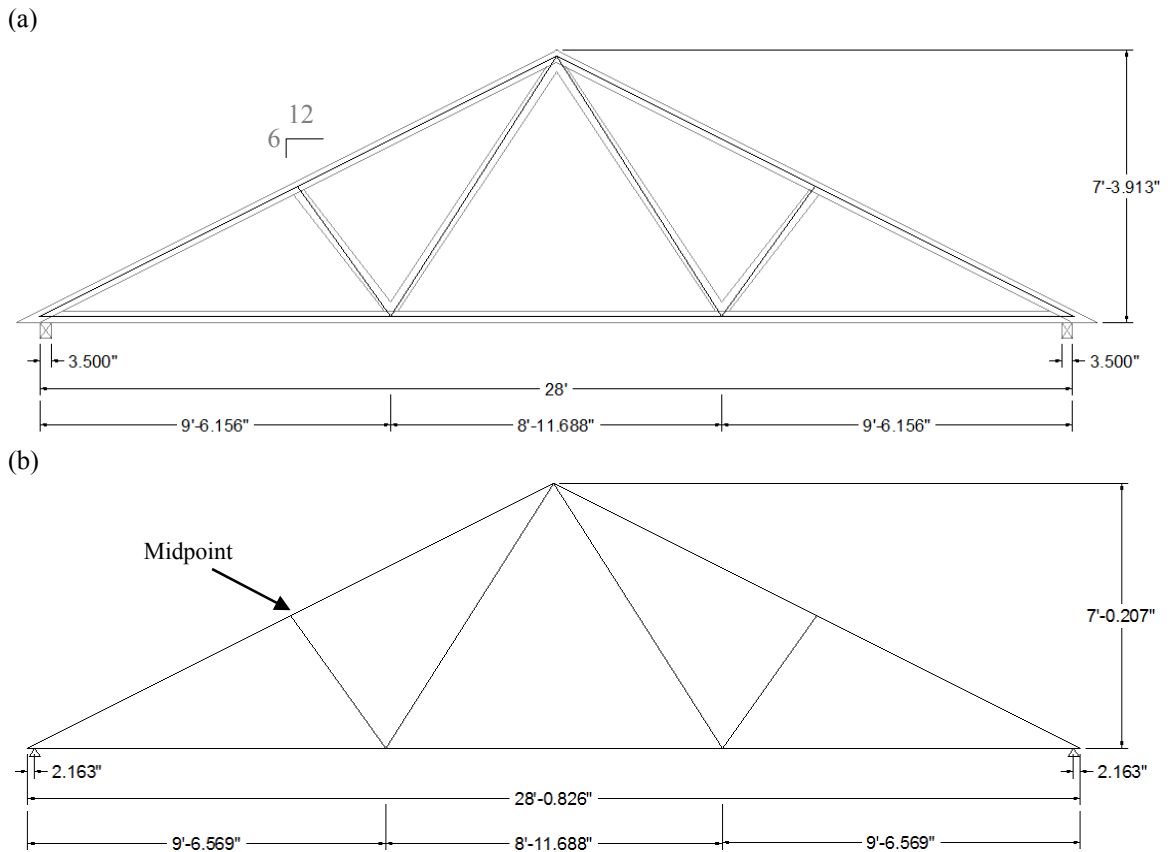


Figure B-1: 6:12 Truss Geometry – (a) Actual truss from Wolfe and LaBissoniere (1991) and (b) centerline model used in SAP2000.

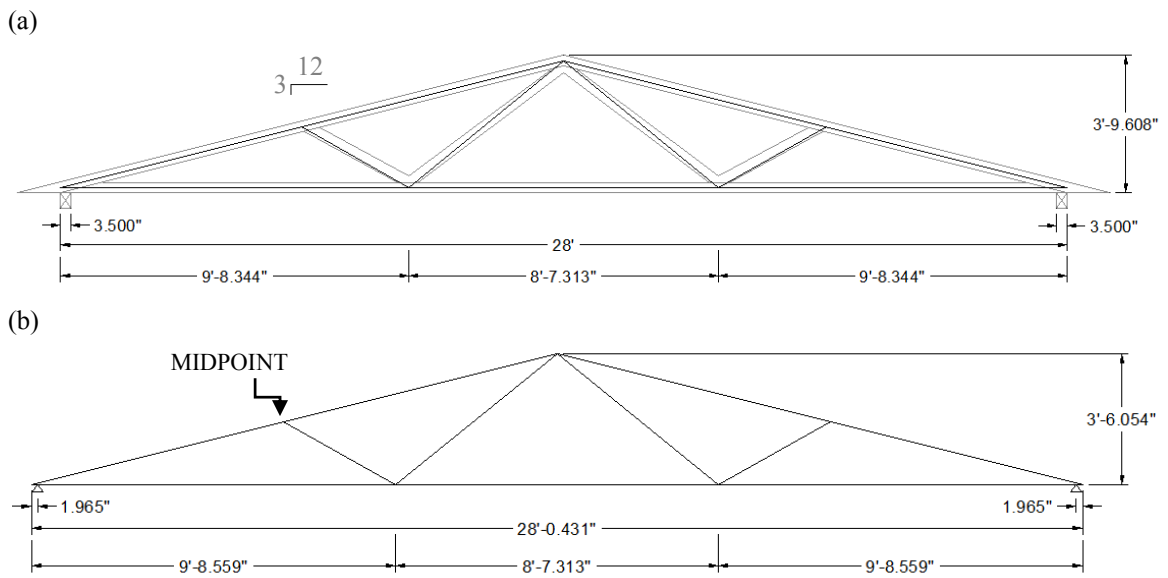


Figure B-2: 3:12 Truss Geometry – (a) Actual truss from Wolfe and LaBissoniere (1991) and (b) centerline model used in SAP2000

Each framing member was assigned a cross section equal to the actual cross section of the lumber used by Wolfe et al. (1986). The connections between members were idealized as either pinned or rigid based on previous studies conducted by Li (1996) and Martin (2010). Pinned connections were used at the ridge and the ends of each web, while rigid connections were used at the truss heels. The splice in the bottom chord of the truss was modeled both as a pinned connection and as a rigid connection, and proved to have negligible effect on the stiffness of the truss model. Figure B-3 shows the connectivity used in the truss models as well as the joint and member labels. Martin (2010) created a similar pinned and rigid model, which closely followed the geometry used by Li (1996) (K. Martin, personal communication, July 27, 2010).

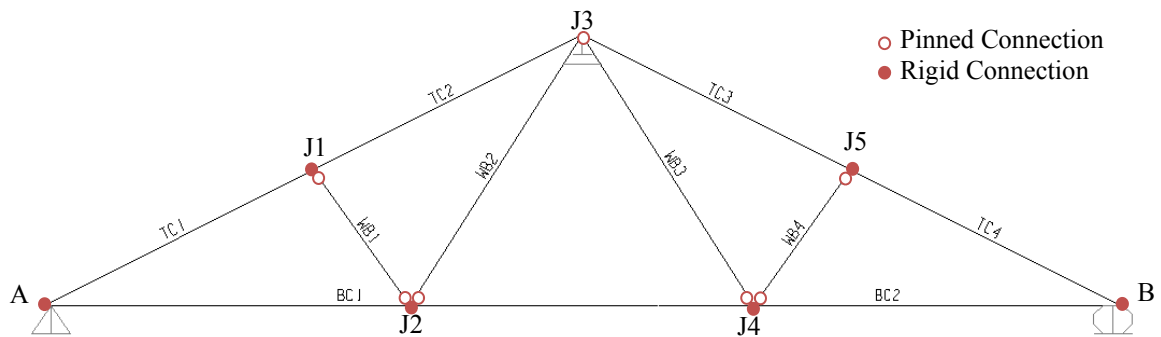


Figure B-3: Connectivity and Element Labels for 2D Truss Model –J3 was restrained in the R2 direction (in-plane rotation) to prevent instability warnings.

Three sets of material properties for the framing members were explored in this study. First, the 6:12 trusses were modeled using the exact MOEs listed by Wolfe et al. (1986) for each individual member. This allowed for the most accurate comparison between the tested trusses and the modeled trusses. A list of MOEs is included in Table B-1. To simplify the model for practical use in the three-dimensional roof assemblies modeled in Appendix C, the 6:12 and 3:12 trusses were then modeled using average MOEs for each stiffness category applied uniformly to every member of the truss. Averaged MOEs for each category and truss slope are listed in Table B-2.

Table B-1: Modulus of Elasticity Assignments – MOEs per Wolfe et al. (1986).

MOE (MPa)										
Truss	TC1	TC2	TC3	TC4	BC1	BC2	WB1	WB2	WB3	WB4
6L2	7102	8550	9515	9032	8481	8825	7860	9239	6895	8067
6L3	8136	8067	9515	7998	9032	6757	8067	8618	9377	9239
6L5	9032	8687	8825	8550	7653	9446	7033	9653	7308	9239
6L7	7515	8067	8205	8963	9446	9515	9239	8963	7239	9653
6M1	13514	12893	12342	13376	13583	11790	11445	10342	11721	9997
6M2	13238	12342	12893	13031	11997	9722	11101	11445	12893	11170
6M4	12893	11307	9860	13307	13652	11238	13307	11101	10963	11583
6M7	13445	9860	11307	13514	10618	11101	10342	11032	9997	10963
6H1	14755	16341	16341	16410	16616	16892	15513	15513	16272	16272
6H2	14410	15031	15031	17375	15927	15237	16961	16272	17788	16272
6H6	15720	16203	15100	15789	14272	13927	15031	13996	16478	17237
6H7	15996	16203	15100	14479	14272	15168	15031	14203	16823	17237

MOE (ksi)										
Truss	TC1	TC2	TC3	TC4	BC1	BC2	WB1	WB2	WB3	WB4
6L2	1030	1240	1380	1310	1230	1280	1140	1340	1000	1170
6L3	1180	1170	1380	1160	1310	980	1170	1250	1360	1340
6L5	1310	1260	1280	1240	1110	1370	1020	1400	1060	1340
6L7	1090	1170	1190	1300	1370	1380	1340	1300	1050	1400
6M1	1960	1870	1790	1940	1970	1710	1660	1500	1700	1450
6M2	1920	1790	1870	1890	1740	1410	1610	1660	1870	1620
6M4	1870	1640	1430	1930	1980	1630	1930	1610	1590	1680
6M7	1950	1430	1640	1960	1540	1610	1500	1600	1450	1590
6H1	2140	2370	2370	2380	2410	2450	2250	2250	2360	2360
6H2	2090	2180	2180	2520	2310	2210	2460	2360	2580	2360
6H6	2280	2350	2190	2290	2070	2020	2180	2030	2390	2500
6H7	2320	2350	2190	2100	2070	2200	2180	2060	2440	2500

Table B-2: Average MOEs Used for Individual 6:12 Trusses

Slope	Average MOE MPa (ksi)		
	Low	Medium	High
6:12	8515 (1235)	11804 (1712)	15741 (2283)
3:12	8446 (1225)	12080 (1725)	15451 (2241)

Finally, the trusses were assigned a uniform design MOE determined from the 2005 edition of the NDS National Design Specification for Wood Construction. Based on Table 4B from AF&PA (2005a), an MOE value of 11030 MPa (1600 ksi) was chosen for No. 2 grade Southern Pine lumber. No adjustment factors were used since the members were assumed to be of normal moisture content, with no incisions and tested at normal temperatures. This MOE value was applied to both the 3:12 and 6:12 trusses and compared to the overall average deflection of trusses listed in the deflection tables of Wolfe et al. (1986) regardless of MOE category.

The truss models were loaded with the same truss loads used by Wolfe et al. (1986): 0.96 kN/m (66 lb/ft) applied along the top chords of the 6:12 trusses and 0.80 kN/m (55 lb/ft) applied along the top chord of the 3:12 truss. The deflections from joints J1 through J3 were then averaged and compared to the deflections reported by Wolfe et al. (1986).

Results and Discussion

The resulting deflections for each truss model with exact MOE's and averaged MOE's are included in Tables B-3 through B-5. For both the exact MOEs and the averaged MOEs, the models were able to predict the average deflection of the trusses in each stiffness category within 10% of the actual deflections listed by Wolfe et al. 1986. Martin (2010) managed to reduce this discrepancy to less than 5 percent, mainly due to differences in the geometry used to simulate the trusses. As stated before, Martin (2010) used a truss model that was similar to the geometry used by Li (1996), which was 20.3 mm (0.8 in) taller and 88.2 mm (3.47 in) wider than the current model, with the same clear-span.

The models that were assigned a design MOE from AF&PA (2005a) predicted the overall average deflection for both the 3:12 sloped trusses and the 6:12 sloped trusses within 5% of the deflections reported by Wolfe et al. (1986). Table B-6 shows results for the trusses modeled with AF&PA (2005a) properties. In all cases, the truss models were stiffer than the actual tested trusses. This is likely due to the use of a rigid connection at the heels of the truss as opposed to a more realistic semi-rigid connection.

Table B-3: Comparison of Experimental and Model Displacements – Percent differences
between computer models and the experimental data of Wolfe et al. (1986).

Truss	Wolfe et al. (1986)	Current Study		Martin (2010)	
	Deflection mm (in)	Deflection mm (in)	% Diff. from Wolfe et al. (1986)	Deflection mm (in)	% Diff. from Wolfe et al. (1986)
6L2	4.369 (0.172)	4.318 (0.170)	-1%	4.547 (0.179)	4%
6L3	4.572 (0.180)	4.496 (0.177)	-2%	4.724 (0.186)	3%
6L5	4.927 (0.194)	4.267 (0.168)	-14%	4.470 (0.176)	-9%
6L7	5.029 (0.198)	4.242 (0.167)	-16%	4.445 (0.175)	-12%
Average	4.724 (0.186)	4.318 (0.170)	-8%	4.547 (0.179)	-4%
6M1	3.124 (0.123)	2.870 (0.113)	-8%	2.997 (0.118)	-4%
6M2	3.454 (0.136)	3.099 (0.122)	-11%	3.226 (0.127)	-7%
6M4	3.073 (0.121)	3.048 (0.120)	-1%	3.200 (0.126)	4%
6M7	2.972 (0.117)	3.200 (0.126)	8%	3.353 (0.132)	13%
Average	3.150 (0.124)	3.048 (0.120)	-3%	3.200 (0.126)	1%
6H1	2.718 (0.107)	2.260 (0.089)	-17%	2.388 (0.094)	-12%
6H2	2.718 (0.107)	2.362 (0.093)	-13%	2.464 (0.097)	-9%
6H6	2.184 (0.086)	2.438 (0.096)	12%	2.565 (0.101)	17%
6H7	2.718 (0.107)	2.413 (0.095)	-11%	2.591 (0.102)	-5%
Average	2.591 (0.102)	2.362 (0.093)	-8%	2.515 (0.099)	-3%

Table B-4: Comparison of Average Displacements for Simplified 6:12 Trusses using Average MOE Values

Truss	Wolfe et al. (1986)	Current Study with Averaged MOEs	
	Average Disp. mm (in)	Average Disp. mm (in)	% Diff. from Wolfe et al. (1986)
Average L	4.724 (0.186)	4.293 (0.169)	-9%
Average M	3.150 (0.124)	3.100 (0.122)	-2%
Average H	2.591 (0.102)	2.311 (0.091)	-10%

Table B-5: Comparison of Average Displacements for 3:12 Trusses using Average MOE Values - *Note that the deflection tables found in Wolfe et al. (1986) are inconsistent. The average deflections in the 6:12 tables were calculated using the $deflection = A \times (design\ load\ ratio) + B$ equation found at the top of the table, whereas the average deflections for the 3:12 tables were calculated from Column A only. This inconsistency has been corrected in Table A-9 so that the 3:12 averages also incorporate the straight line deflection equation.

Truss	Wolfe et al. (1986)	Current Study with Averaged MOEs	
	Average Disp. mm (in)	Average Disp. mm (in)	% Diff. from Wolfe et al. (1986)
Average L	11.66 (0.459)	11.30 (0.445)	-3%
Average M	8.204 (0.323)	8.026 (0.316)	-2%
Average H	6.833 (0.269)	6.172 (0.243)	-9%

Table B-6: Comparison of Average Displacements for trusses with AF&PA (2005a) design MOE

Truss	Wolfe et al. (1986)	Current Study with AF&PA (2005a) Design MOE	
	Total Average Disp. mm (in)	Average Disp. mm (in)	% Diff. from Wolfe et al. (1986)
3:12 Slope	8.890 (0.350)	8.636 (0.340)	-3%
6:12 Slope	3.480 (0.137)	3.327 (0.131)	-5%

Conclusions

The simplified, linear modeling techniques described in this appendix are sufficient for predicting the behavior of two-dimensional trusses with various pitches and stiffness. Based on the results described above, the following methods were adopted for use in the current study:

- Pinned connections were used at the ends of each web member and at the ridge of the truss. Rigid connections were used along top chords, bottom chords and at truss heels. Figure B-3 shows the connectivity used in the truss models.
- Truss chords and web members were modeled using the SAP2000 frame element with an assigned cross section equal to the actual cross section of the member.

- Material properties for the framing members were assumed to be linear and isotropic. The modulus of elasticity for each member was determined using design properties listed in AF&PA (2005a).

For the three-dimensional truss assembly validation described in Appendix C, the average MOE from Wolfe et al. (1986) for each stiffness category was used in lieu of AF&PA (2005a) design properties so the effects of varying truss stiffness within the assembly could be explored.

APPENDIX C

THREE DIMENSIONAL ROOF ASSEMBLY MODEL VALIDATION

Introduction

Methods for modeling roof assemblies were validated against full-scale tests performed by Wolfe and McCarthy (1989) on two nine-truss gable roof assemblies. One assembly had a 3:12 roof pitch and the other had a 6:12 roof pitch. The trusses, constructed by Wolfe et al. (1986), were spaced 0.61 m (2 ft) on center. As in Wolfe et al. (1986), the trusses were grouped into high (H), medium (M), and low (L) Modulus of Elasticity (MOE) categories based on the individual MOE's of the 2x4 members used to construct the trusses. Within the assemblies, trusses were arranged into a pattern of: M-H-L-M-H-L-L-M-H moving from West to East based on MOE category as shown in Figure C-1.

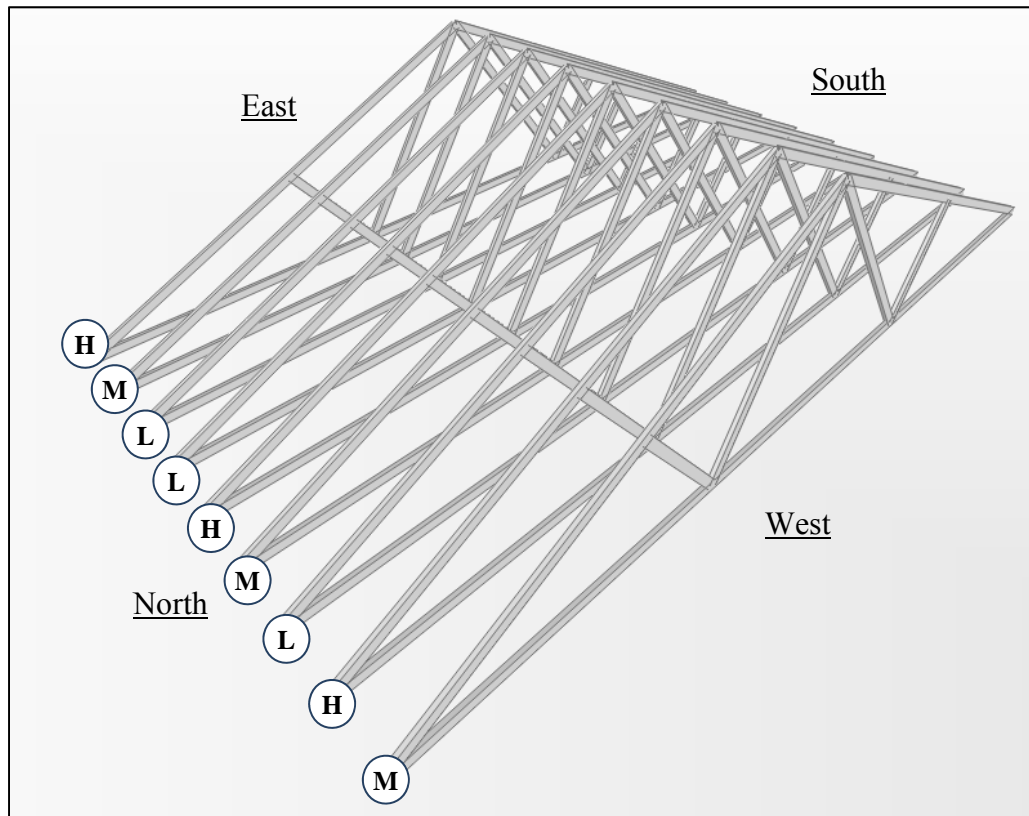


Figure C-1: Pattern of Truss Stiffness in Assemblies – Low MOE (L), Medium MOE (M) and High MOE (H) as used by Wolfe and McCarthy (1989)

The sheathing used in the assembly was 11.9-mm-thick (15/32-in-thick) Southern Pine 3-ply plywood. The average bending stiffness (EI) of the plywood was measured by Wolfe and McCarthy (1989) using a plate bending test and found to be $1.19 \text{ N}\cdot\text{m}^2/\text{m}$ ($196,000 \text{ lb}\cdot\text{in}^2/\text{ft}$). The assembly was supported along the north and south sides by 0.9-m-tall (3-ft-tall) wood framed walls with a clear span of 8.4 m (27 ft, 5 in).

Modeling Methods

Individual Trusses

The trusses in the current study were modeled as described in Appendix B, using only pinned and rigid connections. The MOE for each of the stiffness categories was determined by averaging the individual MOE's of the 2x4's used to construct each of the trusses as shown in Tables C-1 and C-2. The self-weight of the material was not included in the model.

Table C-1: Average MOE's used for Trusses* in 3:12 Truss Assembly

Average MOE MPa (ksi)		
Low: *3L2, 3L4, 3L6	Medium: *3M2, 3M4, 3M6	High: *3H1, 3H3, 3H5
8667 (1257)	11004 (1596)	16443 (2383)

Table C-2: Average MOE's used for Trusses* in 6:12 Truss Assembly

Average MOE MPa (ksi)		
Low: *6L1, 6L4, 6L6	Medium: *6M3, 6M5, 6M6	High: *6H3, 6H4, 6H5
8450 (1226)	12080 (1752)	16171 (2345)

Plywood Sheathing

The sheathing was represented using a continuous, orthotropic “Layered Shell Element” from SAP2000, with a thickness of 11.9 mm (0.469 in) and local coordinates oriented as shown in Figure C-2. The sheathing layer was displaced 50.4 mm (1.98 in) from the centerline of the top chord framing members towards the top surface of the assembly. This was done so that the plywood is modeled at its true physical location rather than through the centerlines of the top chords.

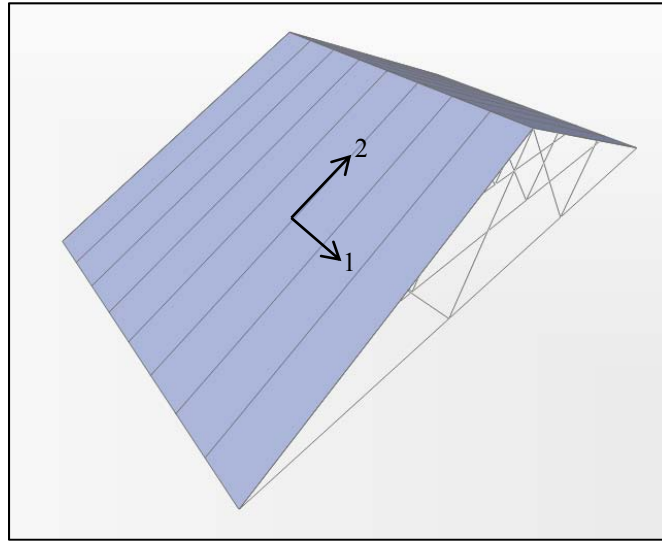


Figure C-2: Local Coordinate Orientation of Thick Shell Elements for Sheathing –
with strong axis (1) running perpendicular to the truss supports

Material properties for the plywood sheathing were calculated using experimentally determined values provided by Wolfe and McCarthy (1989), as well as design specifications and publically available software. A moment of inertia (I) of $1.41 \times 10^{-7} \text{ m}^4/\text{m}$ ($0.103 \text{ in}^4/\text{ft}$) was determined using the 2008 APA Panel Design Specification for 32/15-in-thick, 3-ply plywood from Species Group 1. The MOE along the strong axis (“ E_1 ” as designated by SAP2000) was then determined by dividing the measured EI from Wolfe and McCarthy (1989) by the moment of inertia suggested by APA (2008) to give an MOE of 13,120 MPa (1,903 ksi).

Martin (2010), found the most sensitive material properties for the sheathing to be the MOE along the strong and weak axes (E_1 and E_2 in SAP2000), the in-plane shear modulus (G_{12} in SAP2000), and the Poisson’s Ratio related to E_2 (ν_{12}). It is important to note that the subscript notation for Poisson’s Ratio in SAP2000 is the inverse of conventional notation, where ν_{ij} is typically related to E_i as illustrated in Figure C-3.

$$\begin{bmatrix} \gamma_1 \\ \gamma_2 \\ \gamma_3 \\ \gamma_{23} \\ \gamma_{13} \\ \gamma_{12} \end{bmatrix} = \begin{bmatrix} \frac{1}{E_1} & -\frac{\nu_{21}}{E_2} & -\frac{\nu_{31}}{E_3} & 0 & 0 & 0 \\ -\frac{\nu_{12}}{E_1} & \frac{1}{E_2} & -\frac{\nu_{32}}{E_3} & 0 & 0 & 0 \\ -\frac{\nu_{13}}{E_1} & -\frac{\nu_{23}}{E_2} & \frac{1}{E_3} & 0 & 0 & 0 \\ 0 & 0 & 0 & \frac{1}{G_{23}} & 0 & 0 \\ 0 & 0 & 0 & 0 & \frac{1}{G_{13}} & 0 \\ 0 & 0 & 0 & 0 & 0 & \frac{1}{G_{12}} \end{bmatrix} \begin{bmatrix} \sigma_1 \\ \sigma_2 \\ \sigma_3 \\ \sigma_{23} \\ \sigma_{13} \\ \sigma_{12} \end{bmatrix}$$

$$\begin{bmatrix} \epsilon_{11} \\ \epsilon_{22} \\ \epsilon_{33} \\ \gamma_{12} \\ \gamma_{13} \\ \gamma_{23} \end{bmatrix} = \begin{bmatrix} \frac{1}{e1} & -\frac{u12}{e2} & -\frac{u13}{e3} & 0 & 0 & 0 \\ \frac{1}{e2} & \frac{e3}{-u23} & \frac{1}{e3} & 0 & 0 & 0 \\ \frac{1}{e3} & \frac{1}{e3} & 0 & 0 & 0 & 0 \\ 0 & 0 & 0 & \frac{1}{g12} & 0 & 0 \\ 0 & 0 & 0 & 0 & \frac{1}{g13} & 0 \\ 0 & 0 & 0 & 0 & 0 & \frac{1}{g23} \end{bmatrix} \begin{bmatrix} \sigma_{11} \\ \sigma_{22} \\ \sigma_{33} \\ \sigma_{12} \\ \sigma_{13} \\ \sigma_{23} \end{bmatrix}$$

sym.

Figure C-3: Hooke's Law for Orthotropic Materials – (left) conventional notation from Bodig and Jayne (1982) and (right) SAP2000 notation (CSI Technical Support, personal communication, July 29, 2011).

Since the bending stiffness along the strong axis was the only property provided in the literature, the remainder of the material properties were found using OSULaminates, a publically available software package developed by Dr. John Nairn at Oregon State University (Nairn 2007). Using the software, a 3-ply panel was created with 3.97-mm-thick (0.1563-in-thick) wood-plyes from Species Group 1, alternating 90-degree grain orientations and the strong and weak axes oriented along x and y, respectively. The engineering properties in flexure were used since the roof sheathing is loaded out-of-plane. Table C-3 lists the engineering properties generated by OSULaminates. To better represent the actual material properties of the plywood used in the full-scale tests; E_x , E_y and G_{xy} generated from OSU Laminates were scaled (by a factor of 1.31) equating E_x to the experimental MOE from Wolfe and McCarthy (1989). The remaining orthotropic parameters were found to have a negligible effect on the behavior of the model and were chosen somewhat arbitrarily (Martin 2010).

Table C-3: Engineering Properties in Bending for 3-Ply Panel Generated by OSU Laminates and scaled to Wolfe and McCarthy (1989) – Scaled properties are used in the model

Orthotropic Properties		Generated from OSU Laminates	Scaled to Wolfe and McCarthy (1989)
E_x (E_1 in SAP2000)	MPa (ksi)	9991 (1449)	13120 (1903)
E_y (E_2 in SAP2000)		669 (97)	878 (127)
G_{xy} (G_{12} in SAP2000)		483 (70)	634 (92)
ν_{yx} (ν_{12} in SAP2000)		0.011	0.011

Meshing and Boundary Conditions

As in Martin (2010), the roof sheathing was meshed into elements with a maximum size of 610 mm (24 in) so that the sheathing elements would align with the framing elements of the trusses. This was accomplished using the Automatic Mesh tool in SAP2000.

With respect to boundary conditions, it was reported that the “supports within the assembly behaved as something between [pinned] and roller” (Wolfe and McCarthy 1989). The current study used the “roller-roller” conditions shown in Figure C-4, with horizontal restraint provided at the line of symmetry at the peak. Lateral displacements were measured in the U1 direction at the roller supports of the model during loading and were found to be less than 0.87 mm (0.034 in), which is consistent with the maximum displacement of 0.89 mm (0.035 in) reported by Wolfe and McCarthy (1989).

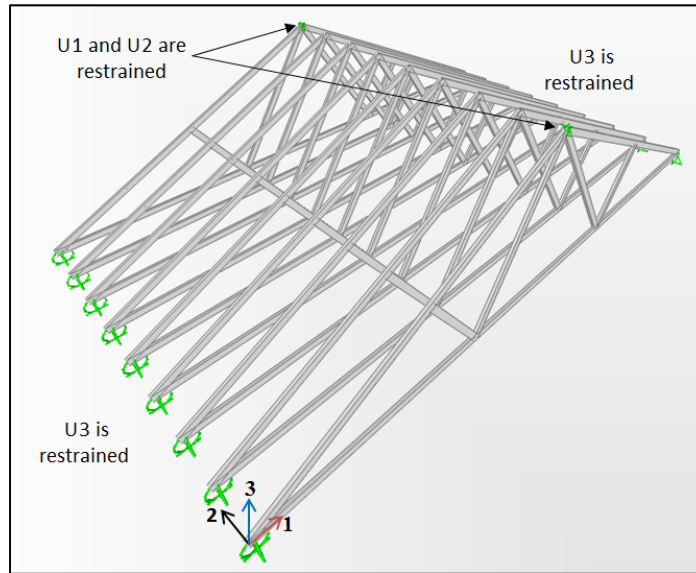


Figure C-4: “Roller-Roller” Support Conditions – for each truss the heel supports are restrained in the U3 (vertical) direction only. The ridge at each end of the assembly is also restrained in the U1 and U2 (lateral) directions to prevent instability warnings.

Loading and Data Collection

Following procedures outlined in Wolfe and McCarthy (1989), the trusses in both the 3:12- and 6:12-sloped assemblies were loaded one at a time. The trusses in the 3:12 assembly were loaded with 803 N/m (55 lb/ft) uniformly distributed along the top chord, and the trusses in the 6:12 assembly were loaded with 963 N/m (66 lb/ft). For each loaded truss, the relative vertical deflections and support reactions of every truss in the assembly were measured and plotted against the results reported in the literature.

Relative vertical reactions (R_{rel}) were determined as the ratio of the total vertical support reaction at each individual truss to the total load applied to the assembly as shown in Equation C-1. For the 3:12 assembly, the total load for a distributed load of 803 N/m (55 lb/ft) along the top chord of a truss was found to be 7068 N (1589 lb). For the 6:12 assembly, the total load for a distributed load of 963 N/m (66 lb/ft) along the top chord of a truss was found to be 9212 N (2071 lb).

$$R_{rel,j} = \frac{R_j}{\sum_{i=1}^9 R_i} \times 100\% \quad \text{For } j = 1 \text{ to } 9 \quad \text{Equation C-1}$$

Note that in Equation C-1, i and j refer to individual trusses within the assembly, where truss 1 is located on the West side of the assembly, and truss 9 is located on the

East side of the assembly. This notation was used for all tables and charts related to the roof assembly validation.

Deflections were measured at four locations on each truss, as shown in Figure C-5, and averaged to determine the average deflection (Δ_{avg}) at each truss. The average deflections of all trusses were then summed to give the total average deflection of the assembly. In accordance with Wolfe and McCarthy (1989), the percent contribution of an individual truss to the total average deflection of the assembly was defined as the “relative deflection” of that truss. The relative deflections (Δ_{rel}) were calculated as shown in Equation C-2.

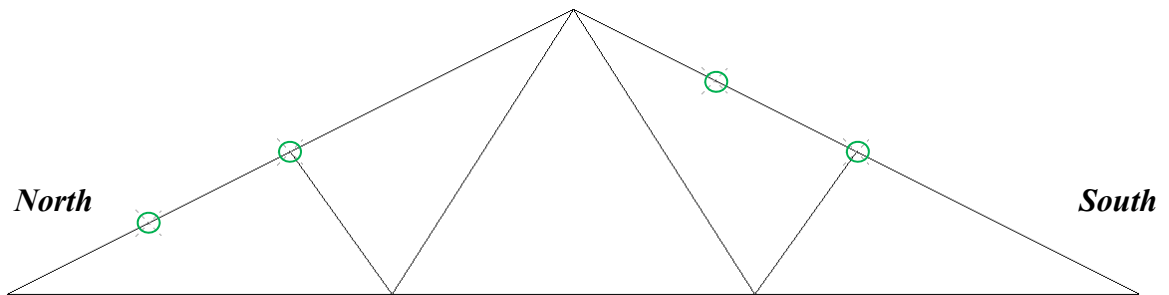


Figure C-5: Locations for Deflection Measurement on Each Truss – The average deflection (Δ_{avg}) at each truss was calculated as the average of the deflections measured at each of the four locations shown.

$$\Delta_{rel,j} = \frac{\Delta_{avg,j}}{\sum_{i=1}^9 \Delta_{avg,i}} \times 100\% \quad \text{For } j = 1 \text{ to } 9 \quad \text{Equation C-2}$$

Results and Discussion

Relative deflections and reactions for the 3:12 and 6:12 assembly models were plotted against results from Wolfe and McCarthy (1989) and organized into influence matrices as shown in Appendix D. The percent error in relative deflections and reactions at the loaded trusses were calculated based on the full-scale tests. At the loaded trusses, relative reactions were predicted with an average error of 9 percent from the full-scale tests in the 3:12 assembly and 17 percent in the 6:12 assembly as shown in Table C-4. Relatively high errors were seen at trusses 2, 5, 6 and 8 in the 6:12 assembly, however, there is not enough information to determine why errors were high at these trusses. Both models accurately predicted the overall load distributions to non-loaded trusses as shown in Figures D-1 through D-18 in Appendix D.

Table C-4: Absolute Error in Predicted Relative Reactions at Loaded Trusses in Each Assembly – Compared to Wolfe and McCarthy (1989)

Loaded Truss #	Percent Error	
	3:12 Assembly	6:12 Assembly
1	3%	7%
2	18%	32%
3	20%	11%
4	1%	11%
5	7%	26%
6	13%	25%
7	11%	7%
8	3%	27%
9	9%	7%
Average	9%	17%

Although the main focus of this study is force distribution through the structure, the relative deflections were also checked to provide additional validation as shown in Table C-5.

Table C-5: Absolute Error in Predicted Relative Deflections at Loaded Trusses in Each Assembly – Compared to Wolfe and McCarthy (1989)

Loaded Truss #	Percent Error	
	3:12 Assembly	6:12 Assembly
1	10%	9%
2	24%	15%
3	38%	0%
4	45%	14%
5	16%	8%
6	30%	9%
7	21%	4%
8	10%	11%
9	21%	0%
Average	24%	8%

At the loaded trusses, the 3:12 model predicted relative deflections with an average error of 24 percent compared to Wolfe and McCarthy (1989). The 6:12 assembly more accurately predicted relative deflections with an average error of only 8 percent. It was observed that the 3:12 model was more accurate in predicting force

distributions than deflections while the 6:12 assembly was more accurate in predicting deflections than force distributions. The reason for this discrepancy is unknown. Overall distributions of relative deflections for each loading scenario were plotted in Figures D-19 through D-36.

Conclusions

The two nine-truss gable roof assemblies with varying slope and individual truss stiffness were adequate in predicting assembly behavior. Based on the results in this appendix, the following modeling methods were adopted for use in the current study:

- Roof sheathing was modeled using a continuous “layered shell element” from SAP2000.
- The plywood layer was displaced from the centerline of the truss top chord so that the bottom surface of the plywood was even with the top surface of the truss top-chord cross section.
- Material properties for the plywood sheathing were assumed to be orthotropic and were determined using flexural engineering properties calculated by OSU Laminates Software.

APPENDIX D

PLOTS FOR ROOF ASSEMBLY MODEL VALIDATION

This appendix contains influence matrices and plots for the 3:12 and 6:12 assemblies that were modeled in Appendix C.

3:12 Assembly – Relative Reactions

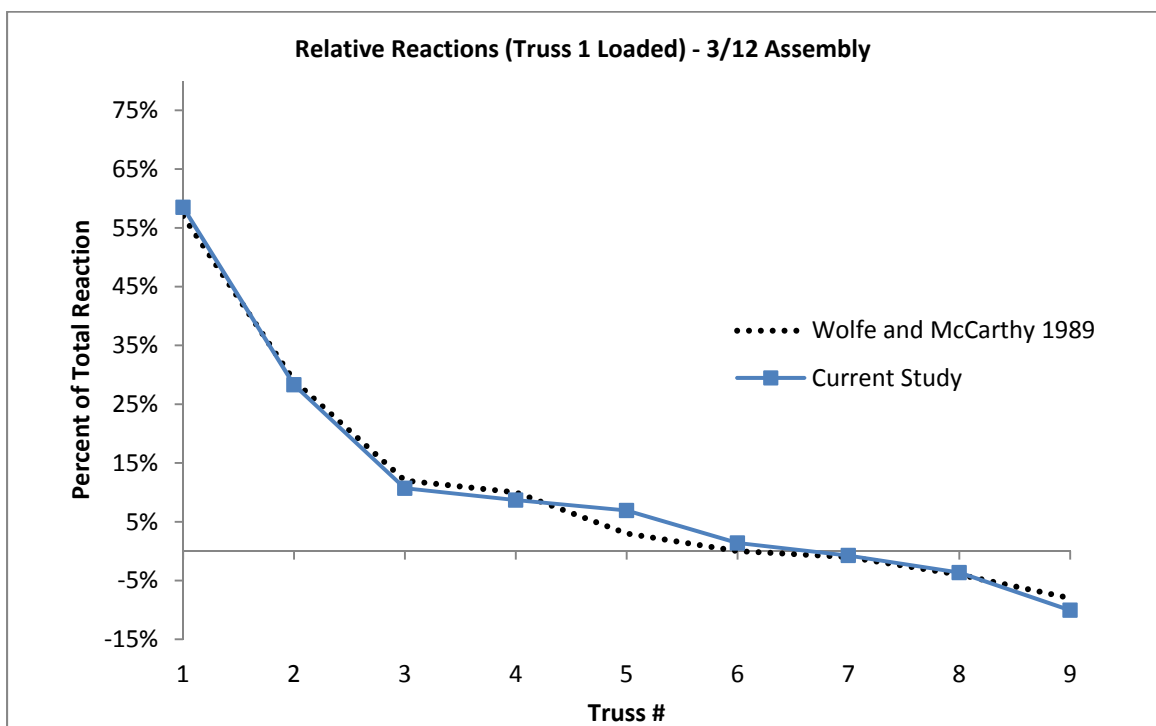


Figure D-1: Relative Reactions for 3:12 Truss Assembly When Truss 1 is Loaded

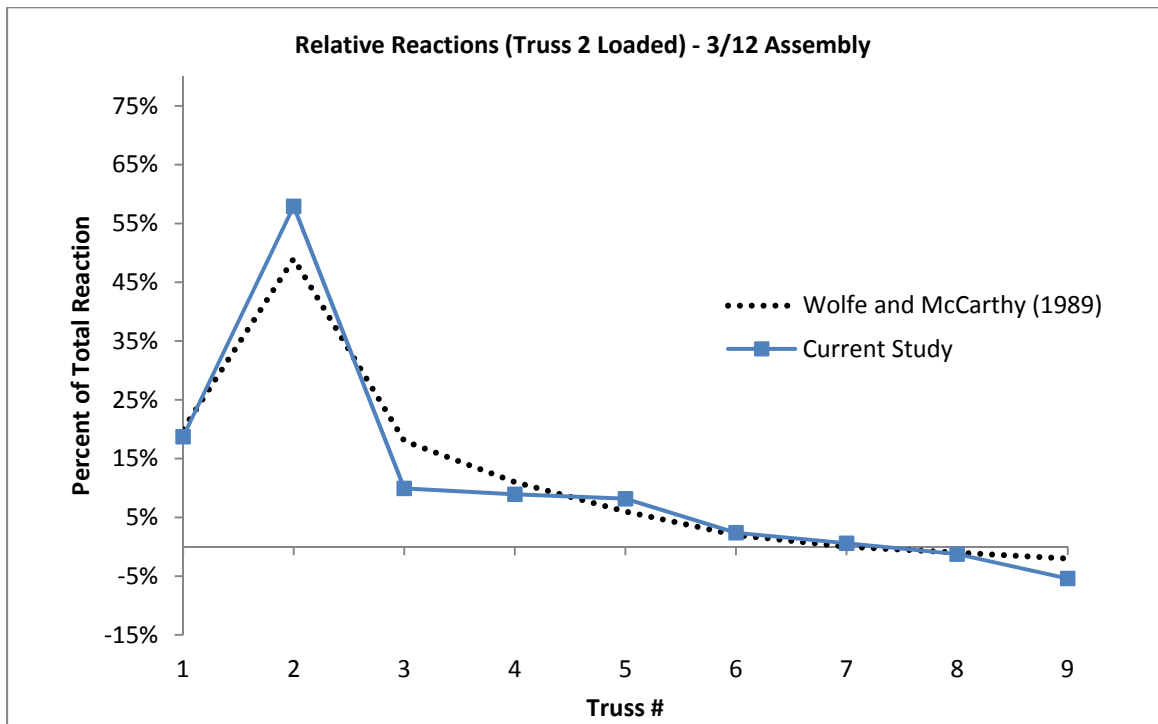


Figure D-2: Relative Reactions for 3:12 Truss Assembly When Truss 2 is Loaded

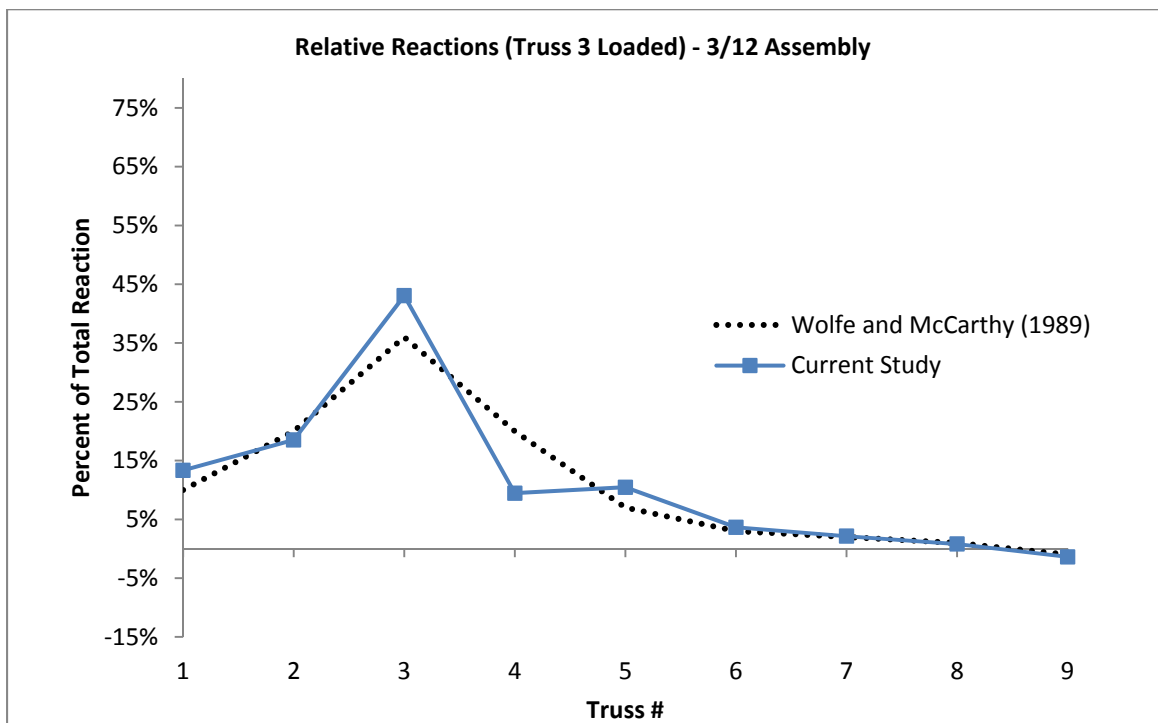


Figure D-3: Relative Reactions for 3:12 Truss Assembly When Truss 3 is Loaded

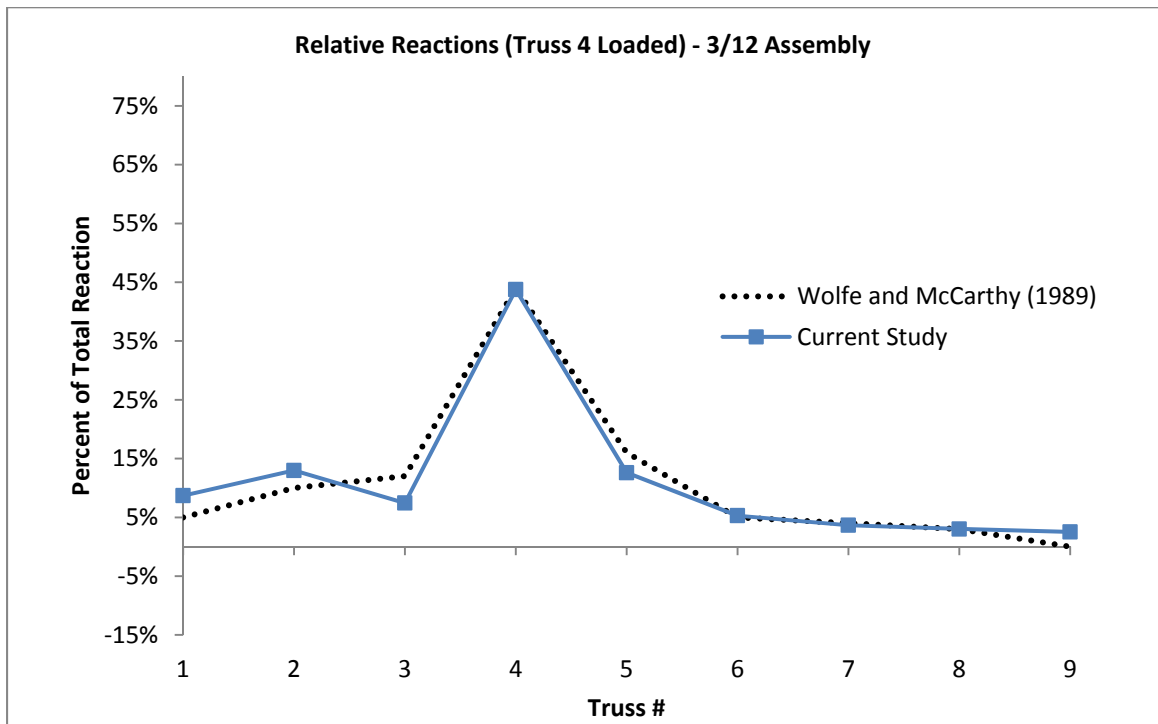


Figure D-4: Relative Reactions for 3:12 Truss Assembly When Truss 4 is Loaded

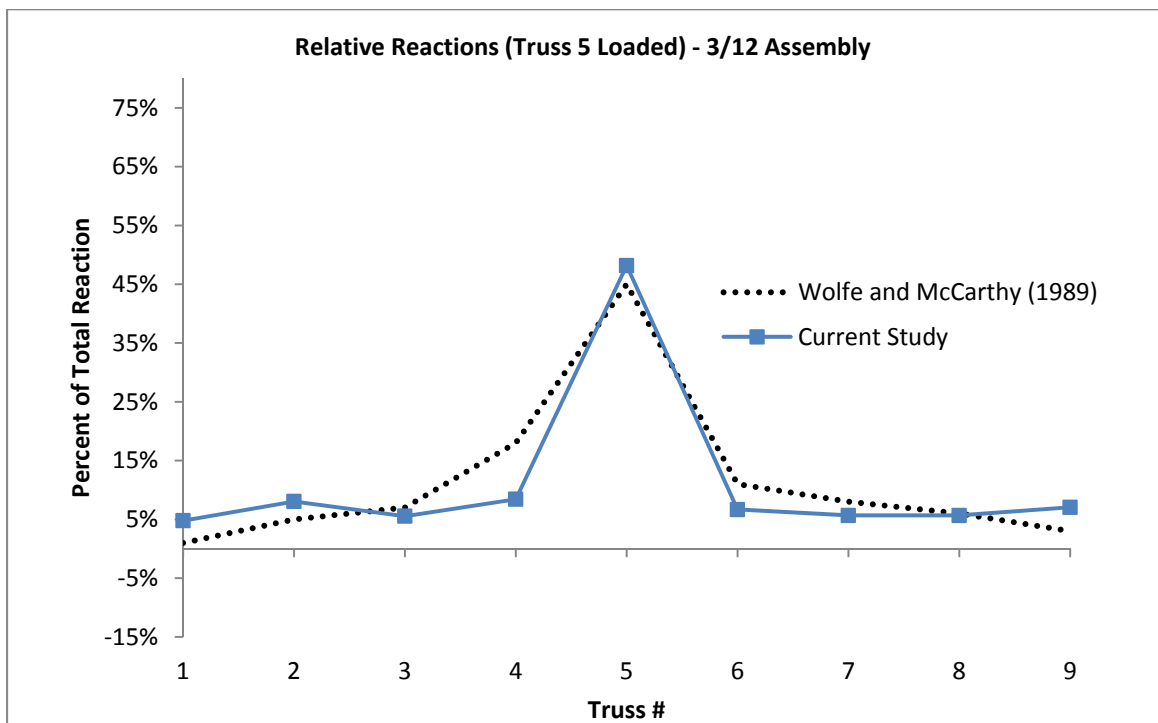


Figure D-5: Relative Reactions for 3:12 Truss Assembly When Truss 5 is Loaded

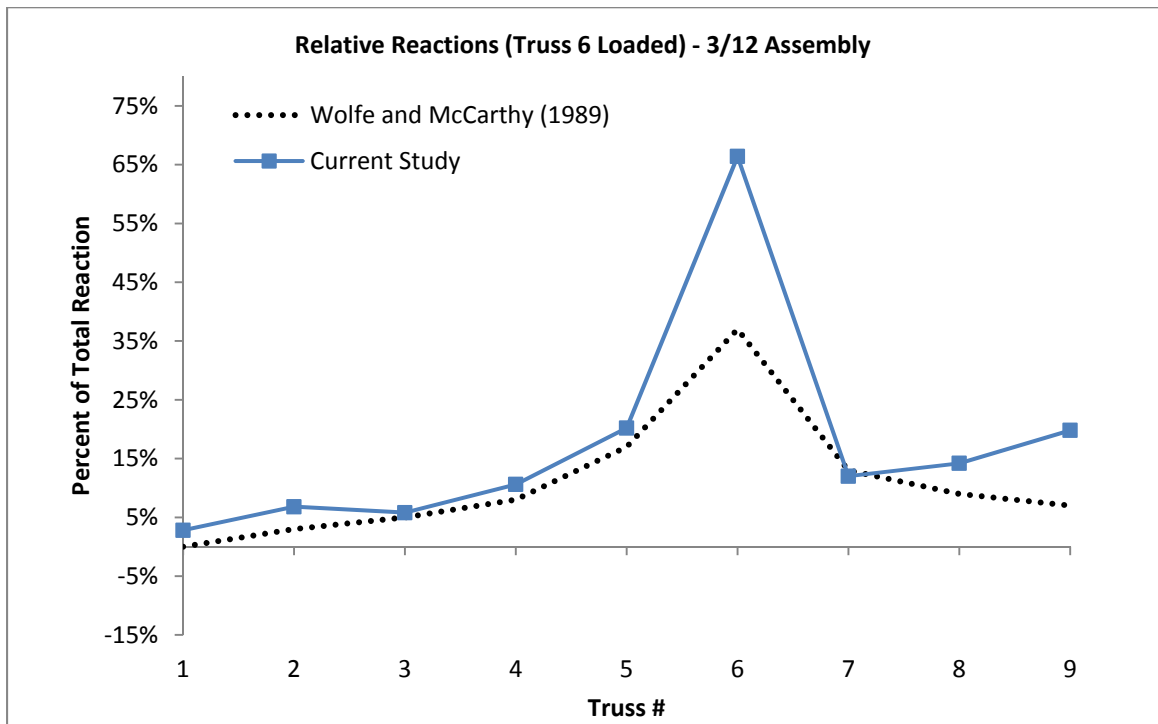


Figure D-6: Relative Reactions for 3:12 Truss Assembly When Truss 6 is Loaded

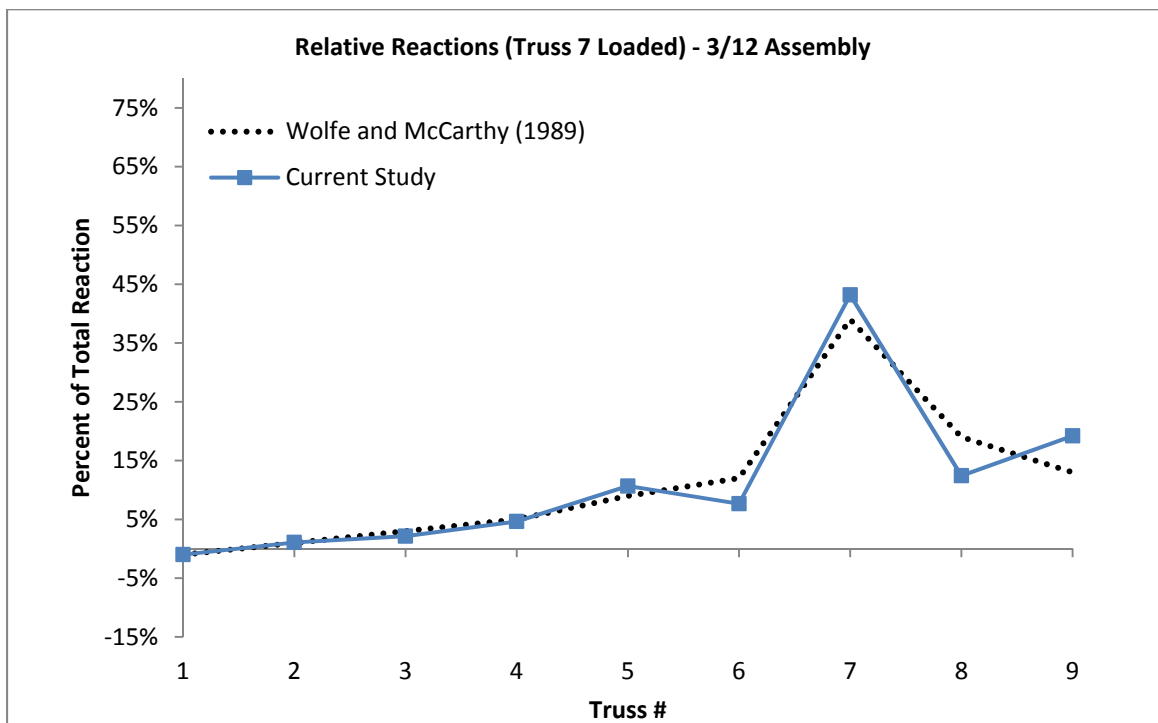


Figure D-7: Relative Reactions for 3:12 Truss Assembly When Truss 7 is Loaded

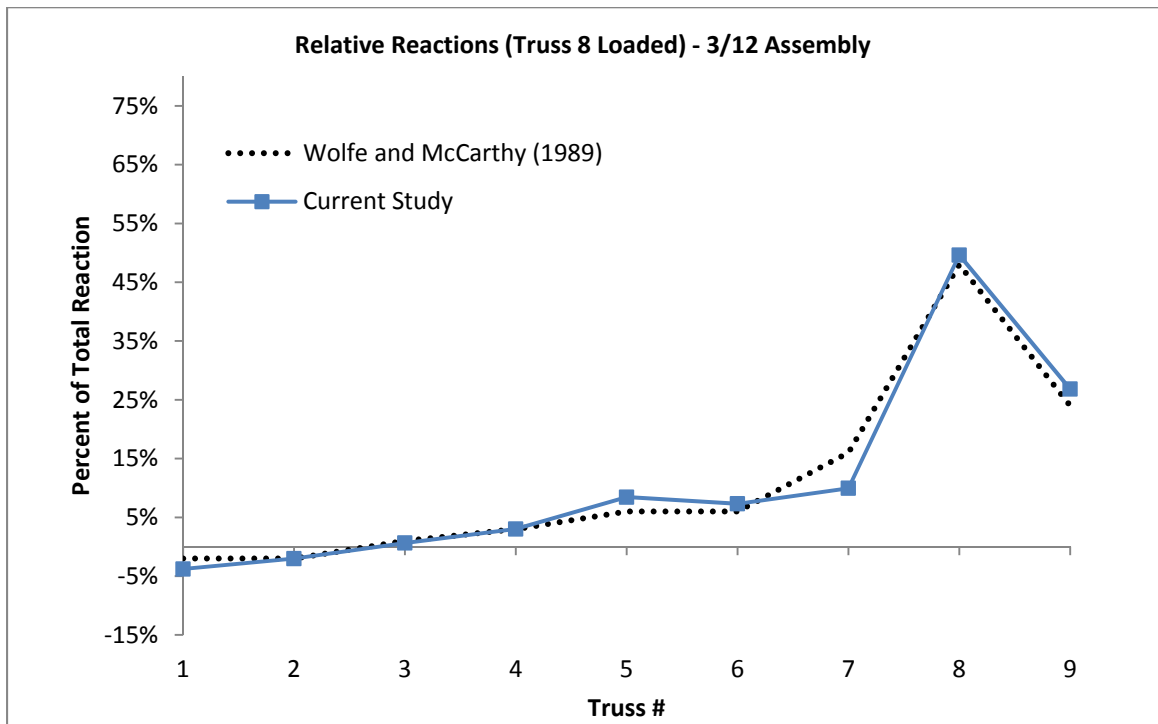


Figure D-8: Relative Reactions for 3:12 Truss Assembly When Truss 8 is Loaded

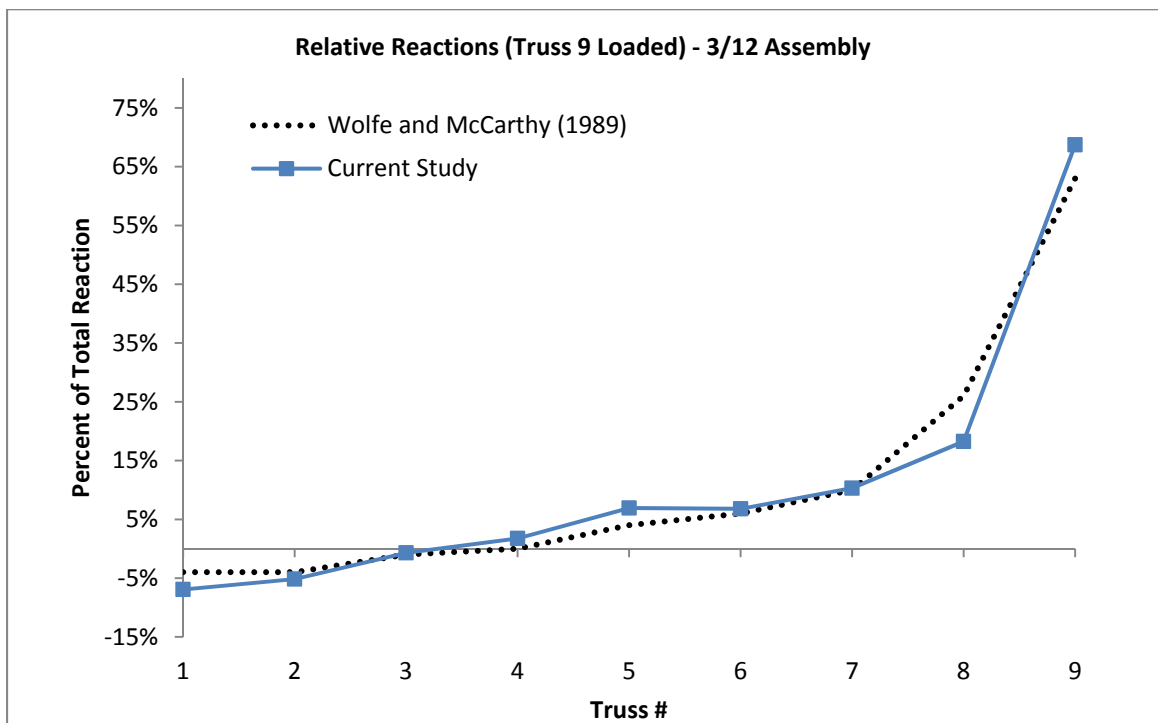


Figure D-9: Relative Reactions for 3:12 Truss Assembly When Truss 9 is Loaded

Influence Matrices for 3:12 Assembly – Relative Reactions

Table D-1: Relative Reactions of Trusses in 3:12 Assembly from Wolfe and McCarthy (1989)

Loaded Truss	Relative Reactions at Truss #								
	1	2	3	4	5	6	7	8	9
1	57%	29%	12%	10%	3%	0%	-1%	-4%	-8%
2	20%	49%	18%	11%	6%	2%	0%	-1%	-2%
3	10%	20%	36%	20%	7%	3%	2%	1%	-1%
4	5%	10%	12%	44%	16%	5%	4%	3%	0%
5	1%	5%	7%	18%	45%	11%	8%	6%	3%
6	0%	3%	5%	8%	17%	37%	13%	9%	7%
7	-1%	1%	3%	5%	9%	12%	39%	19%	13%
8	-2%	-2%	1%	3%	6%	6%	16%	48%	24%
9	-4%	-4%	-1%	0%	4%	6%	10%	26%	63%

Table D-2: Relative Reactions of Trusses in 3:12 Assembly from Current Study

Loaded Truss	Relative Reactions at Truss #								
	1	2	3	4	5	6	7	8	9
1	58%	28%	11%	9%	7%	1%	-1%	-4%	-10%
2	19%	58%	10%	9%	8%	2%	1%	-1%	-5%
3	13%	19%	43%	9%	10%	4%	2%	1%	-1%
4	9%	13%	7%	44%	13%	5%	4%	3%	3%
5	5%	8%	6%	8%	48%	7%	6%	6%	7%
6	2%	4%	4%	7%	13%	42%	8%	9%	12%
7	-1%	1%	2%	5%	11%	8%	43%	12%	19%
8	-4%	-2%	1%	3%	8%	7%	10%	50%	27%
9	-7%	-5%	-1%	2%	7%	7%	10%	18%	69%

Table D-3: Difference in Relative Reactions for 3:12 Assembly

Loaded Truss	Difference in Relative Reactions: (Wolfe and McCarthy 1989) - (Current Study)								
	1	2	3	4	5	6	7	8	9
1	-1%	1%	1%	1%	-4%	-1%	0%	0%	2%
2	1%	-9%	8%	2%	-2%	0%	-1%	0%	3%
3	-3%	1%	-7%	11%	-3%	-1%	0%	0%	0%
4	-4%	-3%	5%	0%	3%	0%	0%	0%	-3%
5	-4%	-3%	1%	10%	-3%	4%	2%	0%	-4%
6	-2%	-1%	1%	1%	4%	-5%	5%	0%	-5%
7	0%	0%	1%	0%	-2%	4%	-4%	7%	-6%
8	2%	0%	0%	0%	-2%	-1%	6%	-2%	-3%
9	3%	1%	0%	-2%	-3%	-1%	0%	8%	-6%

6:12 Assembly – Relative Reactions

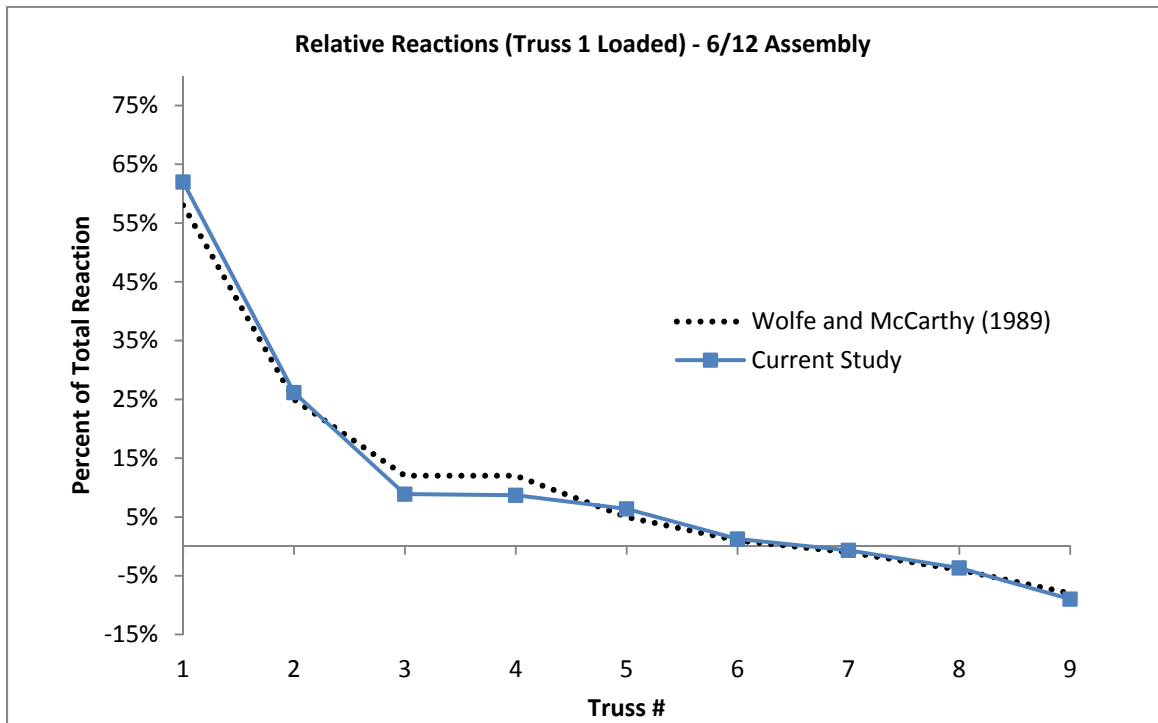


Figure D-10: Relative Reactions for 6:12 Truss Assembly When Truss 1 is Loaded

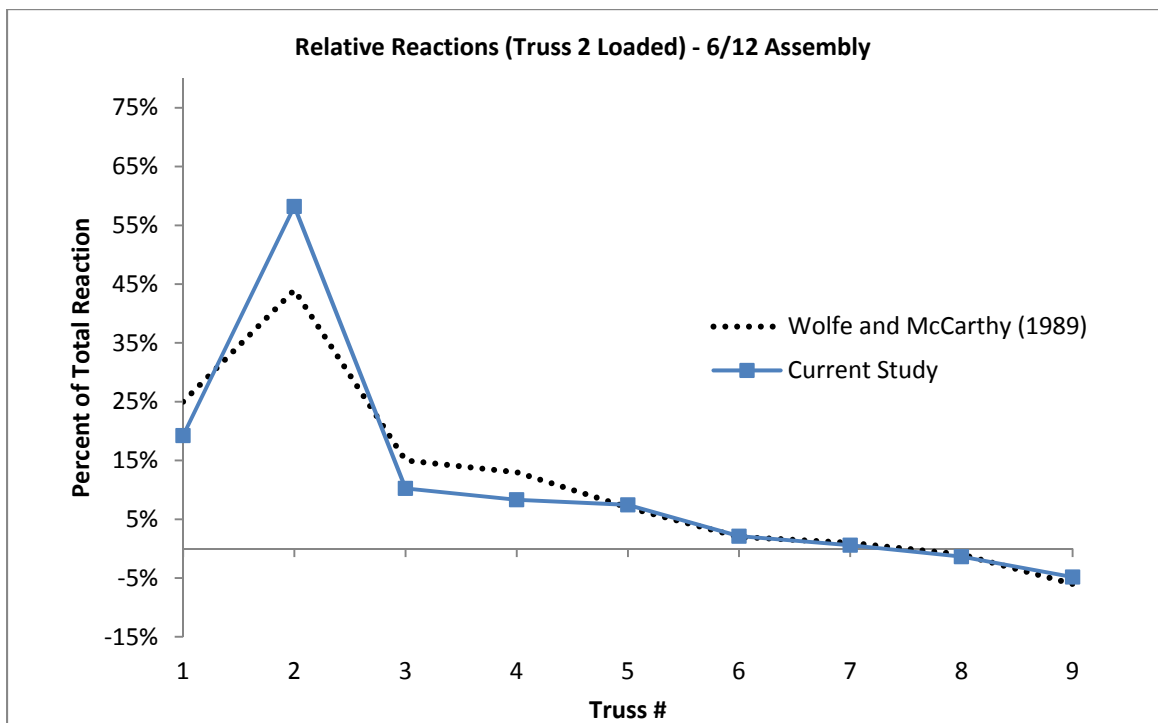


Figure D-11: Relative Reactions for 6:12 Truss Assembly When Truss 2 is Loaded

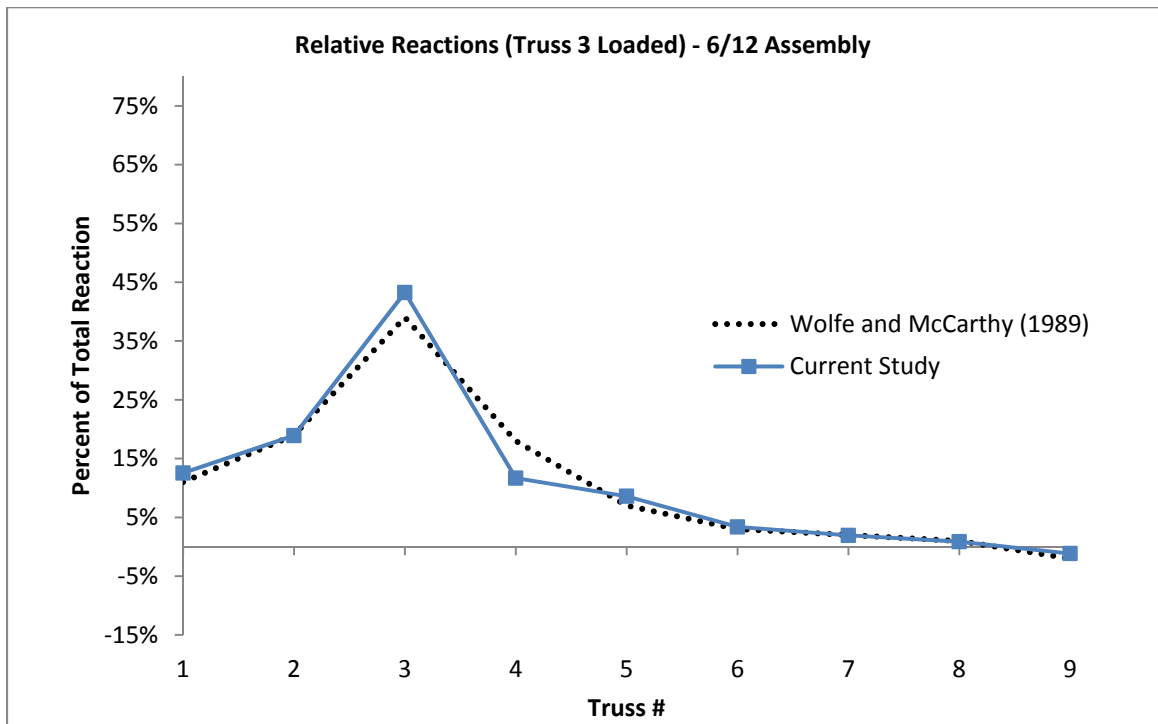


Figure D-12: Relative Reactions for 6:12 Truss Assembly When Truss 3 is Loaded

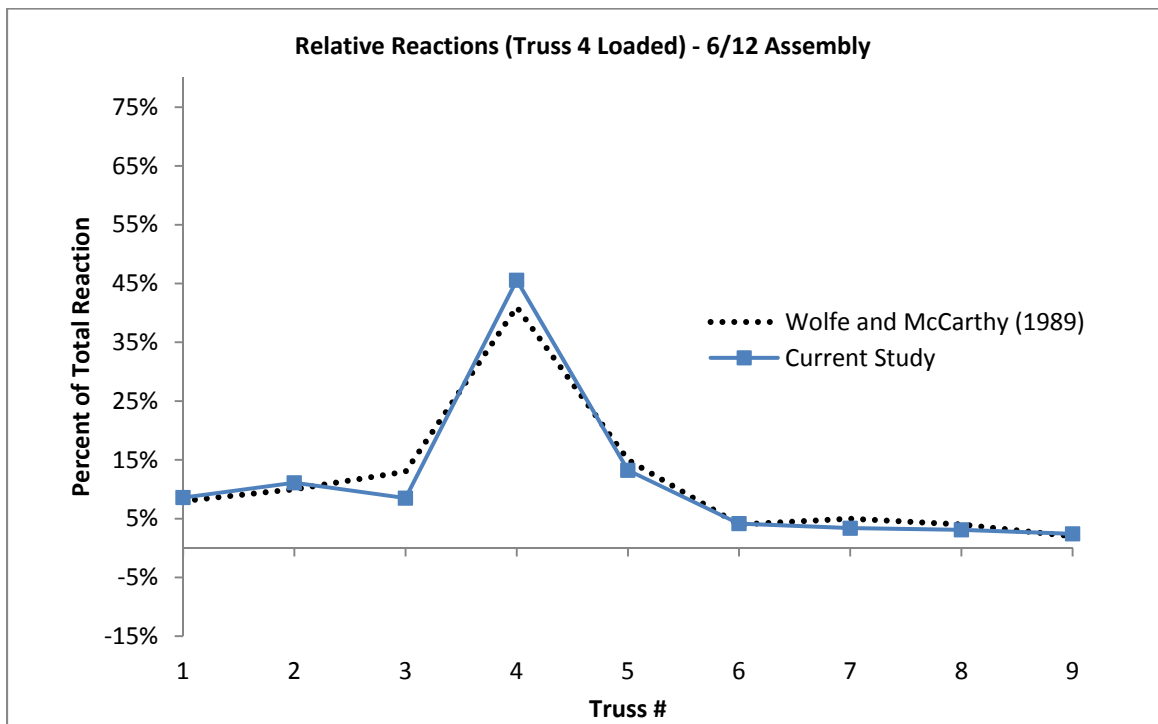


Figure D-13: Relative Reactions for 6:12 Truss Assembly When Truss 4 is Loaded

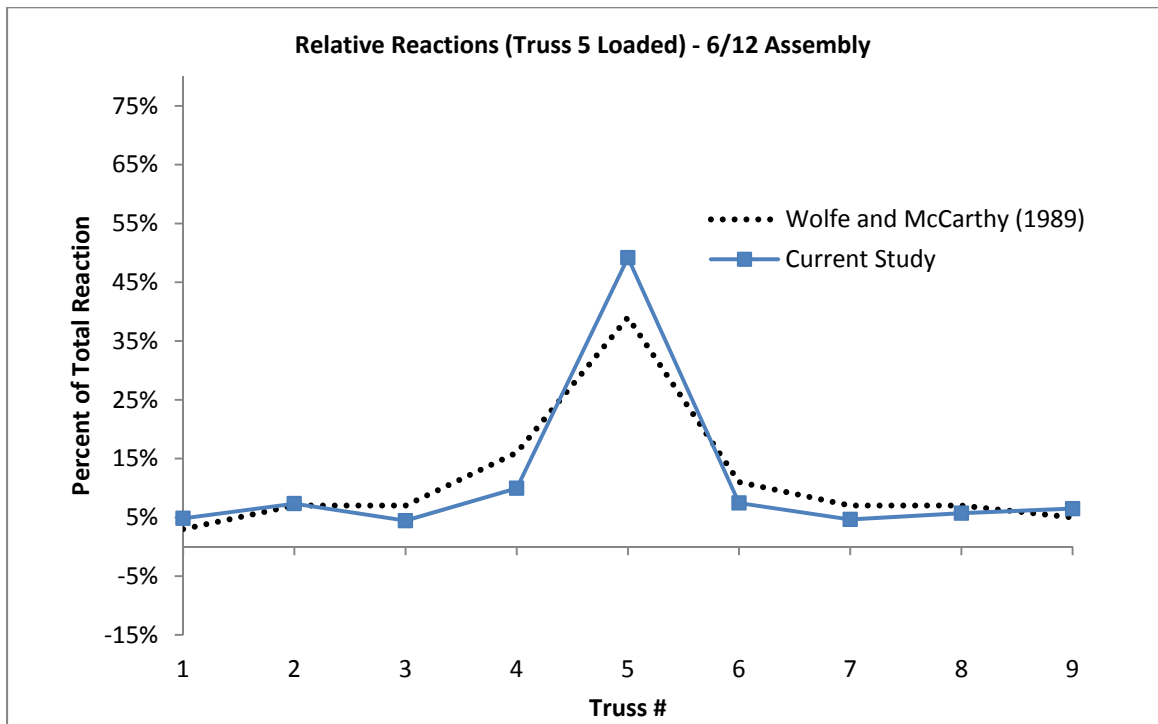


Figure D-14: Relative Reactions for 6:12 Truss Assembly When Truss 5 is Loaded

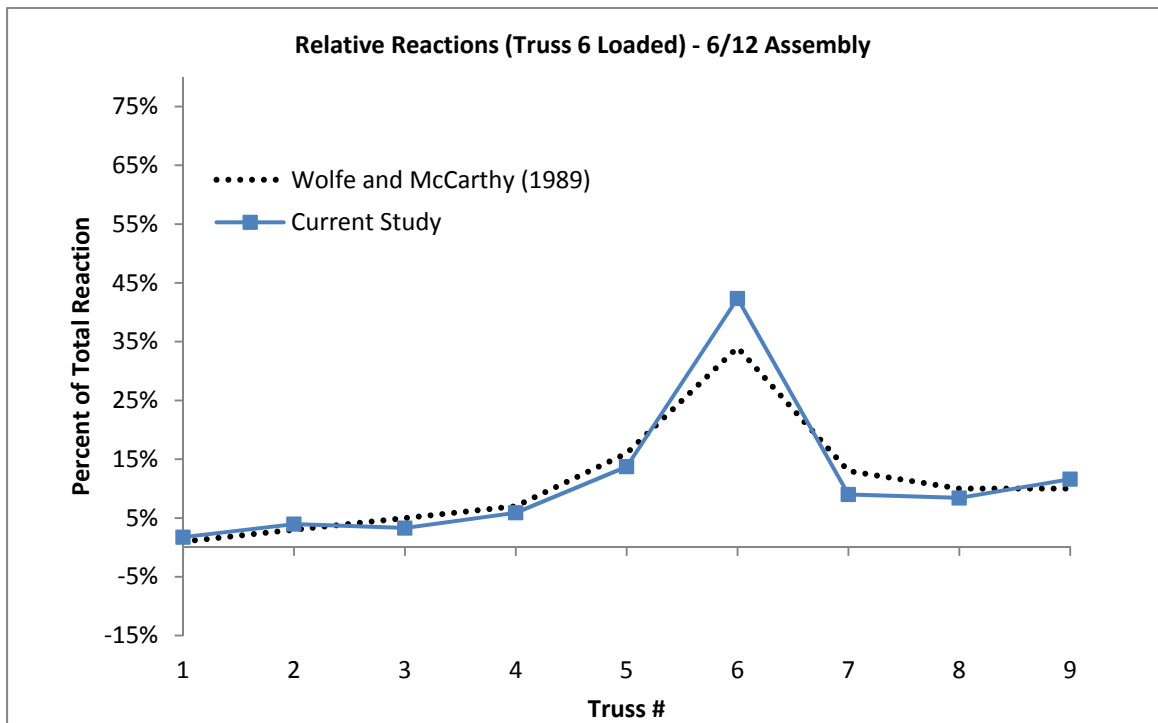


Figure D-15: Relative Reactions for 6:12 Truss Assembly When Truss 6 is Loaded

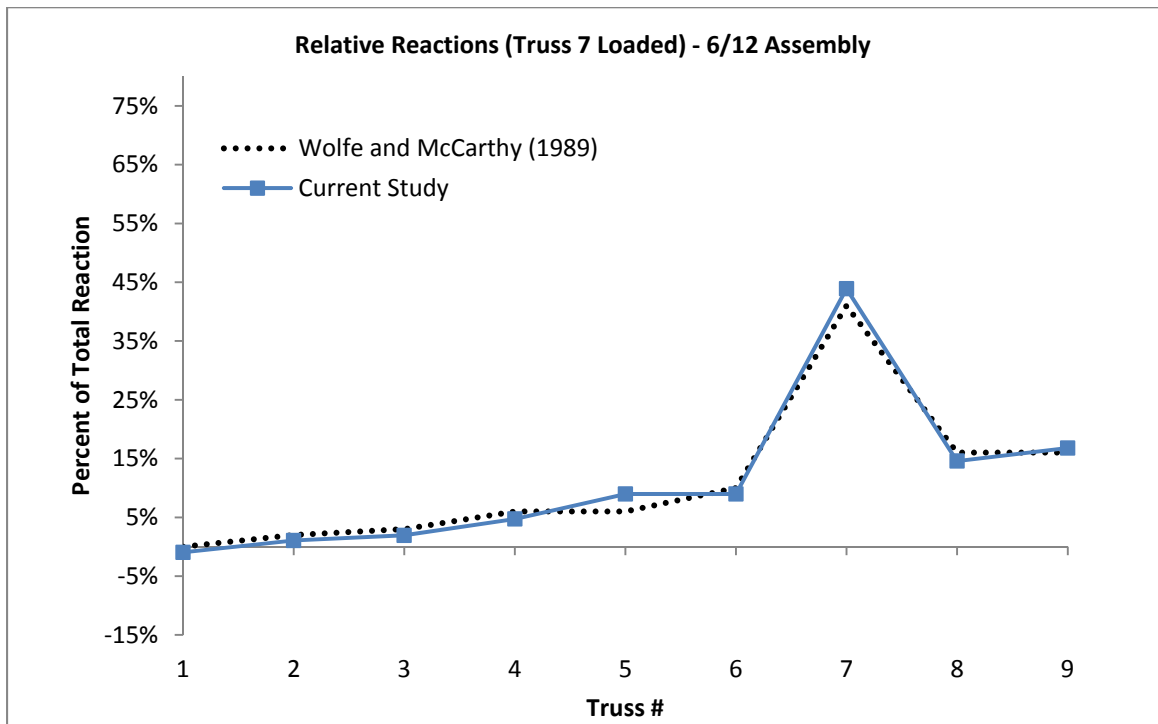


Figure D-16: Relative Reactions for 6:12 Truss Assembly When Truss 7 is Loaded

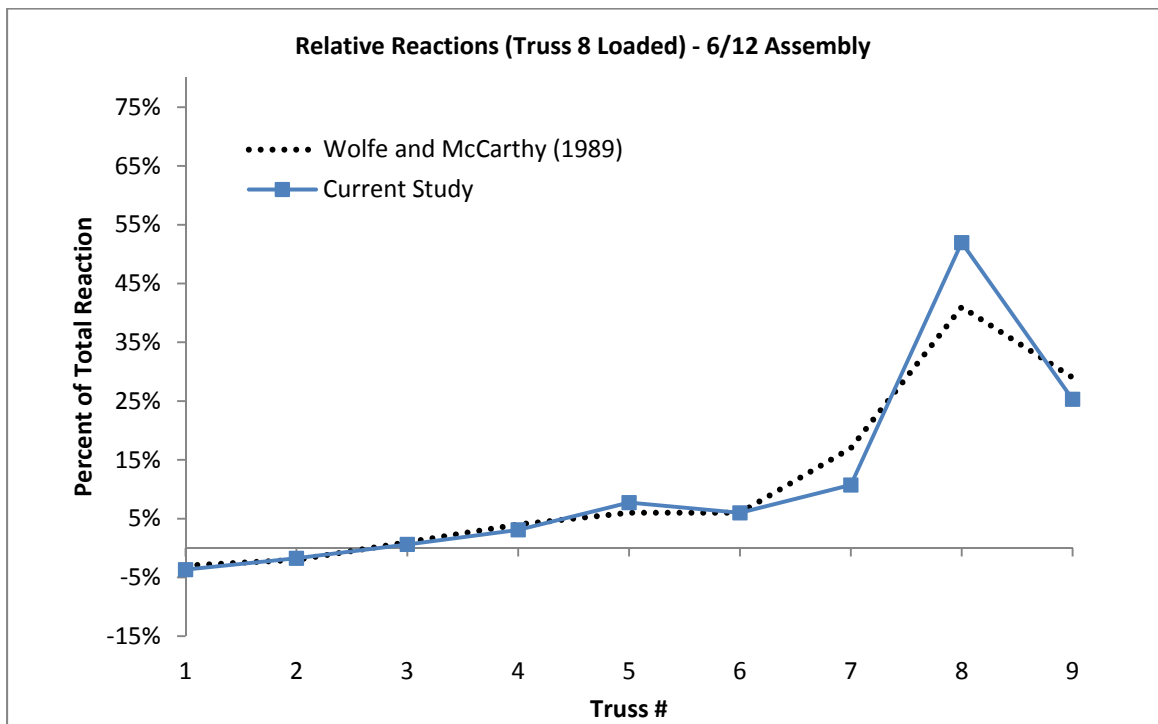


Figure D-17: Relative Reactions for 6:12 Truss Assembly When Truss 8 is Loaded

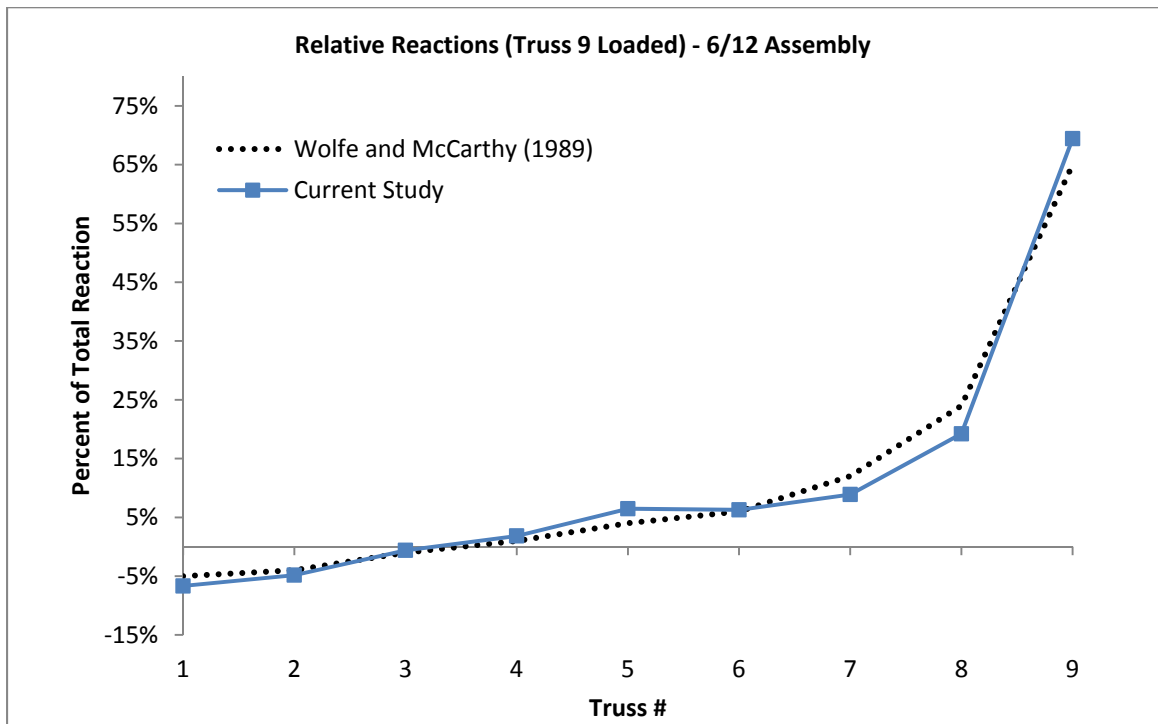


Figure D-18: Relative Reactions for 6:12 Truss Assembly When Truss 9 is Loaded

Influence Matrices for 6:12 Assembly – Relative Reactions

Table D-4: Reactions of Trusses in 6:12 Assembly from Wolfe and McCarthy (1989)

Loaded Truss	Relative Reactions at Truss #								
	1	2	3	4	5	6	7	8	9
1	58%	25%	12%	12%	5%	1%	-1%	-4%	-8%
2	25%	44%	15%	13%	7%	2%	1%	-1%	-6%
3	11%	19%	39%	18%	7%	3%	2%	1%	-2%
4	8%	10%	13%	41%	15%	4%	5%	4%	2%
5	3%	7%	7%	16%	39%	11%	7%	7%	5%
6	1%	3%	5%	7%	16%	34%	13%	10%	10%
7	0%	2%	3%	6%	6%	10%	41%	16%	16%
8	-3%	-2%	1%	4%	6%	6%	17%	41%	29%
9	-5%	-4%	-1%	1%	4%	6%	12%	24%	65%

Table D-5: Reactions of Trusses in 6:12 Assembly from Current Study

Loaded Truss	Relative Reactions at Truss #								
	1	2	3	4	5	6	7	8	9
1	62%	26%	9%	9%	6%	1%	-1%	-4%	-9%
2	19%	58%	10%	8%	7%	2%	1%	-1%	-5%
3	13%	19%	43%	12%	9%	3%	2%	1%	-1%
4	9%	11%	8%	46%	13%	4%	3%	3%	2%
5	5%	7%	4%	10%	49%	7%	5%	6%	6%
6	2%	4%	3%	6%	14%	42%	9%	8%	12%
7	-1%	1%	2%	5%	9%	9%	44%	15%	17%
8	-4%	-2%	1%	3%	8%	6%	11%	52%	25%
9	-7%	-5%	-1%	2%	6%	6%	9%	19%	69%

Table D-6: Difference in Relative Reactions for 6:12 Assembly

Loaded Truss	Difference in Relative Reactions: (Wolfe and McCarthy 1989) - (Current Study)								
	1	2	3	4	5	6	7	8	9
1	-4%	-1%	3%	3%	-1%	0%	0%	0%	1%
2	6%	-14%	5%	5%	0%	0%	0%	0%	-1%
3	-2%	0%	-4%	6%	-2%	0%	0%	0%	-1%
4	-1%	-1%	5%	-5%	2%	0%	2%	1%	0%
5	-2%	0%	3%	6%	-10%	4%	2%	1%	-1%
6	-1%	-1%	2%	1%	2%	-8%	4%	2%	-2%
7	1%	1%	1%	1%	-3%	1%	-3%	1%	-1%
8	1%	0%	0%	1%	-2%	0%	6%	-11%	4%
9	2%	1%	0%	-1%	-2%	0%	3%	5%	-4%

3:12 Assembly – Relative Deflections

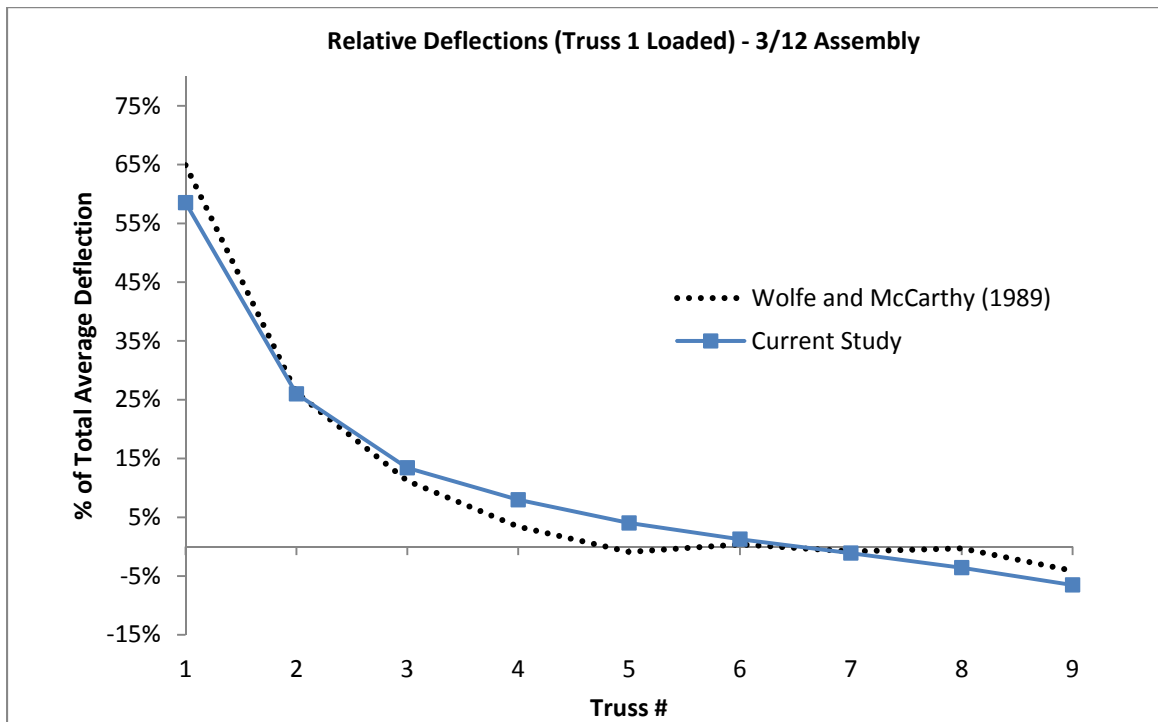


Figure D-19: Relative Deflections for 3:12 Truss Assembly When Truss 1 is Loaded

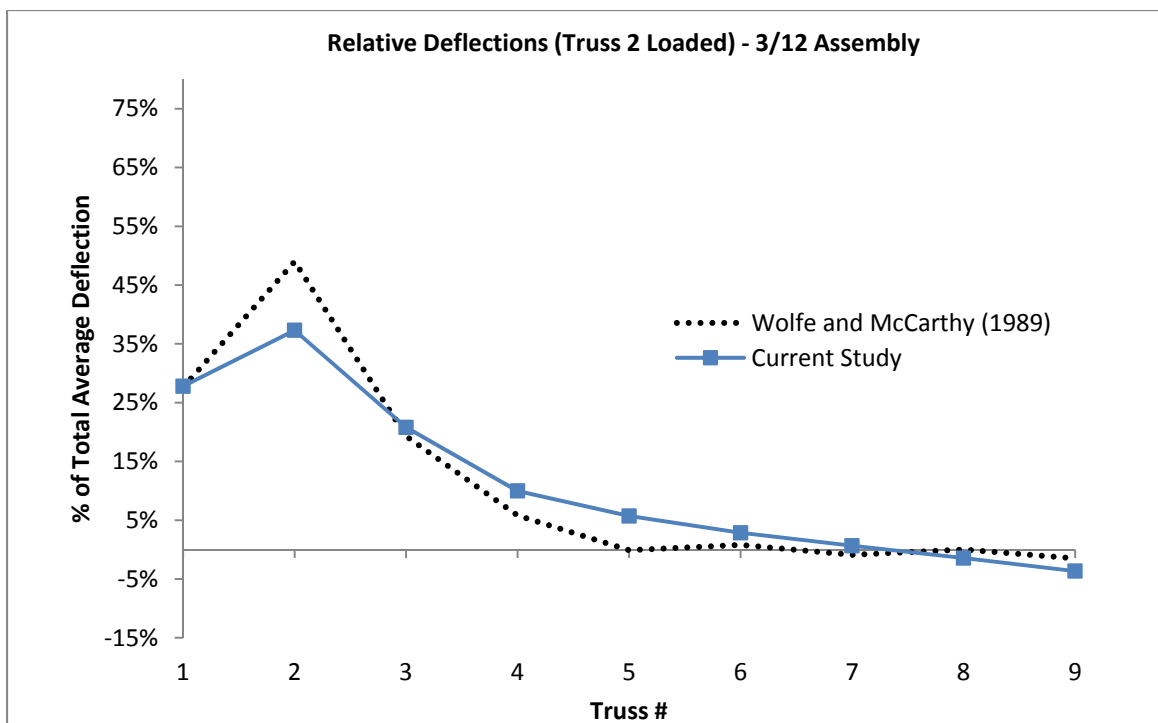


Figure D-20: Relative Deflections for 3:12 Truss Assembly When Truss 2 is Loaded

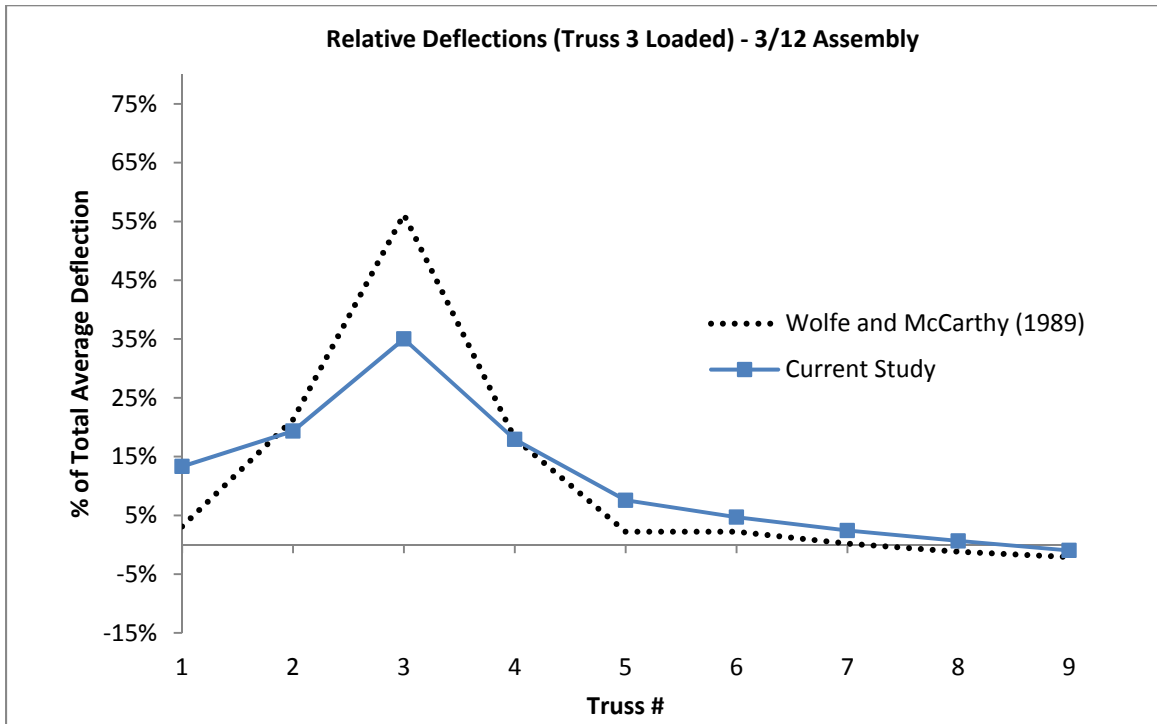


Figure D-21: Relative Deflections for 3:12 Truss Assembly When Truss 3 is Loaded

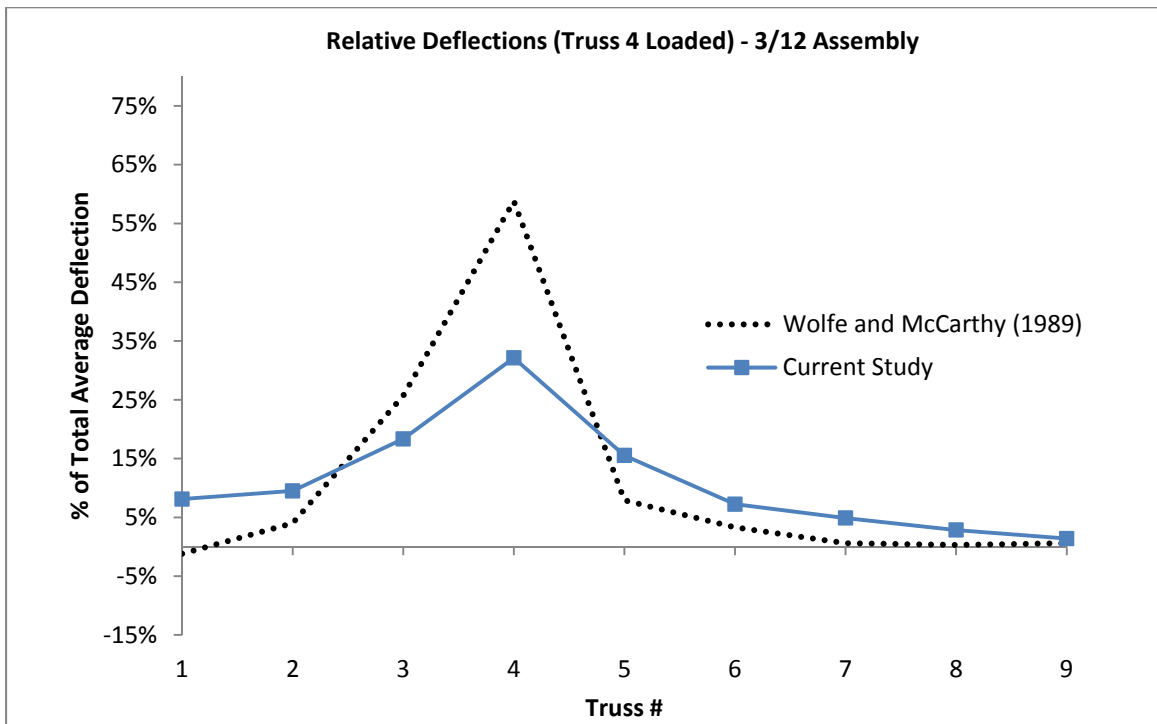


Figure D-22: Relative Deflections for 3:12 Truss Assembly When Truss 4 is Loaded

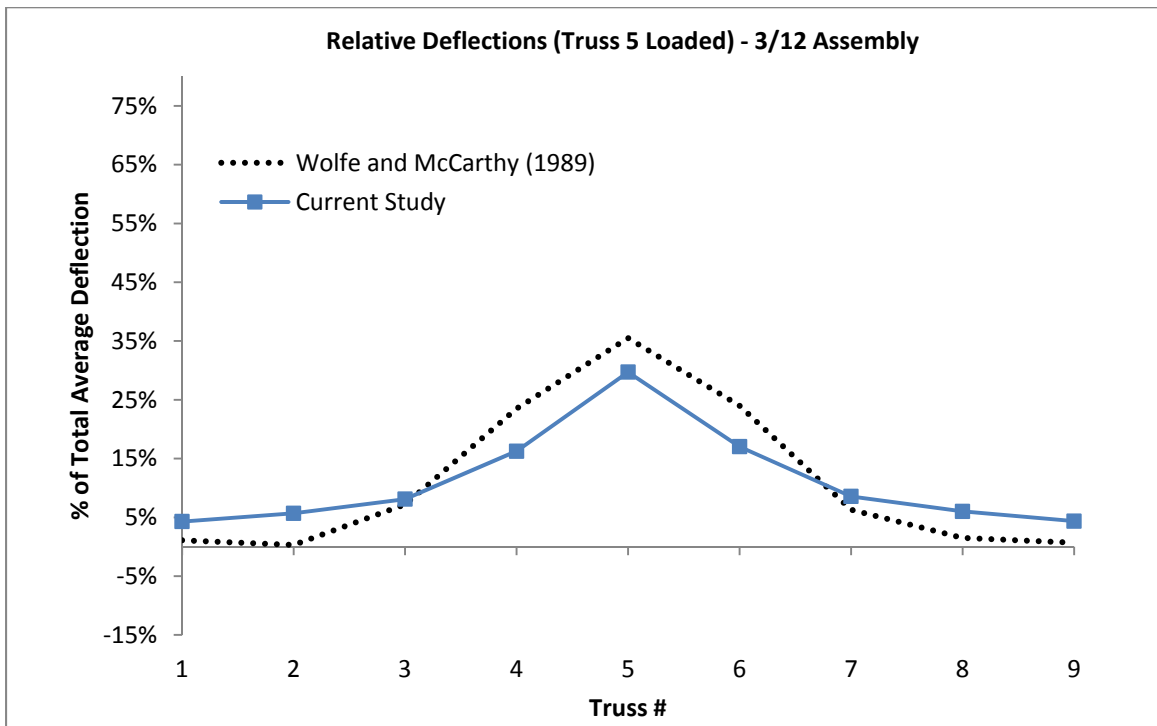


Figure D-23: Relative Deflections for 3:12 Truss Assembly When Truss 5 is Loaded

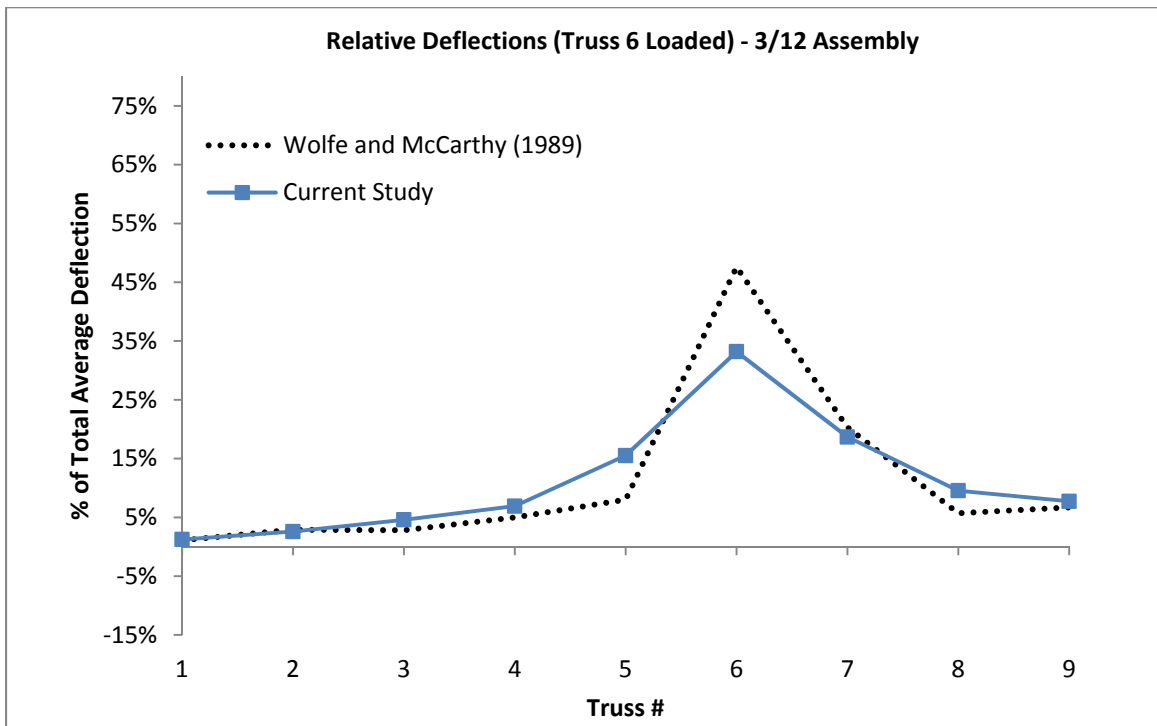


Figure D-24: Relative Deflections for 3:12 Truss Assembly When Truss 6 is Loaded

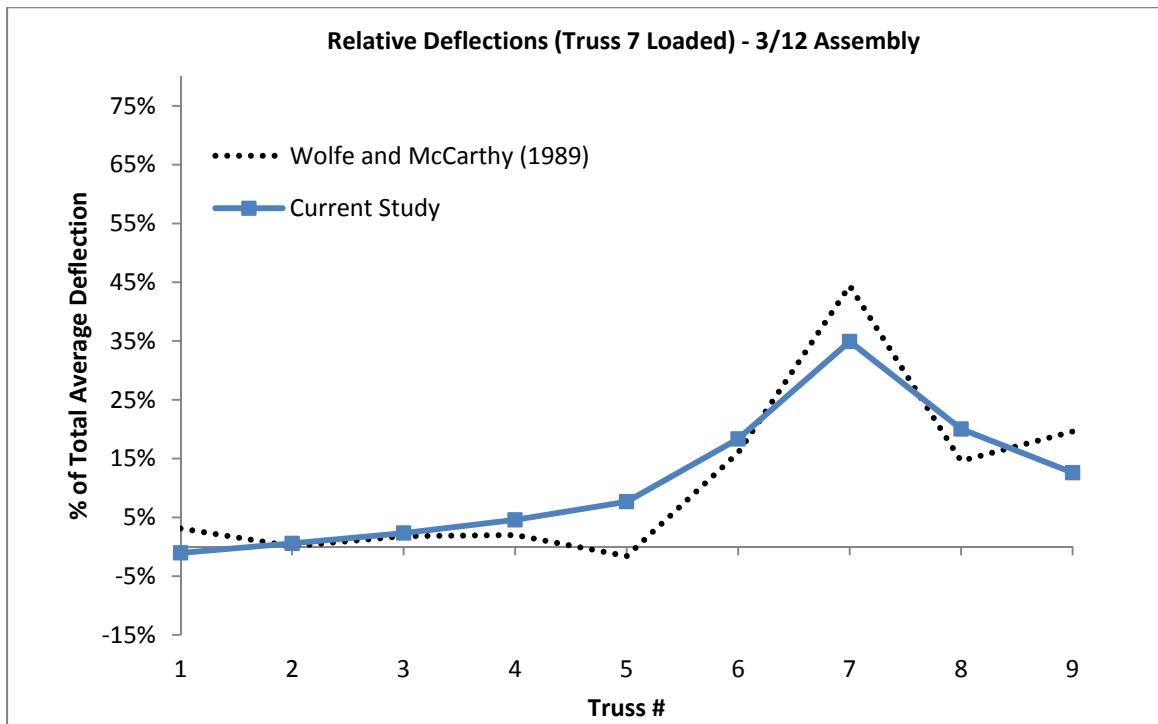


Figure D-25: Relative Deflections for 3:12 Truss Assembly When Truss 7 is Loaded

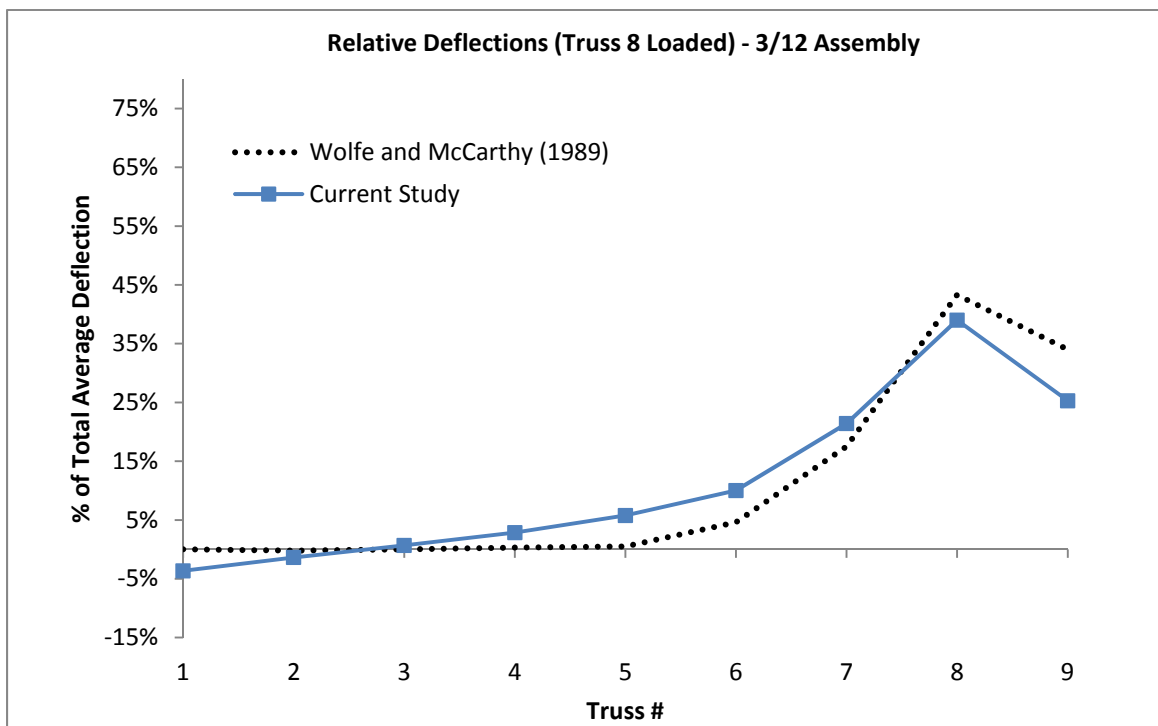


Figure D-26: Relative Deflections for 3:12 Truss Assembly When Truss 8 is Loaded

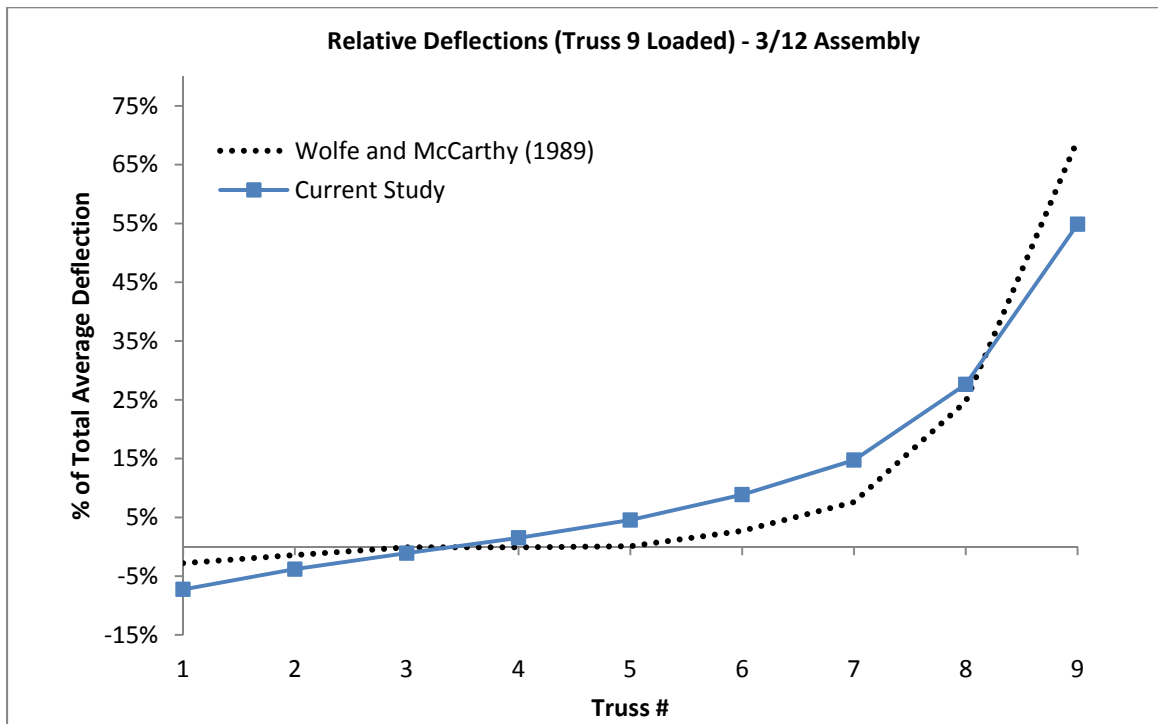


Figure D-27: Relative Deflections for 3:12 Truss Assembly When Truss 9 is Loaded

Influence Matrices for 3:12 Assembly – Relative Deflections

Table D-7: Relative Deflections of Trusses in 3:12 Assembly from Wolfe and McCarthy (1989)

Loaded Truss	Relative Deflections at Truss #								
	1	2	3	4	5	6	7	8	9
1	64.9%	26.2%	11.2%	3.4%	-0.9%	0.4%	-0.8%	-0.3%	-4.1%
2	27.6%	49.0%	19.3%	5.8%	-0.1%	0.8%	-0.9%	0.0%	-1.5%
3	3.1%	21.3%	56.2%	18.1%	2.2%	2.2%	0.2%	-1.2%	-2.1%
4	-1.2%	4.0%	25.7%	58.8%	7.9%	3.3%	0.6%	0.3%	0.6%
5	1.1%	0.3%	7.2%	23.5%	35.5%	24.0%	6.3%	1.5%	0.7%
6	1.1%	2.9%	2.8%	5.0%	8.0%	47.6%	20.3%	5.7%	6.7%
7	3.1%	0.1%	1.8%	2.0%	-1.6%	16.0%	44.4%	14.6%	19.6%
8	0.0%	-0.2%	0.0%	0.3%	0.5%	4.6%	17.5%	43.3%	34.0%
9	-2.8%	-1.4%	-0.1%	-0.1%	0.1%	2.7%	7.6%	24.7%	69.2%

Table D-8: Relative Deflections of Trusses in 3:12 Assembly from Current Study

Loaded Truss	Relative Deflections at Truss #								
	1	2	3	4	5	6	7	8	9
1	58.5%	26.0%	13.4%	8.0%	4.0%	1.3%	-1.1%	-3.6%	-6.5%
2	27.8%	37.3%	20.8%	10.0%	5.7%	2.9%	0.6%	-1.4%	-3.7%
3	13.3%	19.3%	35.0%	17.9%	7.6%	4.7%	2.4%	0.7%	-1.0%
4	8.1%	9.5%	18.4%	32.1%	15.5%	7.2%	4.9%	2.9%	1.4%
5	4.3%	5.7%	8.1%	16.3%	29.7%	17.0%	8.6%	6.0%	4.4%
6	1.2%	2.6%	4.6%	6.9%	15.5%	33.2%	18.7%	9.5%	7.7%
7	-1.0%	0.6%	2.3%	4.6%	7.7%	18.3%	34.9%	20.0%	12.6%
8	-3.6%	-1.4%	0.7%	2.9%	5.8%	10.0%	21.4%	39.0%	25.3%
9	-7.3%	-3.8%	-1.1%	1.5%	4.5%	8.9%	14.7%	27.6%	54.9%

Table D-9: Difference in Relative Deflections for 3:12 Assembly

Loaded Truss	Difference in Relative Deflections: (Wolfe and McCarthy 1989) - (Current Study)								
	1	2	3	4	5	6	7	8	9
1	6%	0%	-2%	-5%	-5%	-1%	0%	3%	2%
2	0%	12%	-1%	-4%	-6%	-2%	-2%	1%	2%
3	-10%	2%	21%	0%	-5%	-3%	-2%	-2%	-1%
4	-9%	-5%	7%	27%	-8%	-4%	-4%	-3%	-1%
5	-3%	-5%	-1%	7%	6%	7%	-2%	-5%	-4%
6	0%	0%	-2%	-2%	-8%	14%	2%	-4%	-1%
7	4%	0%	-1%	-3%	-9%	-2%	9%	-5%	7%
8	4%	1%	-1%	-3%	-5%	-5%	-4%	4%	9%
9	4%	2%	1%	-2%	-4%	-6%	-7%	-3%	14%

6:12 Assembly – Relative Deflections

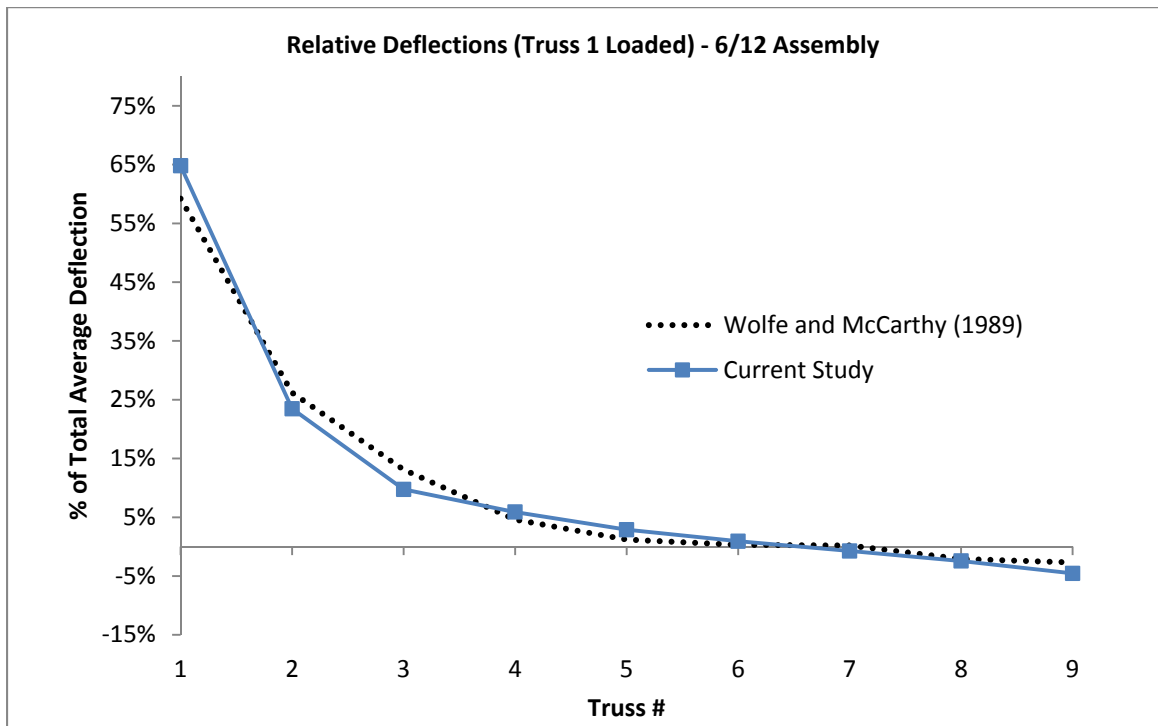


Figure D-28: Relative Deflections for 6:12 Truss Assembly When Truss 1 is Loaded

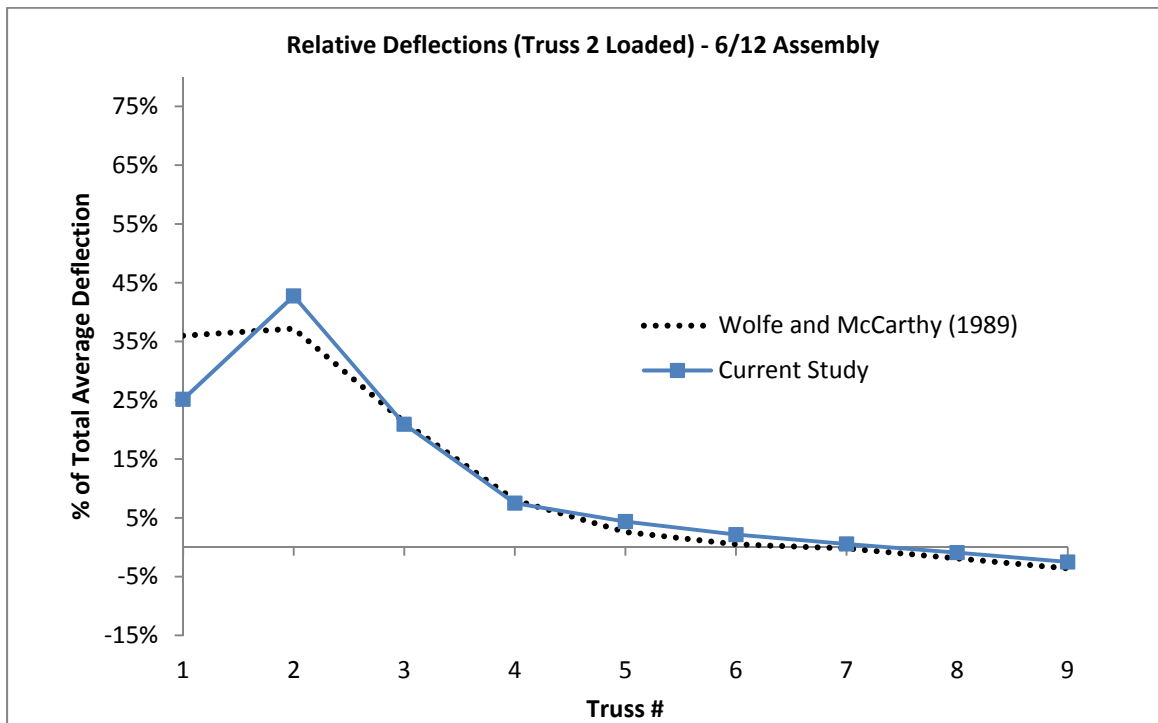


Figure D-29: Relative Deflections for 6:12 Truss Assembly When Truss 2 is Loaded

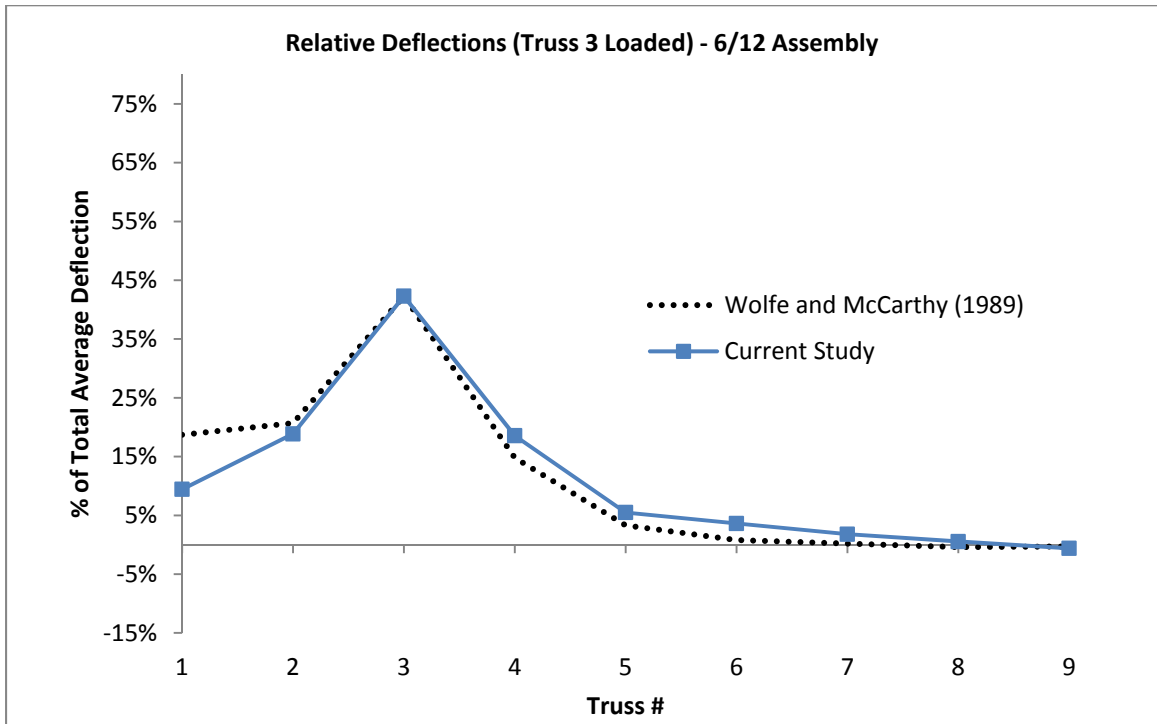


Figure D-30: Relative Deflections for 6:12 Truss Assembly When Truss 3 is Loaded

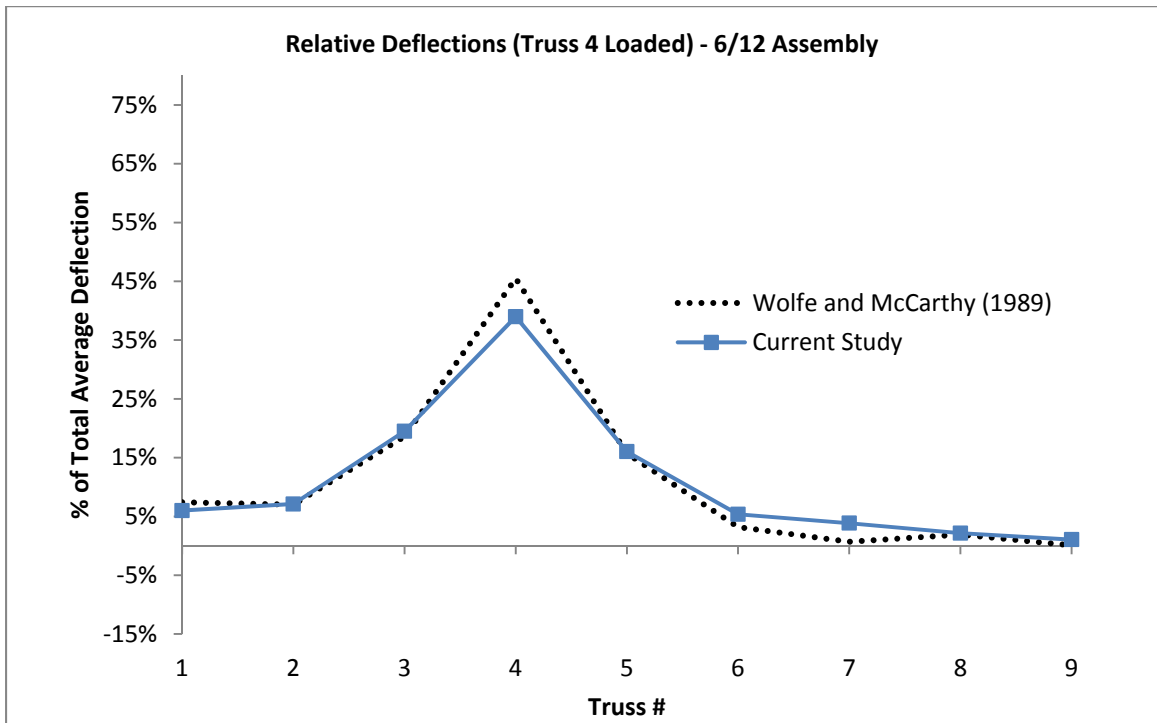


Figure D-31: Relative Deflections for 6:12 Truss Assembly When Truss 4 is Loaded

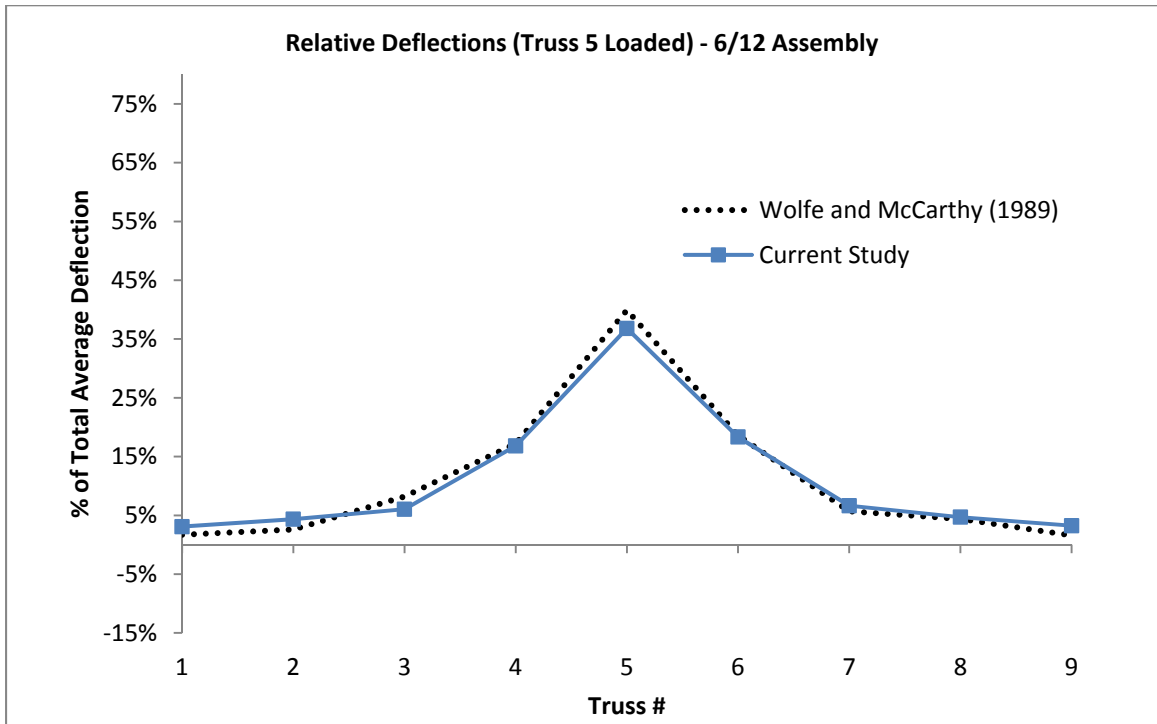


Figure D-32: Relative Deflections for 6:12 Truss Assembly When Truss 5 is Loaded

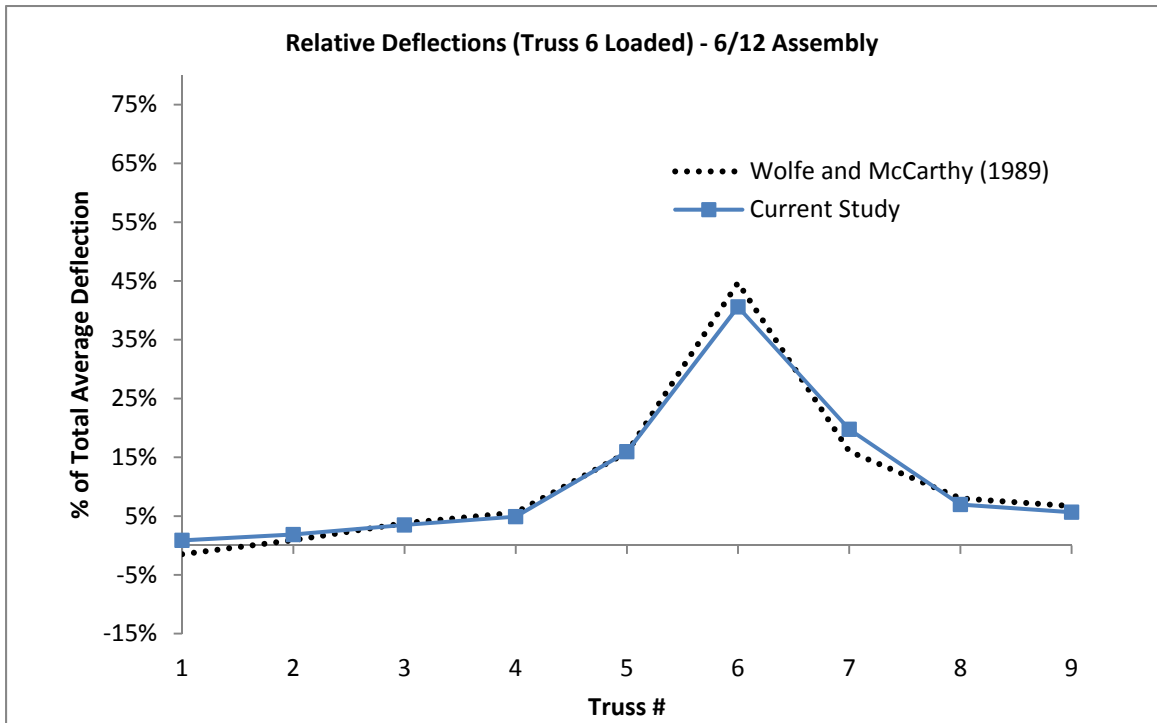


Figure D-33: Relative Deflections for 6:12 Truss Assembly When Truss 6 is Loaded

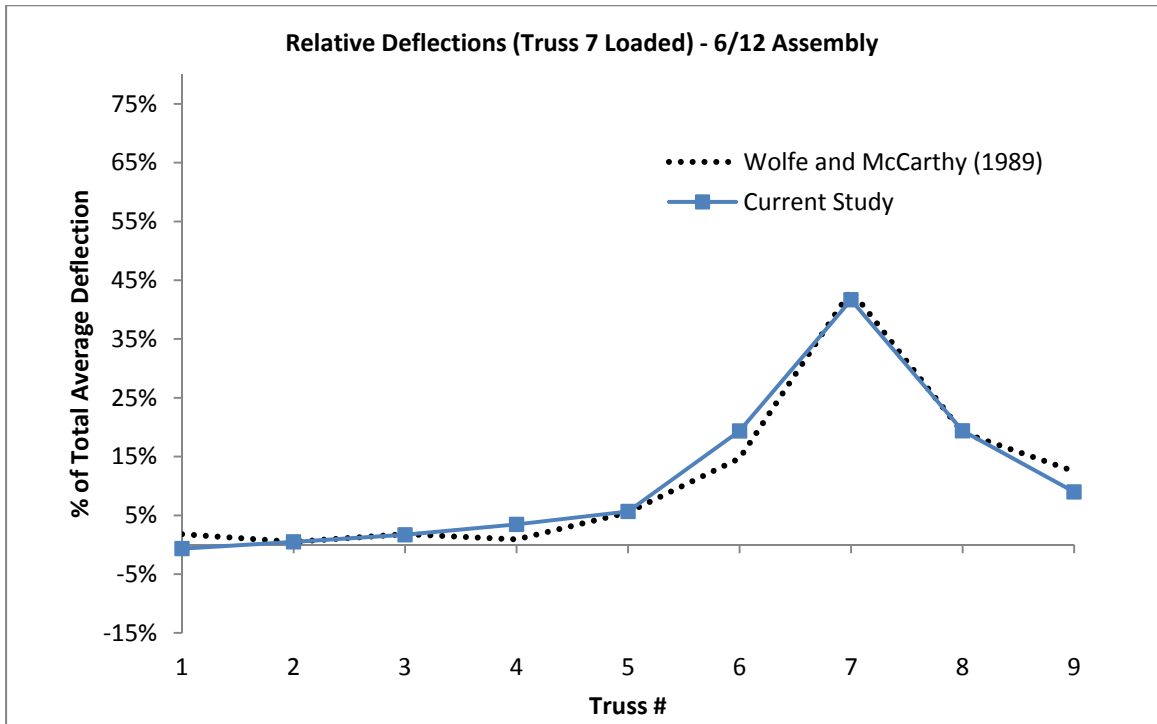


Figure D-34: Relative Deflections for 6:12 Truss Assembly When Truss 7 is Loaded

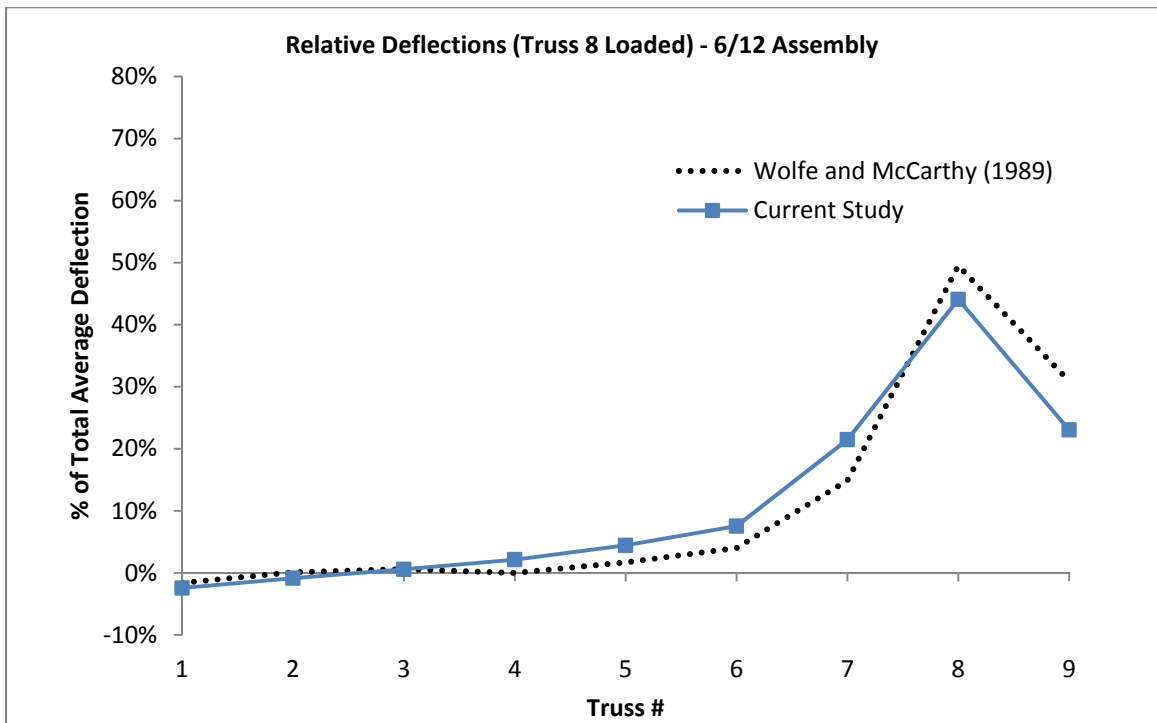


Figure D-35: Relative Deflections for 6:12 Truss Assembly When Truss 8 is Loaded

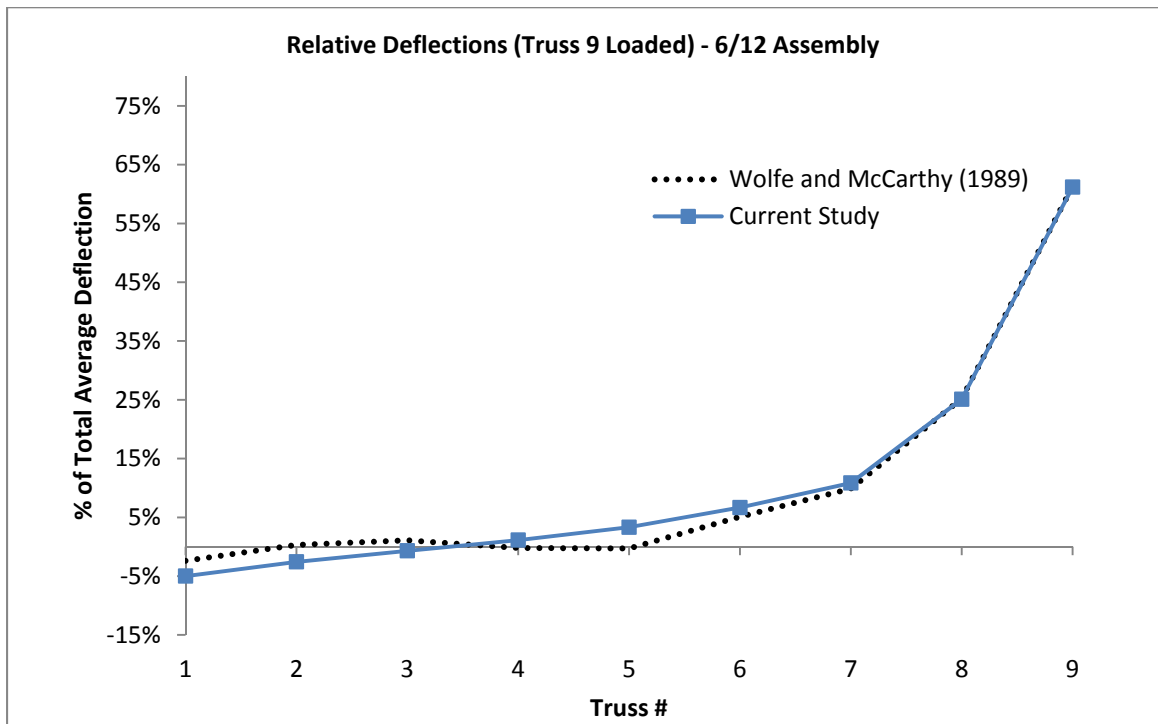


Figure D-36: Relative Deflections for 6:12 Truss Assembly When Truss 9 is Loaded

Influence Matrices for 6:12 Assembly – Relative Deflections

Table D-10: Relative Deflections of Trusses in 6:12 Assembly from Wolfe and McCarthy (1989)

Loaded Truss	Relative Deflections at Truss #								
	1	2	3	4	5	6	7	8	9
1	59.2%	26.2%	13.1%	4.6%	1.2%	0.3%	0.2%	-2.1%	-2.7%
2	36.0%	37.2%	21.3%	8.0%	2.6%	0.5%	-0.2%	-1.9%	-3.6%
3	18.7%	20.7%	42.3%	14.8%	3.3%	0.8%	0.2%	-0.4%	-0.3%
4	7.4%	7.0%	18.6%	45.5%	15.7%	3.2%	0.7%	1.9%	0.1%
5	1.7%	2.6%	8.2%	17.2%	39.9%	18.6%	5.7%	4.4%	1.6%
6	-1.5%	0.9%	3.8%	5.6%	15.8%	44.7%	16.0%	8.0%	6.7%
7	1.8%	0.5%	1.8%	0.9%	5.5%	14.7%	43.3%	19.1%	12.5%
8	-1.6%	0.1%	0.6%	0.0%	1.7%	4.0%	14.9%	49.5%	30.9%
9	-2.4%	0.3%	1.1%	-0.2%	-0.3%	5.1%	9.9%	25.2%	61.3%

Table D-11: Relative Deflections of Trusses in 6:12 Assembly from Current Study

Loaded Truss	Relative Deflections at Truss #								
	1	2	3	4	5	6	7	8	9
1	64.8%	23.5%	9.7%	5.9%	2.9%	0.9%	-0.7%	-2.4%	-4.6%
2	25.2%	42.7%	20.9%	7.5%	4.4%	2.1%	0.6%	-0.9%	-2.5%
3	9.4%	18.9%	42.3%	18.6%	5.5%	3.6%	1.8%	0.6%	-0.6%
4	6.0%	7.1%	19.5%	39.0%	16.0%	5.4%	3.9%	2.2%	1.1%
5	3.1%	4.3%	6.0%	16.8%	36.8%	18.3%	6.6%	4.7%	3.2%
6	0.9%	1.9%	3.5%	4.9%	15.9%	40.6%	19.8%	7.0%	5.7%
7	-0.7%	0.5%	1.7%	3.5%	5.7%	19.4%	41.7%	19.4%	9.0%
8	-2.4%	-0.9%	0.6%	2.1%	4.4%	7.5%	21.5%	44.1%	23.0%
9	-5.0%	-2.6%	-0.7%	1.1%	3.3%	6.7%	10.9%	25.1%	61.2%

Table D-12: Difference in Relative Deflections for 3:12 Assembly

Loaded Truss	Difference in Relative Deflections: (Wolfe and McCarthy 1989) - (Current Study)								
	1	2	3	4	5	6	7	8	9
1	-6%	3%	3%	-1%	-2%	-1%	1%	0%	2%
2	11%	-6%	0%	0%	-2%	-2%	-1%	-1%	-1%
3	9%	2%	0%	-4%	-2%	-3%	-2%	-1%	0%
4	1%	0%	-1%	7%	0%	-2%	-3%	0%	-1%
5	-1%	-2%	2%	0%	3%	0%	-1%	0%	-2%
6	-2%	-1%	0%	1%	0%	4%	-4%	1%	1%
7	2%	0%	0%	-3%	0%	-5%	2%	0%	4%
8	1%	1%	0%	-2%	-3%	-4%	-7%	5%	8%
9	3%	3%	2%	-1%	-4%	-2%	-1%	0%	0%

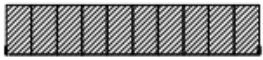




APPENDIX E

TWO-DIMENSIONAL SHEAR WALL MODEL VALIDATION

Introduction

Modeling methods for two-dimensional shear walls were validated against full-scale tests performed by Dolan and Johnson (1996). Ten light-frame, wood shear walls were tested: two from each of the five configurations shown in Table E-1 (Dolan and Johnson 1996). Shear wall types A through D were used for validation in the current study. All shear walls were 12.2 m (40 ft) long, and sheathed on both sides (one side with plywood and the other with gypsum wall board). No. 2, Spruce-Pine-Fir (SPF) sawn lumber was used for all wall framing members including studs, plates and headers. A detailed description of materials and fabrication methods used by Dolan and Johnson (1996) is included in Table E-2 and the connectors and connector spacing used in the wall assemblies are listed in Table E-3.

Table E-1: Description of Shear Wall Configurations (Dolan and Johnson 1996)

Wall Configuration ¹	Wall Type	Sheathing Area Ratio, (r)	Opening Size	
			Door	Window ²
	A	1.0	-	-
	B	0.76	6'-8" x 4'-0"	5'-8" x 7'-10 ¹ / ₂ "
	C	0.55	6'-8" x 4'-0"	4'-0" x 11'-10 ¹ / ₂ " 4'-0" x 7'-10 ¹ / ₂ "
	D	0.48	6'-8" x 4'-0" 6'-8" x 12'-0"	4'-0" x 7'-10 ¹ / ₂ "
	E	0.30	(Sheathed at ends) ³ 8'-0" x 28'-0"	-

1: All walls are framed with studs spaced at 16 inches on center. Shaded areas represent sheathing.
 2: The top of each window is located 16 inches from the top of the wall.
 2: Wall E has studs along the full length of wall but is sheathed only at the ends of the wall.

Table E-2: Description of Materials and Construction Methods (Dolan and Johnson 1996)

Component	Fabrication and Materials
Framing Members	No. 2, Spruce-Pine-Fir, 2 x 4 inch nominal
Sheathing:	
Exterior	Plywood, 15/32 in., 4 ply, Structural I. 4 ft. x 8 ft. sheets installed vertically.
Interior	Gypsum wallboard, 1/2 in., installed vertically, joints taped
Headers:	
4'-0" opening	(2) 2x4's with intermediate layer of 15/32 in. plywood. One jack stud at each end.
7'-10½" opening	(2) 2x8's with intermediate layer of 15/32 in. plywood. Two jack studs at each end.
11' - 10½" opening	(2) 2x12's with intermediate layer of 15/32 in. plywood. Two jack studs at each end.
Tie-down	Simpson HTT 22, nailed to end studs with 32 16d sinker nails. 5/8 in. diameter A307 bolt to connect to foundation.
Anchor Bolts	5/8 in. diameter A307 bolt with 3 in. square x 1/4 in. steel plate washers.

Table E-3: Description of Connections used in Construction (Dolan and Johnson 1996)

Connection Description	No. and Type of Connector	Connector Spacing
Framing		
Top Plate to Top Plate (Face-nailed)	16d common	per foot
Top / Bottom Plate to Stud (End-nailed)	2-16d common	per stud
Stud to Stud (Face-nailed)	2-16d common	24 in. o.c.
Stud to Header (Toe-nailed)	2-16d common	per stud
Header to Header (Face-nailed)	16d common	16 in. o.c. along edges
Tie-down Anchor/ Anchor Bolts		
Tie-down Anchor to Stud (Face-nailed)	32-16d sinker	per tie-down
Tie-down Anchor to Foundation	1-A307 5/8 in. dia. bolt	per tie-down
Anchor bolts	1-A307 5/8 in. dia. bolt	24 in. o.c. and within 1 ft. of wall ends, using 3 x 3 x ¼ in. steel plate washers
Sheathing:		
Plywood	8d	6 in. edge / 12 in. field (2 rows for end stud)
Gypsum wall board	13 ga x 1½ in. (3/8 in. head)	7 in. edge / 10 in. field

The shear walls were tested horizontally, in-plane to the wall using the apparatus shown in Figure E-1 (Dolan and Johnson 1996). The top and bottom chords of the walls were anchored to steel tubes to prevent out-of-plane displacement during testing. A series of increasing horizontal displacements were applied along the top chord of each wall, representing increasing degrees of inter-story drift. The resultant force was then measured and plotted against inter-story drift in a $P-\Delta$ plot. An “equivalent energy elastic-plastic curve” was then developed for each wall configuration and used to determine an equivalent elastic stiffness for each wall configuration (Dolan and Johnson 1996).

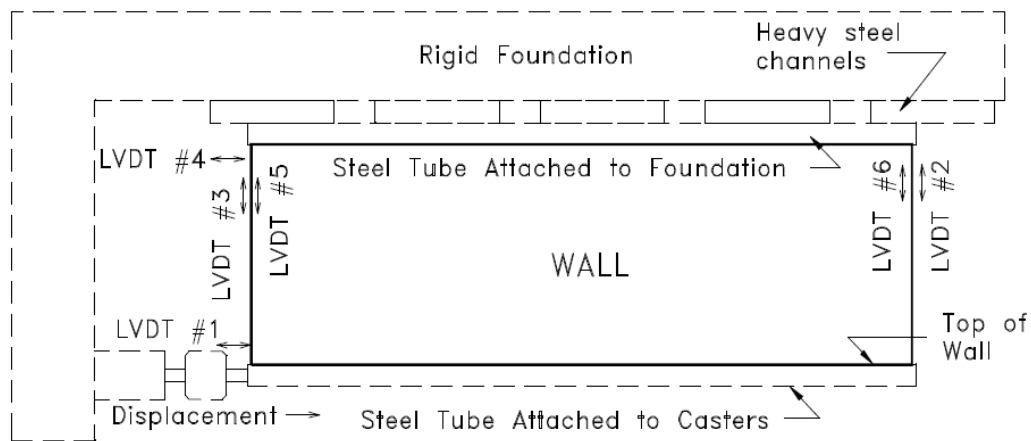


Figure E-1: Testing Apparatus and Sensor Locations (Dolan and Johnson 1996)

Modeling Methods

Framing Members

Studs, plates (top and bottom) and headers were modeled using SAP2000’s frame elements. Opening headers constructed by Dolan and Johnson (1996) consisted of two pieces of dimension lumber with an intermediate layer of plywood. To simplify the modeling process, headers in the model were represented as one framing element with a cross section equal to the total cross section of the header assembly and material properties for the sawn lumber only. Table E-4 lists the frame element sections used in the SAP2000 model.

Table E-4: Frame Sections Used for Modeling in SAP2000 – modeled through center of cross-section unless otherwise noted

Name of Frame Section	Cross Section Dimensions
2x4 header	89 x 89 mm (3.5 x 3.5 in)
2x8 header	89 x 184 mm (3.5 x 7.25 in)
2x12 header	286 x 89 mm (3.5 x 11.25 in)
Single Stud	38 x 89 mm (1.5 x 3.5 in)
Double Stud/Single Jack	76 x 89 mm (3.0 x 3.5 in)
Double Jack	76 x 89 mm (4.5 x 3.5 in)
Double Top Plate	89 x 76 mm (3.5 x 3 in) <i>(modeled through top of section)</i>
Bottom Plate	89 x 38 mm (3.5 x 1.5 in) <i>(modeled through bottom of section)</i>

Figures E-2 and E-3 show an example of the framing layout for the wall Type D model. All frame elements were assigned linear, isotropic material properties. A modulus of elasticity (MOE) of 9653 MPa (1400 ksi) was determined from AF&PA (2005a) Table 4A for No. 2 SPF. No adjustment factors were used since the members were assumed to be of normal moisture content (less than 19 percent), with no incisions and tested at normal temperatures.

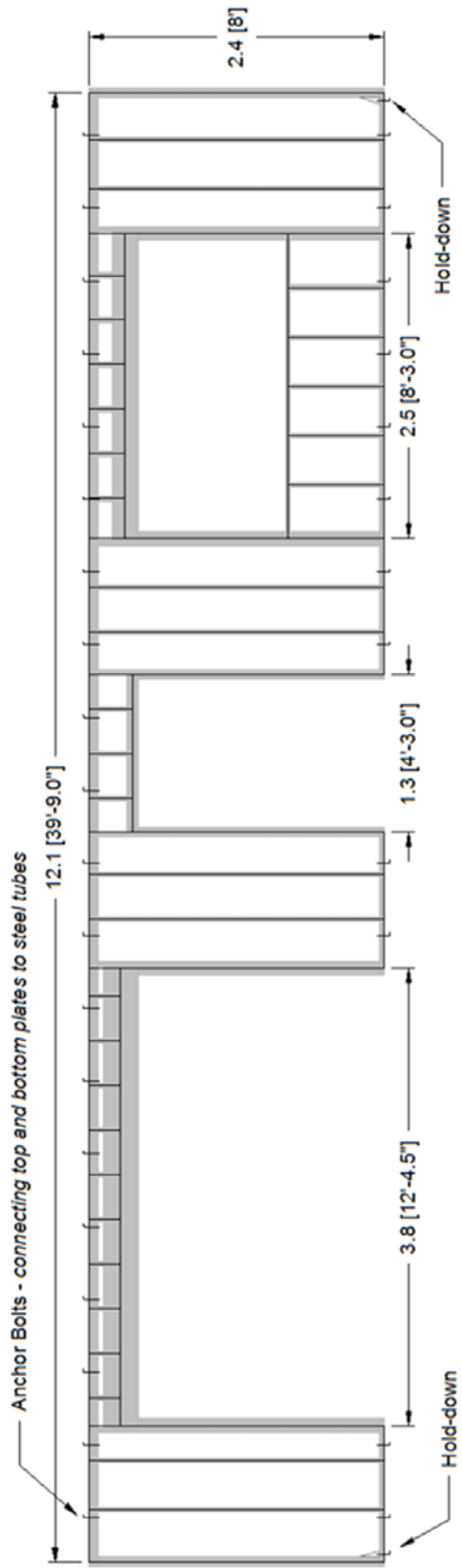


Figure E-2: Example of Assumed Wall Framing with SAP2000 Wire Frame Overlay for Type D Shear Wall – Dimensions are in (ft-in)

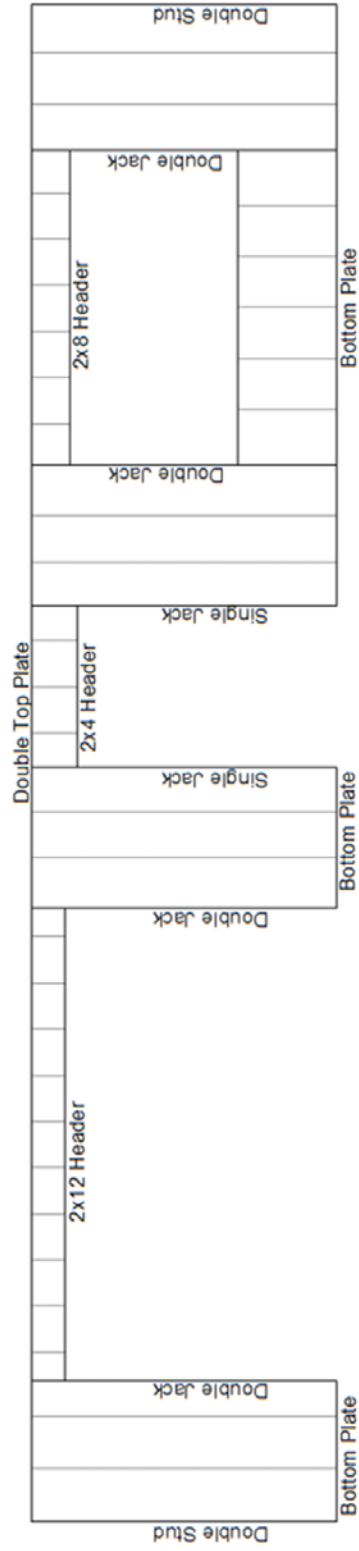
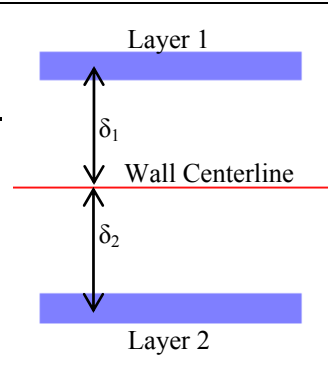


Figure E-3: Example Frame Section Assignment for Type D Shear Wall – All non-labeled members are assigned “Single Stud” frame sections

Plywood and Gypsum Wall Board Sheathing

Plywood and GWB sheathing were modeled using SAP2000's layered shell element as described in Table E-5 (with local axis 1 oriented parallel to the long side of the plywood and local axis 3 oriented through the thickness of the plywood). The shell element was modeled through the centerline of the wall with the plywood and GWB layers displaced a distance of half the thickness of the wall framing members plus half the thickness of the sheathing to either side of the wall centerline. In concurrence with Martin (2010), one continuous shell element applied to each wall and meshed into smaller, approximately square shaped elements for analysis.

Table E-5: Layered Shell Element Used for Modeling Sheathing in SAP2000

Layer	Thickness	Displacement (δ): from centerline of wall to centerline of layer	
Layer 1: Plywood Sheathing	11.9 mm (15/32 in)	50.4 mm (1.984 in)	
Layer 2: Gypsum Wall Board	12.7 mm (1/2 in)	50.8 mm (2 in)	

Linear, orthotropic material properties for the plywood sheathing were determined using the in-plane engineering properties from OSULaminates with the following inputs:

- Number of Plies = 4
- Ply Thickness = 3.97 mm (0.156 in)
- Ply Orientation = 0° - 90° - 90° - 0°
- Plywood Species Group 1

The gypsum wallboard was assigned linear isotropic properties using the orthotropic input in SAP2000 so that the shear modulus, G_{12} , could be adjusted freely to account for edge nail spacing (discussed later in this appendix and in Appendix F). The modulus of elasticity for the GWB was determined as the average of the stiffness range listed by the

Gypsum Association (2010). An value of 0.3 was used for Poisson's ratio. Table E-6 contains a full list of material properties assigned to each sheathing layer.

Table E-6: Material Properties Used for Modeling in SAP2000

Sheathing Material Properties	
Plywood Sheathing <i>(In-Plane Properties)</i>	<ul style="list-style-type: none"> • Orthotropic Properties • $E_1 = 5337$ MPa (774 ksi) • $E_2 = 5337$ MPa (774 ksi) • $U_{12} = 0.021$ • $G_{12} = 147$ MPa (21.3 ksi) <div style="display: flex; align-items: center; justify-content: flex-end; margin-left: 20px;"> <div style="font-size: 3em; margin-right: 5px;">}</div> <div style="text-align: left;"> <p><i>Calculated using OSULaminates</i></p> <p><i>See Appendix F</i></p> </div> </div>
Gypsum Wall Board	<ul style="list-style-type: none"> • Orthotropic Properties • $E_1 = 1820$ MPa (264 ksi) • $E_2 = 1820$ MPa (264 ksi) • $U_{12} = 0.3$ • $G_{12} = 641$ MPa (9.3 ksi) <div style="display: flex; align-items: center; justify-content: flex-end; margin-left: 20px;"> <div style="text-align: left;"> <p><i>Gypsum Association (2010)</i></p> <p><i>See Appendix F</i></p> </div> </div>

Connectivity and Anchorage

Simple pinned connections were used to connect all framing members so that the assembly stiffness of each wall could be controlled using the shear modulus (G_{12}) of each sheathing layer. Overall wall assembly stiffness (based on edge nail spacing and wall length) was predicted using shear wall deflection equations from AF&PA (2005b) *Special Design Provisions for Wind and Seismic*. Values of G_{12} for each sheathing layer were then adjusted to reflect the predicted wall stiffness through a procedure similar to the sheathing correlation procedure developed by Martin (2010). The procedure used in the current study is described in detail in Appendix F.

Anchor bolts and hold-downs were modeled using directional linear spring elements. The anchor bolts were represented using three springs: one oriented in the Z-direction (representing the axial stiffness of each bolt) and two oriented in the X- and Y-directions (representing the shear stiffness of each bolt). Hold-down devices were represented with only one spring oriented in the Z-direction. Figure E-4 illustrates the

local axes orientation used for each anchorage device (Martin 2010). Figure E-5 shows the location of the anchor bolts and hold-downs in the model.

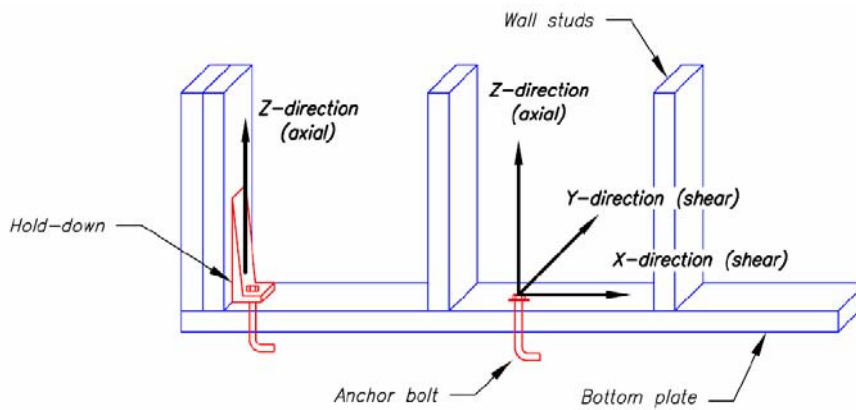


Figure E-4: Local Axes for Anchor Bolts and Hold-downs (Martin 2010)

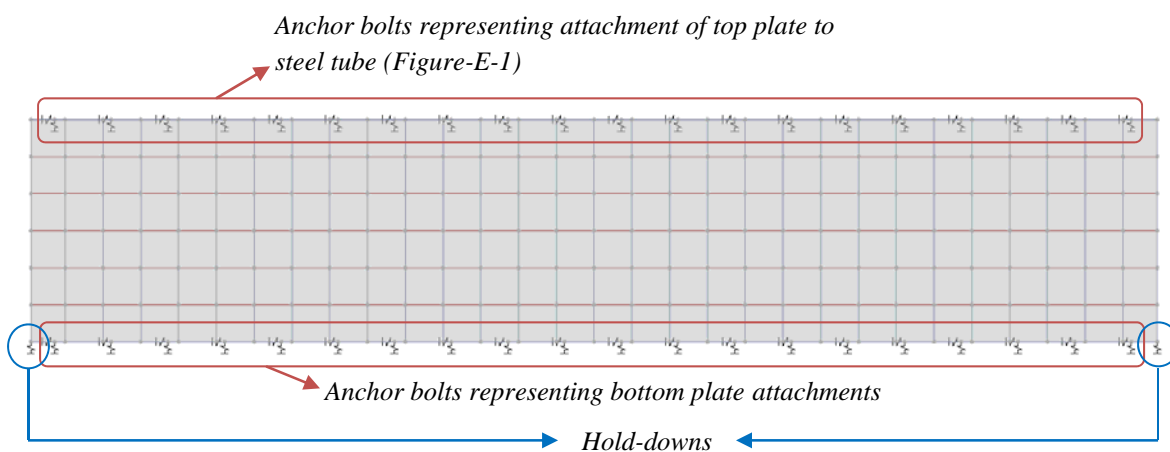


Figure E-5: Anchor Bolt and Hold-Down Placement in SAP2000 Model

Stiffness properties for anchorage devices are listed in Table E-7. The axial stiffness for the anchor bolts was determined experimentally by Seaders (2004) and incorporates wood crushing as well as bolt elongation and slip. The shear stiffness was determined using Equation E-1, below, taken from AF&PA (2005a) Section 10.3.6 for load/slip modulus, γ (kips/in), of dowel type connectors with diameter, D (in).

$$\gamma = 270000(D^{1.5}) \quad \text{Equation E-1}$$

The axial stiffness of the hold-down device was determined using the allowable tension load and displacement at allowable tension load reported by Simpson Strong-Tie (2012b) for an HTT5 hold down with 16d fasteners connected to SPF wood. The HTT5 connector is listed by Simpson Strong-Tie (2012a) as the recommended alternative to the HTT22 since the HTT22 has been discontinued.

Table E-7: Properties for Wall Anchorage used for Modeling in SAP2000

Anchorage Device	Stiffness		Placement
	Shear	Axial	
Anchor Bolts	23.3 kN/mm (133 kip/in)*	6.1 kN/mm (35 kip/in)**	Spaced 0.6 m (2 ft) on center and within 0.3 m (1 ft) of wall ends
Hold-Downs	---	5674 kN/m (32.4 kip/in)***	One at each end of wall

*Calculated from AF&PA (2005a) Section 10.3.6

**From Seaders (2004)

***Simpson Strong-Tie (2012b)

Results and Discussion

The stiffness of each shear wall model was found by displacing the top plate of the model 8 mm (0.32 in) and then summing the lateral reactions at the anchors along the base of the wall. Since the SAP2000 models are linear, the stiffness of the walls remains constant regardless of displacement. Table E-8 compares the stiffness of the SAP2000 wall models to the equivalent elastic stiffness experimentally determined by Dolan and Johnson (1996). For all cases, the models were able to predict the experimental elastic stiffness of the walls within 5 percent error. The models were also accurate in predicting the reduction in stiffness due to the addition of openings.

Table E-8: Stiffness Comparison between the SAP2000 Models from the Current Study and Tests from Dolan and Johnson (1996)

<i>Wall Type</i>	<i>Dolan and Johnson (1996)</i>		<i>Current Study</i>		<i>% Difference</i>
	Equivalent Elastic Stiffness kN/mm (kip/in)	% Stiffness Reduction from Type A	Model Stiffness kN/mm (kip/in)	% Stiffness Reduction from Type A	
A	11.1 (63.6)	---	11.6 (66.4)	---	4%
B	7.6 (43.5)	32%	7.2 (41.3)	38%	-5%
C	3.8 (21.5)	66%	3.7 (21.2)	68%	-1%
D	3.3 (18.6)	71%	3.2 (18.1)	73%	-3%

Conclusions

The modeling procedures used in this appendix to represent light-frame, wood shear walls were accurate in predicting the behavior of two-dimensional shear walls with various opening configurations. Based on the results described in this appendix, the following shear wall modeling methods were adopted for use in the current study:

- Framing members were modeled using the SAP2000 frame element with cross sections equal to either the actual cross section of the member or the sum of the cross sections when multiple members are placed side by side (as in double top plates or built-up headers).
- Isotropic material properties for the framing members were determined using design properties listed in AF&PA (2005a).
- Plywood and GWB sheathing were represented using a layered shell element with each layer displaced as shown in Table E-5.
- Orthotropic material properties for the plywood sheathing were determined using in-plane engineering properties from OSULaminates.
- Isotropic material properties for the GWB sheathing were determined from properties published by the Gypsum Association (2010) and inserted into the model using orthotropic material assignments.

- The effects of edge nail spacing and wall length were incorporated by adjusting the shear modulus (G_{12}) for the plywood sheathing and GWB based on the procedure described in Appendix F.
- Anchor bolts and hold-downs were modeled using directional linear spring elements oriented as shown in Figure E-4.
- Anchor bolt axial stiffness was determined from the experimental results of Seaders (2004) and shear stiffness was calculated from AF&PA (2005a).
- Hold-down stiffness was determined from publications provided by the manufacture.

APPENDIX F

SHEATHING G_{12} ADJUSTMENT PROCEDURE FOR EDGE NAIL SPACING

The effects of edge nail spacing on shear wall stiffness were incorporated through a procedure similar to that used by Martin (2010). The shear modulus (G_{12}) of the sheathing was adjusted in SAP2000 to control the stiffness of the shear wall. This was done by equating the deflection of a simple “calibration model” in SAP2000 to an expected deflection calculated using Equation C4.3.2-2 (Equation F-1, below) from AF&PA (2005b). The deflection of the calibration model is controlled by altering the G_{12} of the sheathing. Equation F-1 gives a linear approximation for shear wall deflections based on “framing bending deflection, panel shear deflection, deflection from nail slip, and deflection due to tie-down slip” (AF&PA 2005b). The effects of panel shear and nail slip are incorporated into an apparent stiffness term, G_a . Values for G_a are tabulated in AF&PA (2005b) based on sheathing material, framing lay-out and edge-nail spacing.

$$\delta_{AF\&PA} = \frac{8vh^3}{EAb} + \frac{vh}{1000G_a} + \frac{h}{b}\Delta_a \quad \text{Equation F-1}$$

Where: $\delta_{AF\&PA}$ = Expected shear wall deflection (in)
 v = Induced unit shear (plf)
 h = Shear wall height (ft)
 E = Modulus of elasticity of end posts (psi)
 A = Area of end post cross-section (in²)
 b = Shear wall length (ft)
 G_a = Apparent shear wall shear stiffness (kips/in)
 Δ_a = Total vertical elongation of wall anchorage system (in)

The following is a step-by-step example for determining the value of G_{12} for the plywood sheathing used on the shear walls in Appendix E:

Step 1: A simple calibration model was created in SAP2000 for a 12.2-m-long (40-ft-long) shear wall sheathed on one side, only, with the plywood used in shear wall validation (Appendix E). Section and material properties for the plywood are listed in Tables E-5 and E-6. In place of anchor bolts and hold-downs, rigid supports were used in the calibration model as shown in Figure F-1.

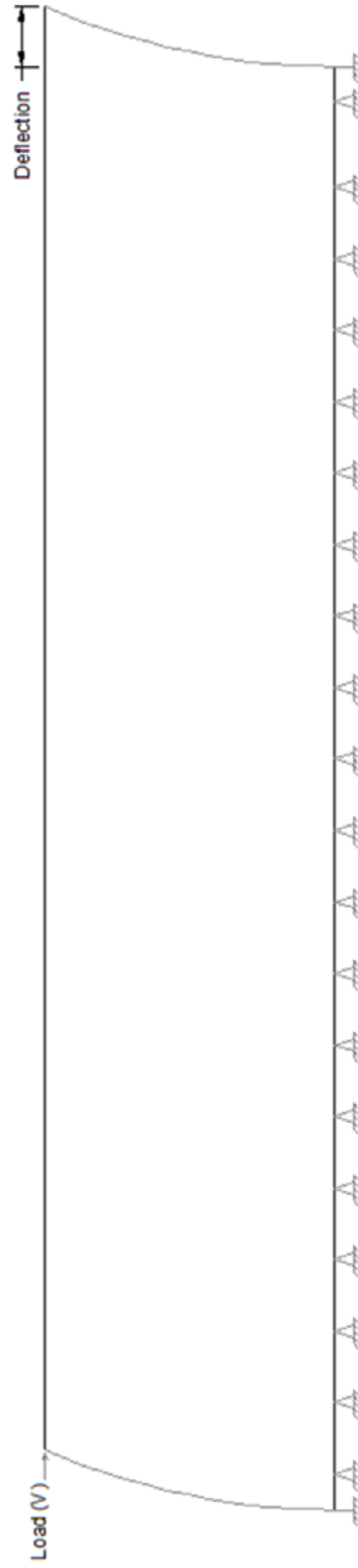
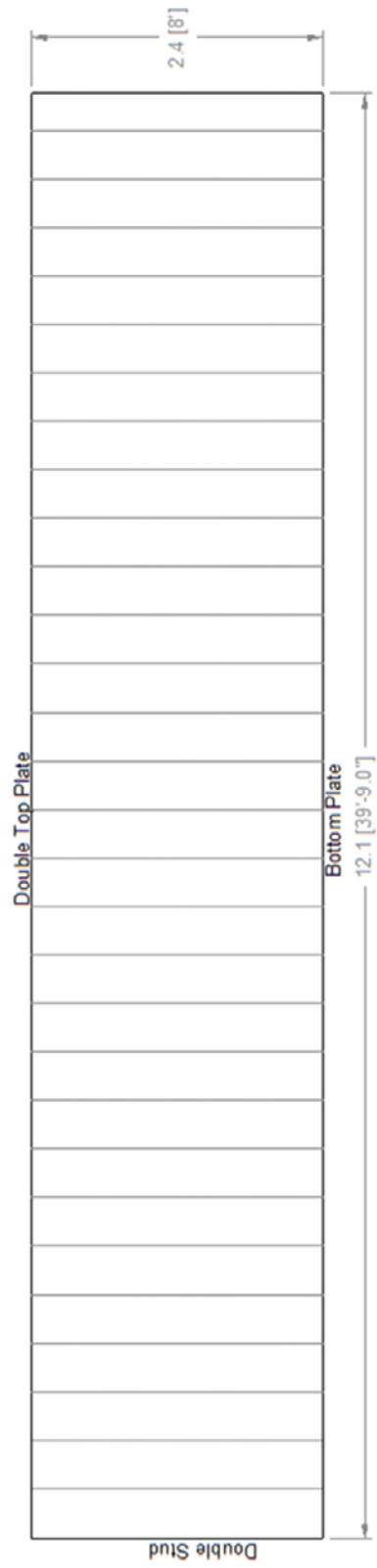


Figure F-1: (Top) framing plan for example calibration (grey studs are single studs) and (Bottom) support and loading conditions for calibration model - m (ft-in)

This was done so that the vertical elongation of wall anchorage, Δ_a , in Equation F-1 could be set equal to zero. The purpose of the calibration model is to determine the required stiffness of the plywood sheathing for a specific edge nail spacing and wall length. The effects of the anchor bolts and hold downs are incorporated into the actual wall models later on by using linear springs with realistic stiffness properties as explained in Appendix E and listed in Table E-7.

Step 2: A range of values for G_{12} of the plywood sheathing were entered into the calibration model in SAP2000. For each value of G_{12} , the deflection of the model under an applied shear force, V , of 13.3 kN (3 kips) was recorded as shown in Table F-1. G_{12} vs. deflection for the calibration model was then plotted in Figure F-2, and fitted with a power curve described by Equation F-2.

Table F-1: Example of Shear Wall Deflections vs. Sheathing Shear Modulus, G_{12} in SAP2000

Plywood Sheathing Properties used in SAP2000				Wall Deflection at $V = 13.3$ kN (3 kips) mm (in)
E_1 MPa (ksi)	E_2 MPa (ksi)	Poisson's Ratio, U_{12}	G_{12} MPa (ksi)	
5337 (774)	5337 (774)	0.021	414 (60)	0.356 (0.014)
			276 (40)	0.584 (0.023)
			138 (20)	1.295 (0.051)
			69 (10)	2.743 (0.108)

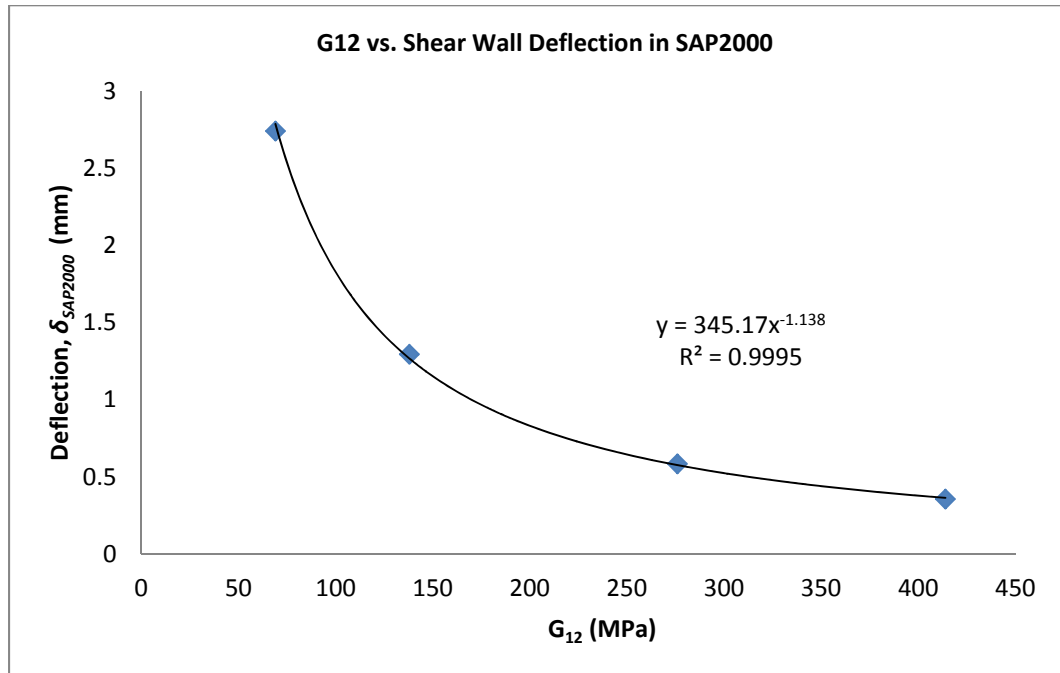


Figure F-2: Sheathing G_{12} vs. Shear Wall Deflection in SAP2000 for Example Calibration Model

$$\delta_{SAP2000} = 345.17(G_{12})^{-1.138} \quad \text{Equation F-2}$$

Where: $\delta_{SAP2000}$ = Model shear wall deflection (mm)
 G_{12} = Sheathing shear modulus (MPa)

Step 3: Using equation F-1, an expected deflection, $\delta_{AF\&PA}$, of 1.17 mm (0.046 in) was calculated for an equivalent wall with an edge nail spacing of 162 mm (6 in) and an applied shear force, V , of 13.3 kN (3 kips) as shown in Table F-2. The vertical elongation of wall anchorage, Δ_a , was set to zero as explained in Step 1.

Table F-2: Example Shear Wall Deflection Calculation using Equation F-1 (AF&PA 2005b Equation C4.3.2-2) – in specified units

Edge Nail Spacing =	6	<i>(in o.c.)</i>
Shear Wall Height (h) =	8	<i>(ft)</i>
Shear Wall Length (b) =	40	<i>(ft)</i>
¹ Modulus of Elasticity of End Posts (E) =	1.4×10^6	<i>(psi)</i>
² Area of End Post Cross-Section (A) =	10.5	<i>(in²)</i>
³ Apparent Shear Wall Shear Stiffness (G_a) =	13.2	<i>(kip/in)</i>
Total Vertical Elongation of Anchorage (Δ_a) =	0	<i>(in)</i>
⁴ Force applied to top of wall =	3	<i>(kips)</i>
Induced Unit Shear (v) =	75	<i>(plf)</i>
Calculated Deflection =	0.046	<i>(in)</i>
	1.17	<i>(mm)</i>

¹AF&PA (2005a) Table 4A

²For two 38 x 89 mm (1.5 x 3.5 in) studs

³AF&PA (2005b) Table A.4.3A (increased by 1.2 for 4-ply sheathing per Table A.4.3A, Footnote 2)

⁴Chosen arbitrarily

Step 4: Finally, the required sheathing shear modulus, G_{12} , was determined by equating $\delta_{SAP2000}$ in Equation F-2 to $\delta_{AF\&PA}$ (converted to mm) calculated in step 3. Solving for G_{12} gives a required shear modulus of 147 MPa (21.3) ksi for an edge nail spacing of 162 mm (6 in). Repeating this method for several shear walls of various lengths reveals that the required G_{12} for a specific edge nail spacing changes approximately linearly with wall length as shown in Figure F-3. Thus, for a building with multiple wall lengths and uniform edge nail spacing, this procedure is only necessary for the shortest wall and the longest wall in the building. Linear interpolation can be used for all other wall lengths.

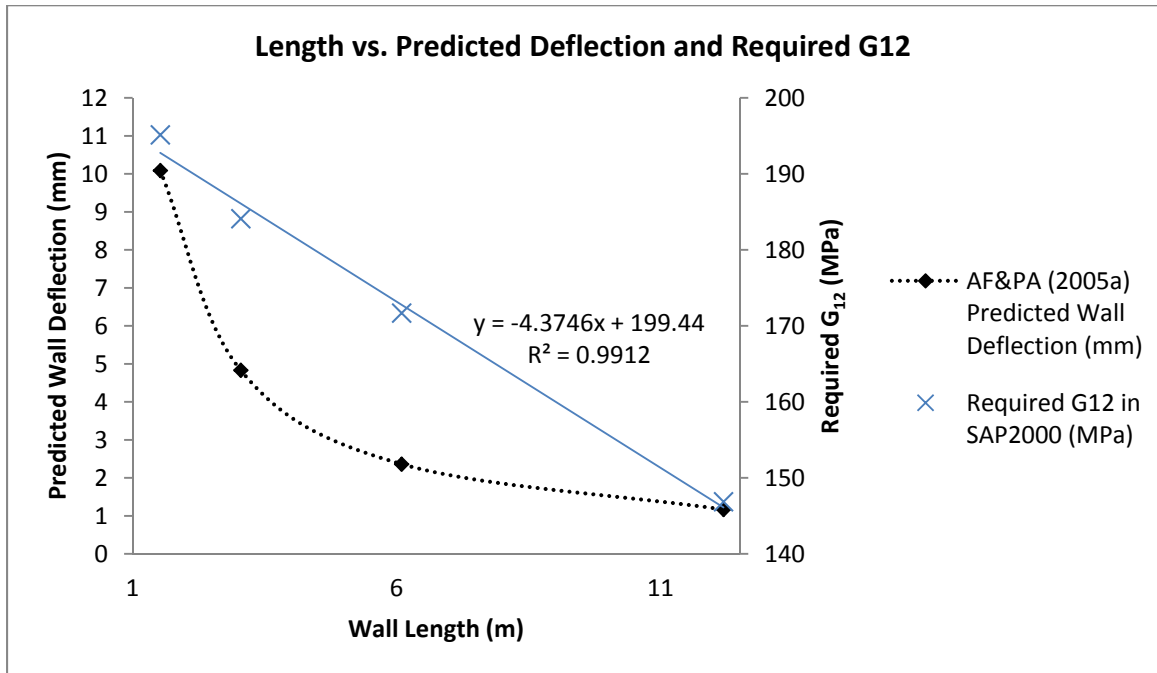


Figure F-3: AF&PA (2005b) Predicted Deflection and Required G₁₂ in SAP2000 vs. Wall Length

Through a series of tests performed on shear walls sheathed on one and two sides, Patton-Mallory et al. (1984) found that the stiffness of a shear wall sheathed on two sides is equal to the sum of two shear walls sheathed on one side only. Based on this finding, it was decided that the properties for plywood sheathing and GWB sheathing could be determined separately using the procedure above for a wall sheathed on one side only. The resulting sheathing properties can then be applied to each side of a wall sheathed on two sides.

APPENDIX G

DETAILS FOR FULL BUILDING MODEL OF PAEVERE ET AL. (2003) HOUSE

The final validation study for the modeling methods described in this paper was performed using the full-scale, realistic, L-shaped house tested by Paevere et al. (2003). The full-scale house was designed jointly by the National Association of Home Builders (NAHB) Research Center in the United States and the Commonwealth Scientific & Industrial Research Organization (CSIRO) to reflect a typical North American “stick frame” house (Paevere et al. 2003). Construction and testing of the house was done at the CSIRO division of Building, Construction and Engineering testing facility in Melbourne, Australia using equivalent Australian construction materials.

This Appendix contains construction and modeling details used for the Paevere et al. (2003) house. Additional details for the house can be found in Paevere (2002). The methods used to model the trusses, roof assemblies and wall assemblies are the same methods described in detail in Appendices B through H. It is important to note the following details:

- A modulus of elasticity of 10000 MPa (1450 ksi) given by Paevere (2002) was used for the framing members in lieu of design properties from AF&PA (2005) since radiata pine is not included in the AF&PA (2005a) NDS.
- The interior walls were modeled 25mm lower than the exterior walls so that the roof trusses spanned the exterior walls only.
- Wall 3 was connected to the roof trusses using 2-joint link elements in SAP2000 to represent the slotted brackets used by Paevere (2002). Walls 6 and 8 were not connected to the trusses.
- Wall corner framing was represented as one 90 x 90 mm (3.5 x 3.5 in) member to simplify the modeling process.

Table G-1: Construction Details from Paevere (2002)

<p><i>Wall Framing:</i></p> <p><u>Studs:</u> 90x35 mm Machine Graded Pine (MGP) 10 spaced 400 mm on center without blocking</p> <p><u>Bottom Plate:</u> 90x45 mm MGP 10</p> <p><u>Top Plate:</u> double 90x35 mm MGP 10</p> <p><u>Header Plate:</u> 190x90 mm (short span) or 290x90 mm (long span)</p> <p><u>MOE:</u> 10000 MPa (short duration)</p> <p><u>Average Density at 12% MC:</u> 550 kg/m³</p>
<p><i>Bottom Plate Anchorage:</i></p> <p><u>Anchor Bolts:</u> 12.7 mm bolts with plate washers spaced approximately 1000 mm</p>
<p><i>Roof Framing:</i></p> <p><u>Trusses:</u> Pre-fabricated 'gang-nailed' pine trusses spaced 600 mm on center without blocking</p> <p><u>Truss Connectors:</u> Connected to top plate with pryda 'triple-grip' plate connectors</p> <p><u>Truss Top and Bottom Chords:</u> 90x35 mm MGP 10</p> <p><u>Truss Web Members:</u> 70x35 mm MGP 10</p>
<p><i>Plywood Bracing:</i></p> <p><u>Walls:</u> 2400x1200x9.5 mm F11 Bracing Ply (Laid Vertically)</p> <p><u>Roof:</u> 2400x1200x12.5 mm F11 Ply (Laid Horizontally)</p> <p><u>Bending MOE:</u> 10500 MPa</p>
<p><i>Gypsum Board Lining:</i></p> <p>1200x2400x13 mm Gypsum Wall Board (Laid Horizontally)</p>
<p><i>Sheathing Nails:</i></p> <p>2.87x50 mm machine driven nails spaced 150 mm on perimeter and 300 mm in field</p>
<p><i>Gypsum Board Lining:</i></p> <p>6 gauge x 30 mm Needle-point Type 1 Gypsum Board Screws spaced 300 mm</p>

Table G-2: Frame Sections Used in SAP2000 Model: Modeled through center of cross section unless otherwise noted.

Name of Frame Section	Cross Section Dimensions
190x90 Header	190 x 90 mm (7.5 x 3.5 in)
290x90 Header	290 x 90 mm (11.4 x 3.5 in)
35x90 Header	35 x 90 mm (1.4 x 3.5 in) <i>(used above doorways in interior walls)</i>
290x90 Garage Beam	290 x 90 mm (11.4 x 3.5 in) <i>(modeled through top of section)</i>
Single Stud	35 x 90 mm (1.4 x 3.5 in)
Double Stud	70 x 90 mm (2.8 x 3.5 in)
Corner Stud	90 x 90 mm (3.5 x 3.5 in)
Double Top Plate	90 x 70 mm (3.5 x 2.8 in) <i>(modeled through top of section)</i>
Bottom Plate	90 x 45 mm (3.5 x 1.8 in) <i>(modeled through bottom of section)</i>
Truss Chord	35 x 90 mm (1.4 x 3.5 in) <i>(modeled through bottom of section)</i>
Truss Web	35 x 70 mm (1.4 x 2.8 in) <i>(modeled through bottom of section)</i>

Table G-3: Sheathing Material Properties used in SAP2000 Model

^aPlywood Sheathing (for roof)	Orthotropic Properties <ul style="list-style-type: none"> • $E_1 = 8280$ MPa (1201 ksi) • $E_2 = 2393$ MPa (347 ksi) • $U_{12} = 0.011$ • $G_{12} = 482$ MPa (70 ksi) } <i>From OSULaminates (Flexural Properties)</i>
^bPlywood Sheathing (for walls)	Orthotropic Properties <ul style="list-style-type: none"> • $E_1 = 7017$ MPa (1018 ksi) • $E_2 = 3657$ MPa (530 ksi) • $U_{12} = 0.016$ • $G_{12} = \text{See Figure G-1(a)}$ } <i>From OSULaminates (In-Plane Properties)</i>
Gypsum Wall Board (for walls and ceiling)	Isotropic Properties <ul style="list-style-type: none"> • $E_1 = E_2 = 1820$ MPa (264 ksi) • $U_{12} = 0.3$ • $G_{12} = \text{See Figure G-1(b)}$ } <i>Gypsum Association (2010)</i>

a. Assumed: 5-ply sheathing, 0°-90°-0°-90°-0° ply orientation, species group 1

b. Assumed: 3-ply sheathing, 0°-90°-0° ply orientation, species group 1

Table G-4: Properties for Wall Anchorage used for SAP2000 Model

Anchorage Device	Stiffness		Placement
	Shear ^a	Axial ^b	
Anchor Bolts	16.7 kN/mm (95.5 kip/in)	6.1 kN/mm (35 kip/in)	1.0 m (3.3 ft) maximum (See Figure G-2)

a. Calculated from AF&PA (2005a) Section 10.3.6

b. From Seaders (2004)

Table G-5: Material Densities used for Building Self-Weight

Material	Density kg/m ³ (pcf)	Source
MGP 10 Framing Members	550 (1.07)	<i>Paevere (2002)</i>
F11 Plywood	600 (1.16)	<i>EWPA (2009)</i>
Gypsum Wall Board	772 (1.50)	<i>Gypsum Association (2010)</i>

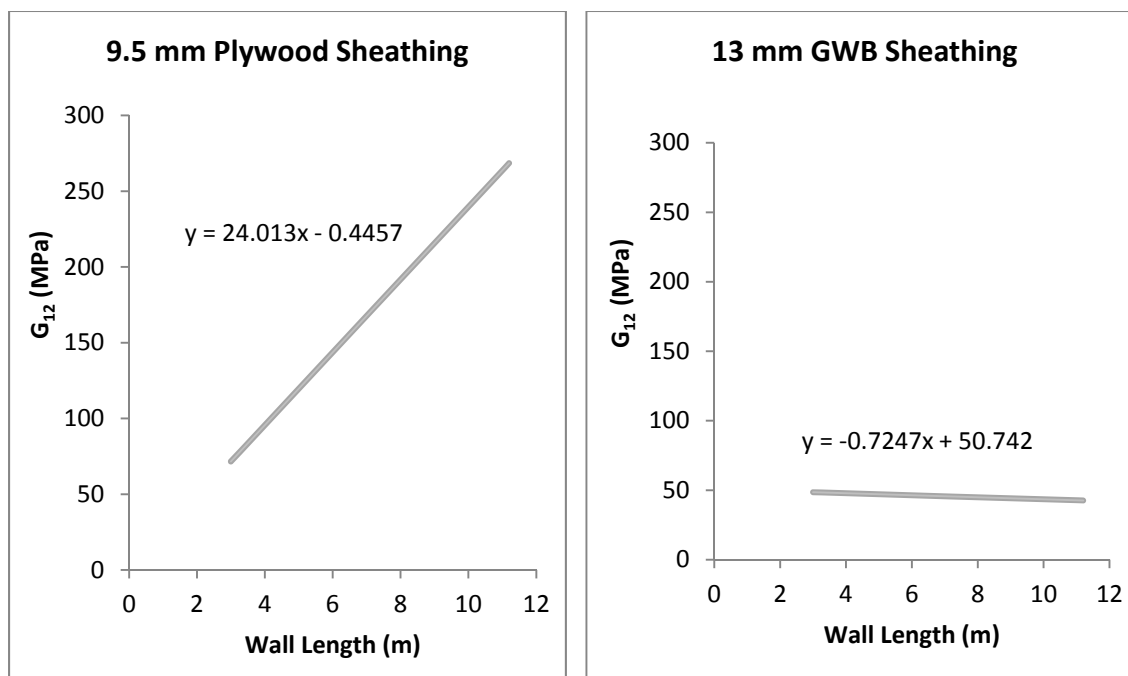


Figure G-1: G_{12} vs. Wall Length for 9.5 mm Plywood and 13 mm GWB Sheathing –
 Calculated using the procedure from Appendix F. Note: parameters for the GWB were determined based on a fastener edge spacing of 200 mm (8 in) rather than 300 mm (12 in) since the latter is not included in AF&PA (2005b) Table 4.3B.

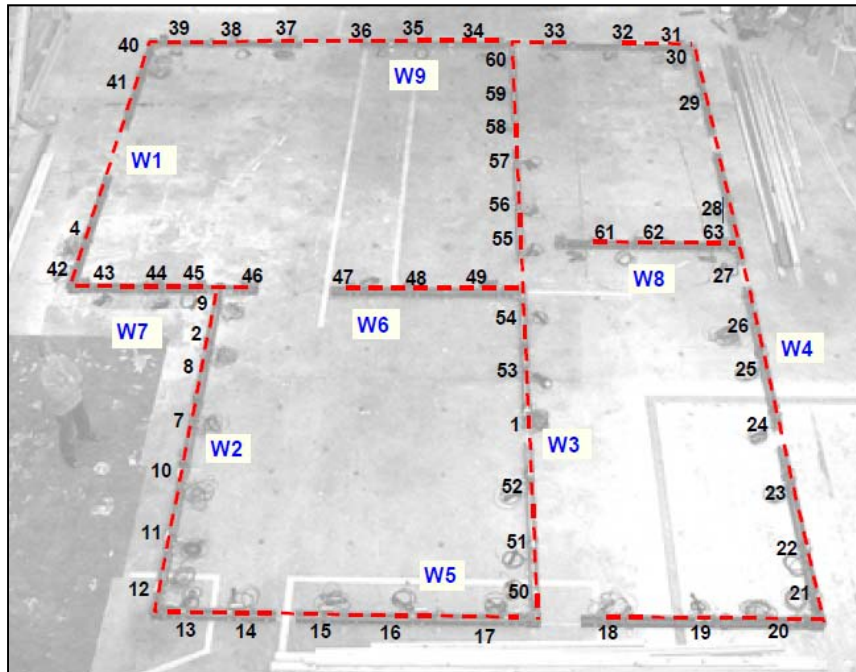


Figure G-2: Anchor Bolt and Load Sensor Placement (Paevere 2002)

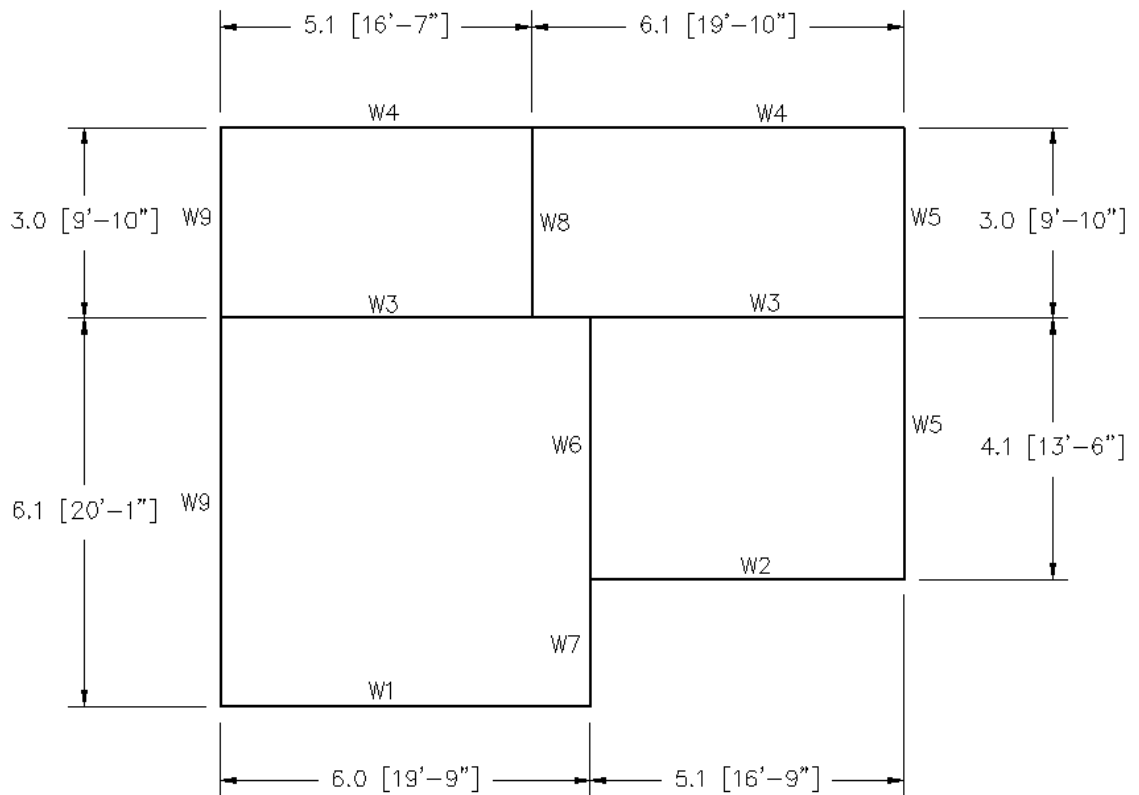


Figure G-3: Wall Locations Used in SAP2000 Model – m (ft-in)

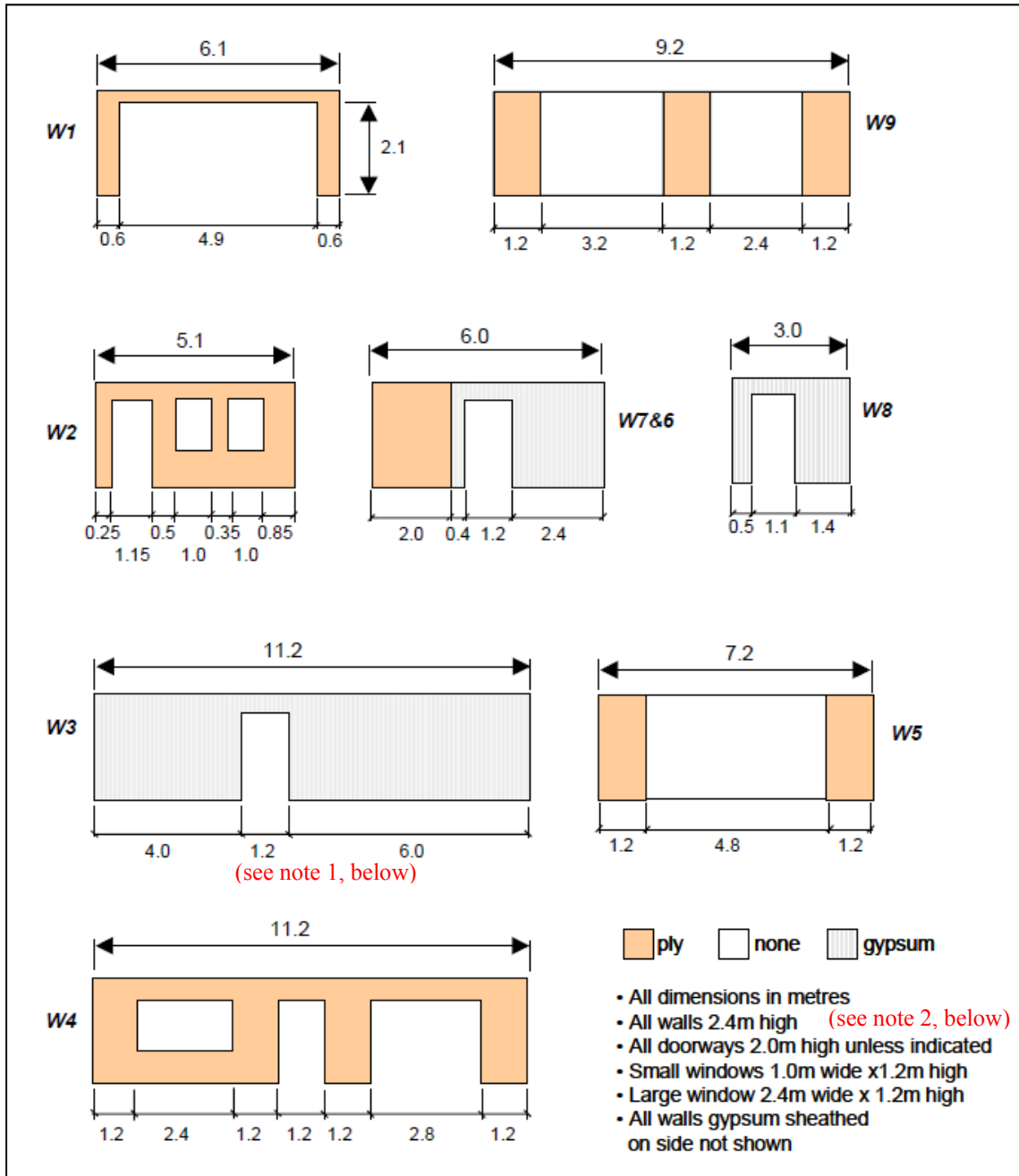


Figure G-4: Wall Configurations (Paevere 2002) – Note: (1) The doorway in W3 was relocated as shown in Figure G-5 based on the point of intersection between W6 and W3.

(2) Interior walls were modeled 25 mm shorter than the exterior walls (Dr. Phillip Paevere, personal communication, June 25, 2012).

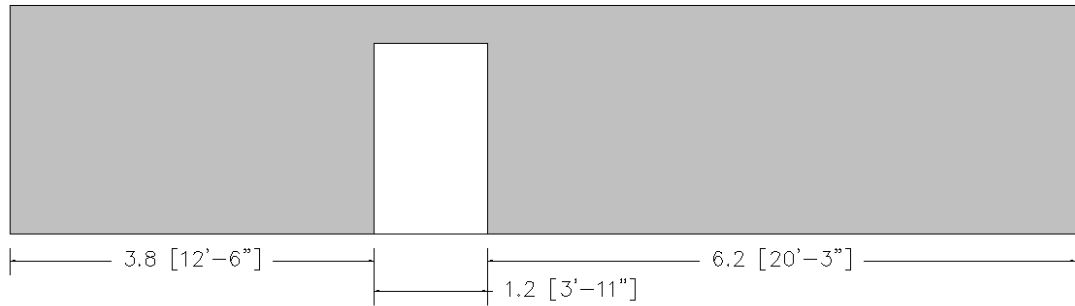


Figure G-5: Wall 3 Configuration used for SAP2000 Model – m (ft-in)

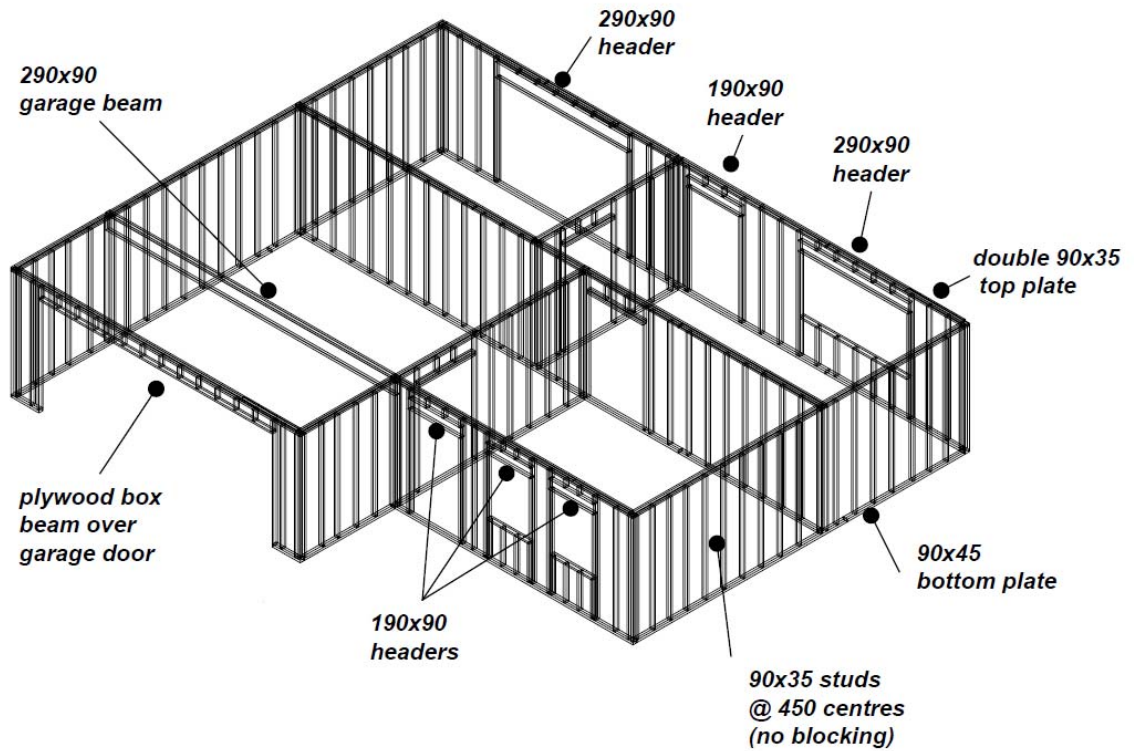


Figure G-6: Wall Framing (Paevere 2002)

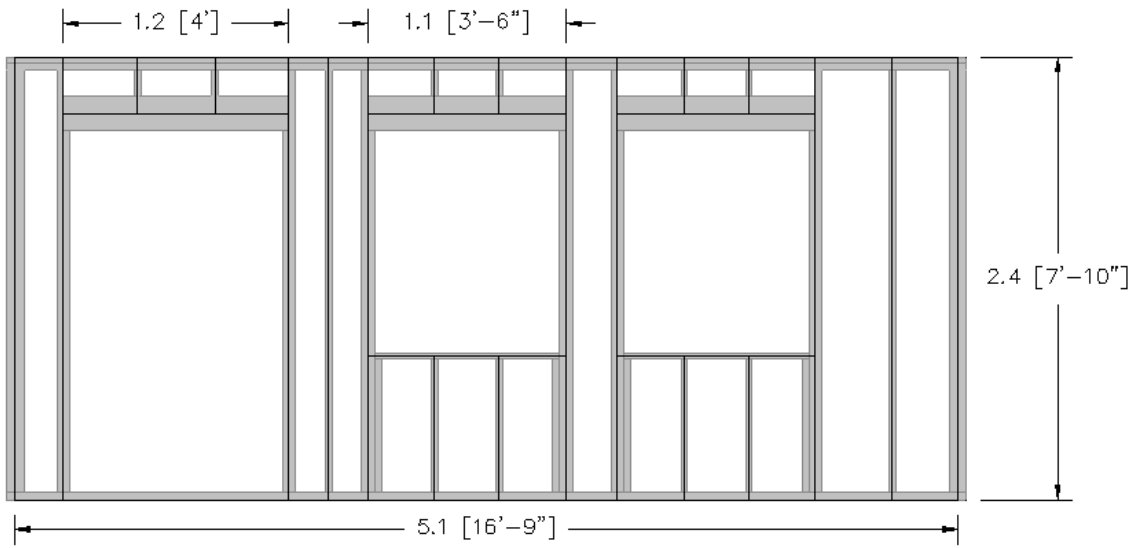


Figure G-7: Example of Assumed Framing with SAP2000 Wire Frame Overlay for Wall 2 – m (ft-in)

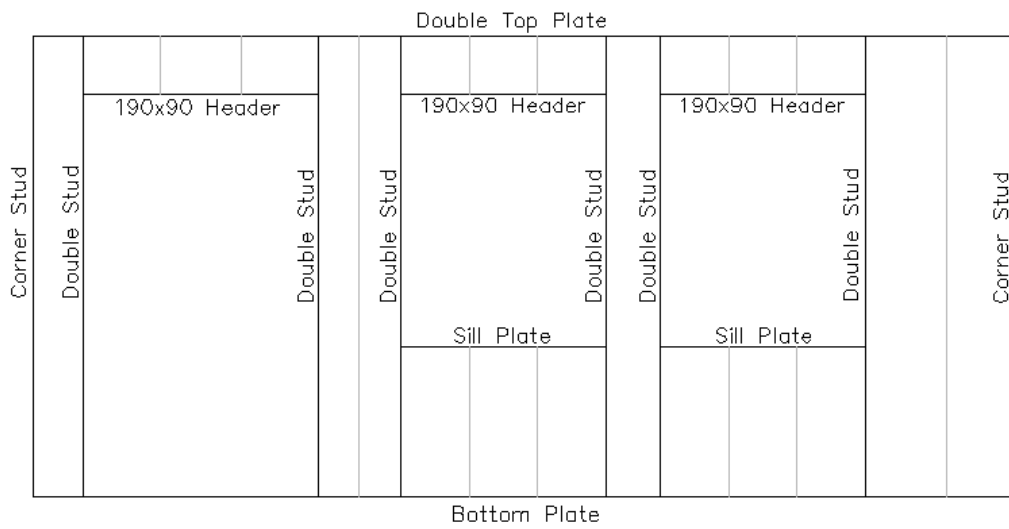


Figure G-8: Example Frame Section Assignment for Wall 2 – All connections are pinned

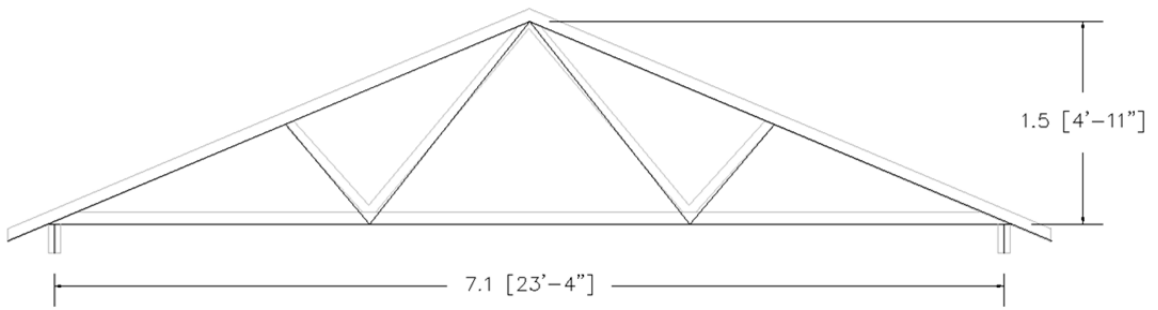


Figure G-9: Assumed Framing with SAP2000 Wire Frame Overlay for Type A Trusses – m (ft-in)

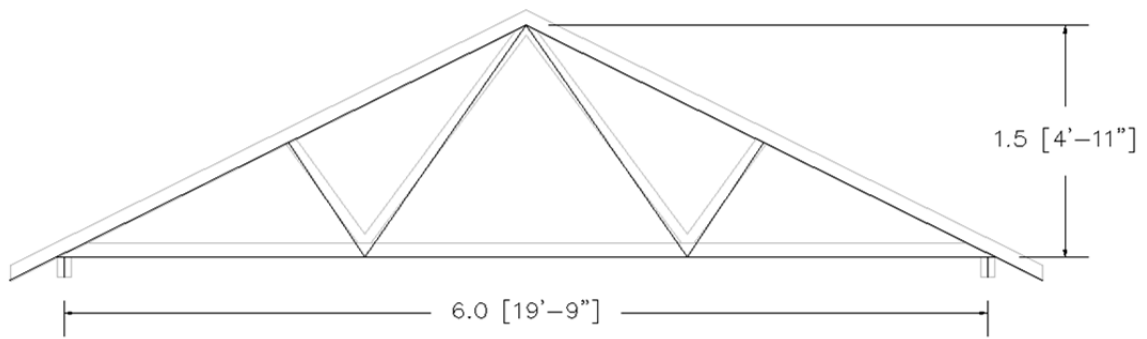


Figure G-10: Assumed Framing with SAP2000 Wire Frame Overlay for Type B Trusses – m (ft-in)

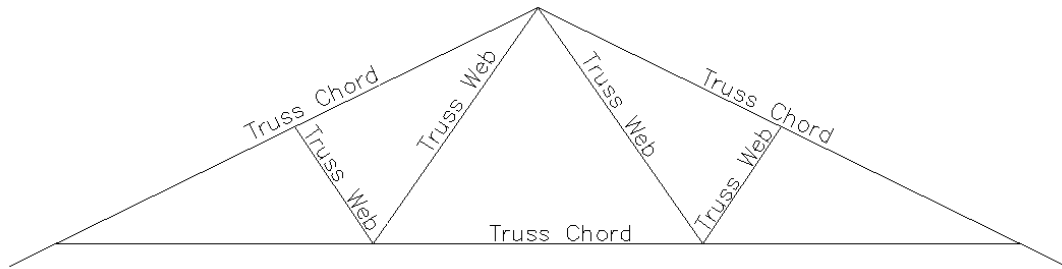


Figure G-11: Example Frame Section Assignment used for Trusses

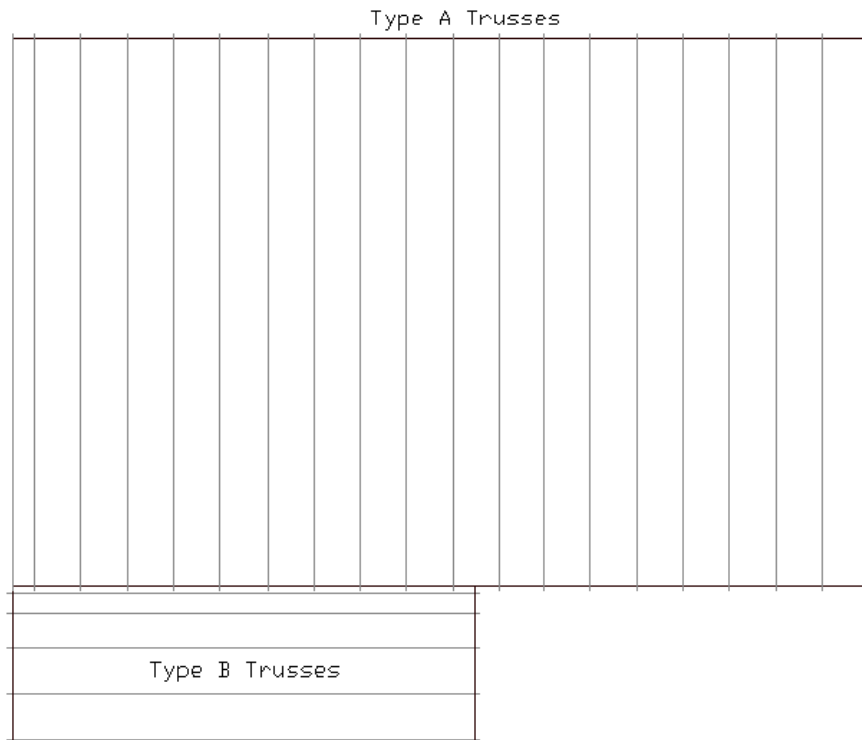


Figure G-12: Truss Layout for Type A and Type B Trusses

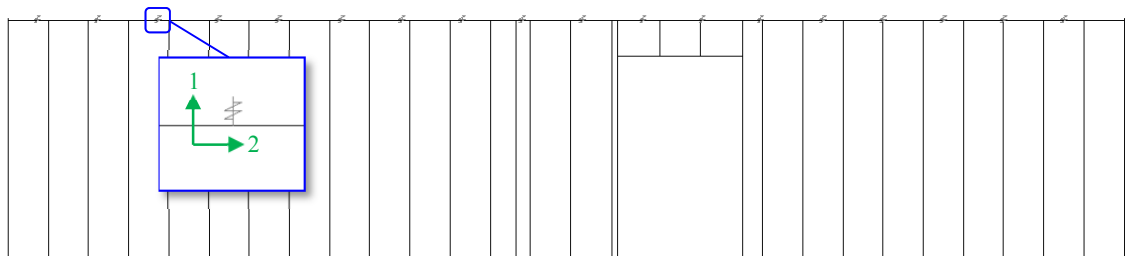


Figure G-13: 2-Joint Links used to Connect Wall 3 to Truss Bottom Chords – U2
 (translation along the wall) is “fixed” for all links

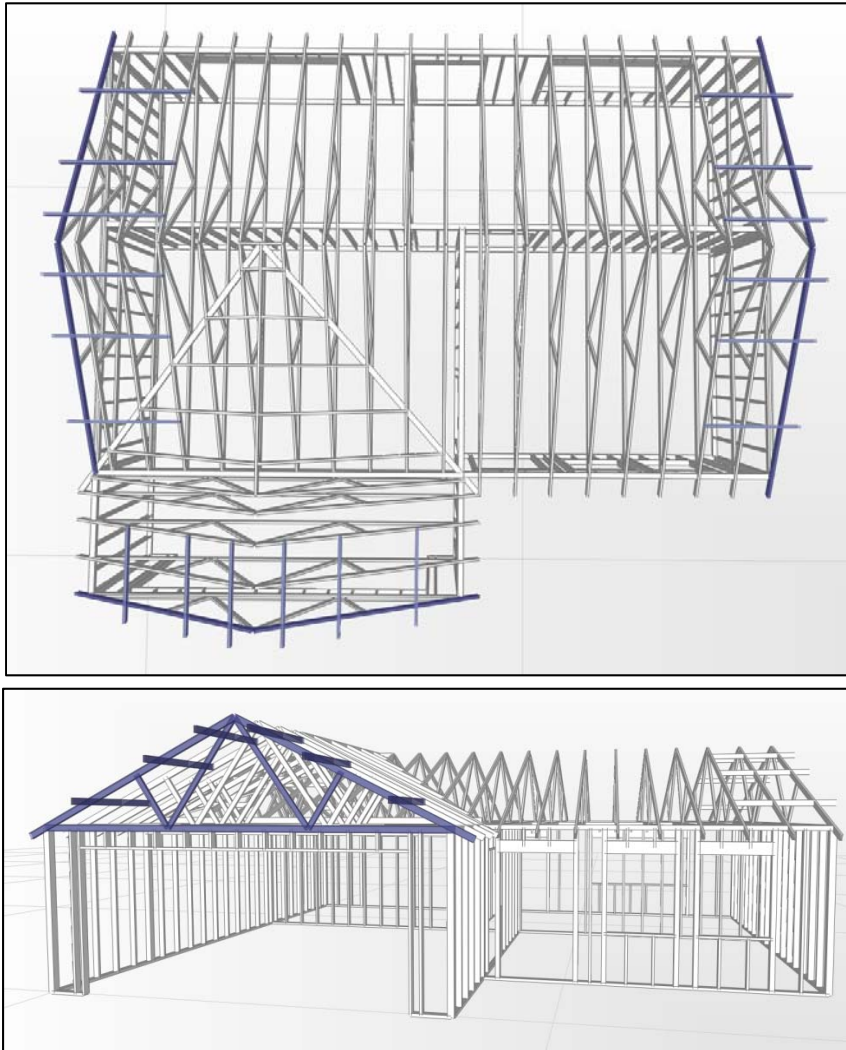


Figure G-14: Gable-End Overhang Framing used in SAP2000 Model

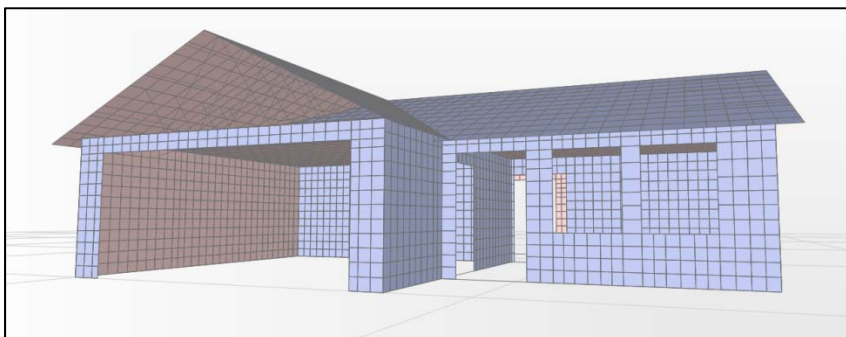


Figure G-15: Gable-End Sheathing Placement used in SAP2000 Model

APPENDIX H

FULL BUILDING MODEL VALIDATION

Paevere et al. (2003) ran a series of static load tests on the full- scale house described in Appendix G including:

- Gravity loads only (load case 1)
- Lateral point loads applied in N-S and E-W directions at various locations along the top plates of the walls (load cases 2 through 12)
- Lateral point loads applied at various angles to the roof ridge above wall 5 (load cases 13 through 15)

This appendix contains plots comparing the load distributions in the house tested by Paevere et al. (2003) to the SAP2000 model from the current study for load cases 2 through 15. The load distributions were determined by summing the reactions in the direction parallel to the applied loads at the anchor bolts underneath the in-plane walls. For load cases 13 through 15, where the load is applied at an angle, the load vector was factored into N-S and E-W components applied simultaneously at the ridge.

In Load Case 1 (gravity only loads), Paevere (2002) noted that several load cells were showing negative (uplift) reactions likely due to residual stresses from construction (Paevere (2002)). Consequently, the load distribution to individual walls for Load Case 1 was not considered for this validation. The total self weight of the model was 55.7 kN, which is 9.6% larger than the 50.8 kN reported by Paevere et al (2003). This discrepancy could be due to the previously discussed uplift reactions seen in the tests, differences in modeled and actual material densities and differences in over-framing used to frame the roof above the garage. Details for the over-framing were not included in Paevere et al. (2003). The load cells were zeroed for Load Cases 2 through 15 to negate the effects of self weight, therefore the self weight of the model was also set to zero for these cases.

Load Case 2: Wall 1 Loaded

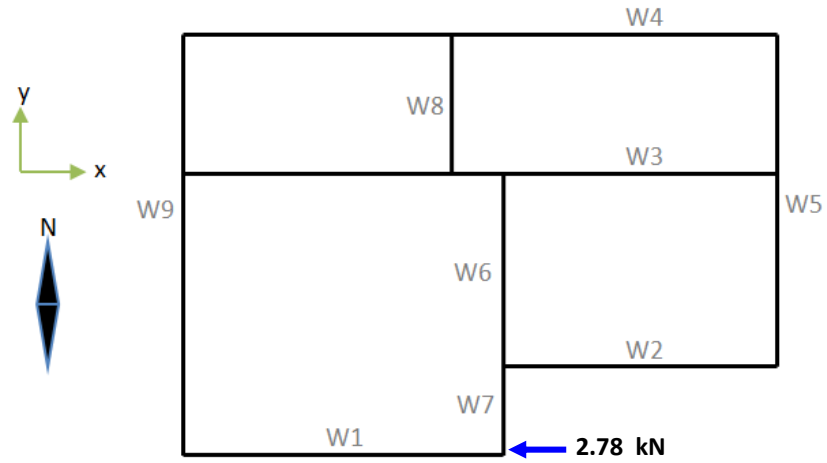


Figure H-1: Load Case 2 – 2.78 kN Applied to Top-Plate at Wall 1

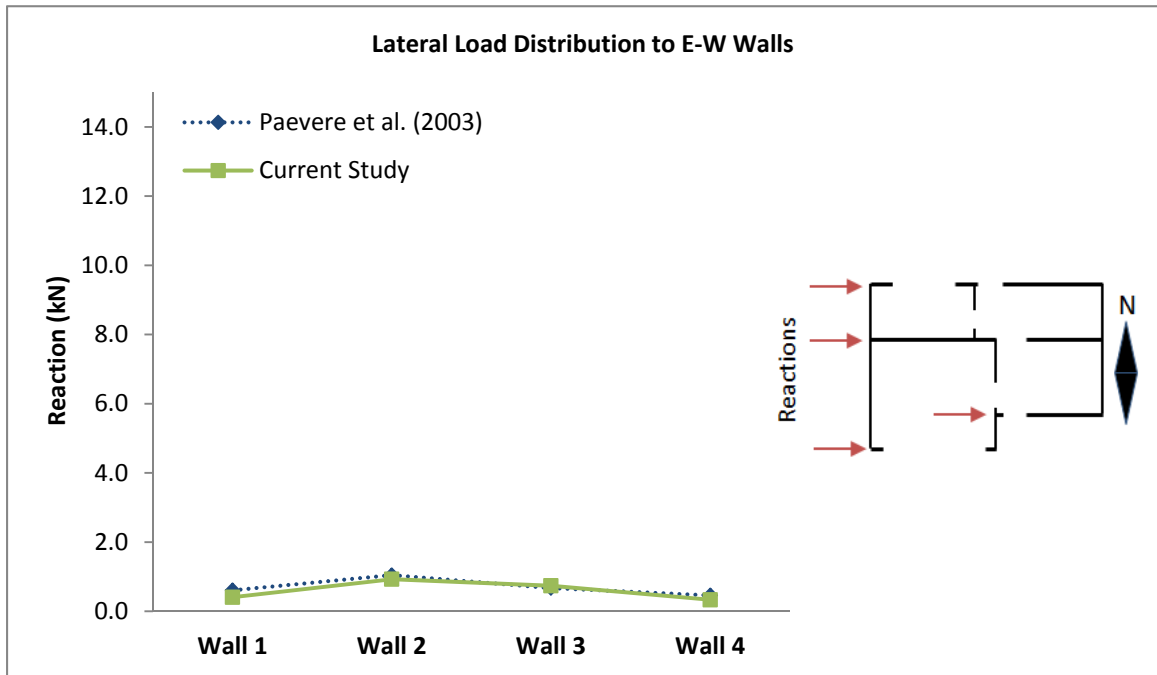


Figure H-2: Lateral Load Distribution to E-W Walls (Load Case 2)

Load Case 3: Wall 2 Loaded

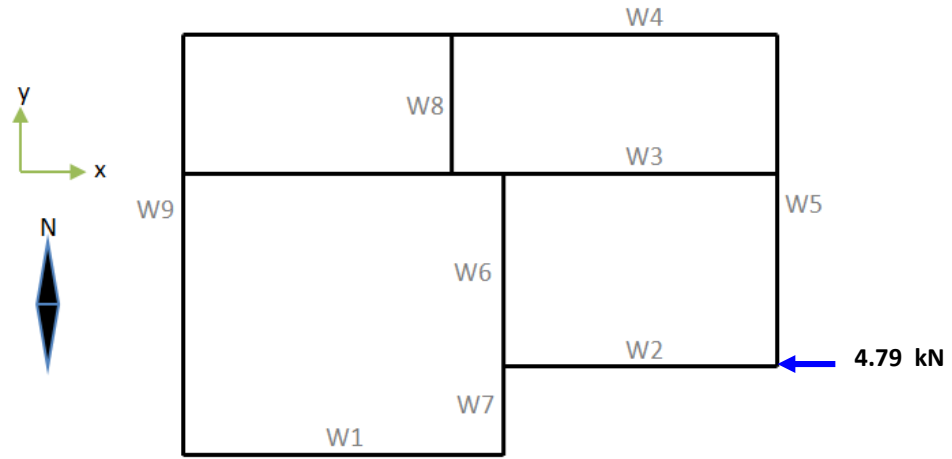


Figure H-3: Load Case 3 – 4.79 kN Applied to Top-Plate at Wall 2

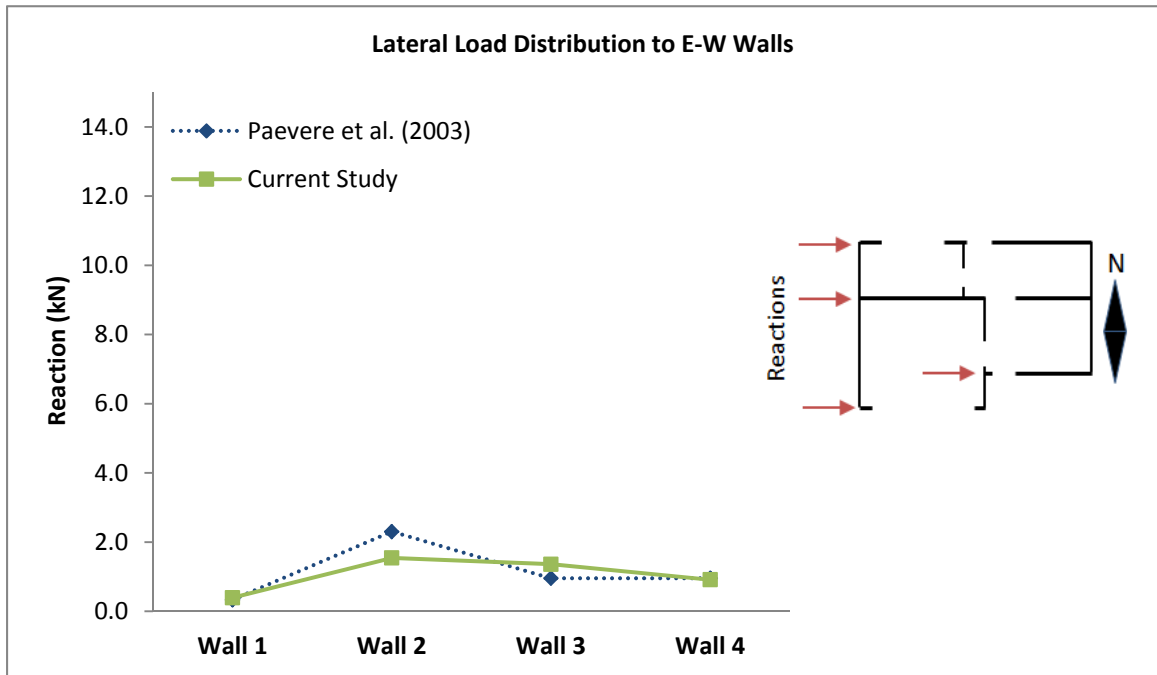


Figure H-4: Lateral Load Distribution to E-W Walls (Load Case 3)

Load Case 4: Wall 3 Loaded

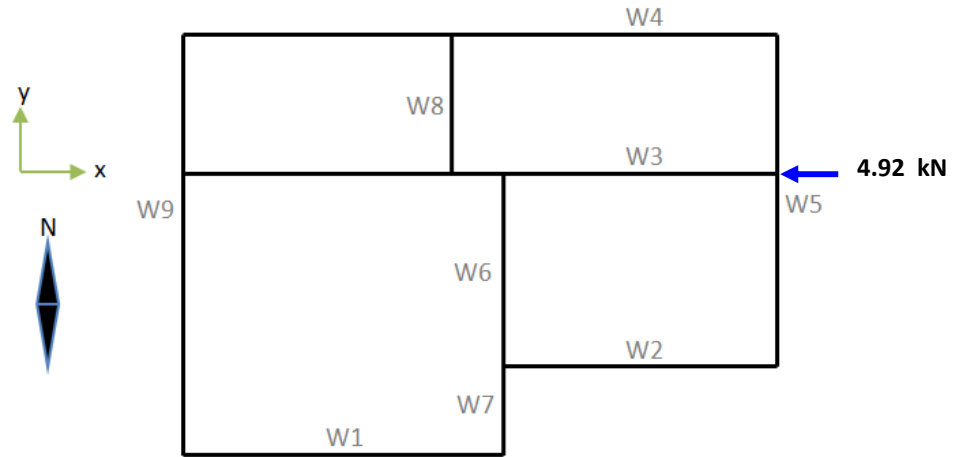


Figure H-5: Load Case 4 – 4.92 kN Applied to Top-Plate at Wall 3

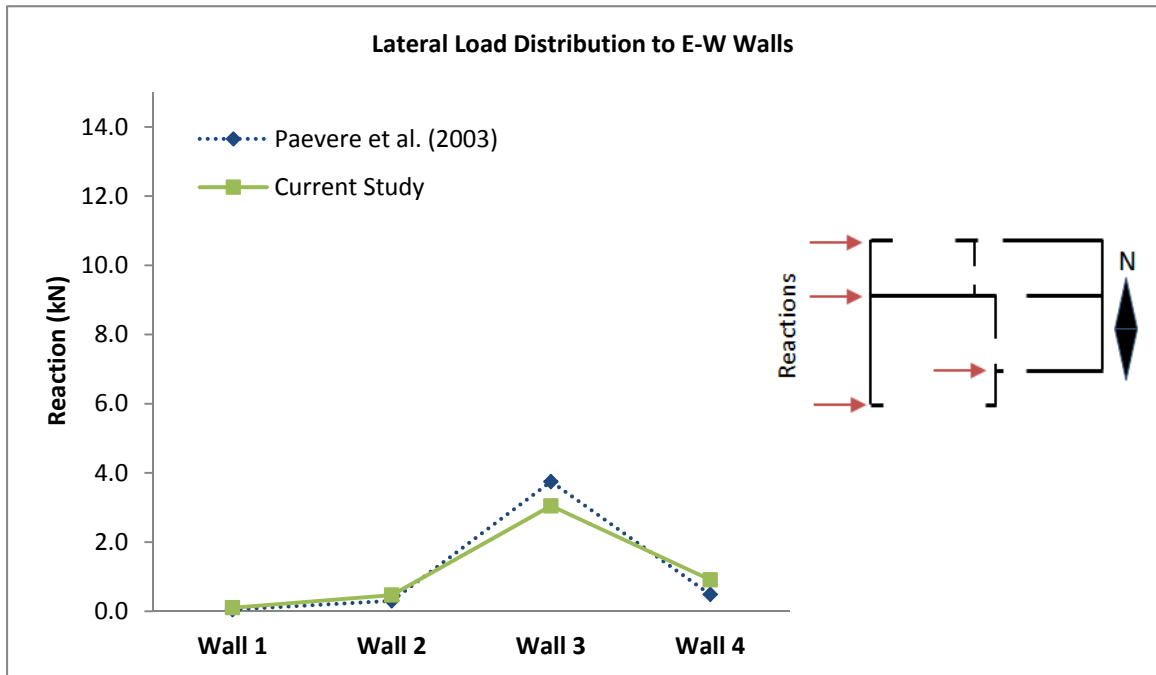


Figure H-6: Lateral Load Distribution to E-W Walls (Load Case 4)

Load Case 5: Wall 4 Loaded

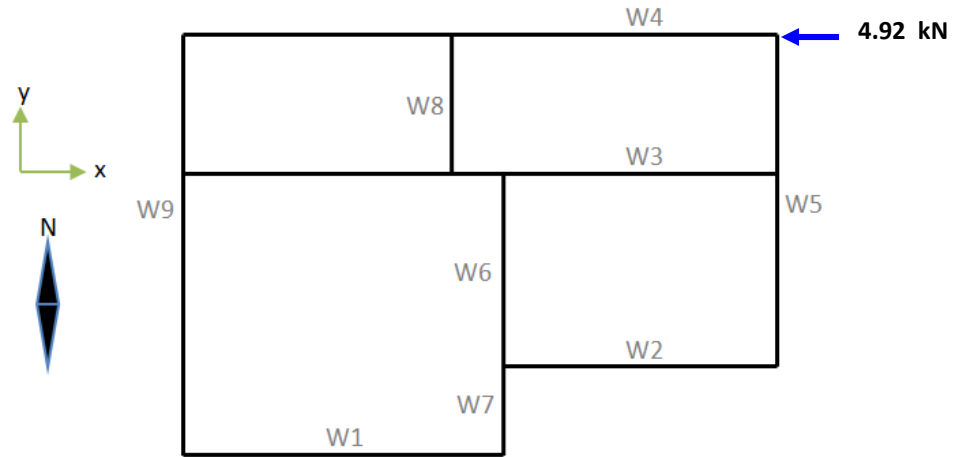


Figure H-7: Load Case 5 – 4.92 kN Applied to Top-Plate at Wall 4

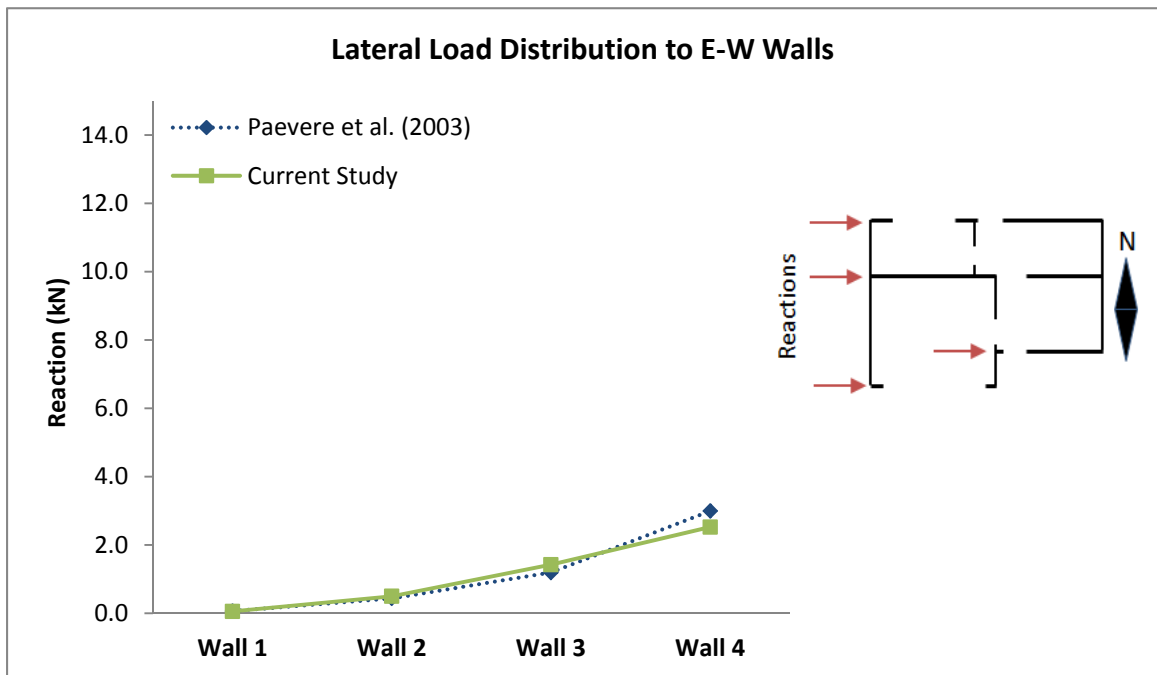


Figure H-8: Lateral Load Distribution to E-W Walls (Load Case 5)

Load Case 6: Wall 8 Loaded

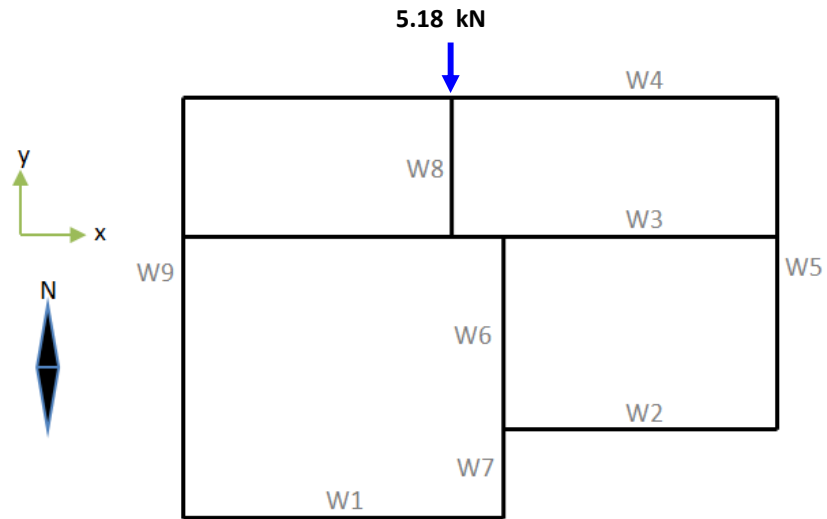


Figure H-9: Load Case 6 – 5.18 kN Applied to Top-Plate at Wall 8

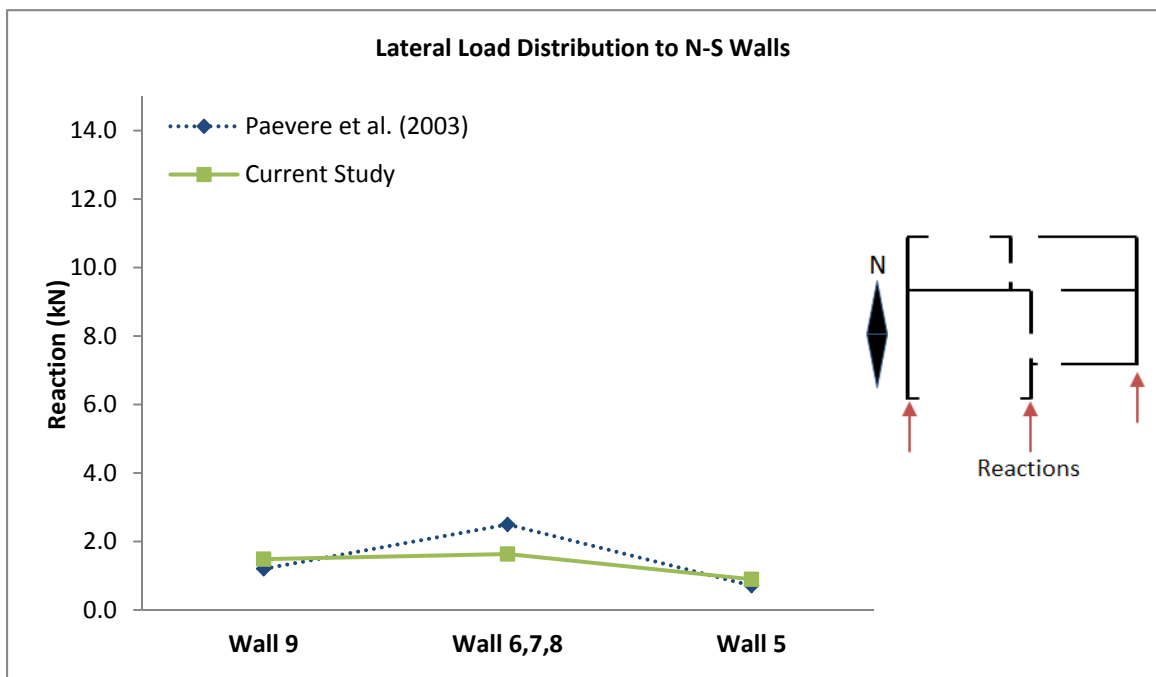


Figure H-10: Lateral Load Distribution to N-S Walls (Load Case 6)

Load Case 7: Walls 2 and 8 Loaded

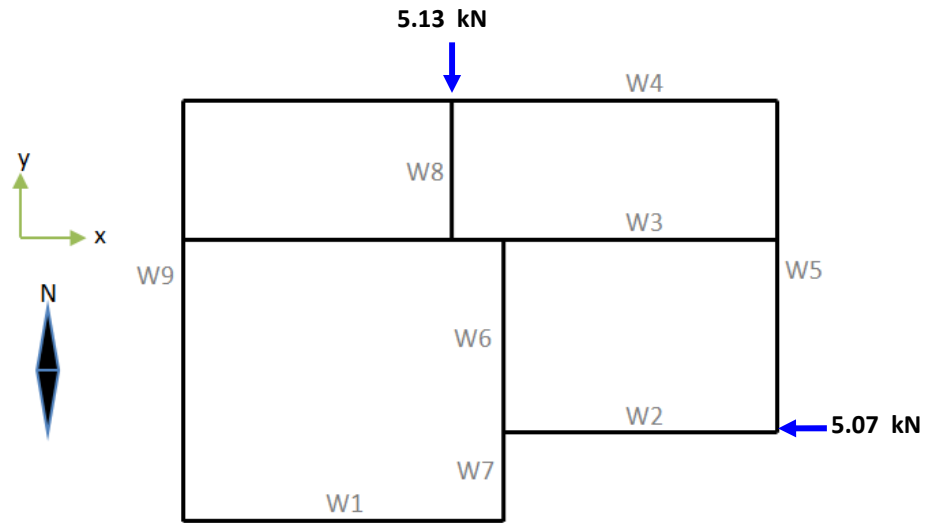


Figure H-11: Load Case 7 – 5.07 kN Applied to Top-Plate at Wall 2 and 5.13 kN Applied to Top-Plate at Wall 8

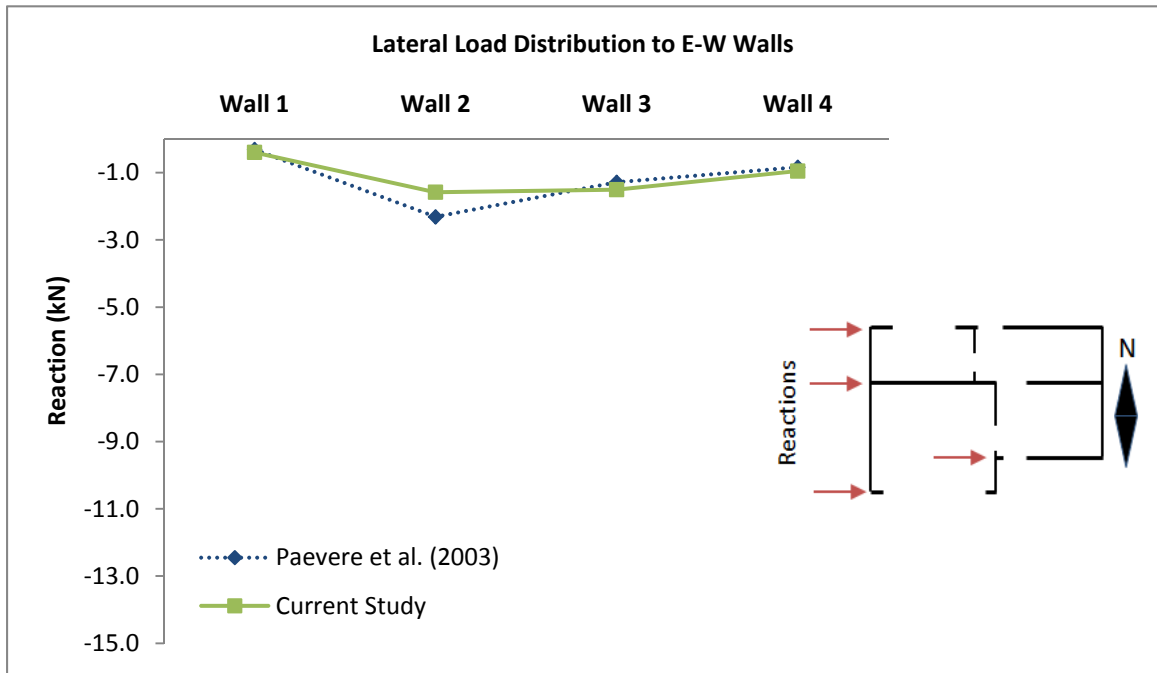


Figure H-12: Lateral Load Distribution to E-W Walls (Load Case 7)

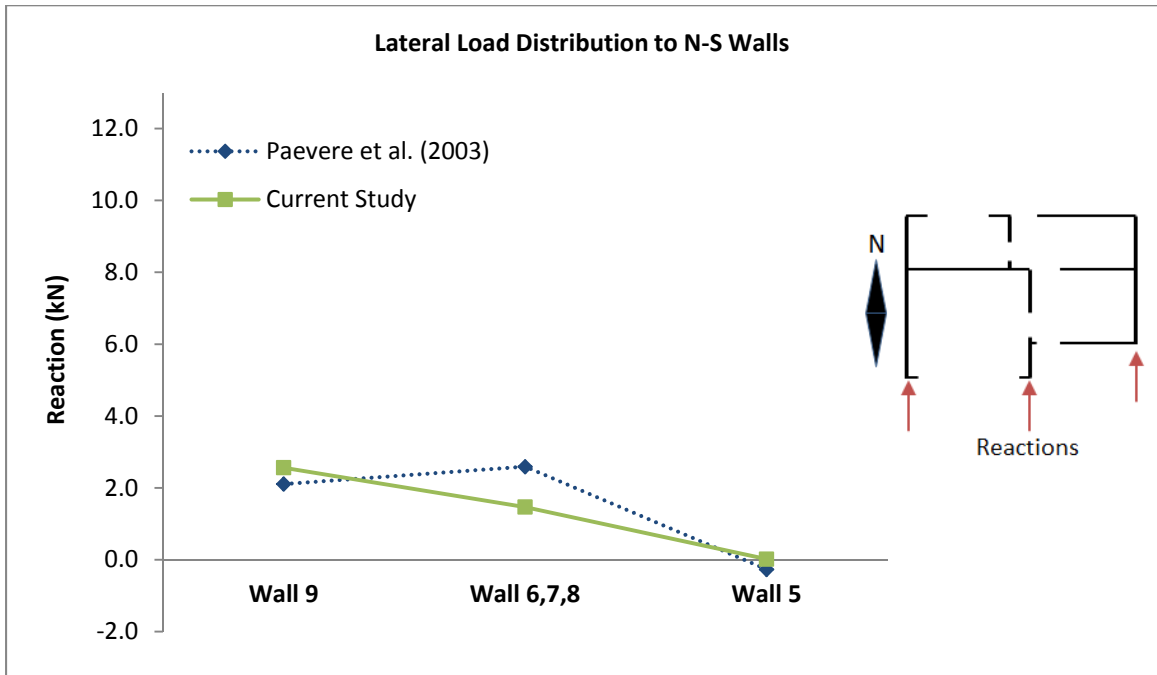


Figure H-13: Lateral Load Distribution to N-S Walls (Load Case 7)

Load Case 8: Wall 5 Loaded

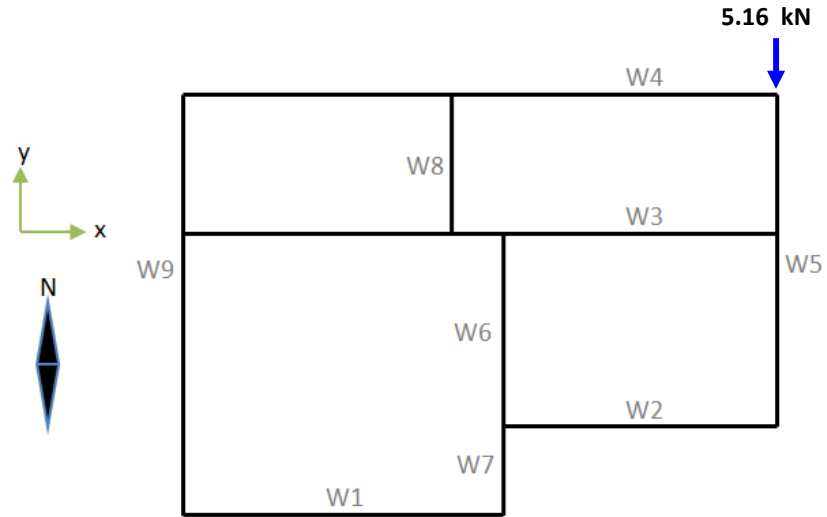


Figure H-14: Load Case 8 – 5.16 kN Applied to Top-Plate at Wall 5

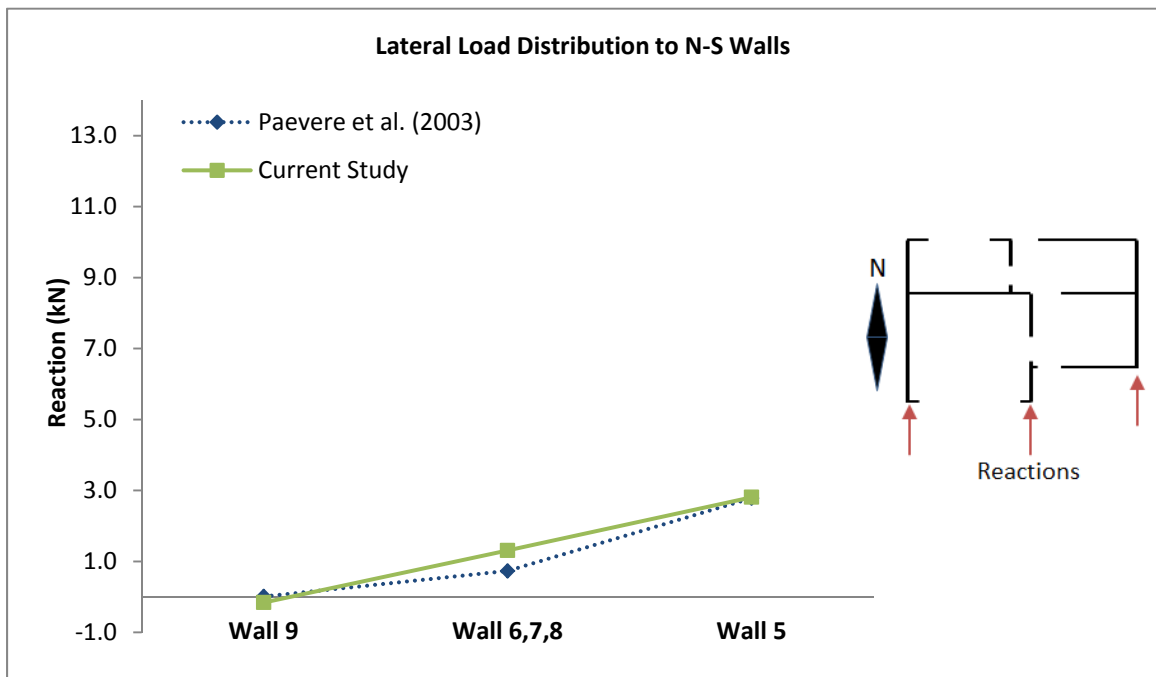


Figure H-15: Lateral Load Distribution to N-S Walls (Load Case 8)

Load Case 9: Walls 4 and 5 Loaded

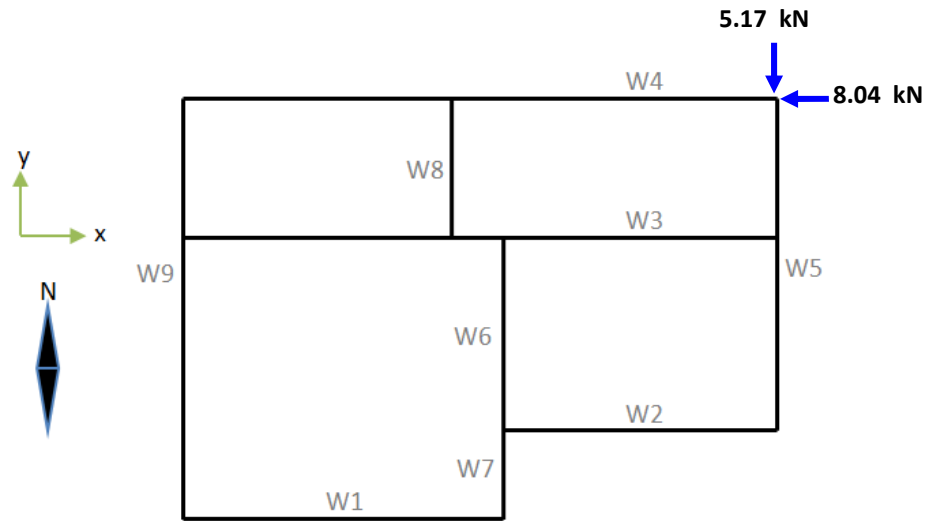


Figure H-16: Load Case 9 – 8.04 kN Applied to Top-Plate at Wall 4 and 5.17 kN Applied to Top-Plate at Wall 5

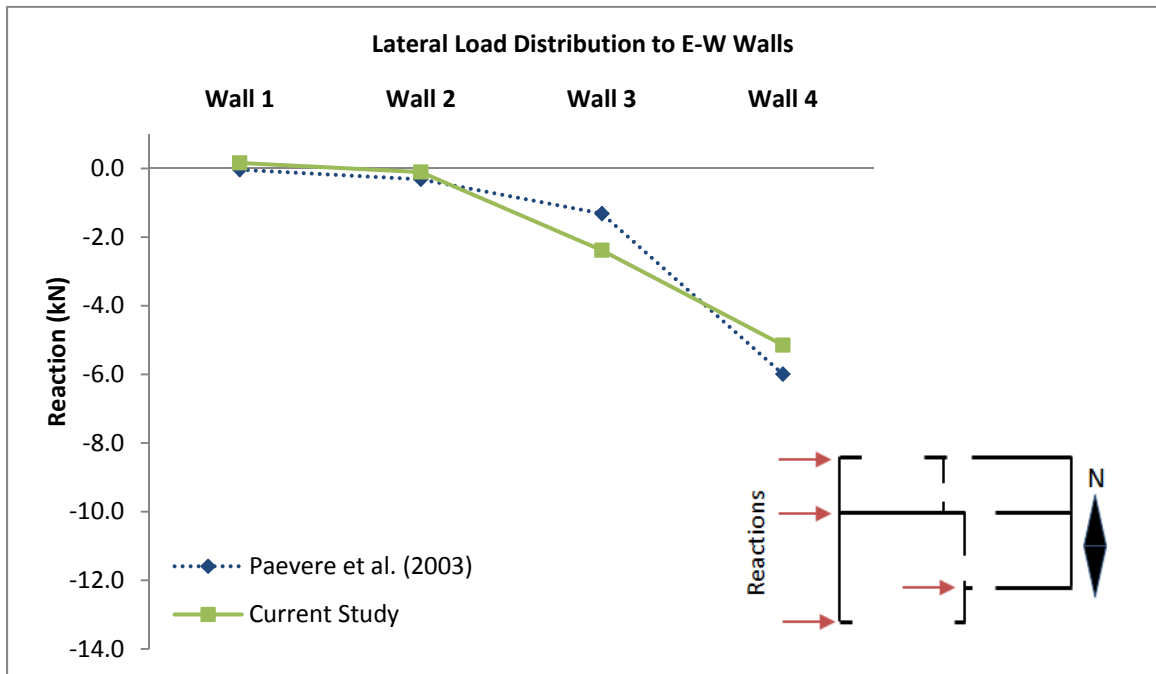


Figure H-17: Lateral Load Distribution to E-W Walls (Load Case 9)

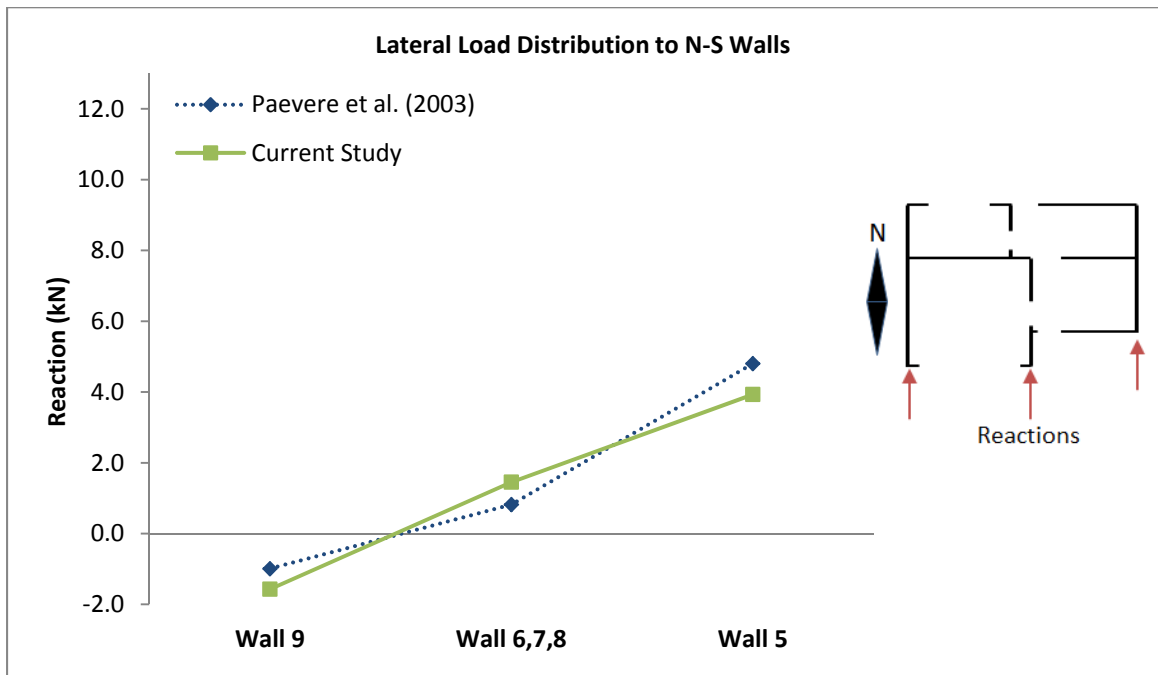


Figure H-18: Lateral Load Distribution to N-S Walls (Load Case 9)

Load Case 10: Walls 2 and 5 Loaded

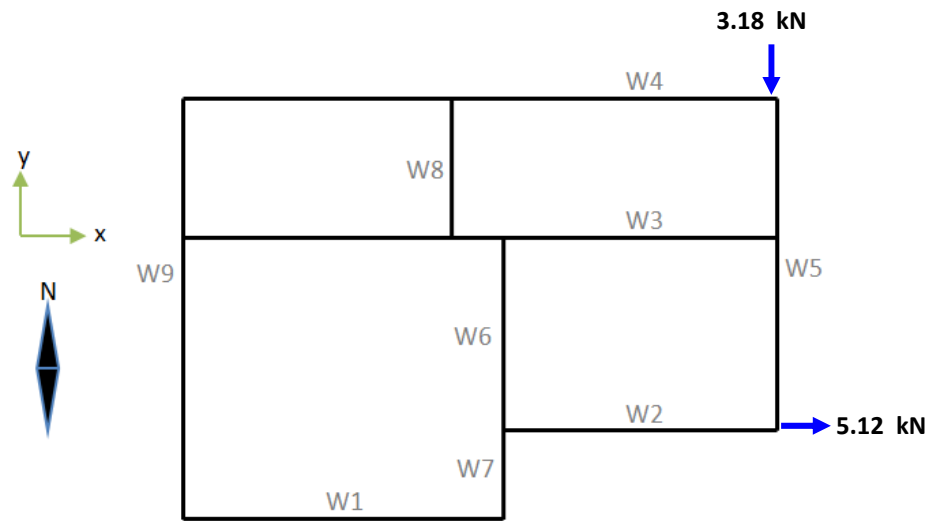


Figure H-19: Load Case 10 – 5.12 kN Applied to Top-Plate at Wall 2 and 3.18 kN Applied to Top-Plate at Wall 5

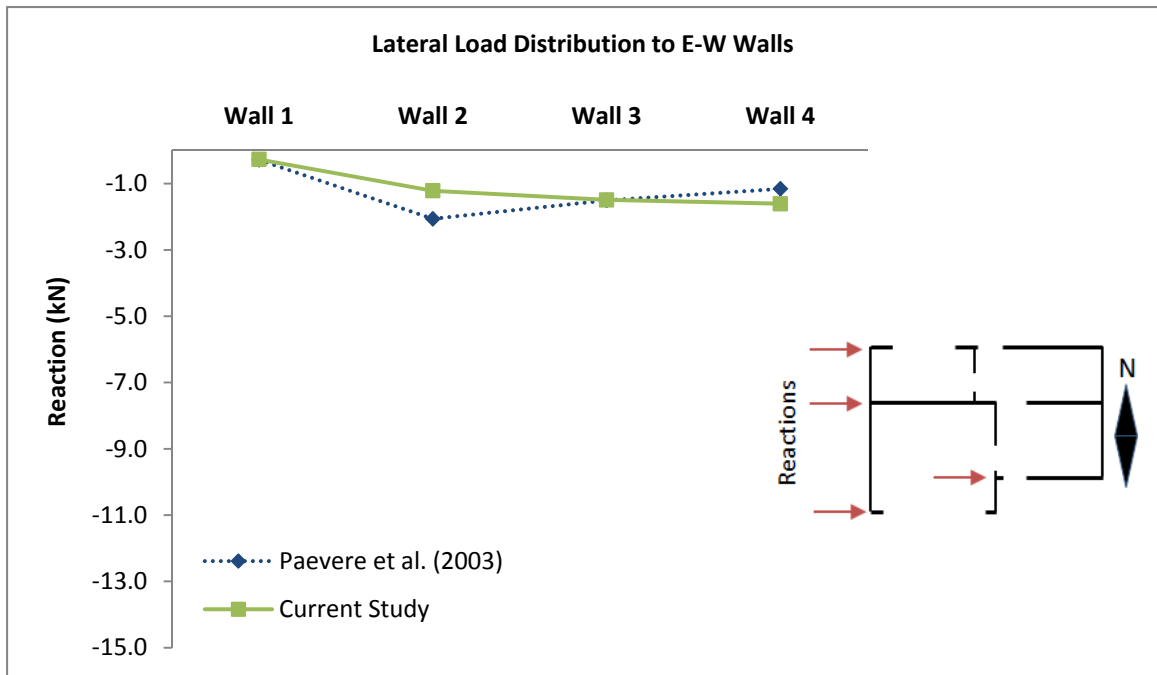


Figure H-20: Lateral Load Distribution to E-W Walls (Load Case 10)

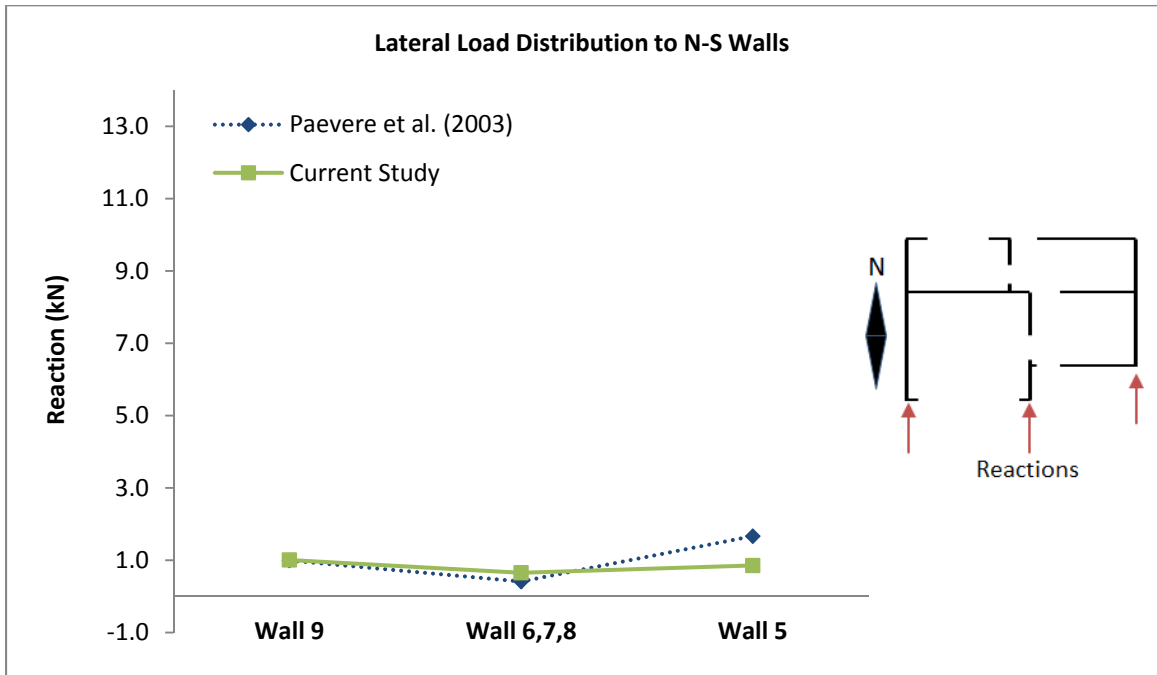


Figure H-21: Lateral Load Distribution to N-S Walls (Load Case 10)

Load Case 11: Load Applied between Walls 2 and 3

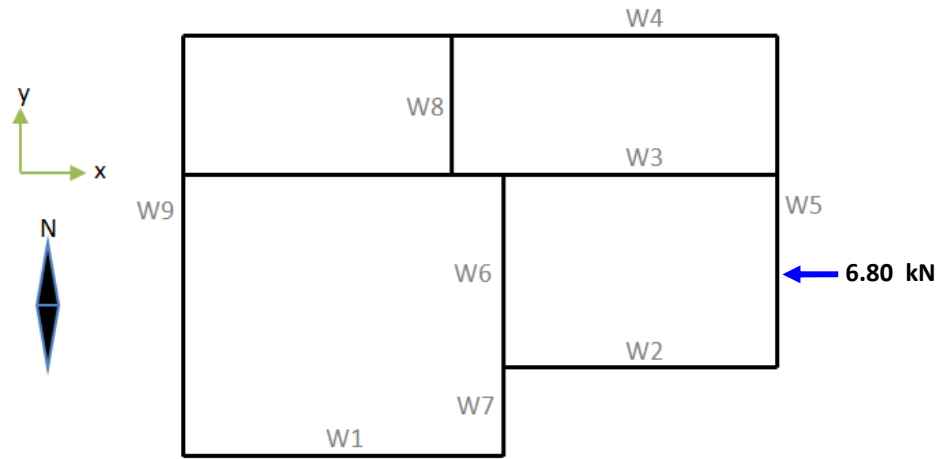


Figure H-22: Load Case 11 – 6.80 kN Applied to Top-Plate between Walls 2 and 3

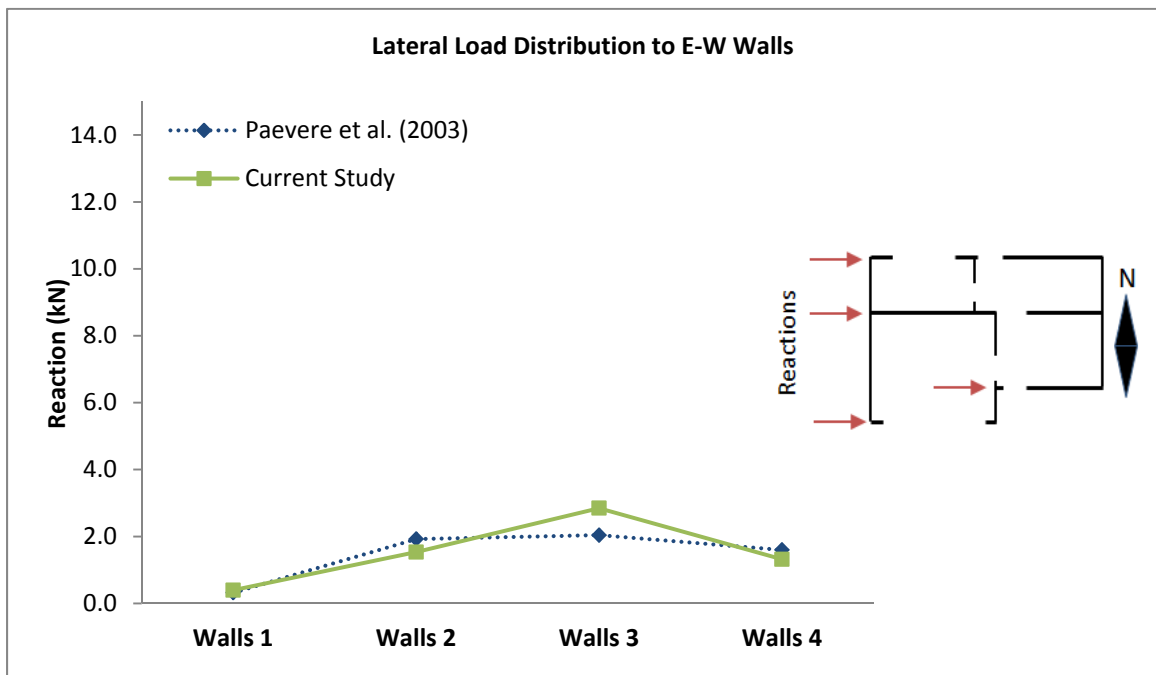


Figure H-23: Lateral Load Distribution to E-W Walls (Load Case 11)

Load Case 12: Load Applied to Walls 1, 2, 3 and 4

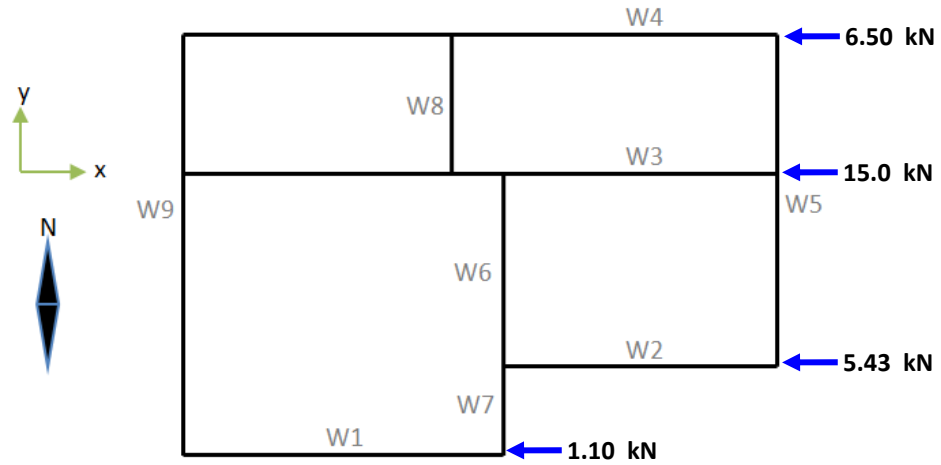


Figure H-24: Load Case 12 – 1.10 kN, 5.43 kN, 15.0 kN and 6.50 kN Applied to Top-Plate at Walls 1, 2, 3 and 4, respectively

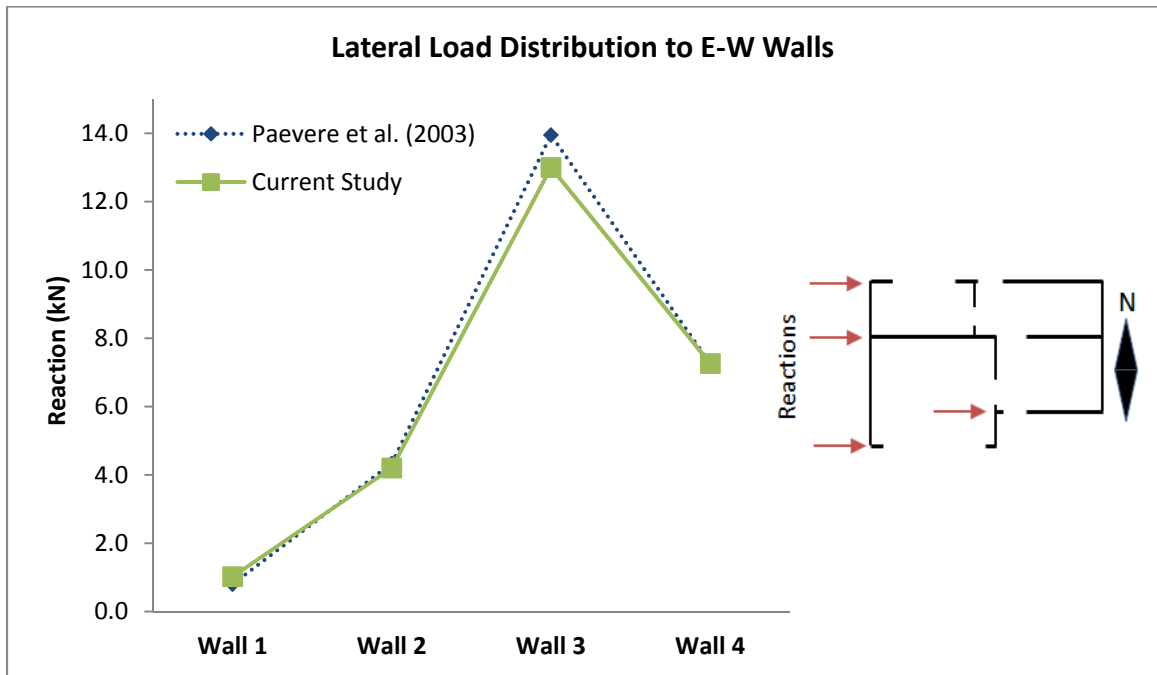


Figure H-25: Lateral Load Distribution to E-W Walls (Load Case 12)

Load Case 13: Load Applied to Roof Ridge (at -5 degrees)

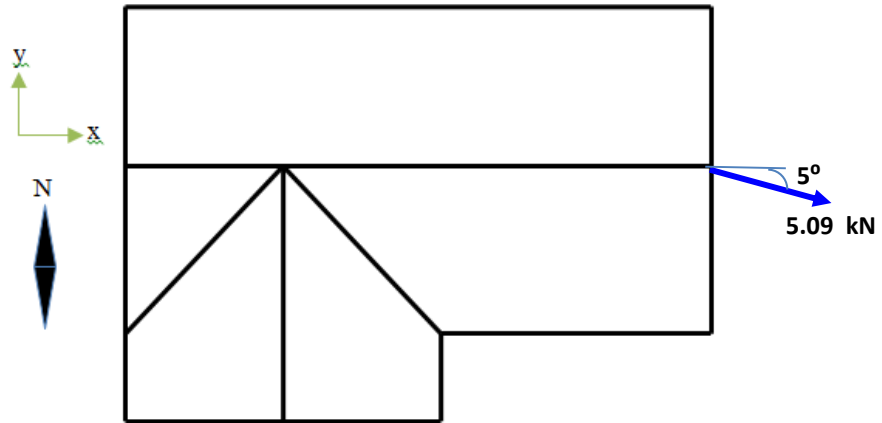


Figure H-26: Load Case 13 – 5.09 kN Applied to Roof Ridge of East Gable-End (at -5 degrees)

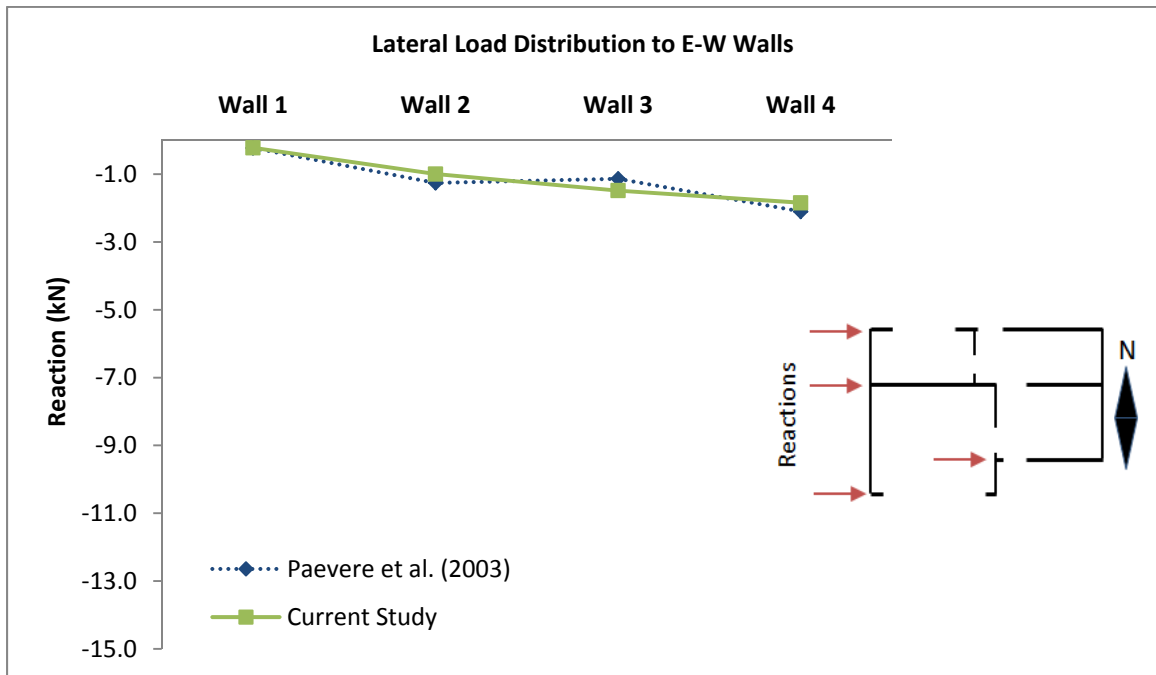


Figure H-27: Lateral Load Distribution to E-W Walls (Load Case 13)

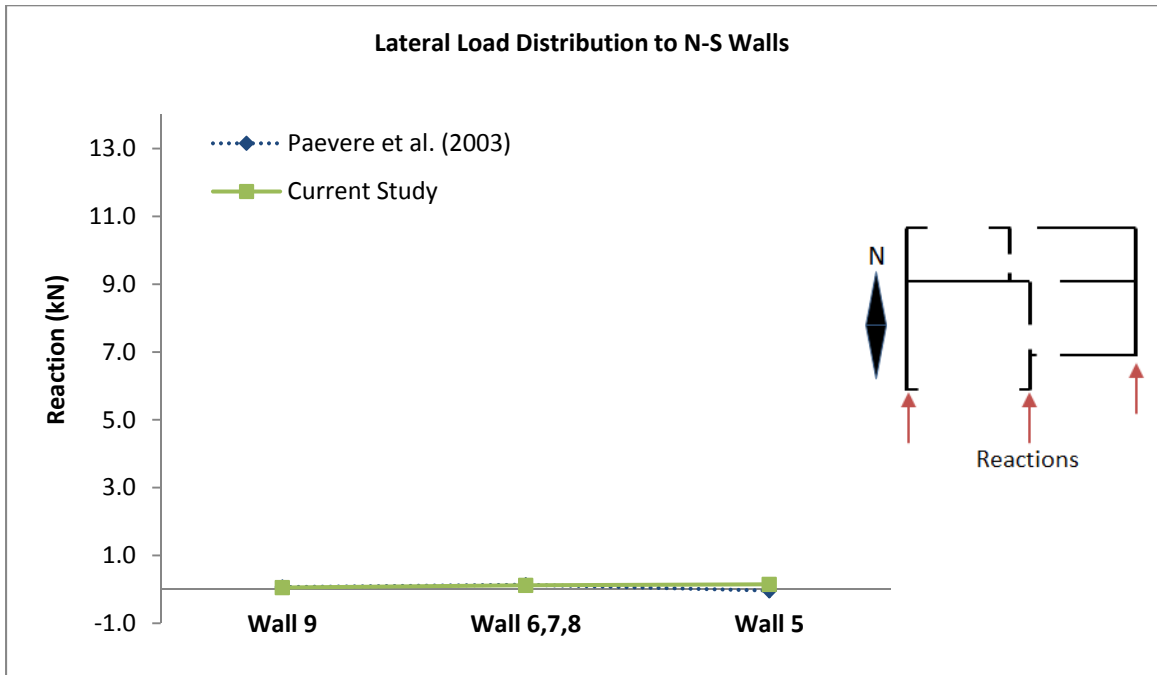


Figure H-28: Lateral Load Distribution to N-S Walls (Load Case 13)

Load Case 14: Load Applied to Roof Ridge (at -10 degrees)

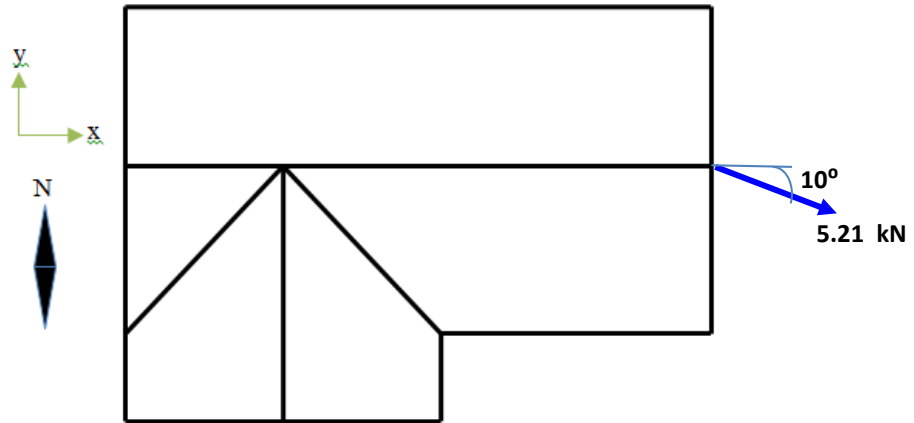


Figure H-29: Load Case 14 – 5.21 kN Applied to Roof Ridge of East Gable-End (at -10 degrees)

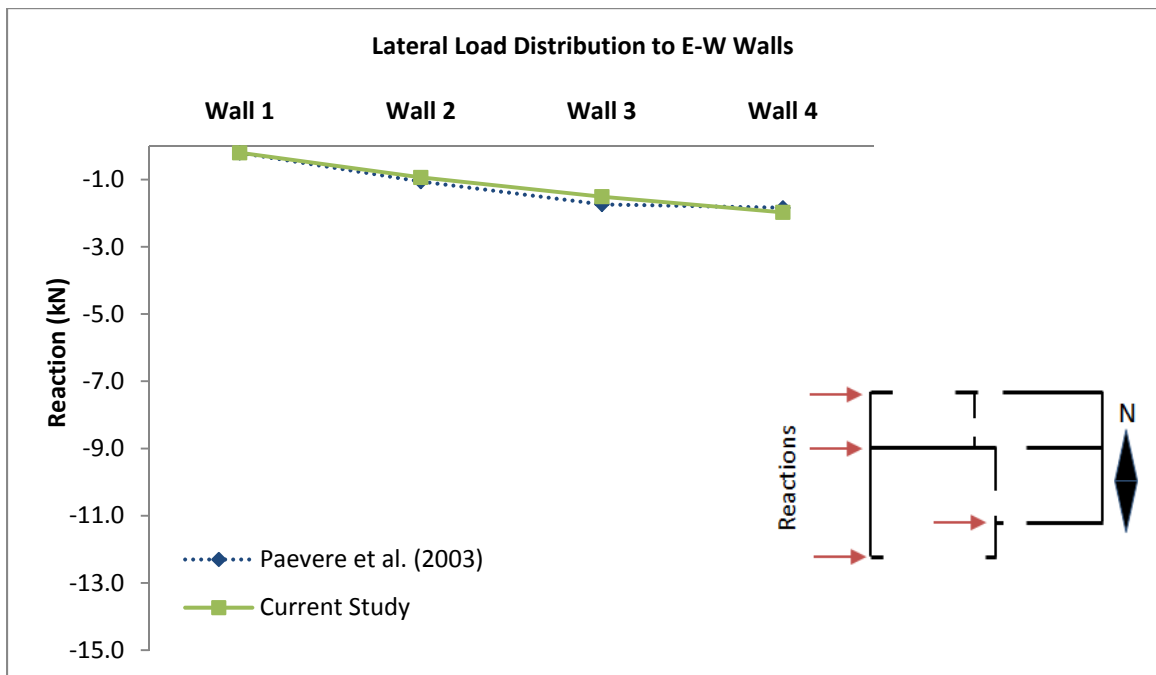


Figure H-30: Lateral Load Distribution to E-W Walls (Load Case 14)

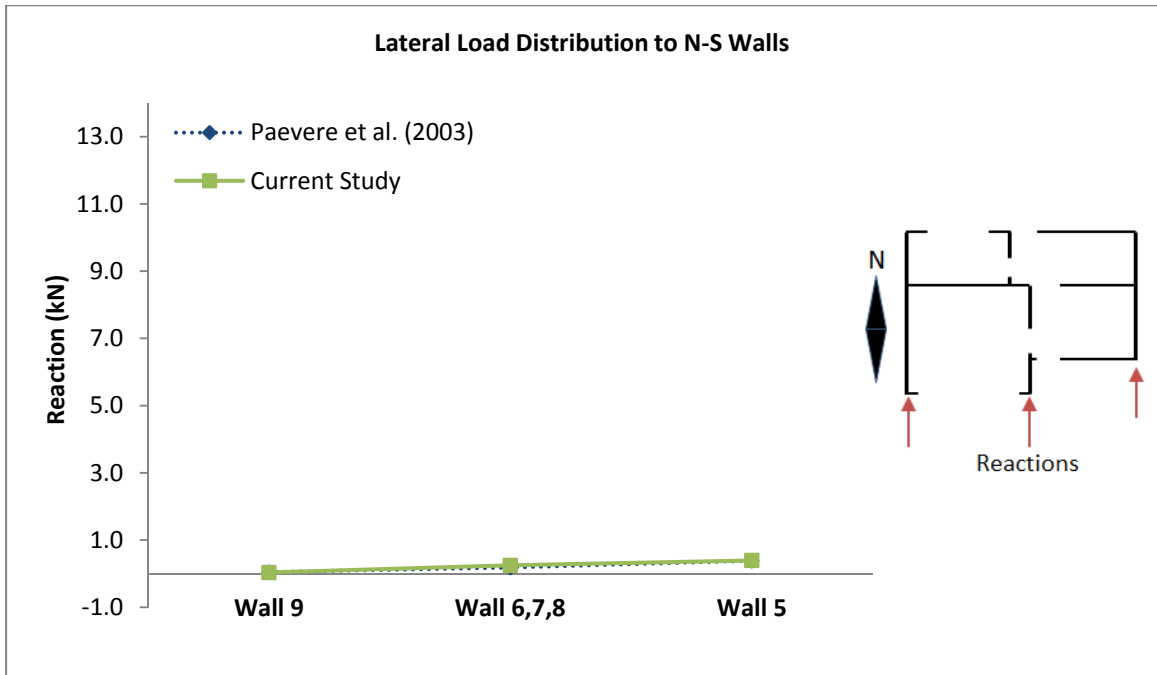


Figure H-31: Lateral Load Distribution to N-S Walls (Load Case 14)

Load Case 15: Load Applied to Roof Ridge (at 20 degrees)

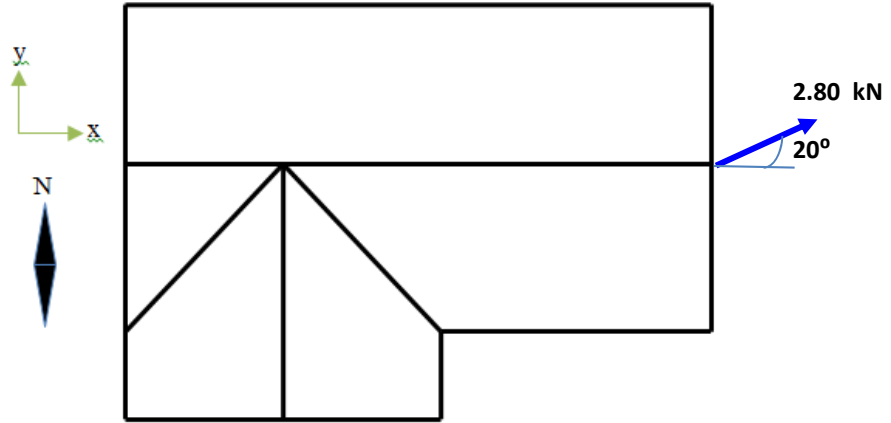


Figure H-32: Load Case 15 – 2.80 kN Applied to Roof Ridge of East Gable-End (at 20 degrees)

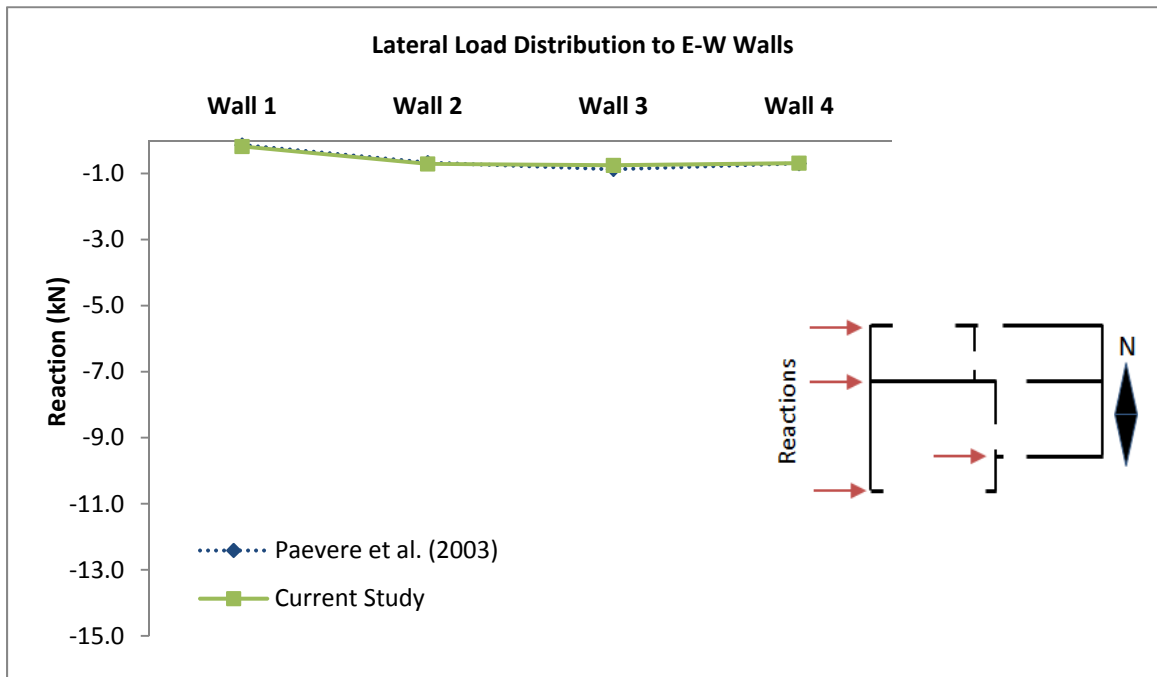


Figure H-33: Lateral Load Distribution to E-W Walls (Load Case 15)

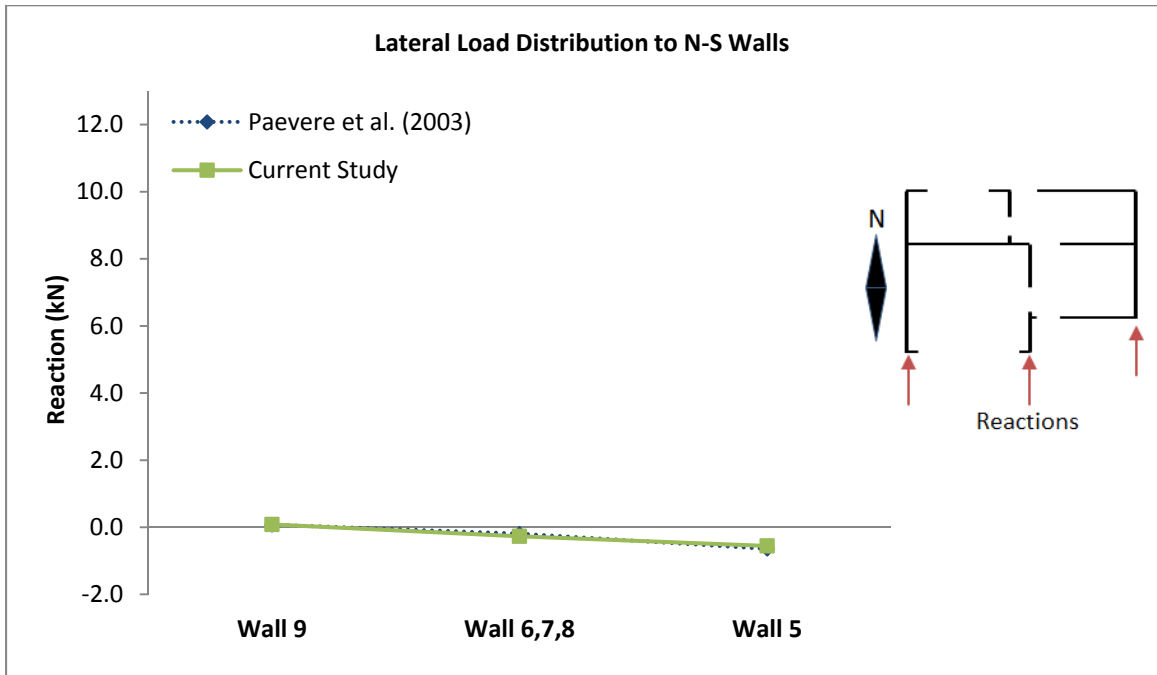


Figure H-34: Lateral Load Distribution to N-S Walls (Load Case 15)

APPENDIX I

MODEL VARIATIONS USED IN UPLIFT AND WIND LOAD INVESTIGATIONS

Using the validated modeling methods discussed in this study, multiple variations of the Paevere et al (2003) house were created for use in uplift and lateral load path investigations. All building variations were based on the same materials and construction methods described in Appendix G, with the following modifications:

- Gable-end overhang framing was modified to reflect out-looker or out-rigger style framing commonly used in North America as shown in Figure I-1 (Martin 2010).
- Gable-end trusses were changed from Fink trusses to non-structural gable-end frames and sheathed with plywood (Figure I-1).
- Simpson Strong-Tie HDU2 hold-downs (also used by Martin 2010) were added to external walls at wall ends and at either side of openings. Hold-downs were modeled with a stiffness of 6.1 kN/m (35 k/in) as listed by the manufacturer (Martin 2010).

Wall designations used by Paevere et al. (2003) were also kept constant throughout the load path investigations.

Two main investigations were performed: (1) an uplift investigation (2) a wind-load (combined lateral and uplift) investigation. For each investigation, an index model was created and systematically modified to explore the effects of geometric variations and retrofits options. This appendix contains details for the buildings used in each investigation. Further information including loading details and results from the investigations are included in Appendices J through L.

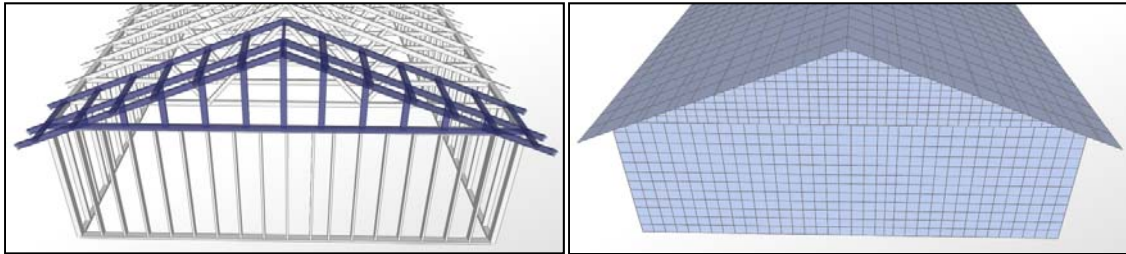


Figure I-1: Gable End-Framing and Sheathing Modifications for Uplift and Wind Load Investigations

Uplift Investigation

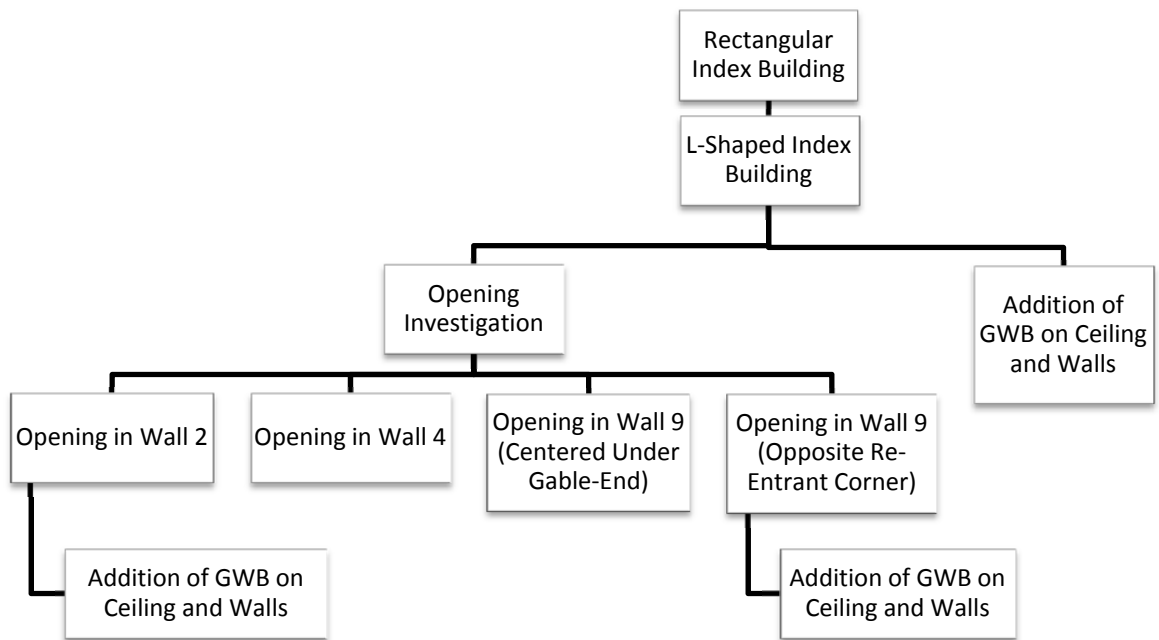


Figure I-2: Progression of Building Variations Used in Uplift Investigation

Rectangular and L-Shaped Index Buildings for Uplift Investigation

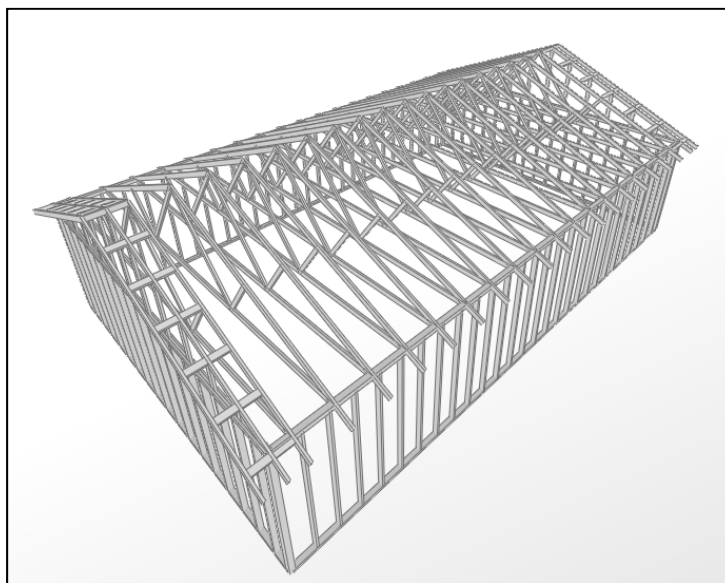


Figure I-3: Rectangular Index Building for Uplift Investigation – rectangular building with no openings, no interior walls and no GWB. Walls and gable-ends are fully sheathed on the exterior with plywood.

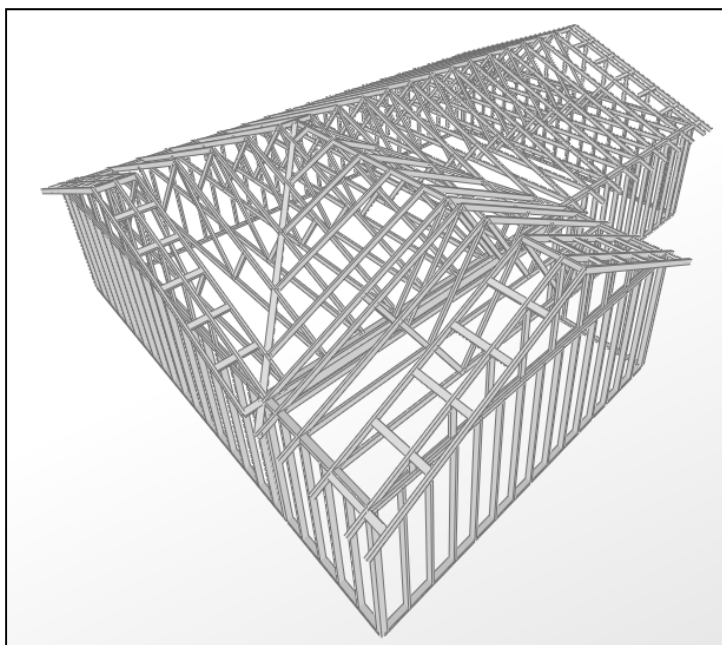


Figure I-4: L-Shaped Index Building for Uplift Investigation – L-Shaped building with no openings, no interior walls and no GWB. Walls and gable-ends are fully sheathed on the exterior with plywood.

Openings Used in Uplift Investigation

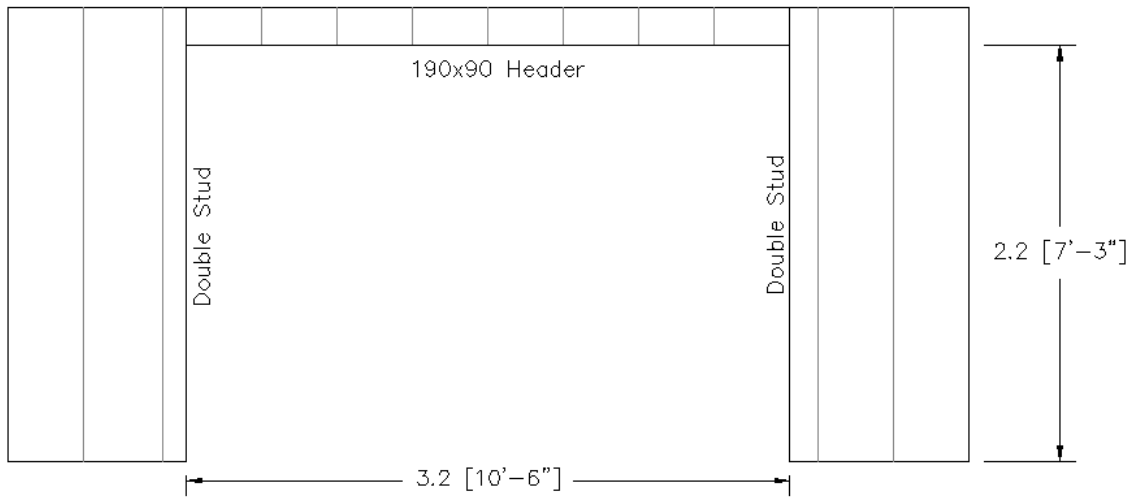


Figure I-5: Framing Detail for Openings used in Uplift Investigation

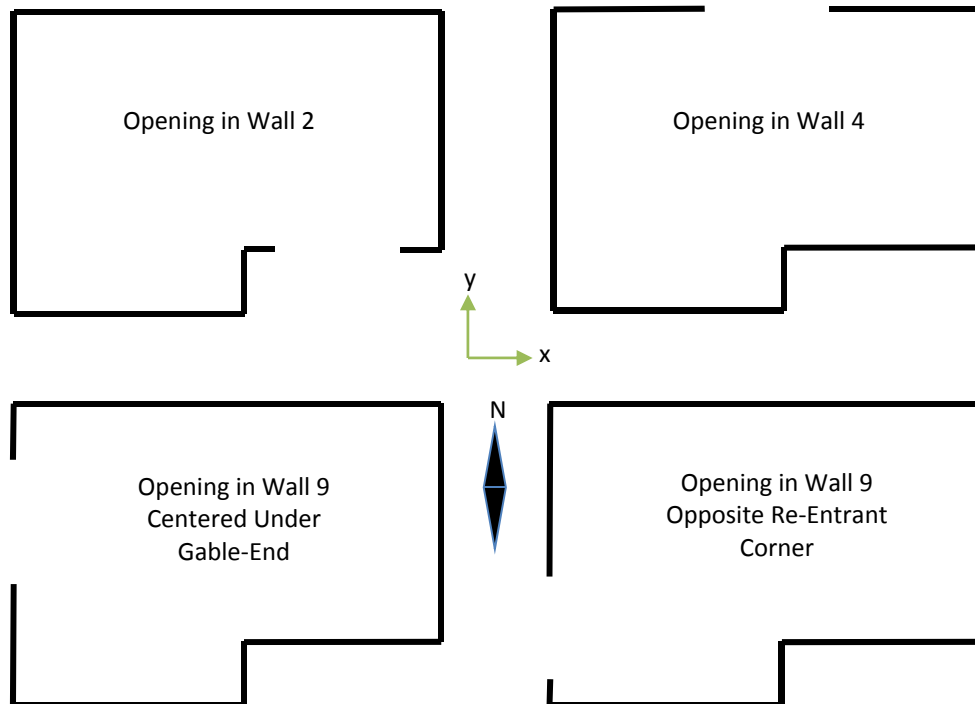


Figure I-6: Locations of Openings Used for Uplift Investigation

Wind Load Investigation

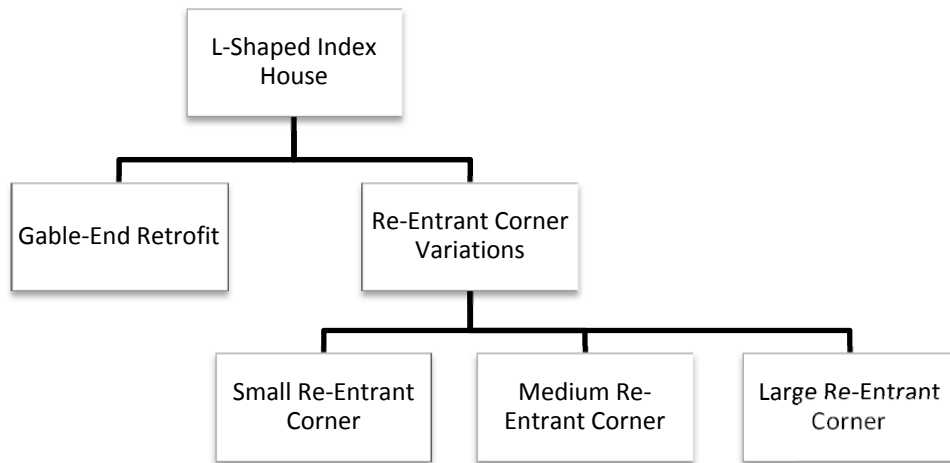


Figure I-7: Progression of Building Variations Used in Wind Load Investigation

L-Shaped Index House for Wind Load Investigation

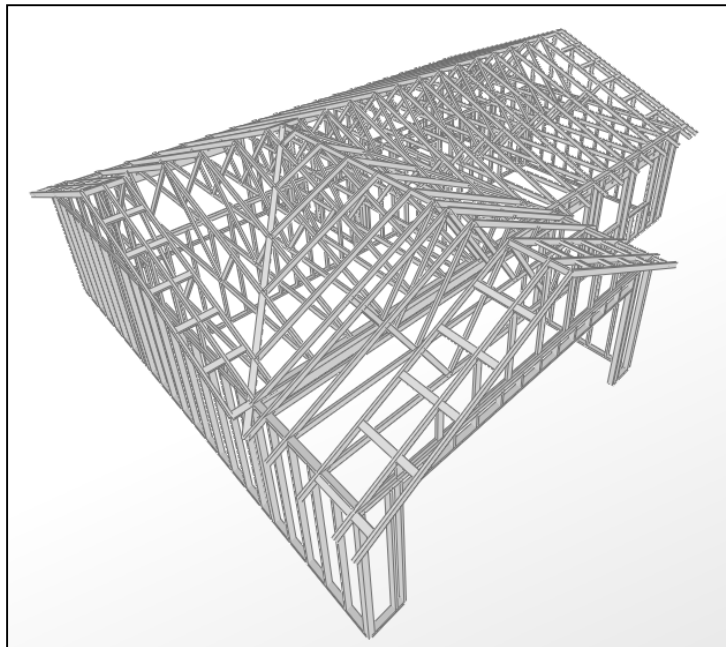


Figure I-8: L-Shaped Index House for Wind Load Investigation – Paevere (2002) house with modified gable-end framing, anchor bolt spacing and addition of hold-downs as described previously. Walls and gable-ends are fully sheathed on the exterior with plywood.

Gable-End Retrofit

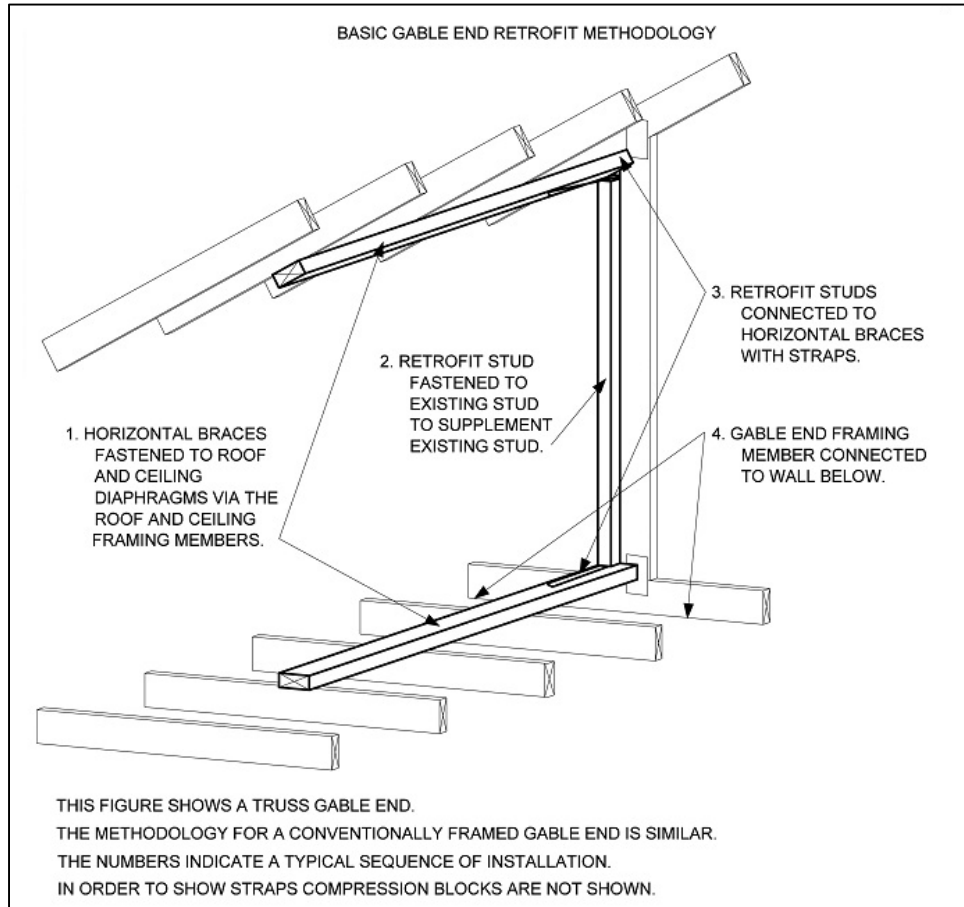


Figure I-9: Gable-End Retrofit Detail from 2010 Florida Building Code (ICC 2011)

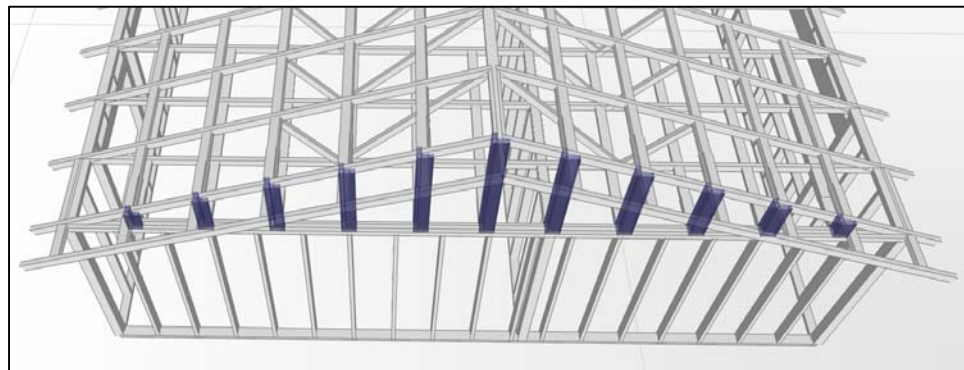


Figure I-10: Gable-End Studs + Retrofit Studs Modeled with L-Shaped Cross-Section

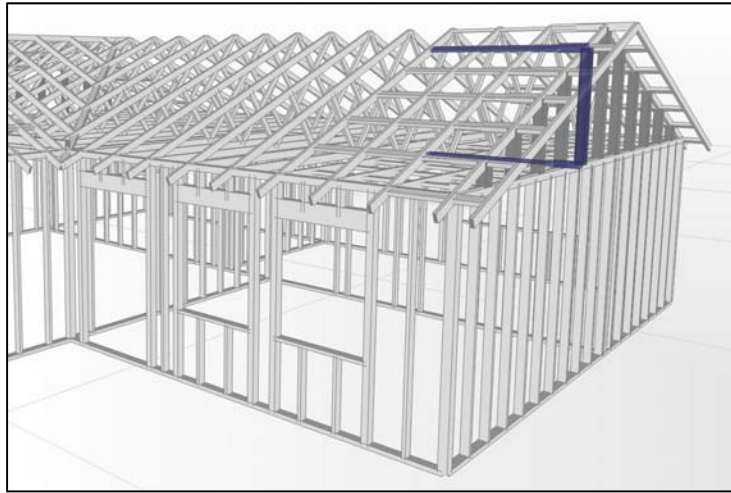


Figure I-11: Example of Gable-End Retrofit in the Model – Retrofits are located at every gable-end stud. Retrofit connections are modeled as rigid connections.

Re-Entrant Corner Variations Used in Wind Load Investigation

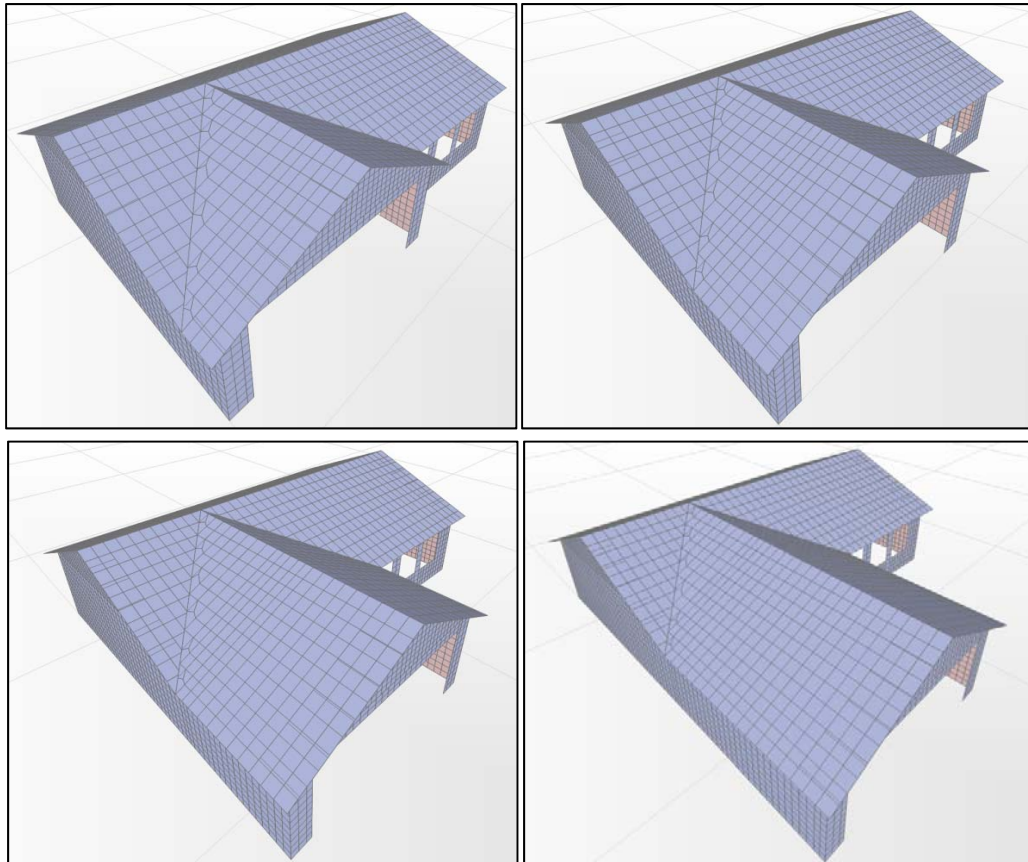


Figure I-12: Re-Entrant Corner Variations Used in Wind Load Investigation – Small re-entrant corner (top left), index (top right), medium (bottom left) and large (bottom right)

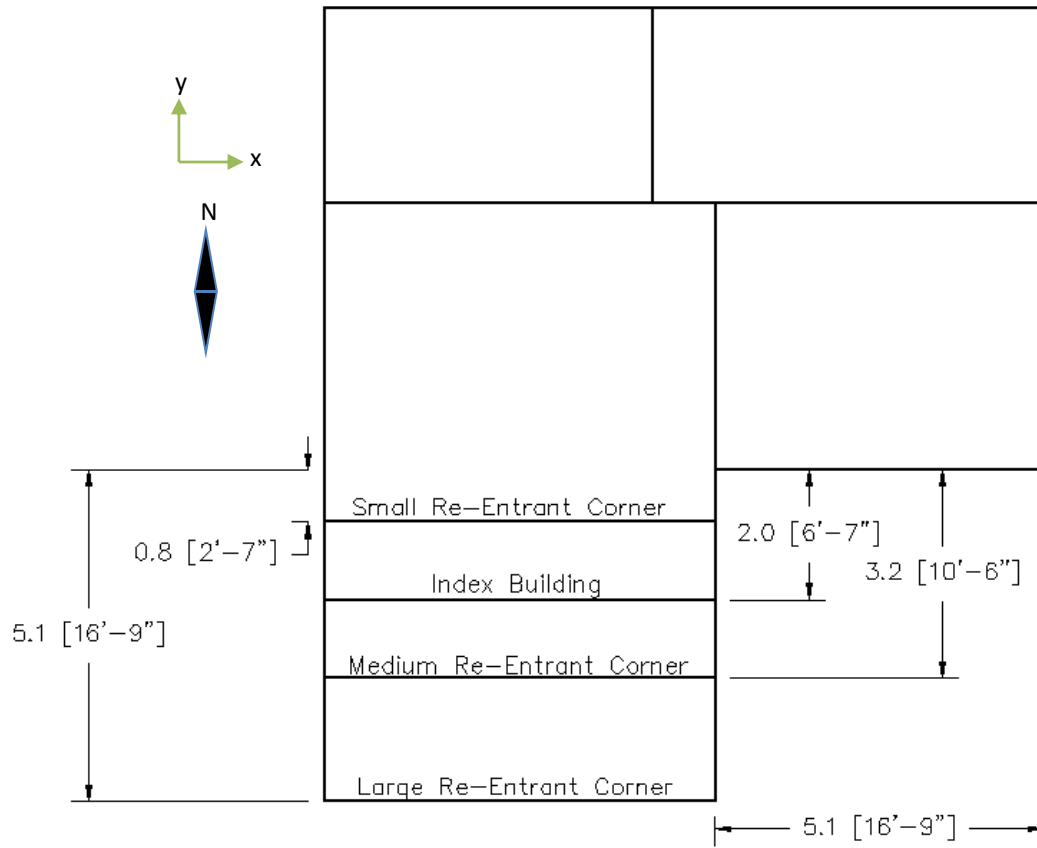


Figure I-13: Re-Entrant Corner Variation Dimensions for Wind Load Investigation – m (ft-in)

APPENDIX J

UNIFORM UPLIFT INVESTIGATION

As a continuation of the research performed by Martin (2010), the propagation and redistribution of uplift load paths due to changes in plan geometry and the addition of openings in a simple light-frame, wood structure were investigated. Model variations used in this study are described in detail in Appendix I and include:

- A rectangular index building with no interior walls, no wall openings and no gypsum wall board lining.
- An L-shaped index building with no interior walls, no wall openings and no gypsum wall board lining.
- Variations of the L-shaped building with openings added one at a time to each of four locations as shown in Figure I-6.
- L-shaped index building with the addition of GWB on the ceiling and on the interior of the walls.
- Two of the wall-opening variations with the addition of GWB on the ceiling and on the interior of the walls.

In concurrence with Martin (2010), a uniform uplift pressure of 2.4 kPa (50 psf) was applied to the roof of the buildings, normal to the surface. The self-weight of the buildings was not included in the uplift investigation (Martin 2010). Resulting reactions and changes in reaction for each building variation are included as “bubble plots” in this appendix. Each bubble represents an individual hold-down or anchor bolt. The size of the bubbles represents the magnitude of either the uplift reaction or change in reaction at each anchorage device.

Index Buildings

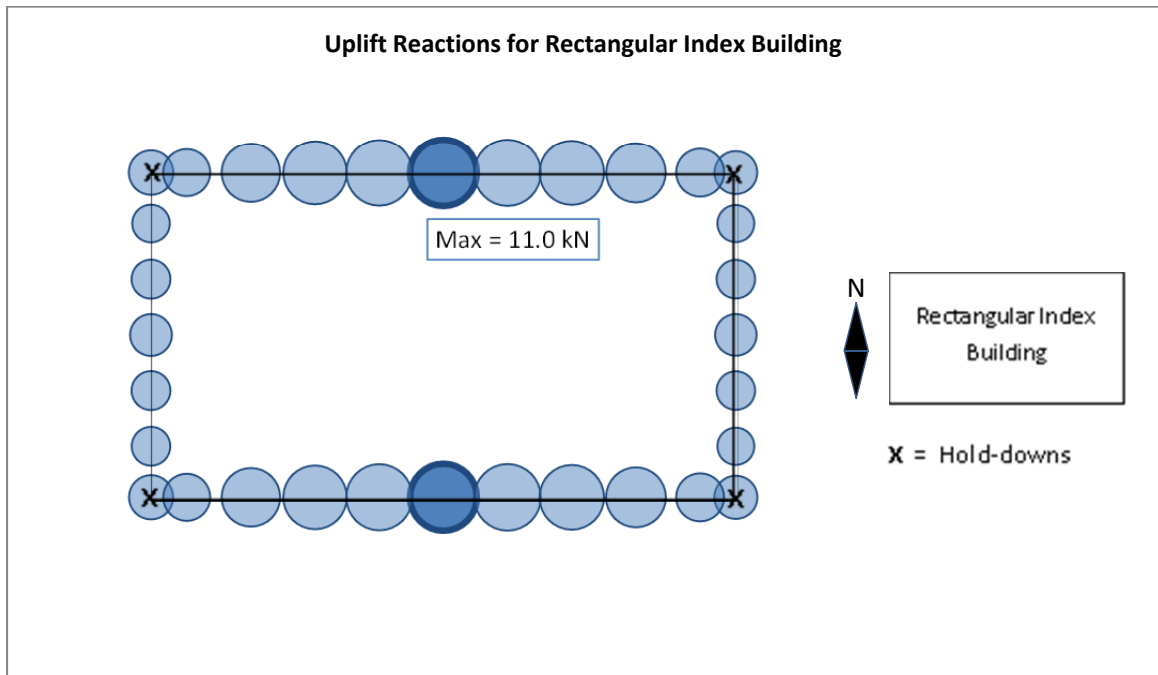


Figure J-1: Uplift Reactions for Rectangular Index Building under Uniform Uplift Pressure

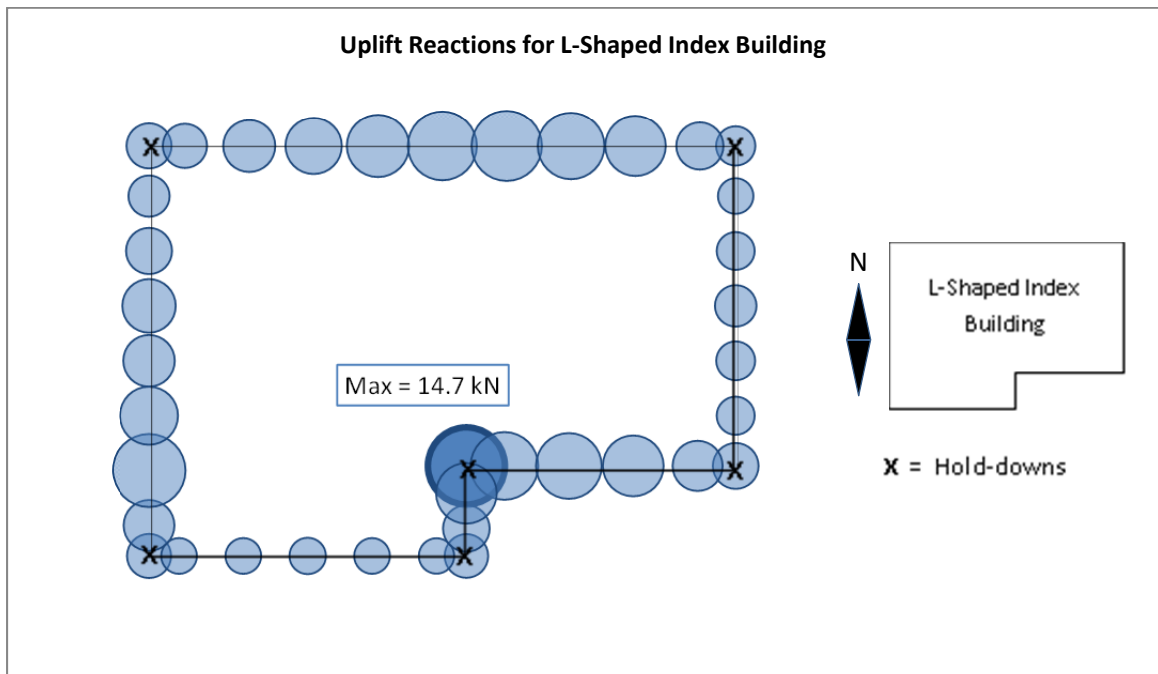


Figure J-2: Uplift Reactions for L-Shaped Index Building under Uniform Uplift Pressure

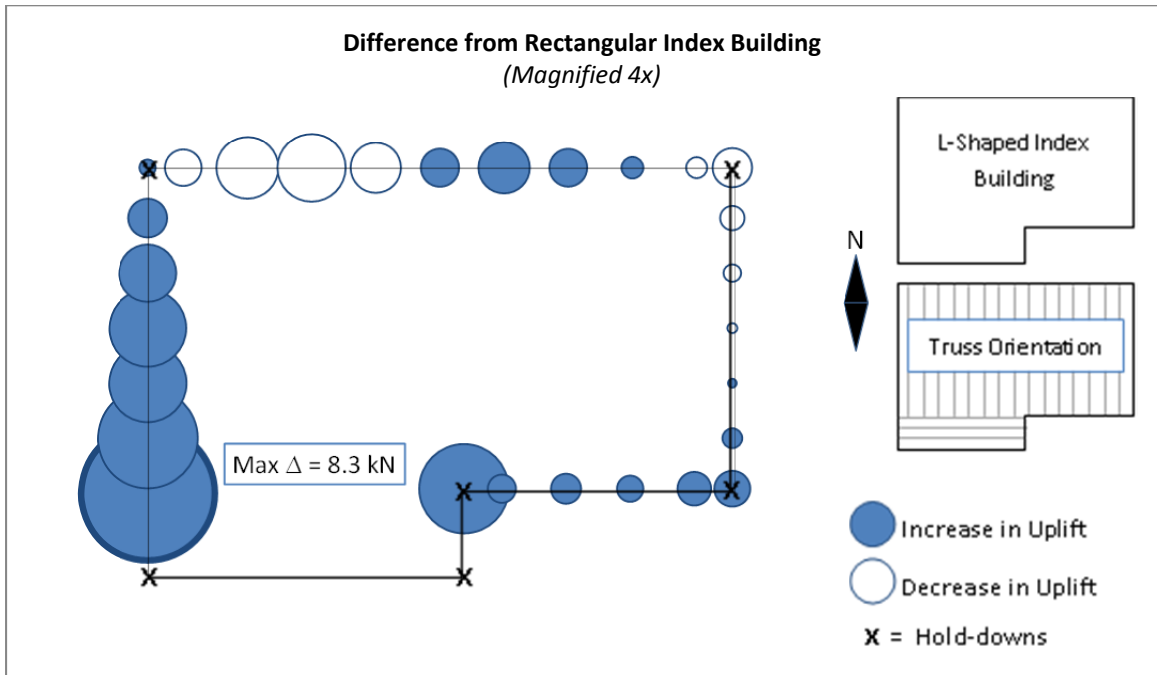


Figure J-3: Difference in Uplift Reactions between Rectangular and L-Shaped Index Buildings under Uniform Uplift Pressure

Opening Investigation

L-Shaped Building with Opening in Wall 2

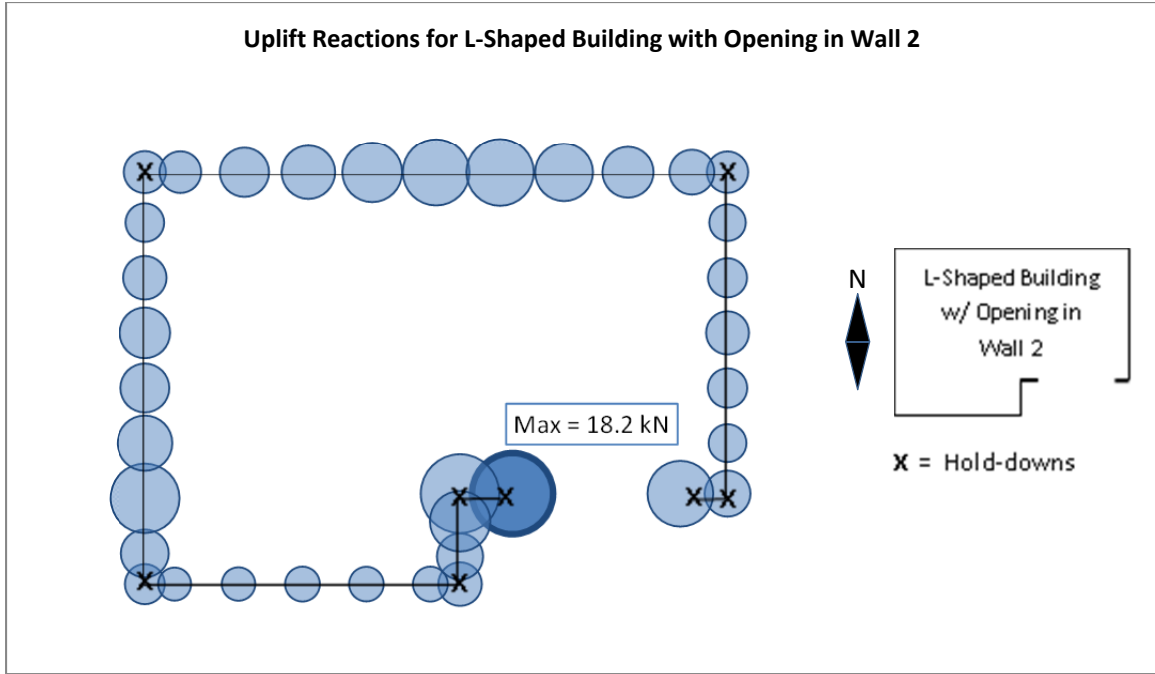


Figure J-4: Uplift Reactions for L-Shaped Building with Opening in Wall 2 (under Uniform Uplift Pressure)

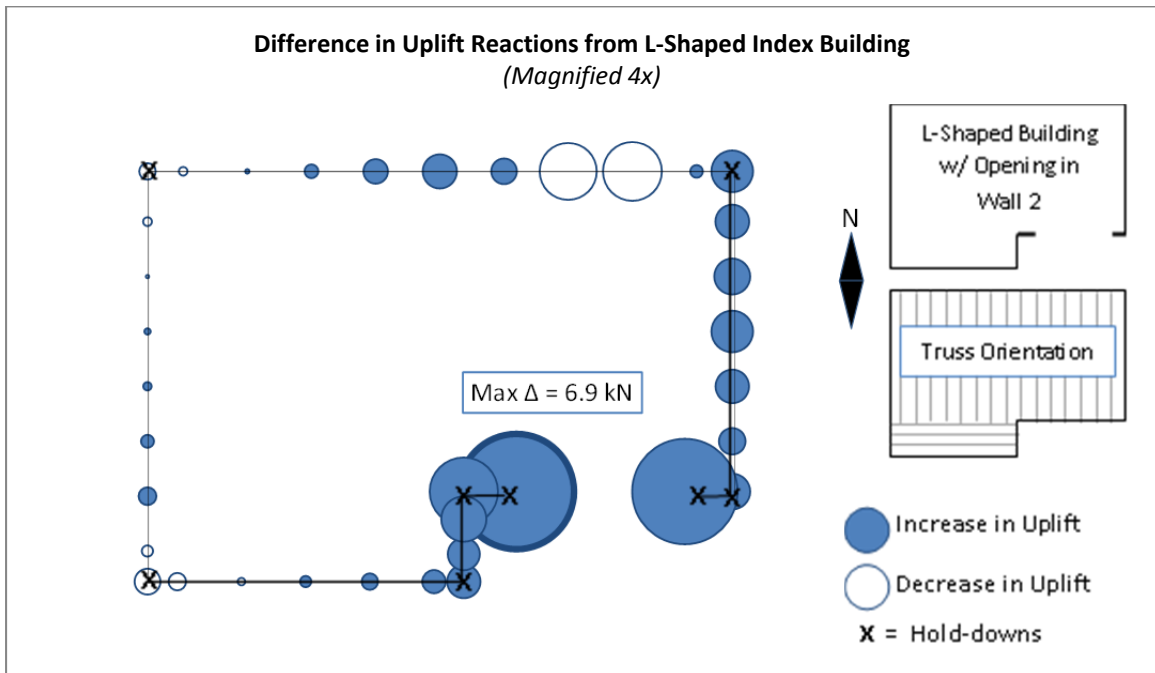


Figure J-5: Difference in Uplift Reactions due to Opening in Wall 2

L-Shaped Building with Opening in Wall 4

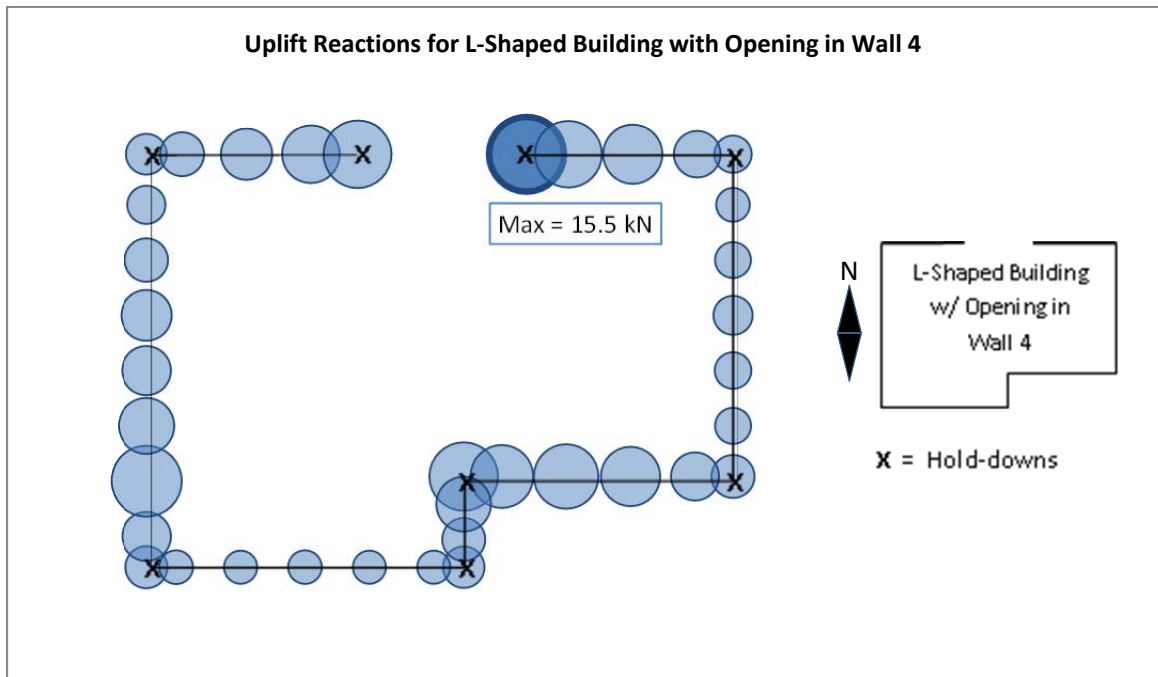


Figure J-6: Uplift Reactions for L-Shaped Building with Opening in Wall 4 (under Uniform Uplift Pressure)

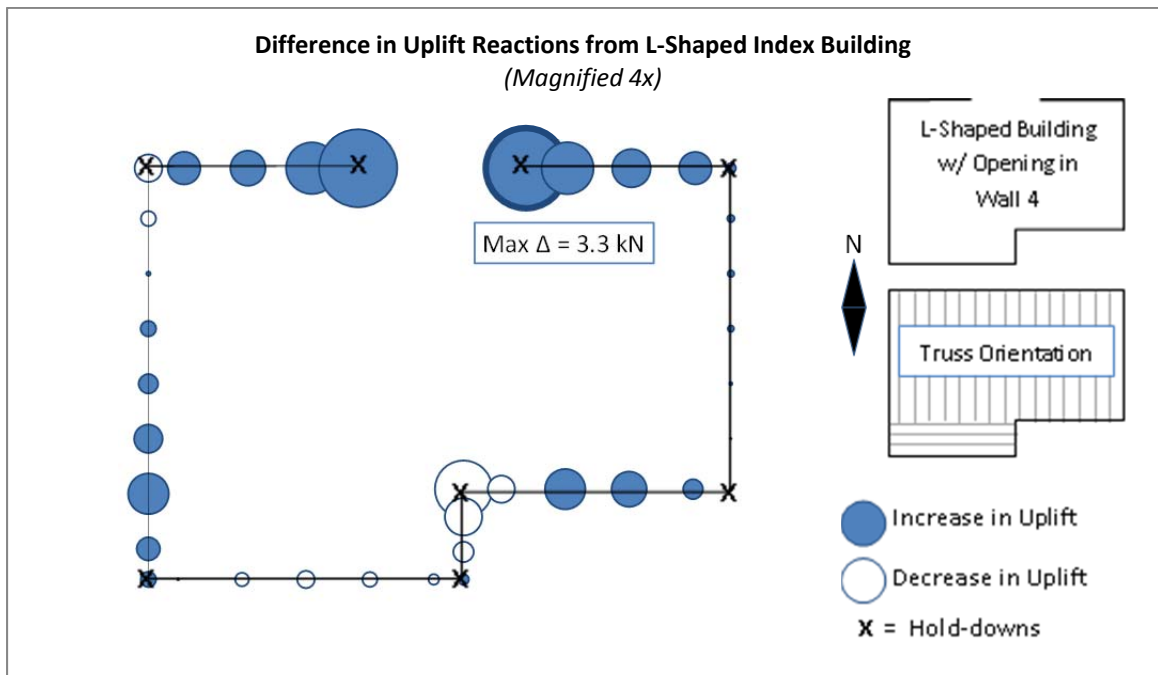


Figure J-7: Difference in Uplift Reactions due to Opening in Wall 4

L-Shaped Building with Opening in Wall 9 (Centered Under Gable-End)

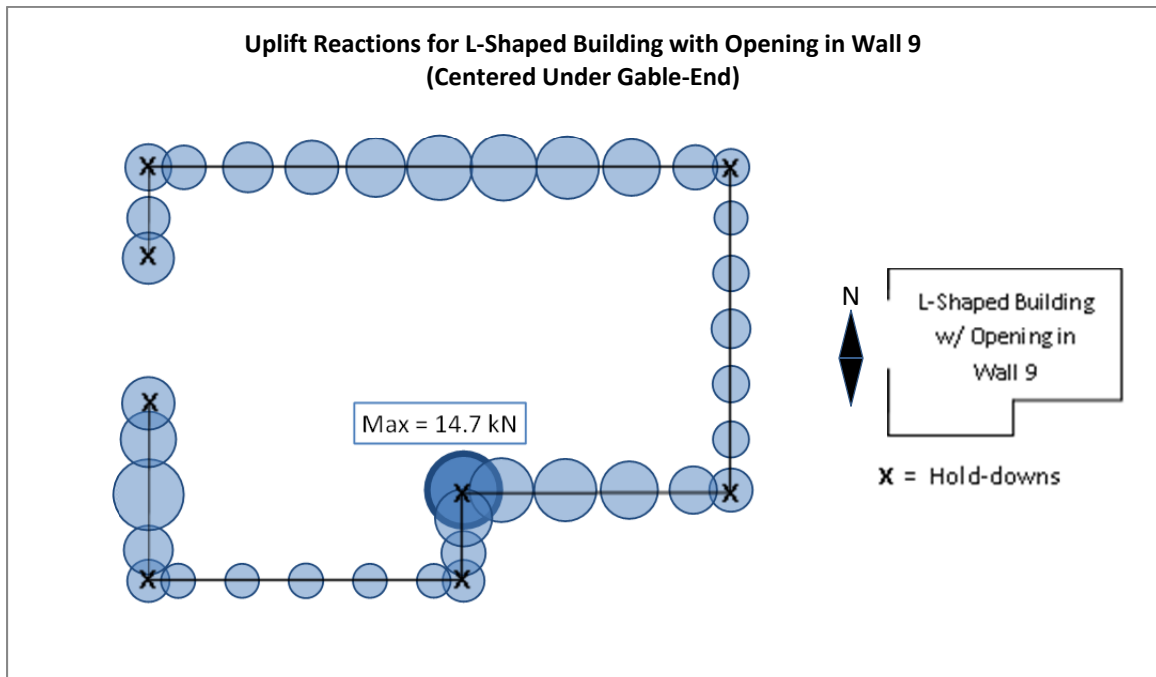


Figure J-8: Uplift Reactions for L-Shaped Building with Opening in Wall 9, Centered Under Gable-End (under Uniform Uplift Pressure)

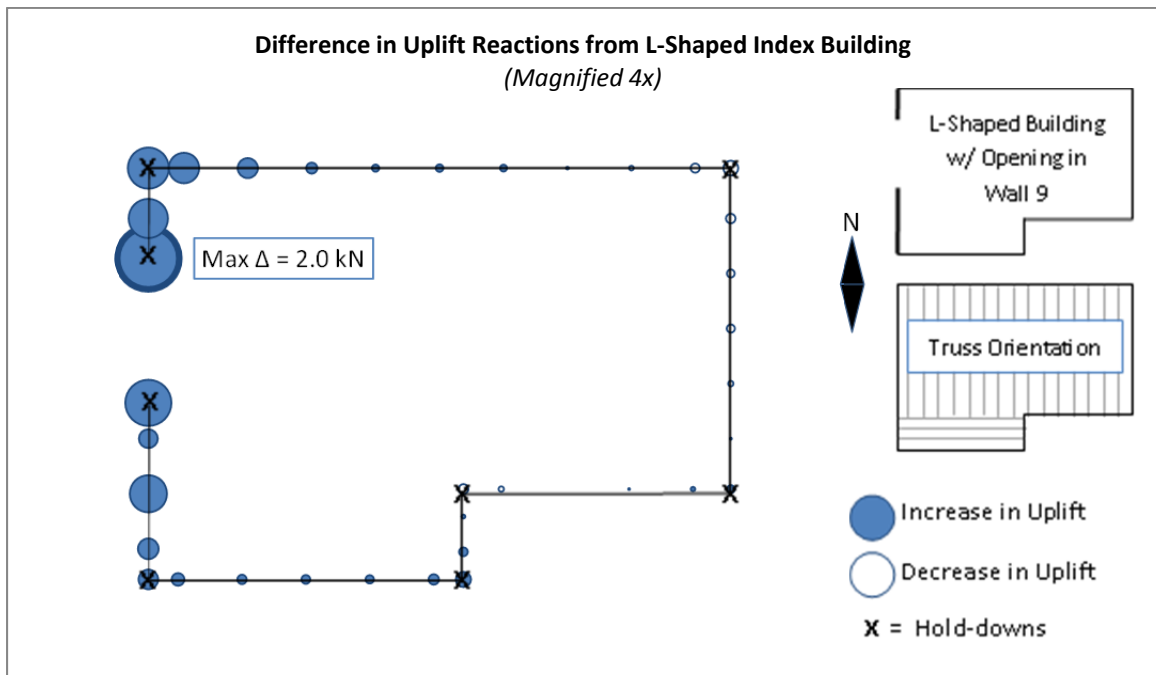


Figure J-9: Difference in Uplift Reactions due to Opening in Wall 9, Centered Under Gable-End

L-Shaped Building with Opening in Wall 9 (Opposite Re-Entrant Corner)

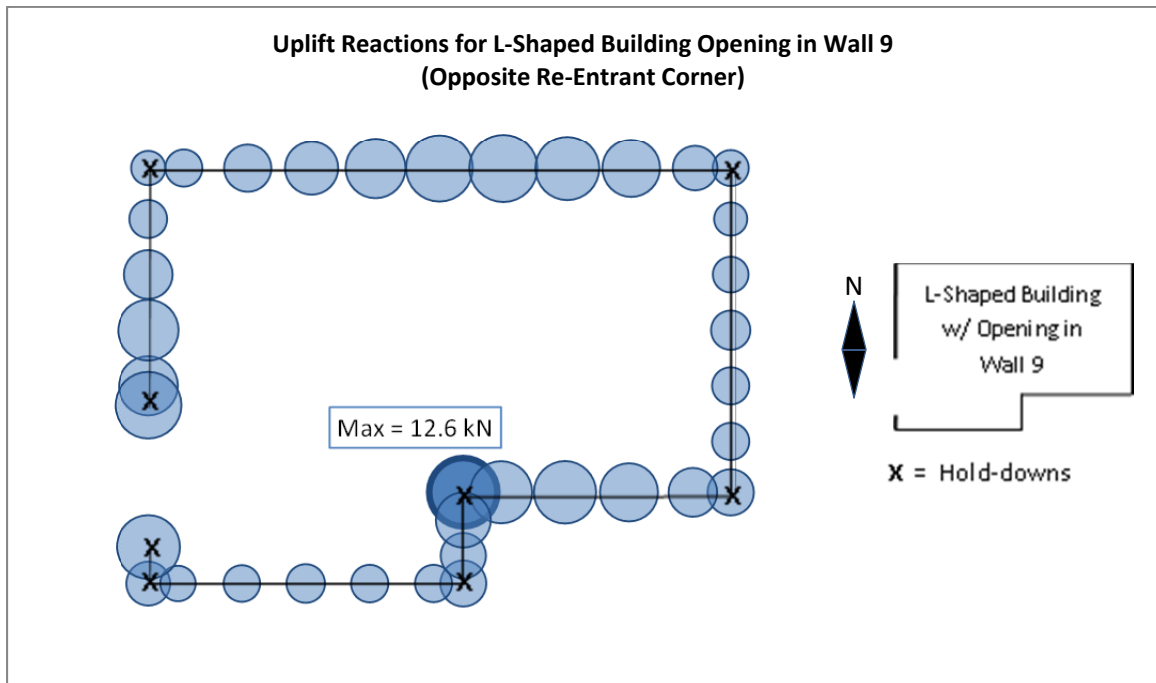


Figure J-10: Uplift Reactions for L-Shaped Building with Opening in Wall 9, Opposite Re-Entrant Corner (under Uniform Uplift Pressure)

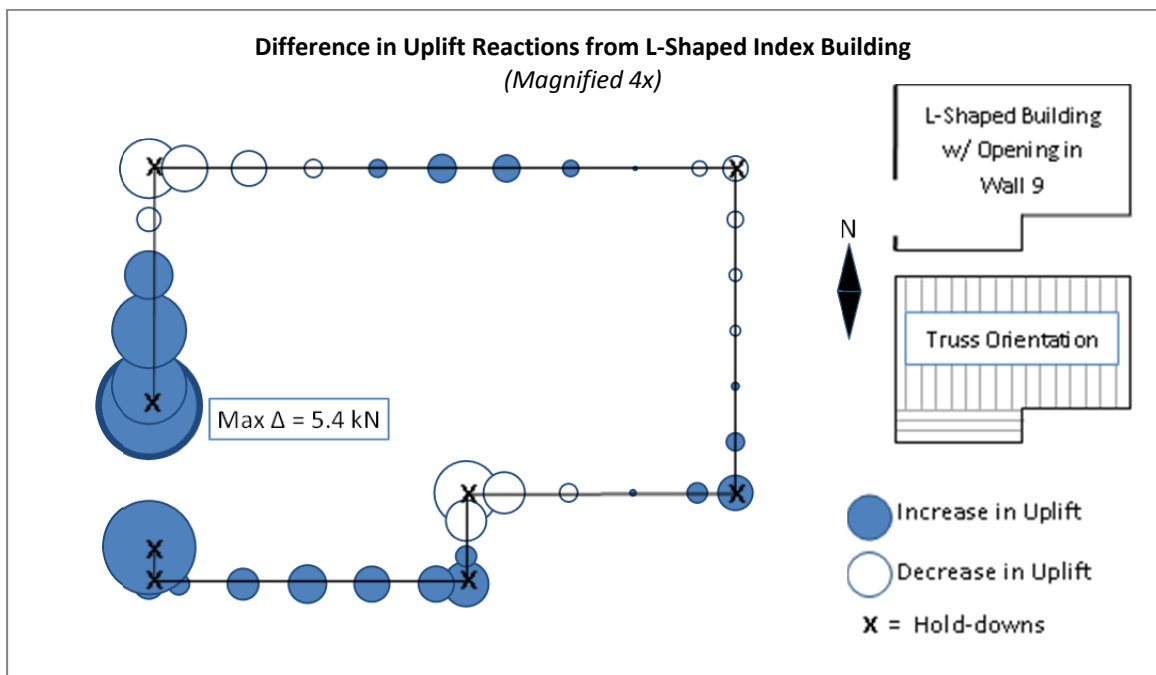


Figure J-11: Difference in Uplift Reactions due to Opening in Wall 9, Opposite Re-Entrant Corner

Effects of Gypsum Wall Board (GWB)

L-Shaped Building with GWB

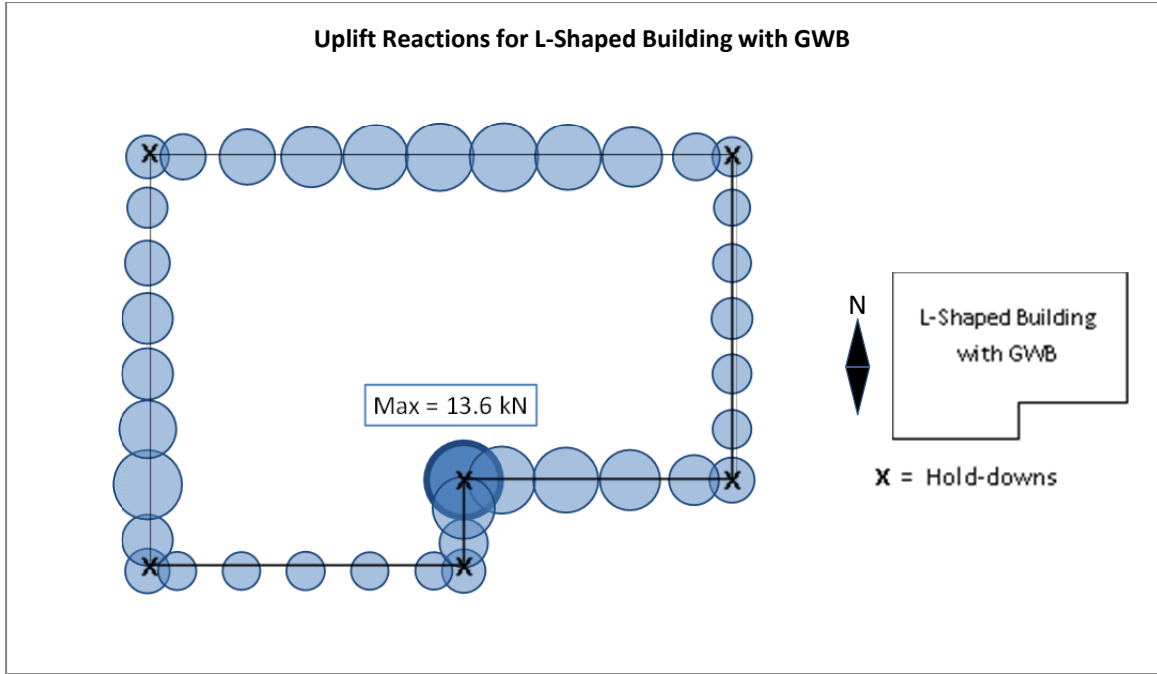


Figure J-12: Uplift Reactions for L-Shaped Building with GWB (under Uniform Uplift Pressure)

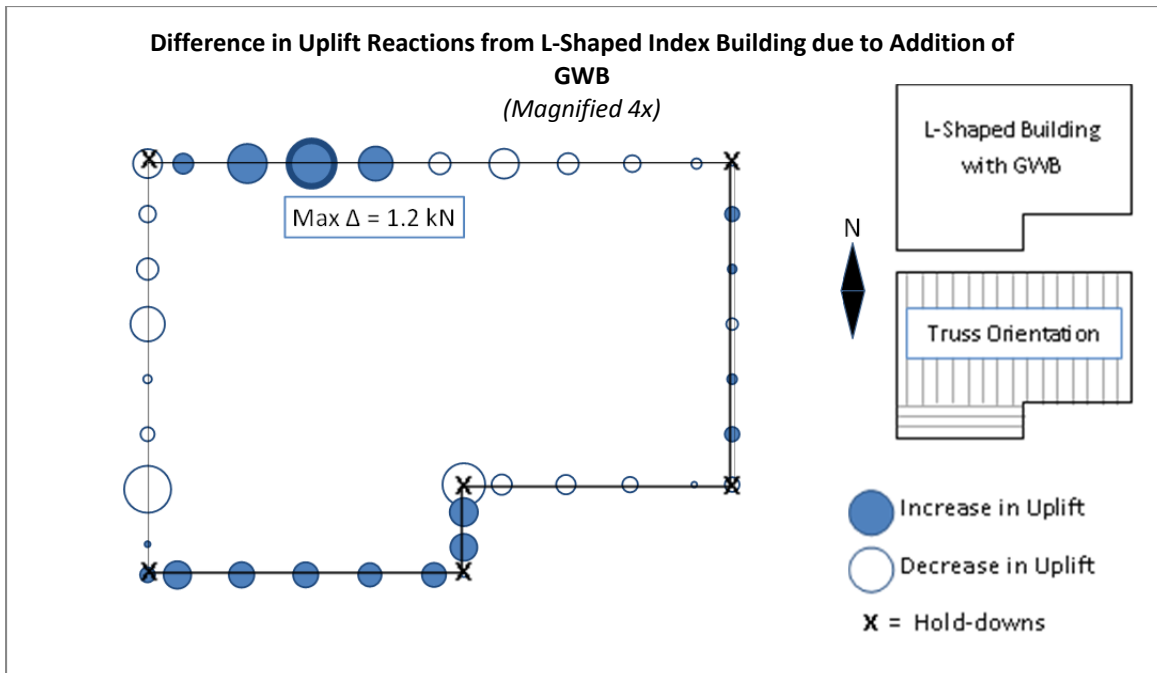


Figure J-13: Difference in Uplift Reactions from L-Shaped Building due to addition of GWB

L-Shaped Building with Opening in Wall 2 and GWB

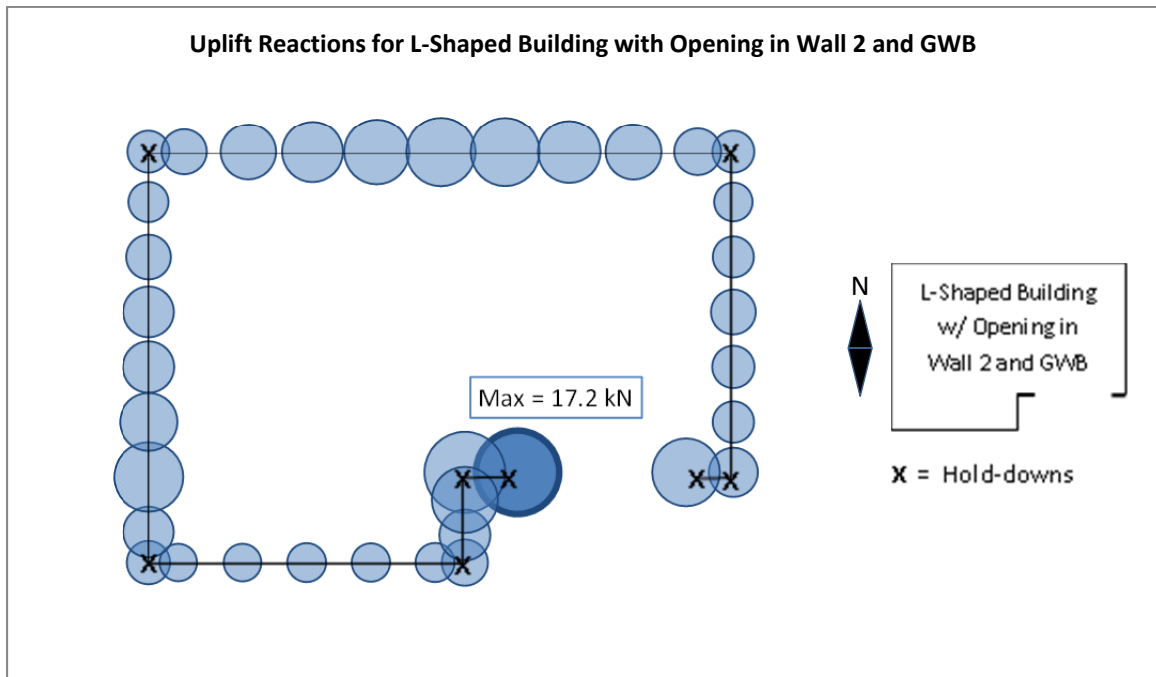


Figure J-14: Uplift Reactions for L-Shaped Building with Opening in Wall 2 and GWB (under Uniform Uplift Pressure)

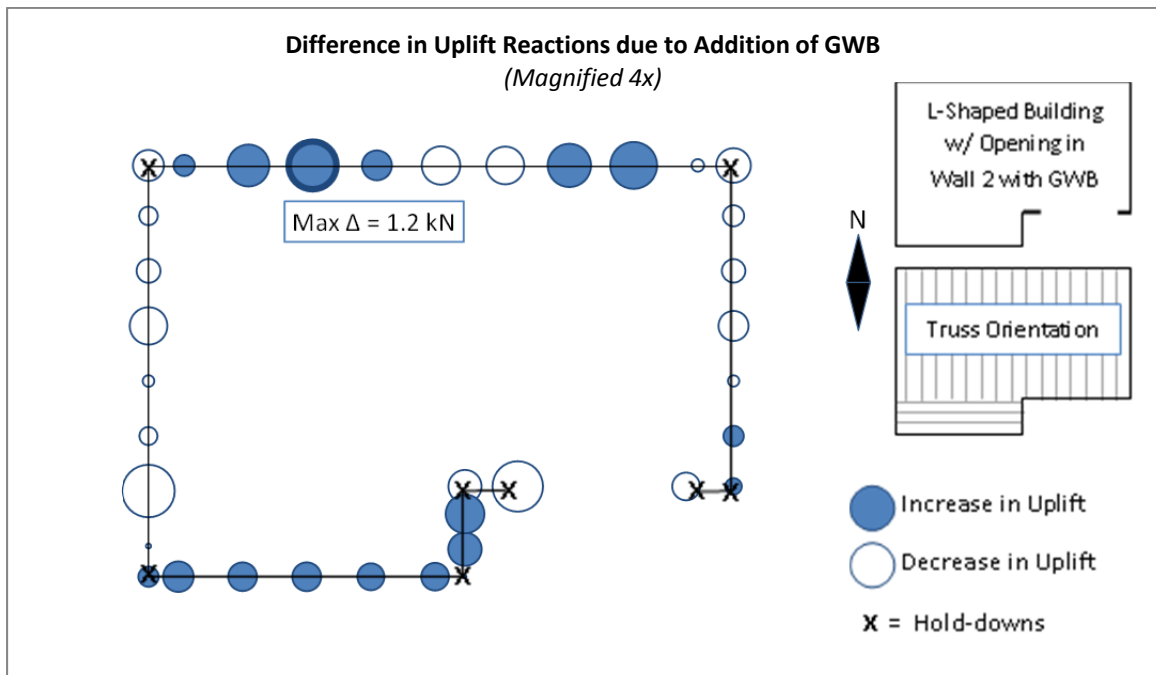


Figure J-15: Difference in Uplift Reactions in L-Shaped Building with Opening in Wall 2 Due to Addition of GWB

L-Shaped Building with Opening in Wall 9 and GWB

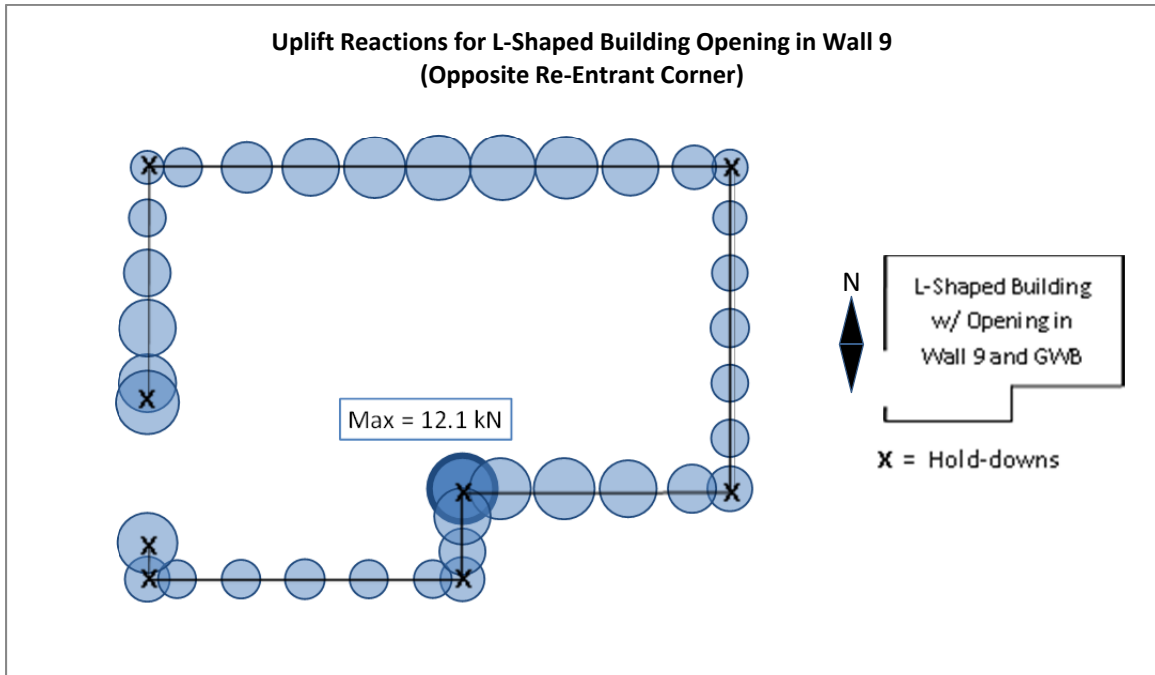


Figure J-16: Uplift Reactions for L-Shaped Building with Opening in Wall 9 and GWB (under Uniform Uplift Pressure)

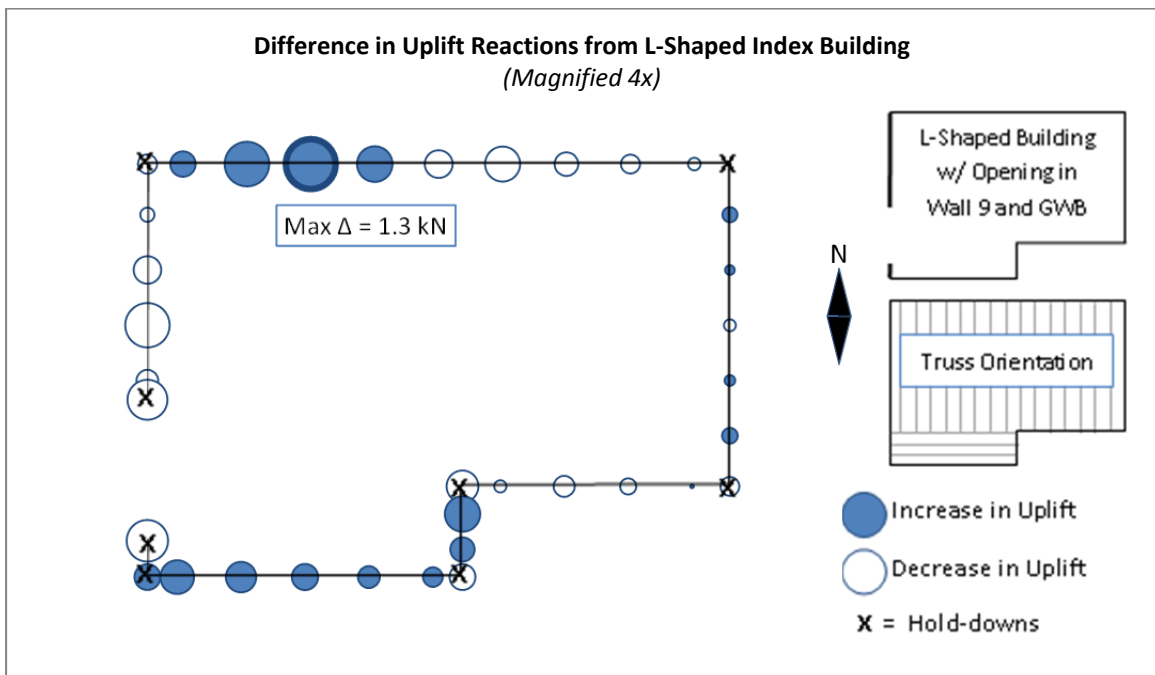


Figure J-17: Difference in Uplift Reactions in L-Shaped Building with Opening in Wall 9 Due to Addition of GWB

APPENDIX K**ASCE 7-05 DESIGN LOADS USED FOR WIND LOAD INVESTIGATION**

Design wind loads for the wind load investigation were calculated using ASCE 7-05 Main Wind Force Resisting System (MWFRS) Method 2 following methods outlined in Mehta and Coulbourne (2010) Example 3.9. Three main wind directions were considered: North-South, West-East and Southeast-Northwest as shown in Figure K-1. ASCE 7-05 Wind Loads for MWFRS Method 2, Case 1 was used for the North-South and West-East wind directions and Case 3 was used for the Southeast-Northwest wind direction (Figure K-2).

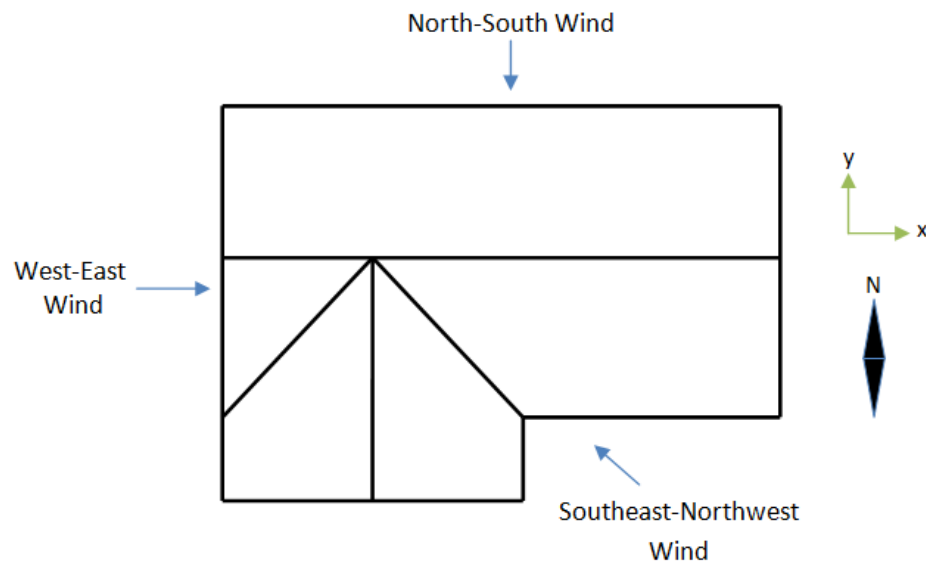


Figure K-1: Wind Directions Considered for Wind Load Investigation

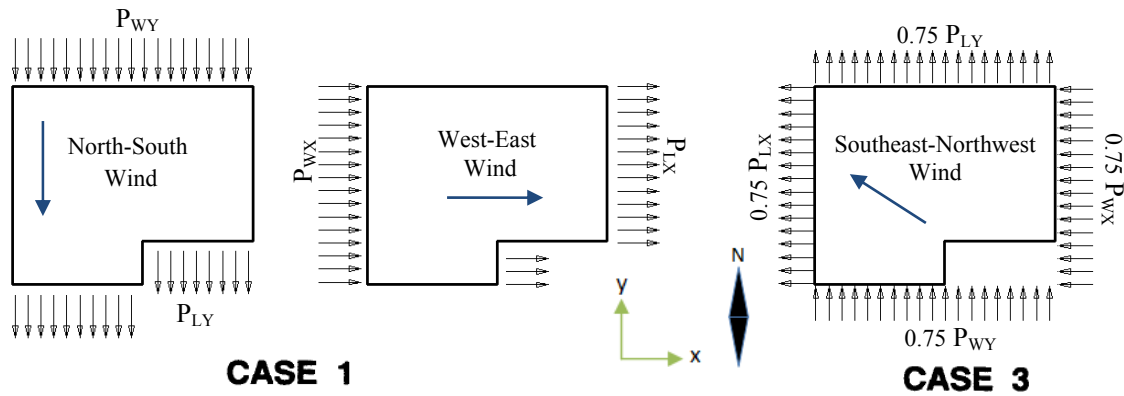


Figure K-2: ASCE 7-05 Design Wind Load Cases for Main Wind Force Resisting System, Method 2 (ASCE 7-05 Figure 6-9) – Case 1 used for North-South and East-West wind directions and Case 3 used for Southeast-Northwest wind direction. P_{WX} , P_{WY} = windward face design pressure acting in the x, y principal axes, respectively and P_{LX} , P_{LY} = leeward face design pressure acting in the x, y principal axes, respectively.

In accordance with Martin (2010), the house was considered to be a rigid, enclosed building with positive internal pressure. Additionally, the parameters for basic wind speed, exposure category, etc., from Martin (2010) were also used in the current study as outlined in Table K-2. Velocity pressure (q_z) and design wind loads (p) were calculated using ASCE 7-05 Equations 6-15 and 6-17 (Equations K-1 and K-2) respectively. Since the building is classified as a low-rise building, the velocity pressure, was evaluated at the mean roof height, only, and designated as q_h in accordance with Section 6.5.6.4.2 of ASCE 7-05.

$$q_z = 0.00256K_zK_{zt}K_dV^2I \quad \text{Equation K-1}$$

$$p = qGC_p - qGC_{pi} \quad \text{Equation K-2}$$

Each surface of the house was designated with a number as shown in Figure K-3. For each wind load direction, surfaces were categorized as a windward surface, leeward surface, side wall, etc., based on expected wind exposure. Wall and roof pressure coefficients (C_p) were then determined using ASCE 7-05 Figure 6-6. Tables K-2 through K-6 show the calculated pressure coefficients and design loads for each surface and wind load direction for the index and gable-end retrofit models. For the re-entrant corner

variations, where the overall dimensions of the house changed, the surface wind loads were adjusted accordingly.

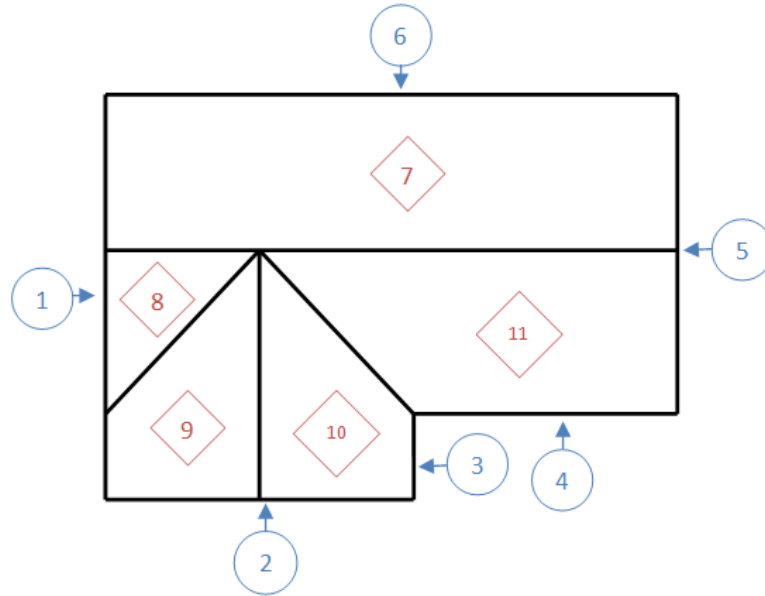


Figure K-3: Surface Designations used for Wind Pressure Calculations

Table K-1: Parameters used for ASCE 7-05 MWFRS Design Wind Loads Method 2
 – Given in specified units for ASCE 7-05 Equation 6-15

Exposure Category =	B	<i>Martin (2010)</i>
Occupancy Category =	II	<i>Martin (2010)</i>
Building Type =	Low-rise, enclosed	
Basic Wind Speed (V) =	130 mph	<i>Martin (2010)</i>
Wind Directionality Factor (K_d) =	0.85	<i>ASCE 7-05 Table 6-4</i>
Importance Factor (I) =	1	<i>Martin (2010)</i>
Topographic Factor (K_{zt}) =	1	<i>Martin (2010)</i>
Internal Pressure Coefficient (GC_{pi}) =	(+) 0.18	<i>ASCE 7-05 Figure 6-5</i>
Gust Factor (G) =	0.85	<i>ASCE 7-05 6.5.8.1 - Rigid Structure</i>
Mean Roof Height (h) =	10.35 ft	
Exposure Category (K_z) = K_h =	0.57	<i>ASCE 7-05 Table 6-3</i>
Velocity Pressure (q_z) = q_h =	20.96 psf	<i>ASCE 7-05 Equation 6-15</i>

Table K-2: Design Pressures for Index House under North-South Wind
ASCE 7-05 Load Case 1 (Figure K-2)

Surface Type	Designation (Figure K-3)	C_p (ASCE 7- 05 Figure 6-6)	External Pressure qGC_p Pa (psf)	(+) Internal Pressure $q_h(GC_{pi})$ Pa (psf)	Net Pressure, p Pa (psf)
Windward Wall	6	0.8	685 (14.3)	182 (3.8)	503 (10.5)
Overhang ^a	6	0.8	685 (14.3)	0	685 (14.3)
Side Wall	1,3,5	-0.7	-599 (-12.5)	182 (3.8)	-776 (-16.2)
Leeward Wall ^b	2,4	-0.5	-426 (-8.9)	182 (3.8)	-608 (-12.7)
Windward Roof ^c	7	-0.28	-239 (-5.0)	182 (3.8)	-421 (-8.8)
Leeward Roof	8,9,10,11	-0.6	-512 (-10.7)	182 (3.8)	-694 (-14.5)

a. $C_p = 0.8$ (ASCE 7-05 Section 6.5.11.4.1)

b. For $L/B = 0.82$

c. Interpolated for $\theta = 23^\circ$ and $h/L = 0.35$

Table K-3: Design Pressures for Index House under West-East Wind
ASCE 7-05 Load Case 1 (Figure K-2)

Surface Type	Designation (Figure K-3)	C_p (ASCE 7- 05 Figure 6-6)	External Pressure qGC_p Pa (psf)	(+) Internal Pressure $q_h(GC_{pi})$ Pa (psf)	Net Pressure, p Pa (psf)
Windward Wall	1	0.8	685 (14.3)	182 (3.8)	503 (10.5)
Overhang ^a	1	0.8	685 (14.3)	0	685 (14.3)
Side Wall	2,4,6	-0.7	-599 (-12.5)	182 (3.8)	-776 (-16.2)
Leeward Wall ^b	3,5	-0.46	-393 (-8.2)	182 (3.8)	-575 (-12.0)
Windward Roof ^c	9	-0.21	-177 (-3.7)	182 (3.8)	-359 (-7.5)
Leeward Roof	10,11	-0.6	-512 (-10.7)	182 (3.8)	-694 (-14.5)
Roof // to Ridge					
<i>0 to 1.6 m</i>	7,8	-0.9	-766 (-16.0)	182 (3.8)	-948 (-19.8)
<i>1.6 m to 3.1 m</i>	7,8	-0.9	-766 (-16)	182 (3.8)	-948 (-19.8)
<i>3.1 m to 6.3 m</i>	7,8	-0.5	-426 (8.9)	182 (3.8)	-608 (-12.7)
<i>> 6.3 m</i>	7,8	-0.3	-254 (-5.3)	182 (3.8)	-436 (-9.1)

a. $C_p = 0.8$ (ASCE 7-05 Section 6.5.11.4.1)

b. For $L/B = 1.2$

c. Interpolated for $\theta = 26^\circ$ and $h/L = 0.28$

Table K-4: ASCE 7-05 Design Pressures for Index House under South-North Wind

Surface Type	Designation (Figure K-3)	C _p (ASCE 7- 05 Figure 6-6)	External Pressure qGC _p Pa (psf)	(+) Internal Pressure q _h (GC _{pi}) Pa (psf)	Net Pressure, p Pa (psf)
Windward Wall	2,4	0.8	685 (14.3)	182 (3.8)	503 (10.5)
Overhang	2,4	0.8	685 (14.3)	0	685 (14.3)
Leeward Wall	6	-0.5	-426 (8.9)	182 (3.8)	-608 (-12.7)
Windward Roof	8,11	-0.28	-239 (-5.0)	182 (3.8)	-421 (-8.8)
Leeward Roof	7	-0.6	-512 (-10.7)	182 (3.8)	-694 (-14.5)

a. C_p = 0.8 (ASCE 7-05 Section 6.5.11.4.1)

b. For L/B = 0.82

c. Interpolated for $\theta = 23^\circ$ and h/L = 0.35

Table K-5: ASCE 7-05 Design Pressures for Index House under East-West Wind

Surface Type	Designation (Figure K-3)	C _p (ASCE 7- 05 Figure 6-6)	External Pressure qGC _p Pa (psf)	(+) Internal Pressure q _h (GC _{pi}) Pa (psf)	Net Pressure, p Pa (psf)
Windward Wall	3,5	0.8	685 (14.3)	182 (3.8)	503 (10.5)
Overhang	3,5	0.8	685 (14.3)	0	685 (14.3)
Leeward Wall	1	-0.46	-393 (-8.2)	182 (3.8)	-575 (-12.0)
Windward Roof	10	-0.21	-177 (-3.7)	182 (3.8)	-359 (-7.5)
Leeward Roof	9,8	-0.6	-512 (-10.7)	182 (3.8)	-694 (-14.5)

a. C_p = 0.8 (ASCE 7-05 Section 6.5.11.4.1)

b. For L/B = 1.2

c. Interpolated for $\theta = 26^\circ$ and h/L = 0.28

Table K-6: Design Pressures for Index Building under Southeast-Northwest Wind = 0.75(S-N) + 0.75(E-W) – ASCE 7-05 Load Case 3 (Figure K-2)

Surface Type	Designation (Figure K-3)	S-N Net Pressure P Pa (psf)	E-W Net Pressure P Pa (psf)	0.75*p Pa (psf)
Windward Wall	2,4	503 (10.5)		378 (7.9)
Overhang	2,4	685 (14.3)		512 (10.7)
Windward Wall	5,3		503 (10.5)	378 (7.9)
Overhang	5,3		685 (14.3)	512 (10.7)
Leeward Wall	6	-608 (-12.7)		-455 (-9.5)
Leeward Wall	1		-575 (-12.0)	-431 (-9.0)
Windward Roof	11	-421 (-8.8)		-316 (-6.6)
Windward Roof	10		-359 (-7.5)	-268 (-5.6)
Leeward Roof	7	-694 (-14.5)		-522 (-10.9)
Leeward Roof	9,8		-694 (-14.5)	-522 (-10.9)

APPENDIX L

WIND LOAD INVESTIGATION

For the wind load investigation, the propagation of lateral and uplift wind loads through an L-shaped house were modeled and analyzed. The house was then systematically modified to study the redistribution of wind loads due to the addition of a gable-end retrofit and various re-entrant corner dimensions. Model variations used for the wind load investigation are detailed in Appendix I and include:

- A model of the Paevere et al. (2003) house with the gable-end framing, hold-down and sheathing modifications described in Appendix I. This building is designated as the *L-shaped index house* for this investigation.
- The L-shaped index house with the addition of *gable-end retrofits* as recommended in the 2010 Florida Building Code (Figure I-9).
- The L-shaped index house with one leg of the “L” shortened/extended as shown in Figure I-13 to create three re-entrant corner variations:
 - *Small re-entrant corner* (leg shortened by 1.2 m)
 - *Medium re-entrant corner* (leg extended by 1.2 m)
 - *Large re-entrant corner* (leg extended to create a re-entrant corner with 1:1 dimensional ratio)

All model variations in this investigation include the self weight of the construction materials for realistic results. Models were loaded with ASCE 7-05 design wind loads for each of the three wind directions described in Appendix K. Uplift and change in uplift reactions for each building were plotted using the same “bubble plots” used in Appendix J. Lateral load distributions to in-plane walls were also plotted for each model and load case.

L-shaped index house

North to South Wind Loads

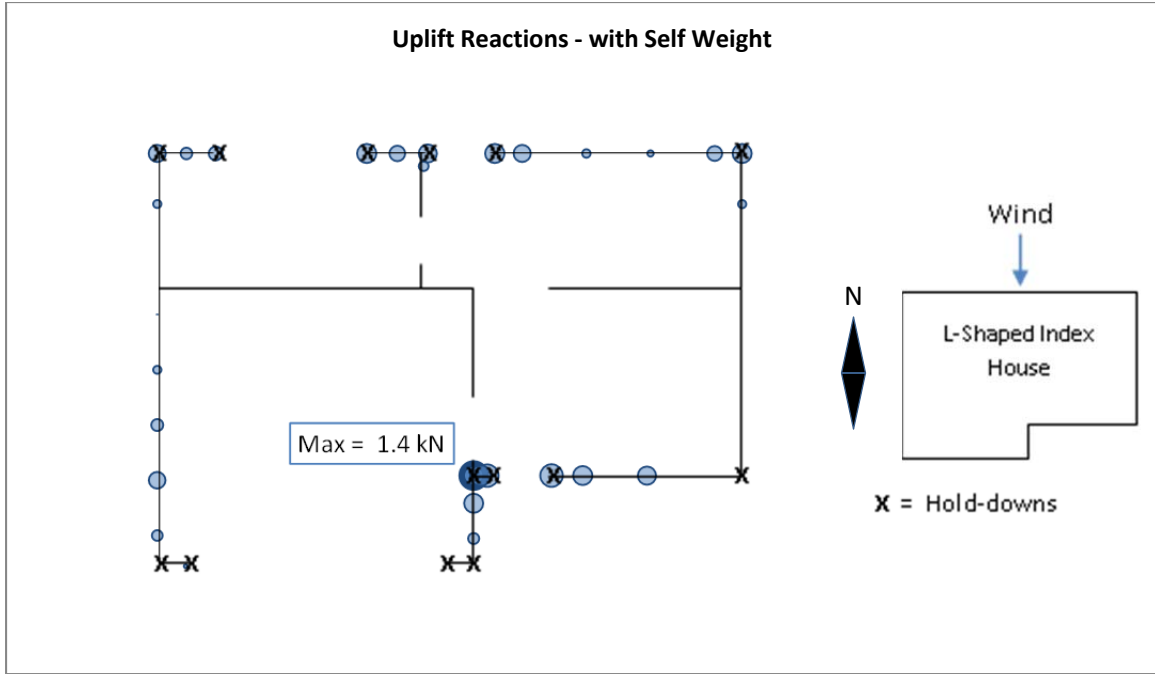


Figure L-1: Uplift Reactions for L-shaped index house under North-South Wind Loads (with Self Weight)

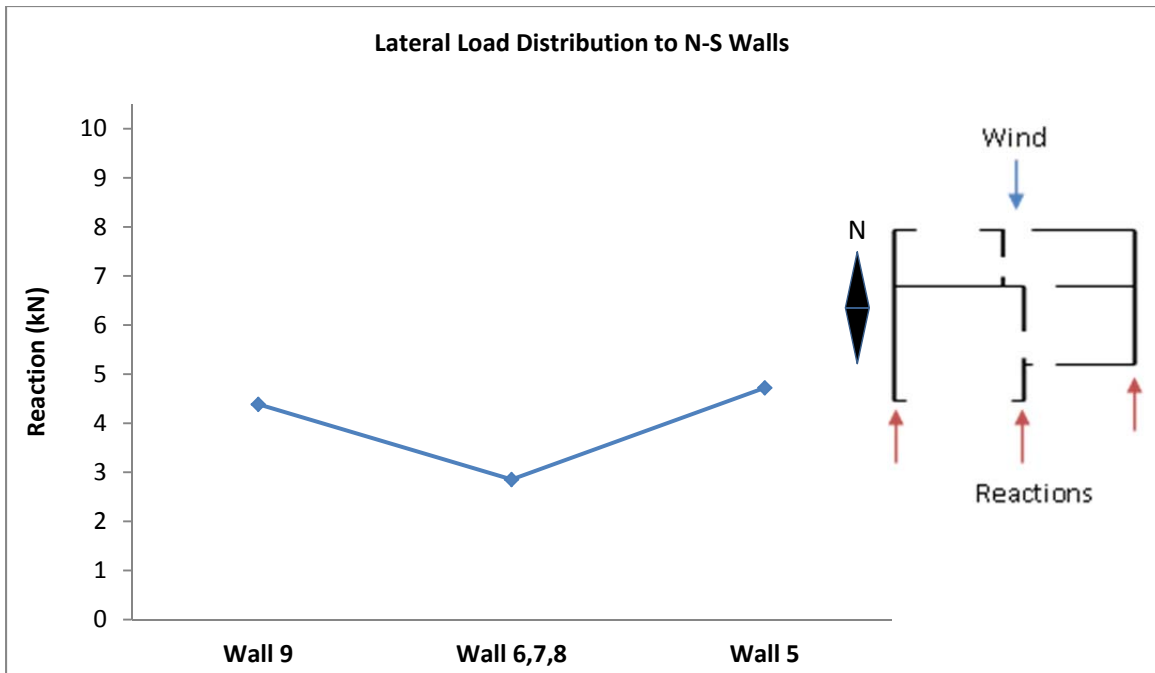


Figure L-2: Lateral Load Distribution to North-South walls under North-South Wind Loads (with Self Weight)

West to East Wind Loads

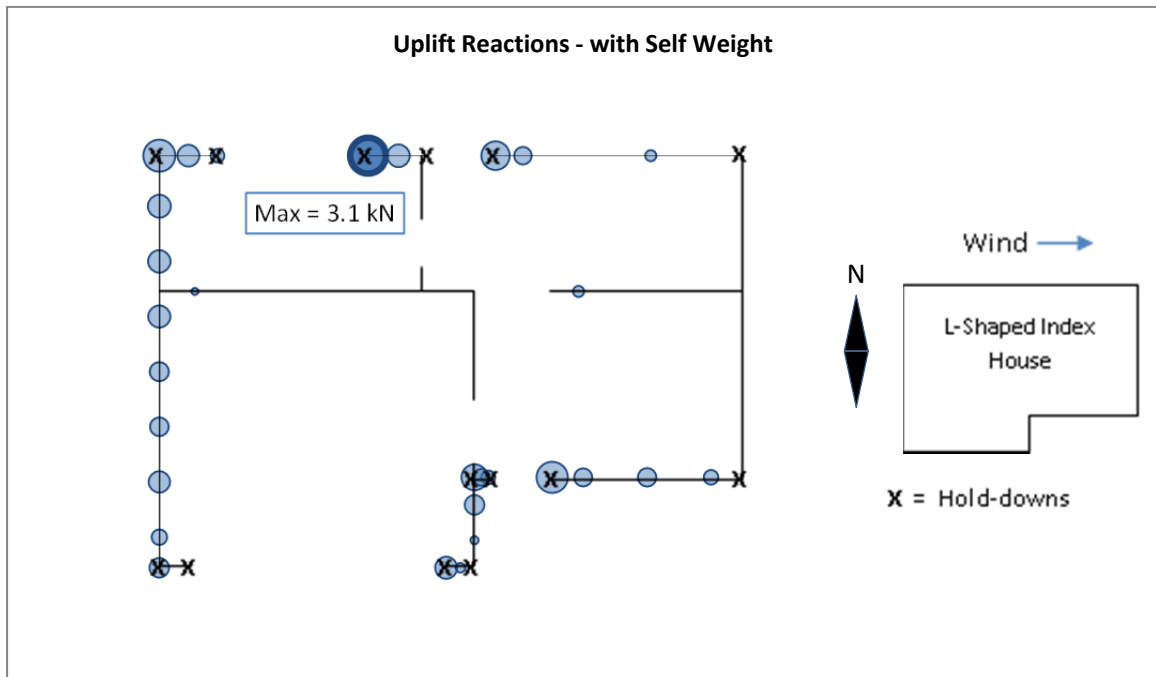


Figure L-3: Uplift Reactions for L-shaped index house under West-East Wind Loads (with Self Weight)

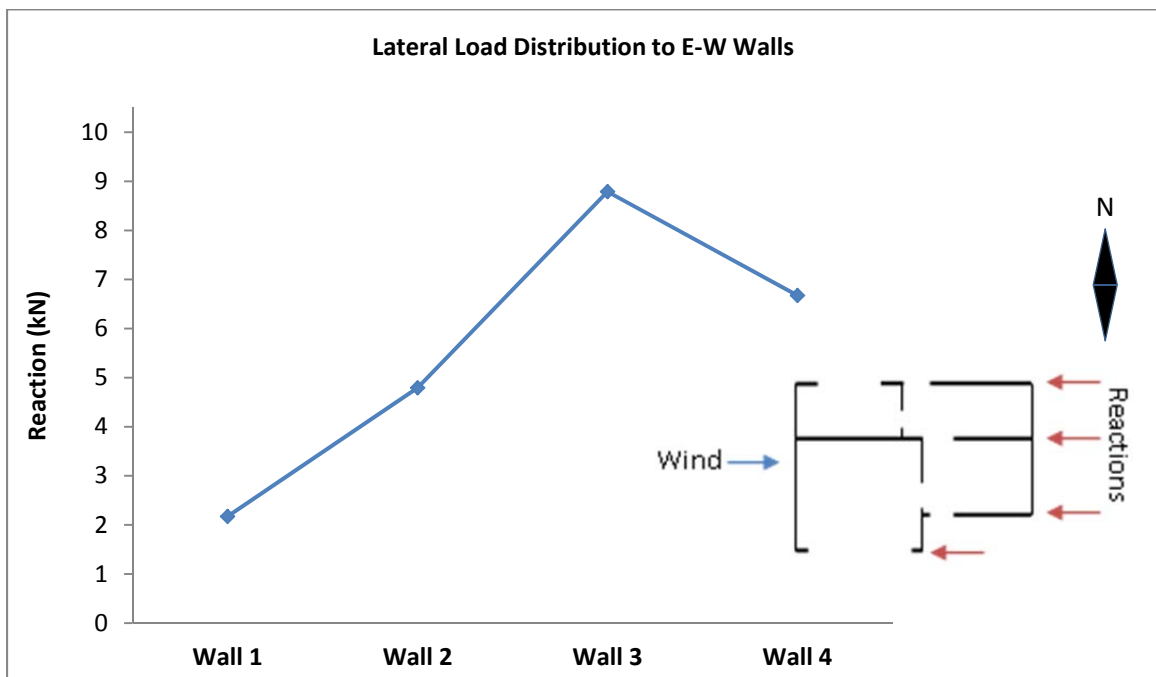


Figure L-4: Lateral Load Distribution to East-West walls under West-East Wind Loads (with Self Weight)

Southeast-Northwest Wind Loads

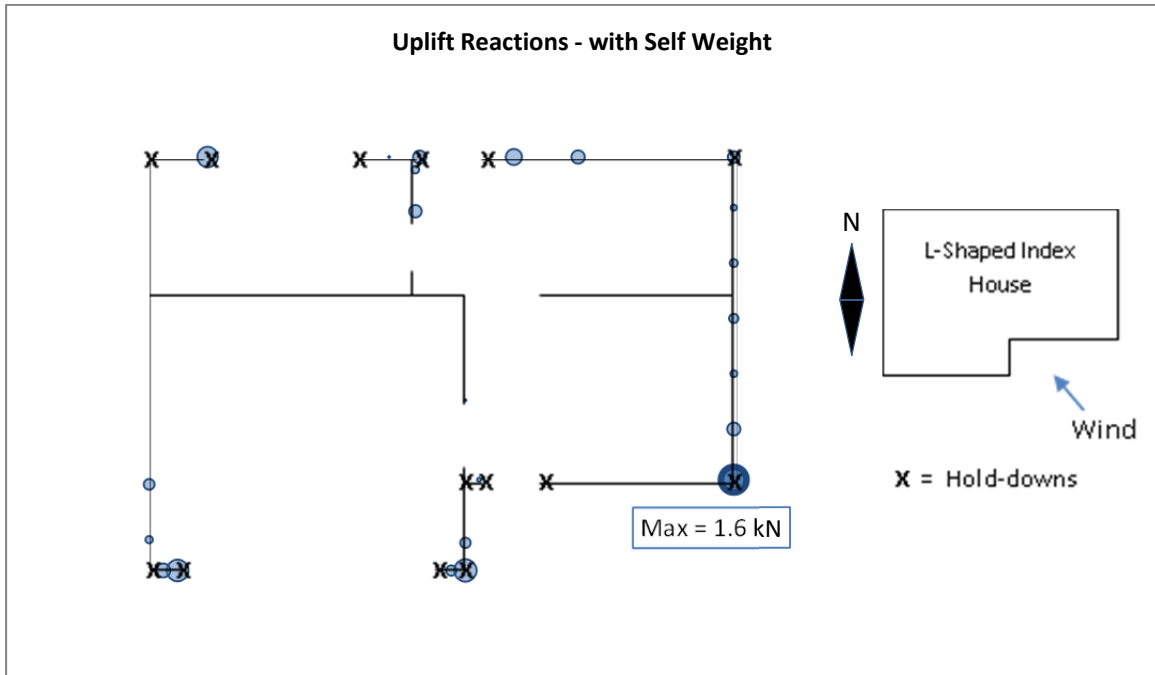


Figure L-5: Uplift Reactions for L-shaped index house under Southeast-Northwest Wind Loads (with Self Weight)

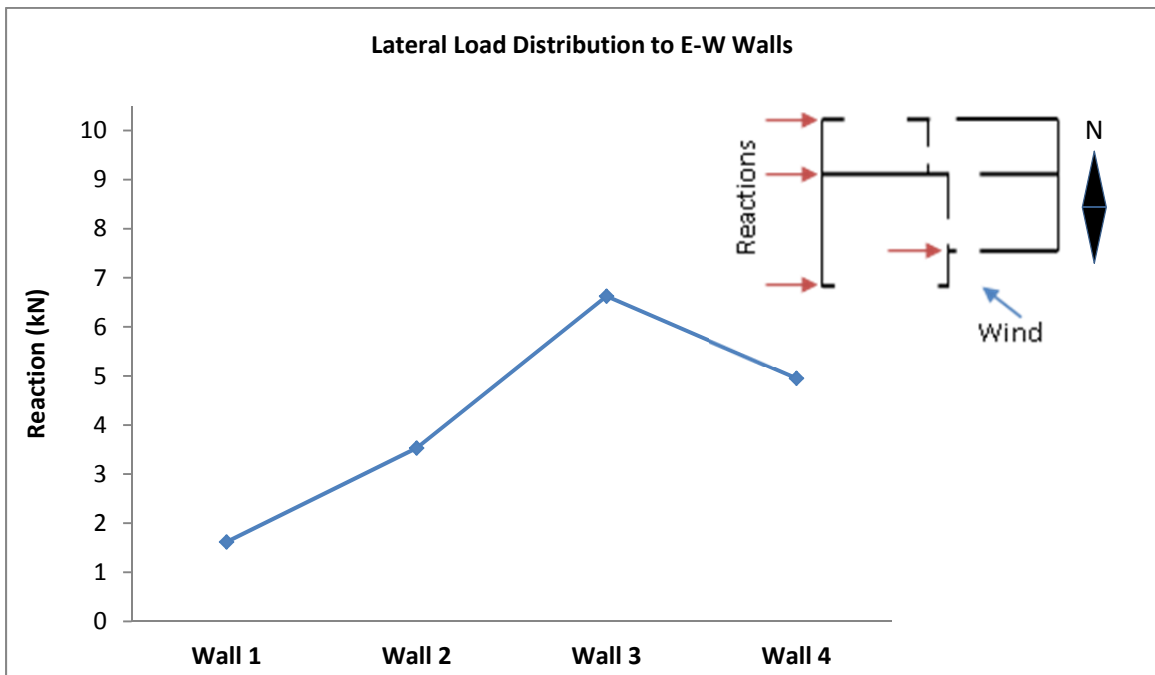


Figure L-6: Lateral Load Distribution to North-South walls under Southeast-Northwest Wind Loads (with Self Weight)

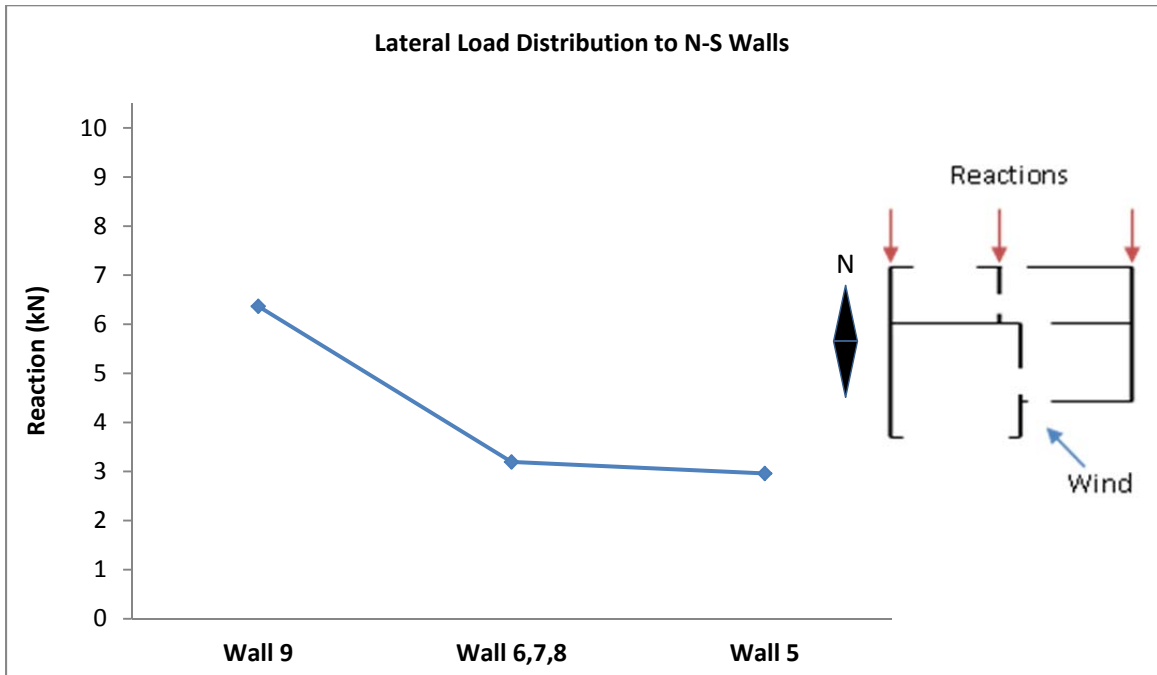


Figure L-7: Lateral Load Distribution to East-West walls under Southeast-Northwest Wind Loads (with Self Weight)

Gable-End Retrofit Investigation

North-South Wind Load

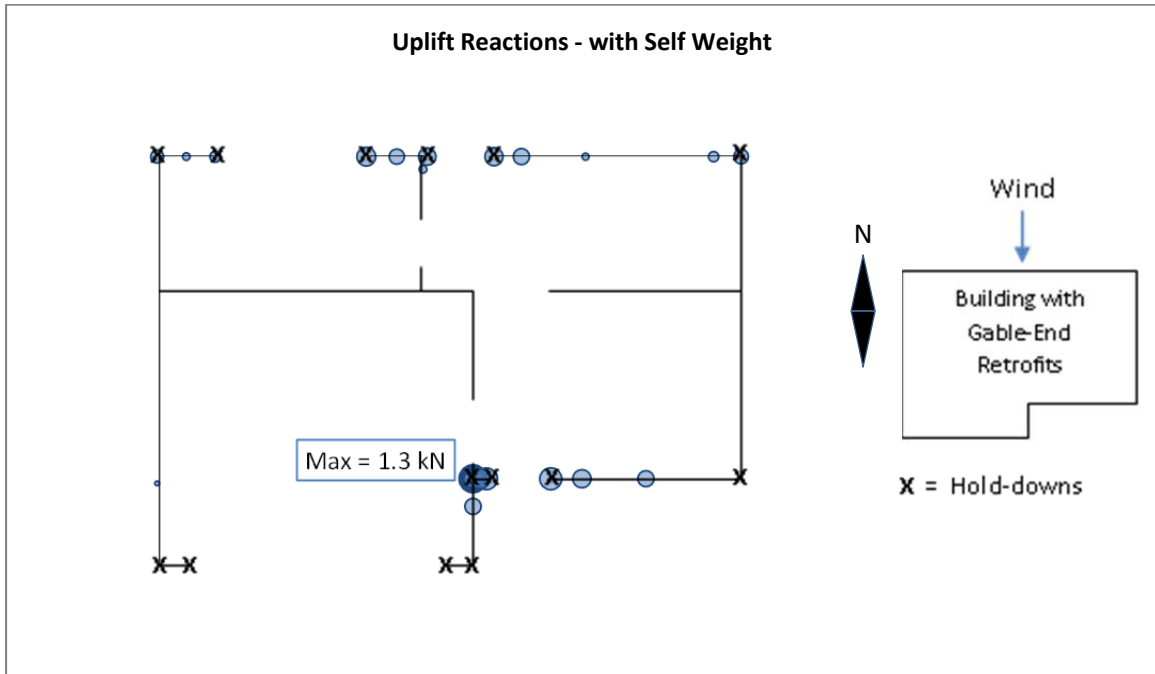


Figure L-8: Uplift Reactions for Building with Gable-End Retrofits under North-South Wind Loads (with Self Weight)

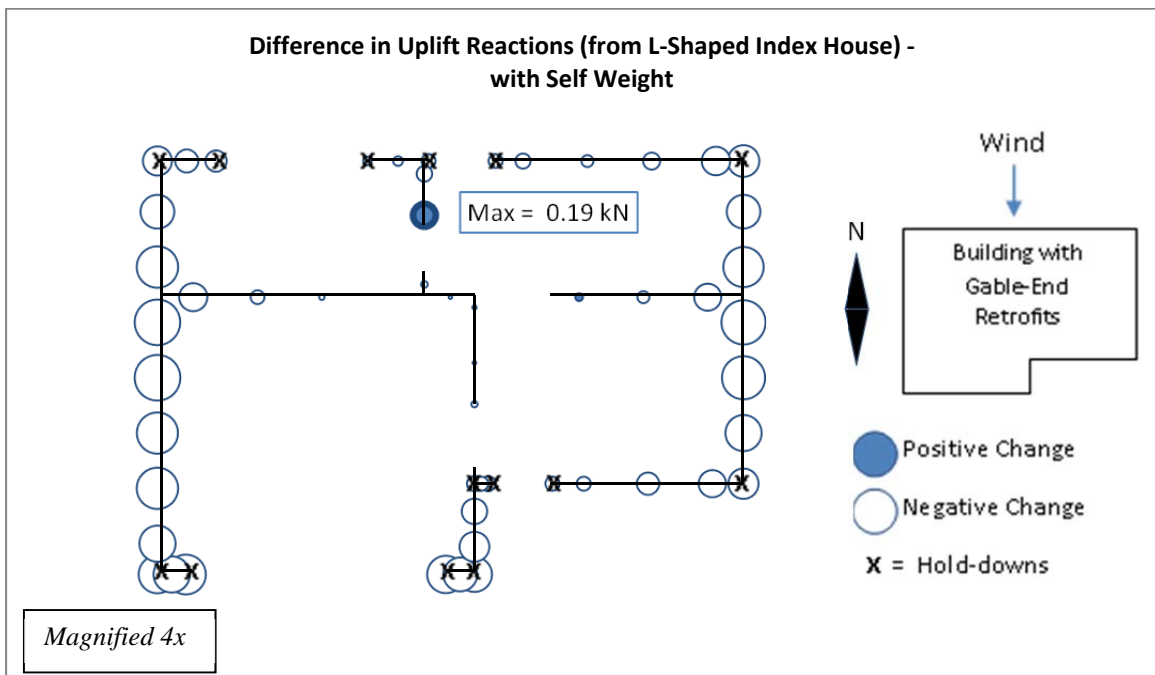


Figure L-9: Difference in Uplift Reactions between Building with Gable-End Retrofits and L-shaped index house under North-South Wind Loads (with Self Weight)

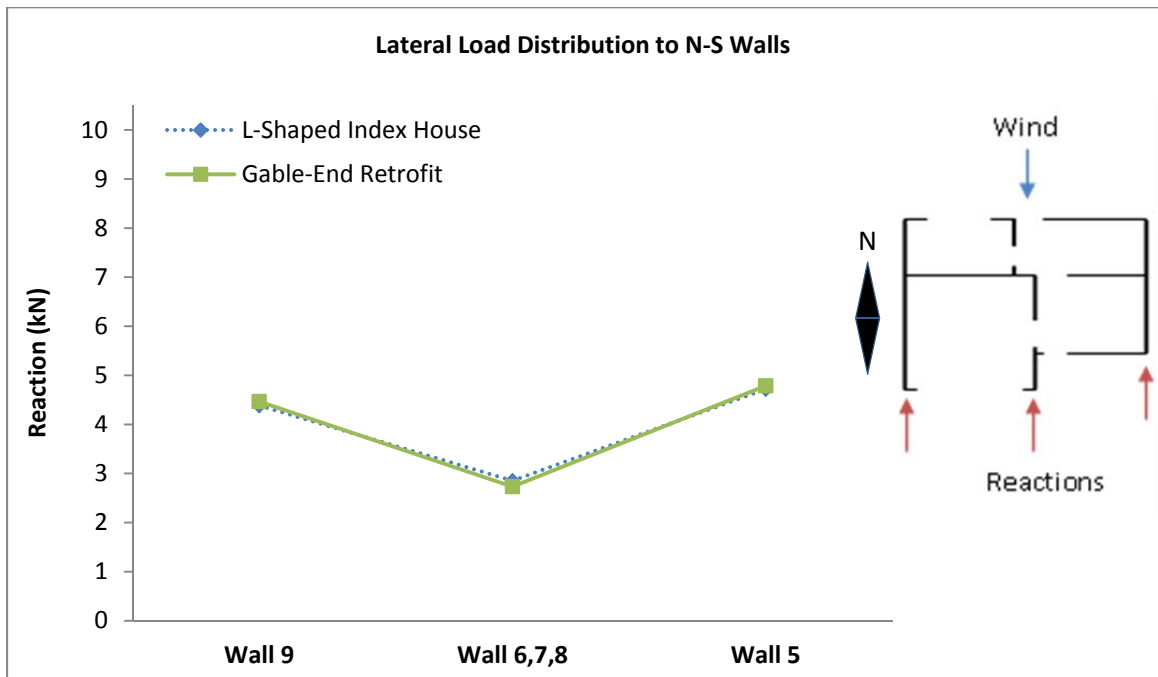


Figure L-10: Lateral Load Distribution to North-South walls under North-South Wind Loads (with Self Weight)

West to East Wind Loads

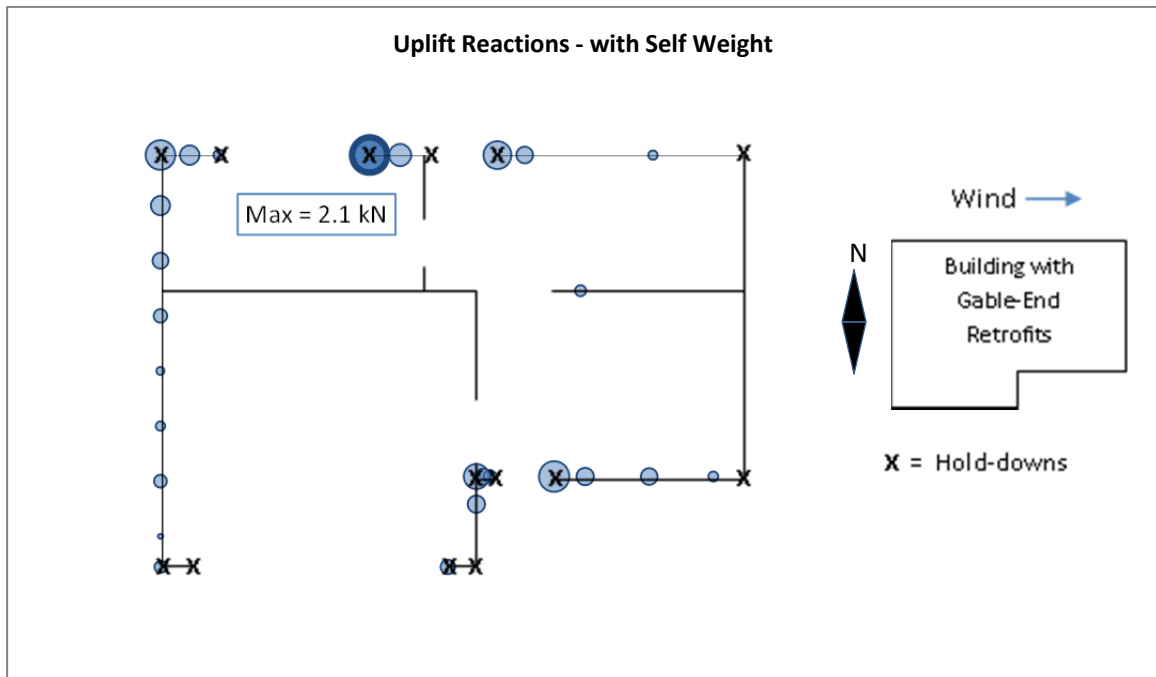


Figure L-11: Uplift Reactions for Building with Gable-End Retrofits under West-East Wind Loads (with Self Weight)

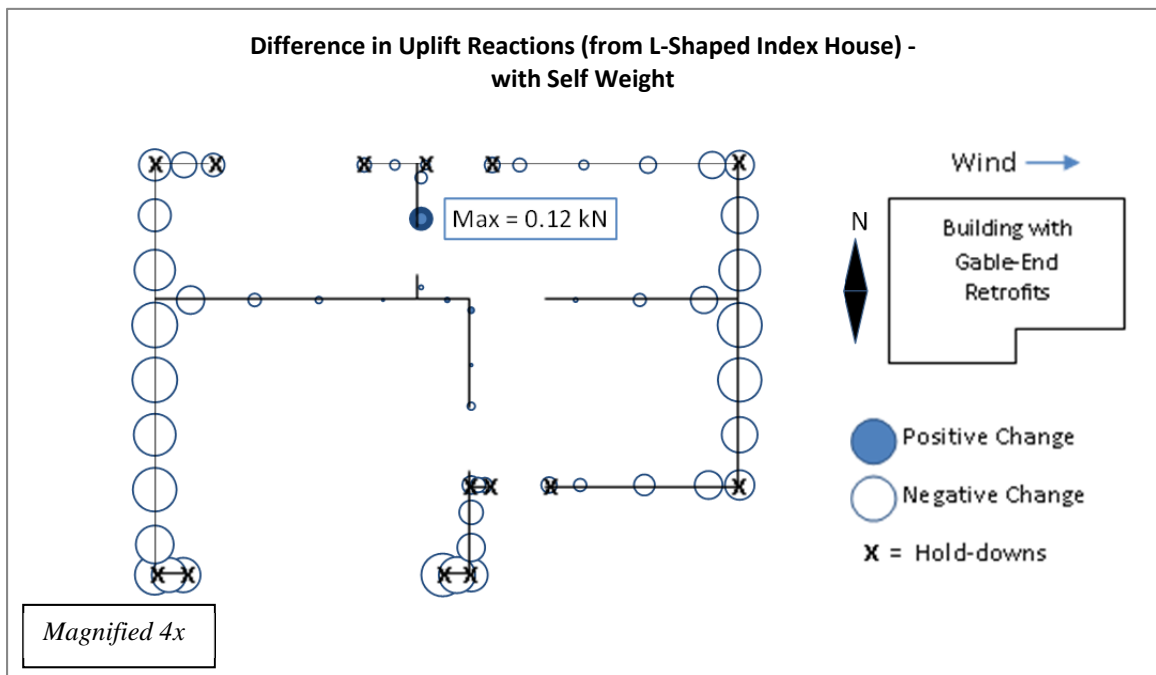


Figure L-12: Difference in Uplift Reactions between Building with Gable-End Retrofits and L-shaped index house under West-East Wind Loads (with Self Weight)

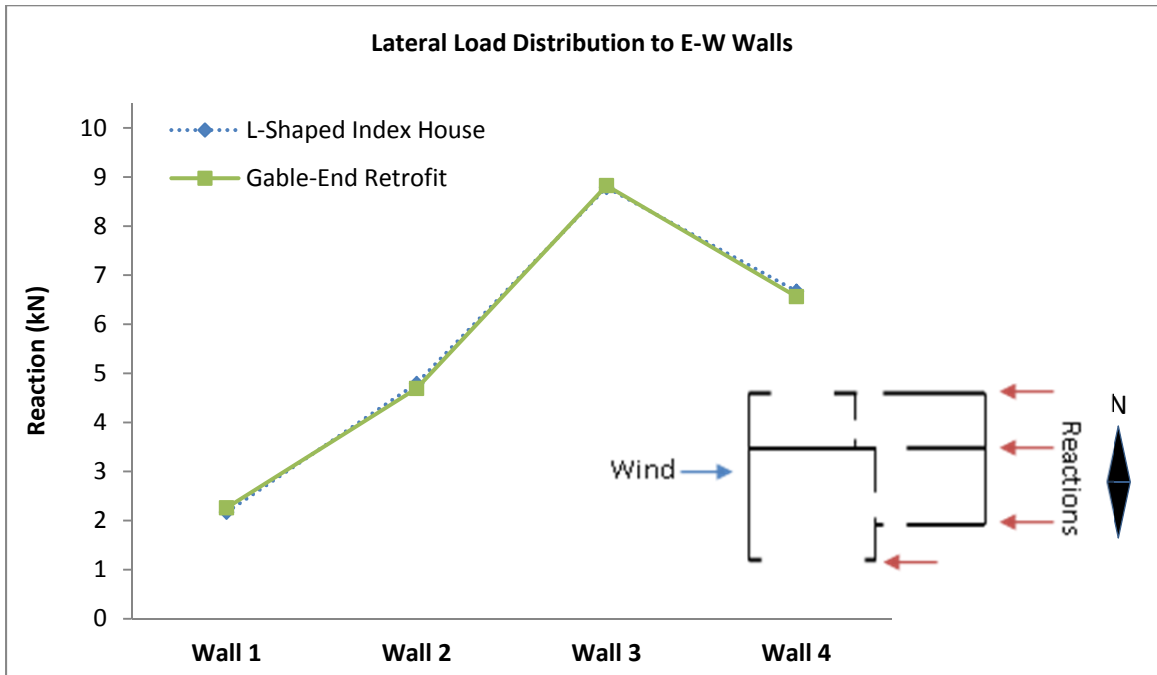


Figure L-13: Lateral Load Distribution to East-West walls under West-East Wind Loads (with Self Weight)

Southeast to Northwest Wind Loads

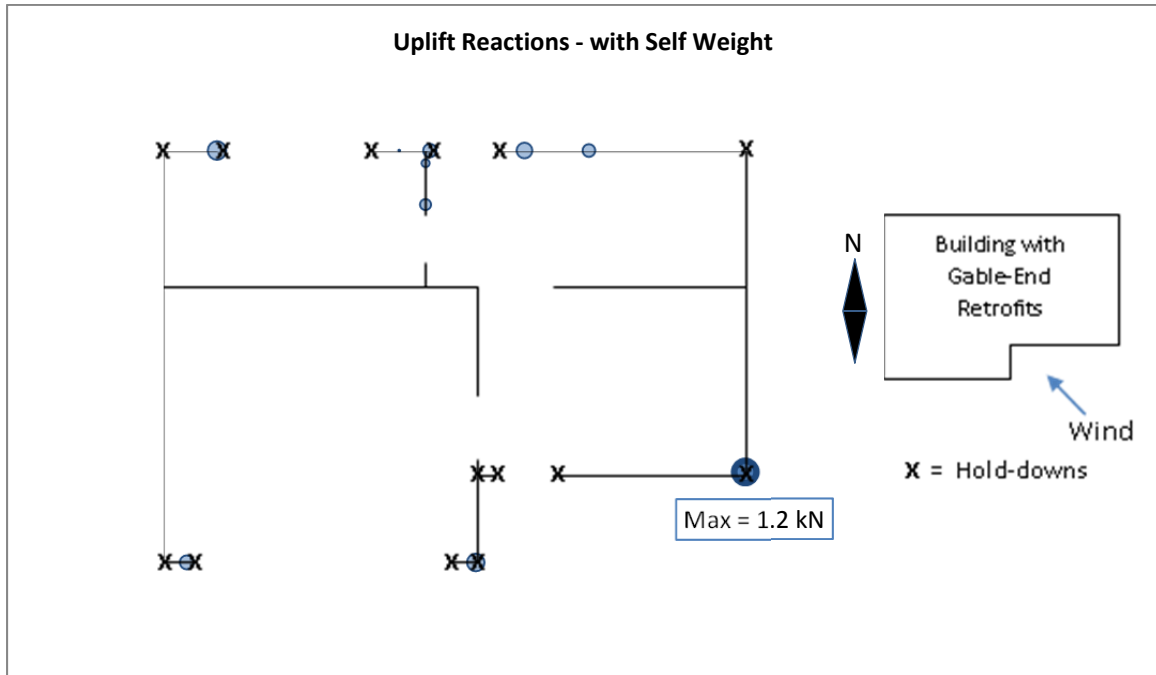


Figure L-14: Uplift Reactions for Building with Gable-End Retrofits under Southeast-Northwest Wind Loads (with Self Weight)

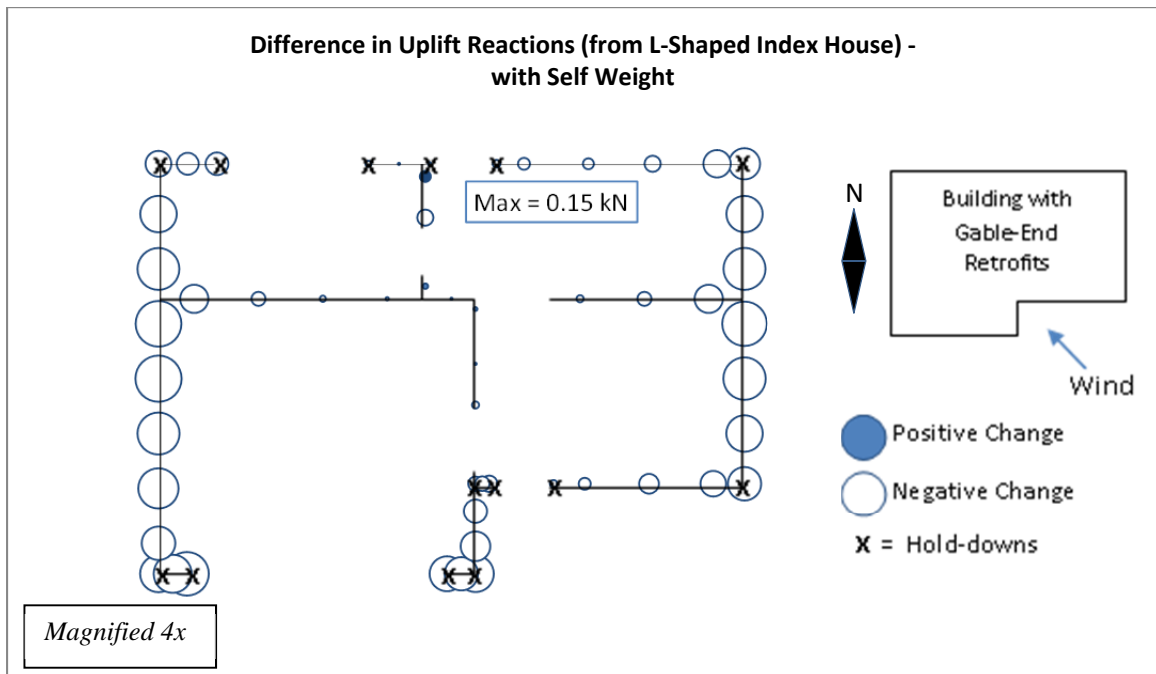


Figure L-15: Difference in Uplift Reactions between Building with Gable-End Retrofits and L-shaped index house under Southeast-Northwest Wind Loads (with Self Weight)

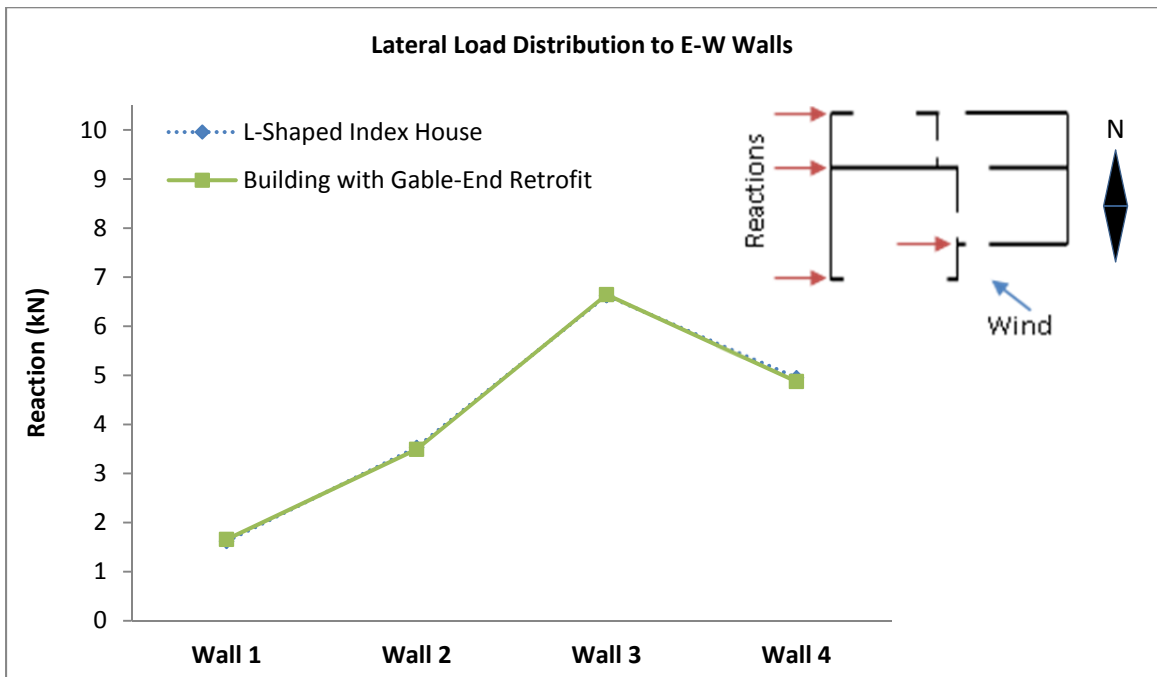


Figure L-16: Lateral Load Distribution to East-West walls under Southeast-Northwest Wind Loads (with Self Weight)

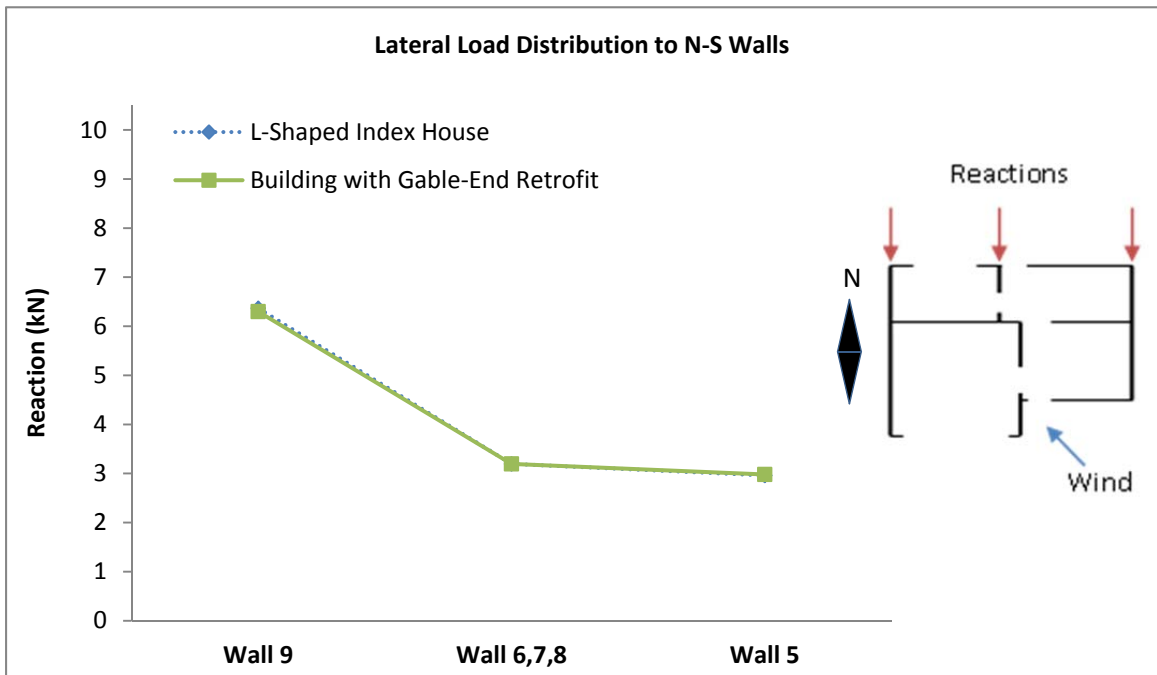


Figure L-17: Lateral Load Distribution to North-South walls under Southeast-Northwest Wind Loads (with Self Weight)

Re-Entrant Corner Investigation

North to South Wind Loads

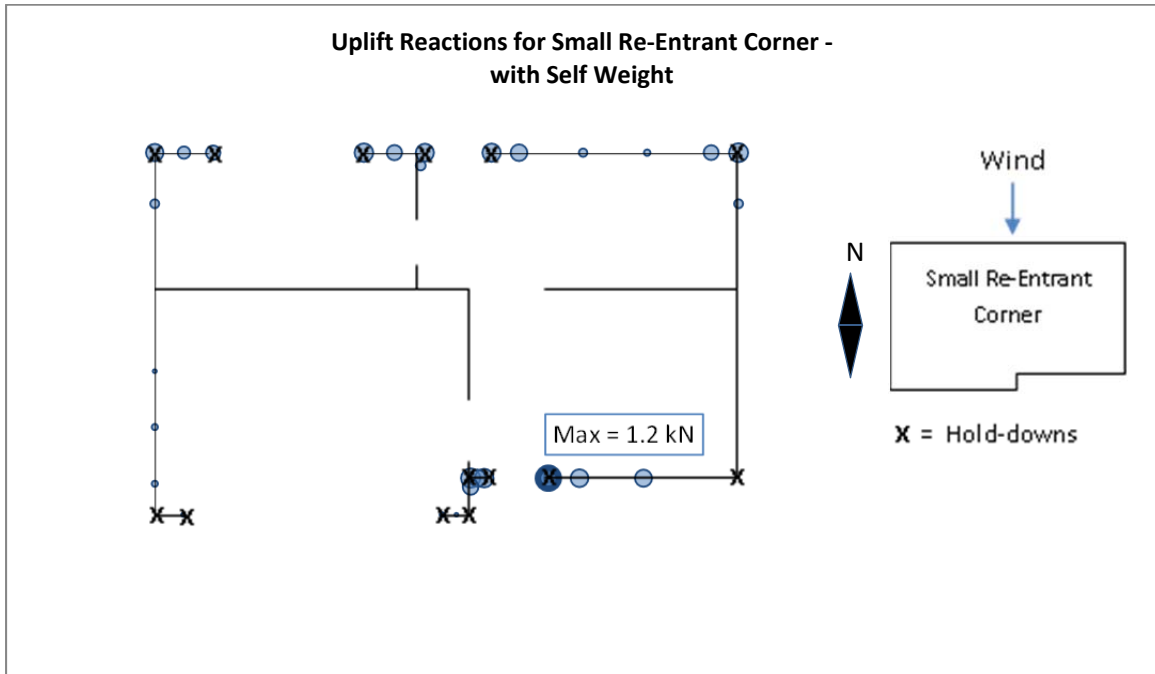


Figure L-18: Uplift Reactions for Building with Small Re-Entrant Corner under North-South Wind Loads (with Self Weight)

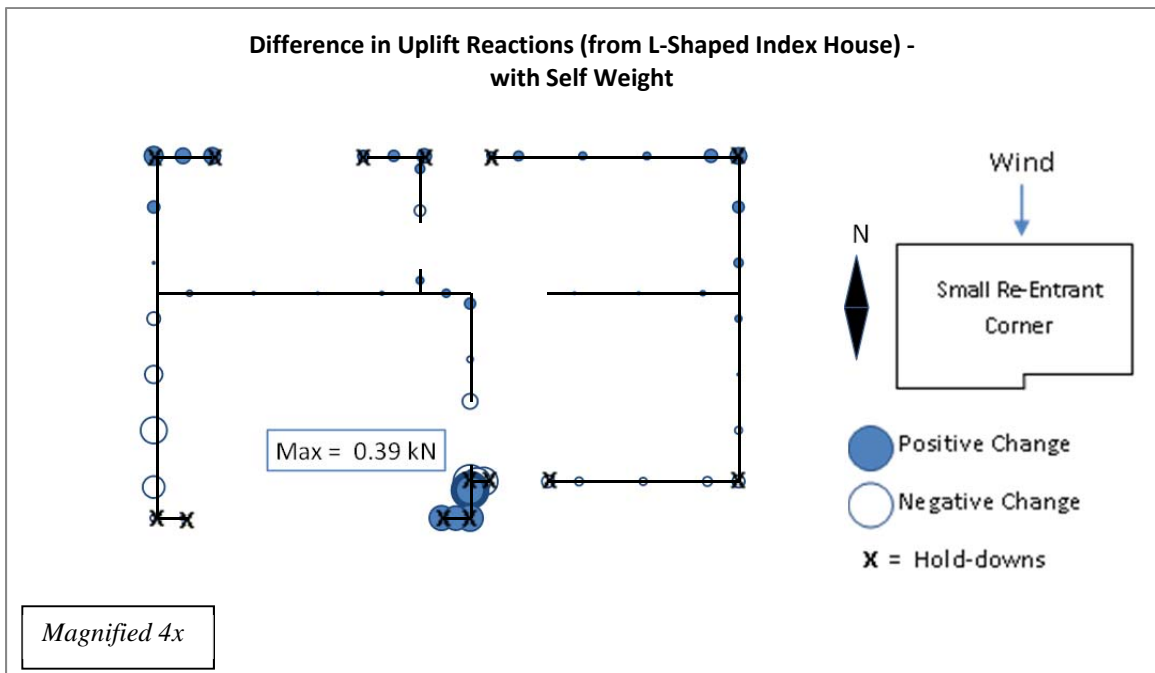


Figure L-19: Difference in Uplift Reactions between Building with Small Re-Entrant Corner and L-shaped index house under North-South Wind Loads (with Self Weight)

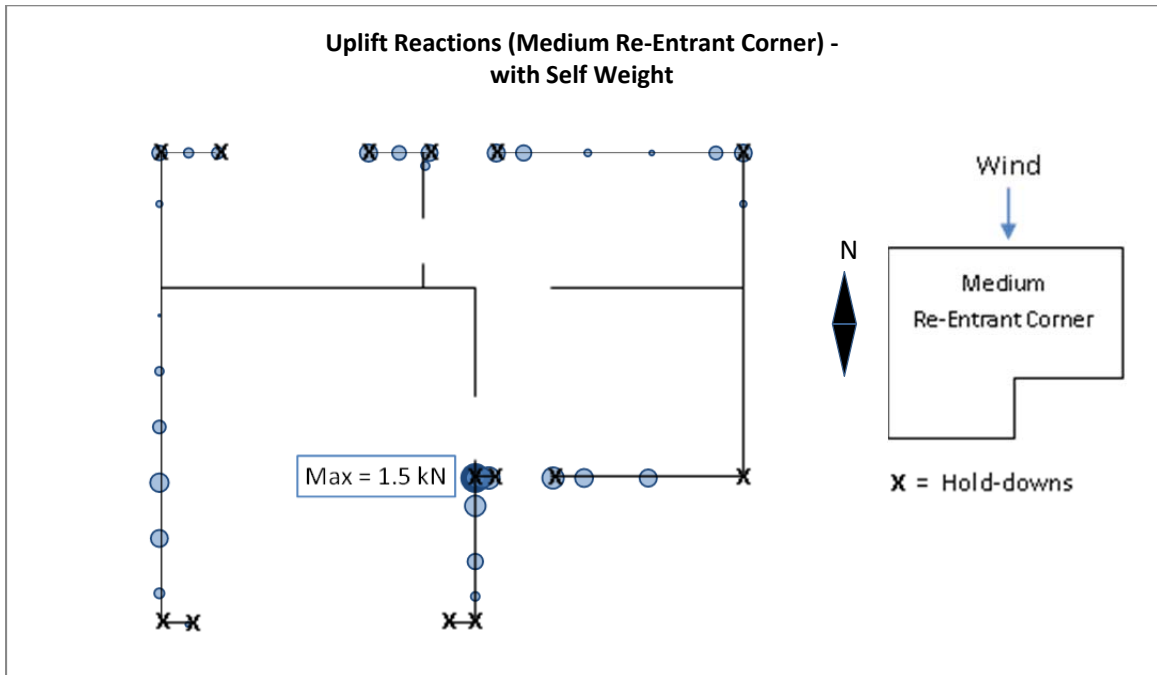


Figure L-20: Uplift Reactions for Building with Medium Re-Entrant Corner under North-South Wind Loads (with Self Weight)

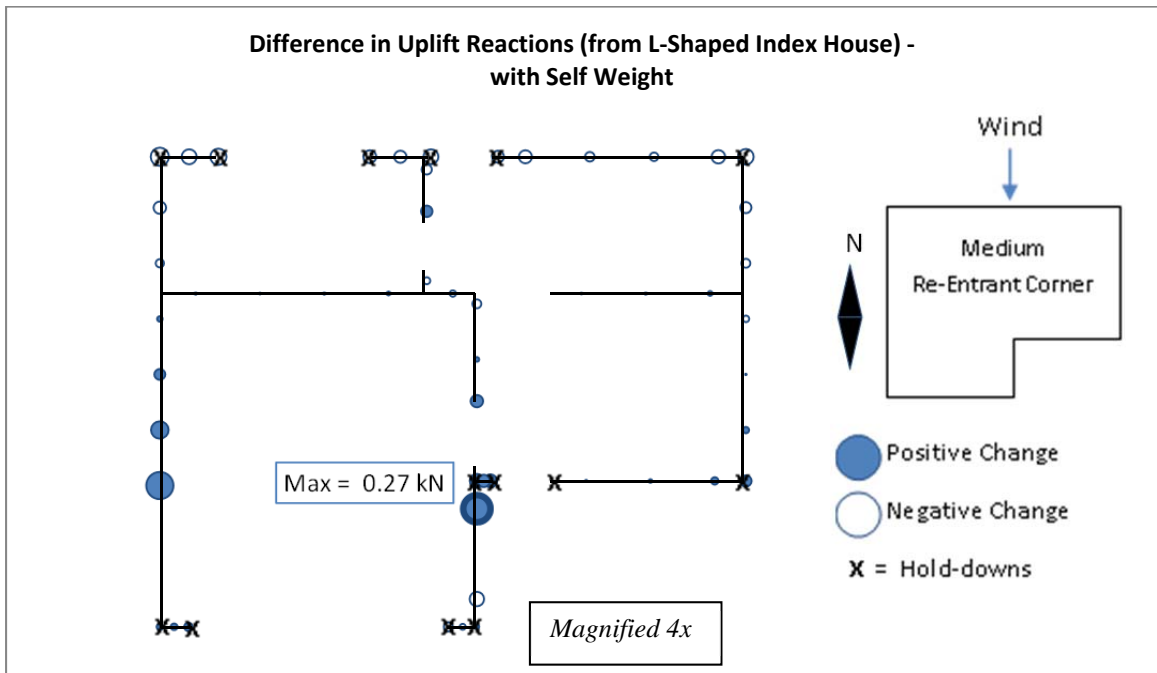


Figure L-21: Difference in Uplift Reactions between Building with Medium Re-Entrant Corner and L-shaped index house under North-South Wind Loads (with Self Weight)

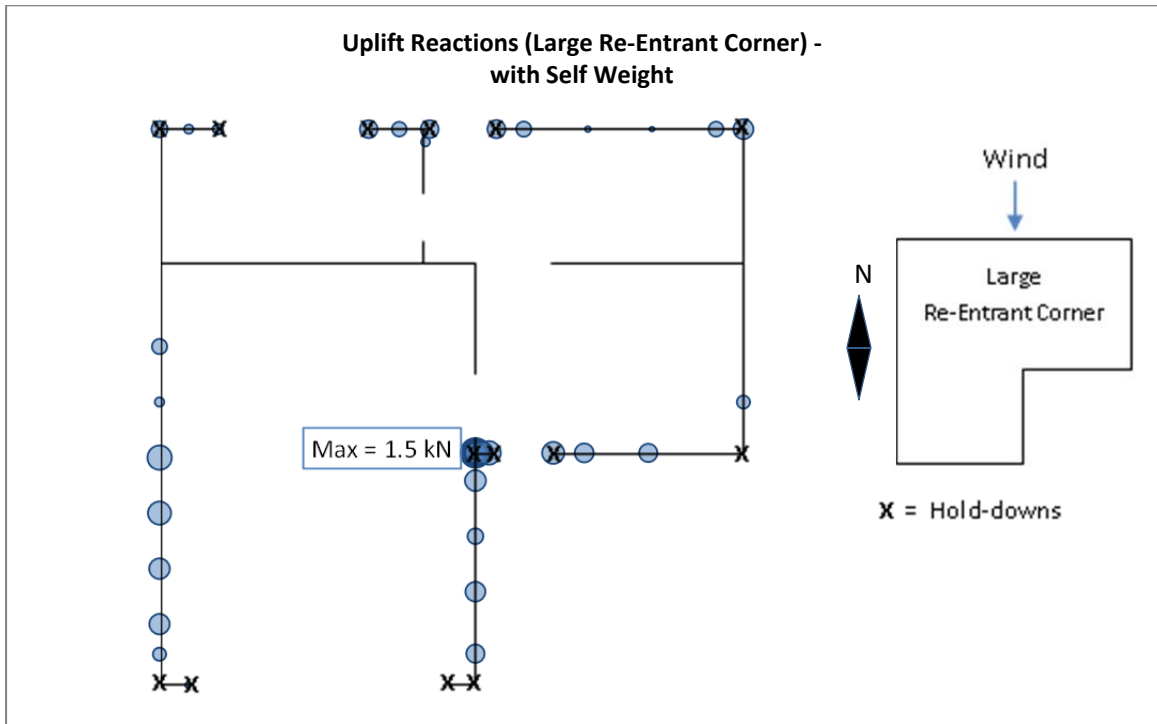


Figure L-22: Uplift Reactions for Building with Large Re-Entrant Corner under North-South Wind Loads (with Self Weight)

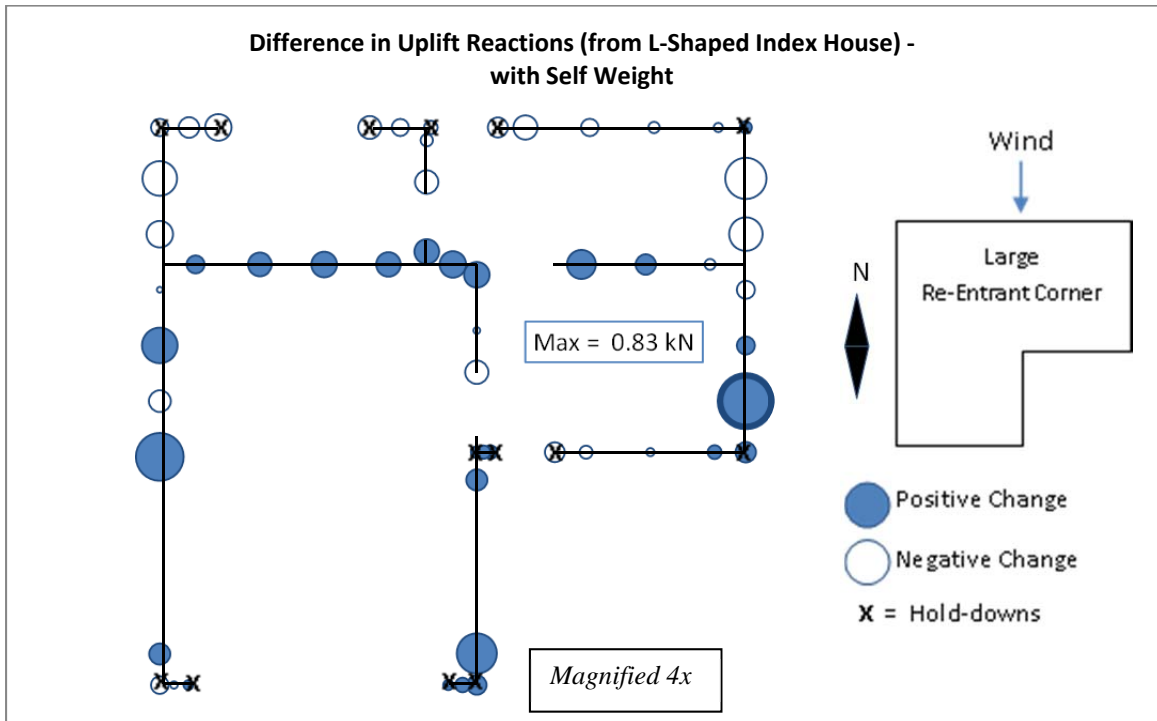


Figure L-23: Difference in Uplift Reactions between Building with Large Re-Entrant Corner and L-shaped index house under North-South Wind Loads (with Self Weight)

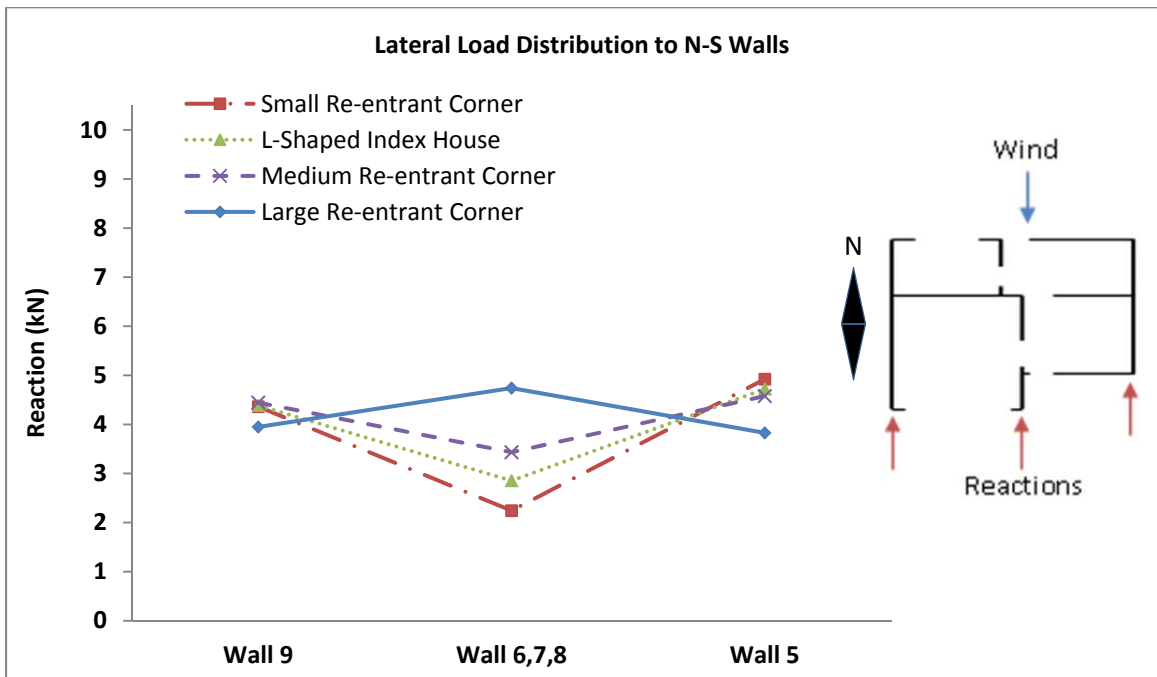


Figure L-24: Lateral Load Distribution to North-South walls under North-South Wind Loads (with Self Weight)

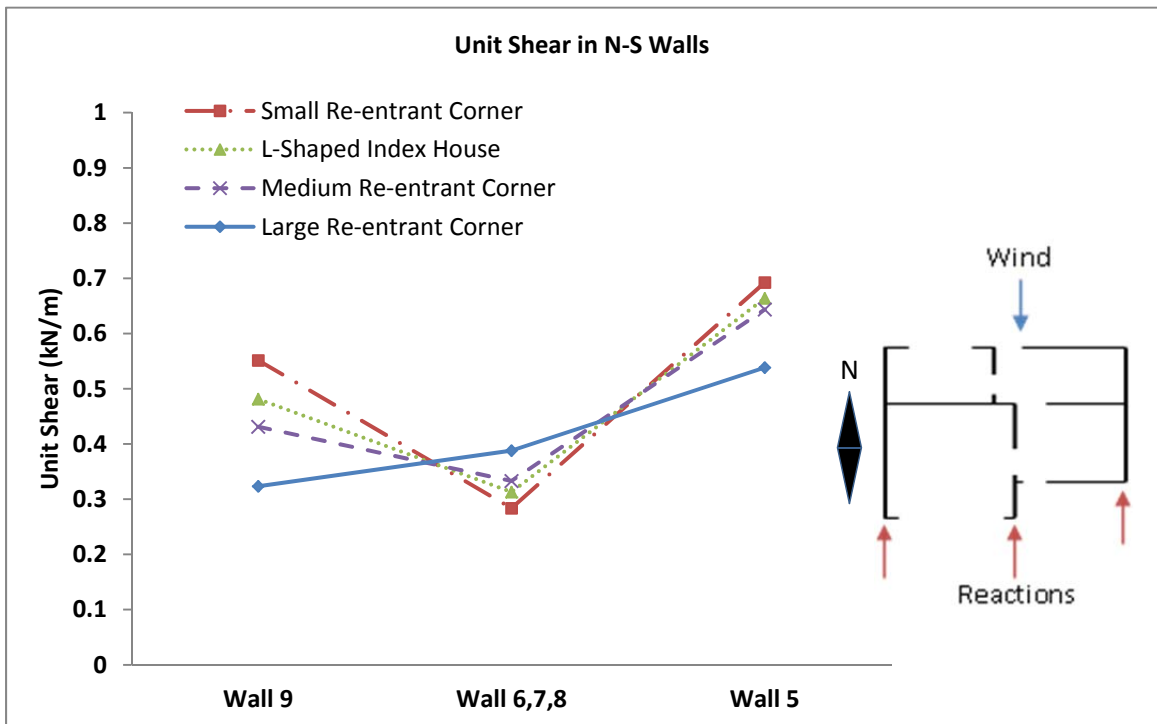


Figure L-25: Unit Shear in North-South walls under North-South Wind Loads (with Self Weight)

West to East Wind Loads

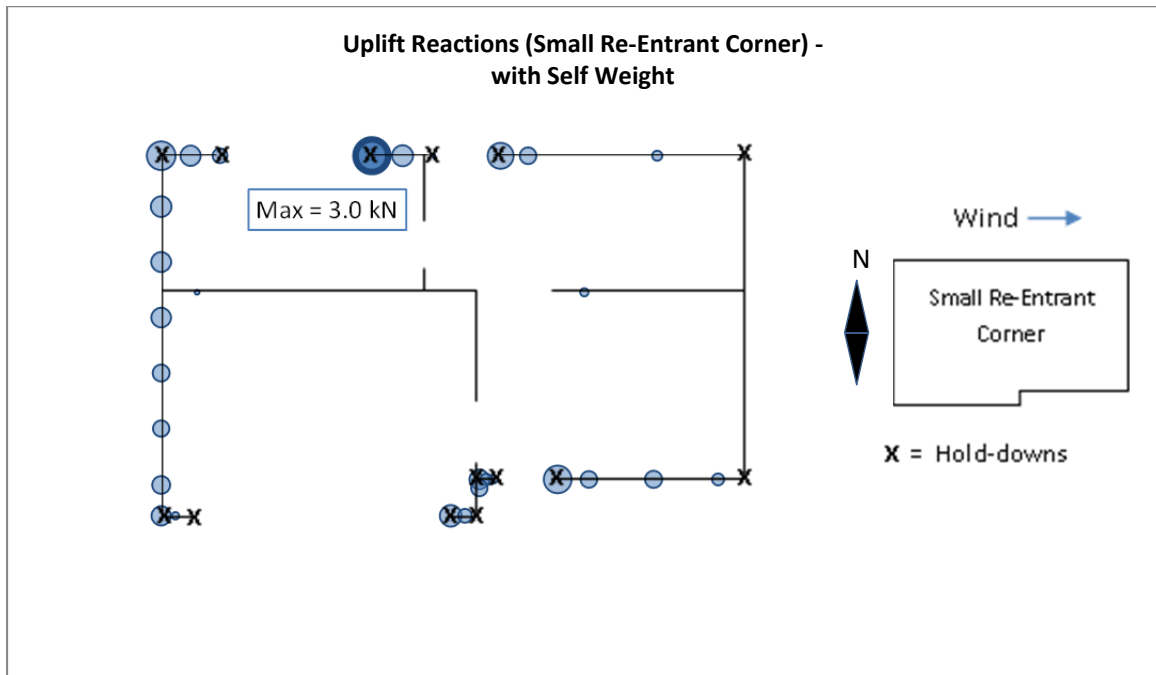


Figure L-26: Uplift Reactions for Building with Small Re-Entrant Corner under West-East Wind Loads (with Self Weight)

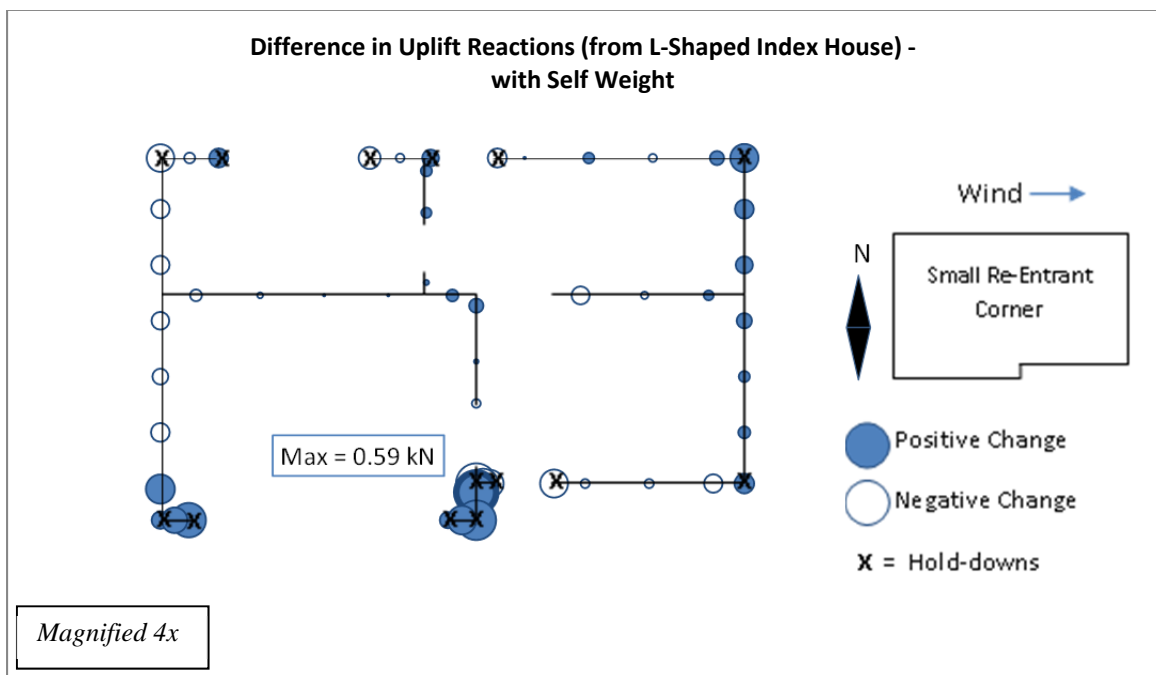


Figure L-27: Difference in Uplift Reactions between Building with Small Re-Entrant Corner and L-shaped index house under West-East Wind Loads (with Self Weight)

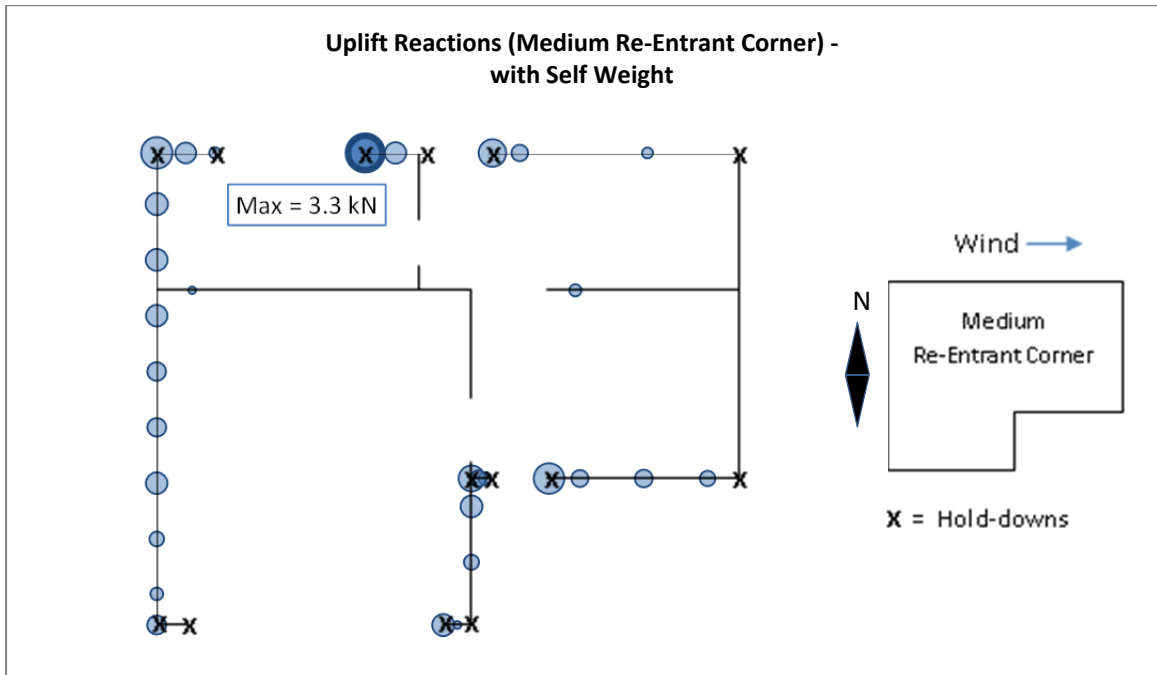


Figure L-28: Uplift Reactions for Building with Medium Re-Entrant Corner under West-East Wind Loads (with Self Weight)

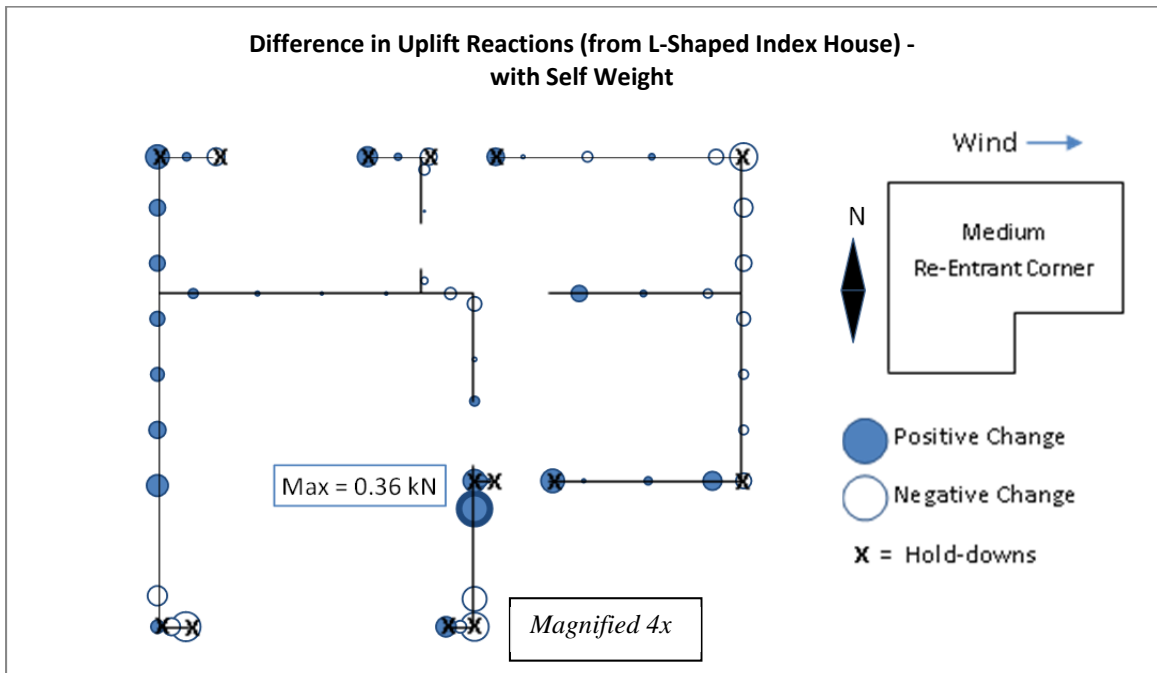


Figure L-29: Difference in Uplift Reactions between Building with Medium Re-Entrant Corner and L-shaped index house under West-East Wind Loads (with Self Weight)

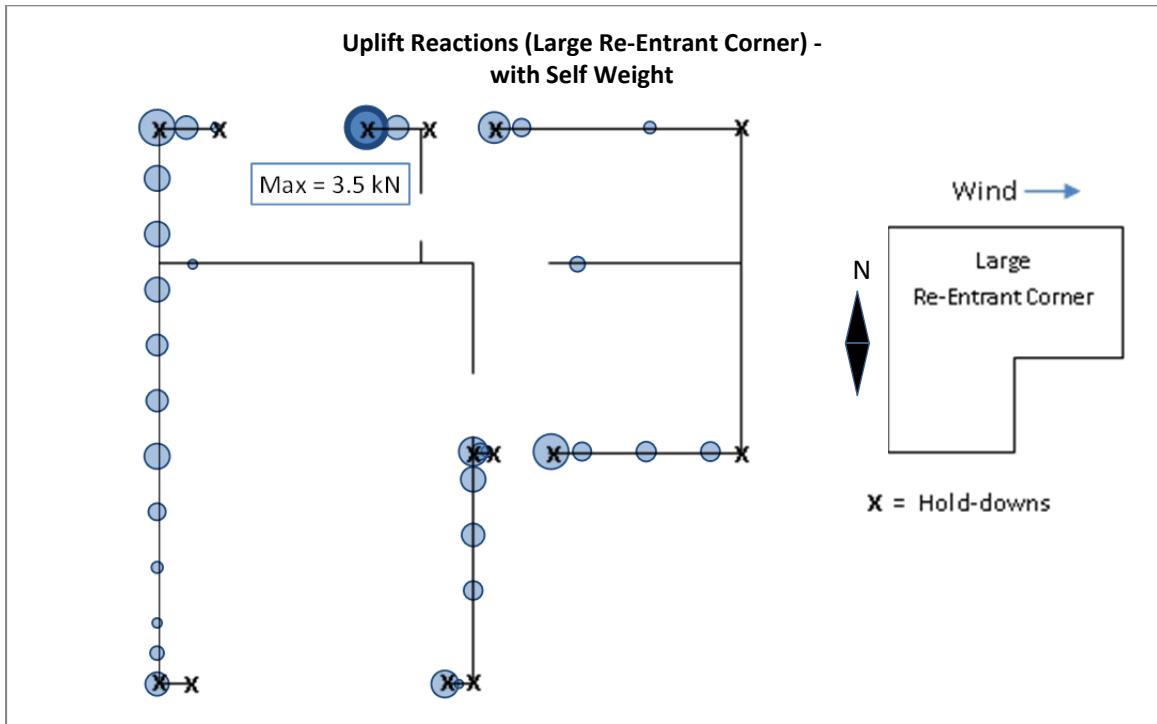


Figure L-30: Uplift Reactions for Building with Large Re-Entrant Corner under West-East Wind Loads (with Self Weight)

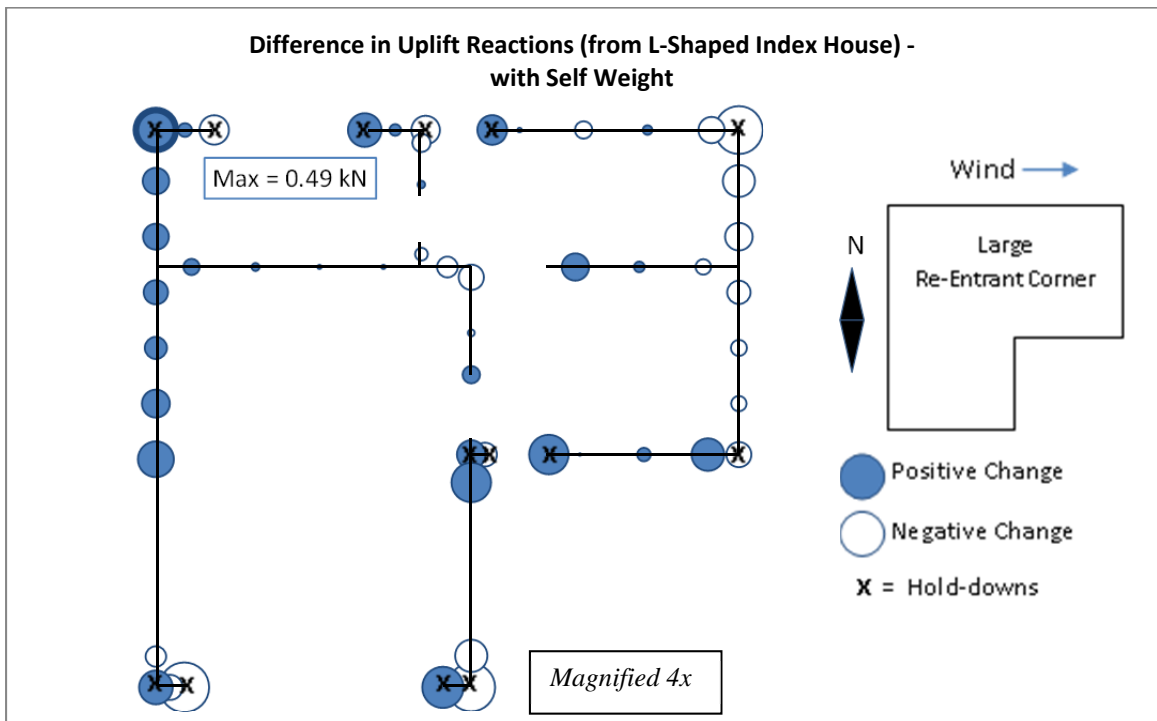


Figure L-31: Difference in Uplift Reactions between Building with Large Re-Entrant Corner and L-shaped index house under West-East Wind Loads (with Self Weight)

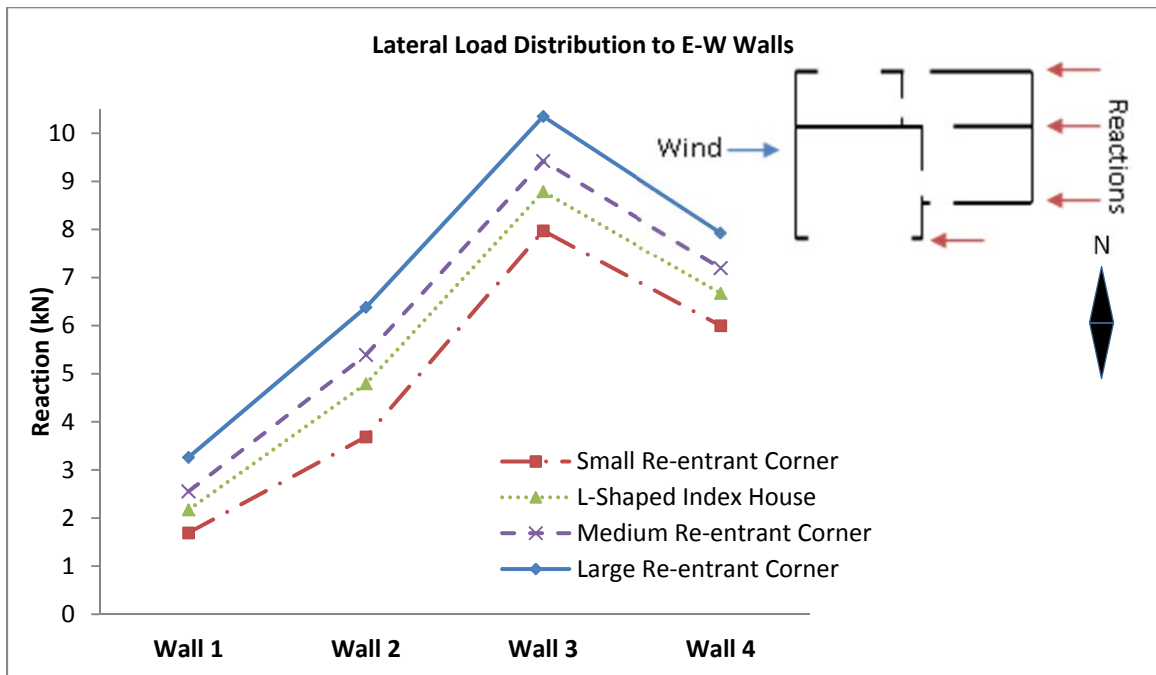


Figure L-32: Lateral Load Distribution to East-West walls under West-East Wind Loads (with Self Weight)

Southeast to Northwest Wind Loads

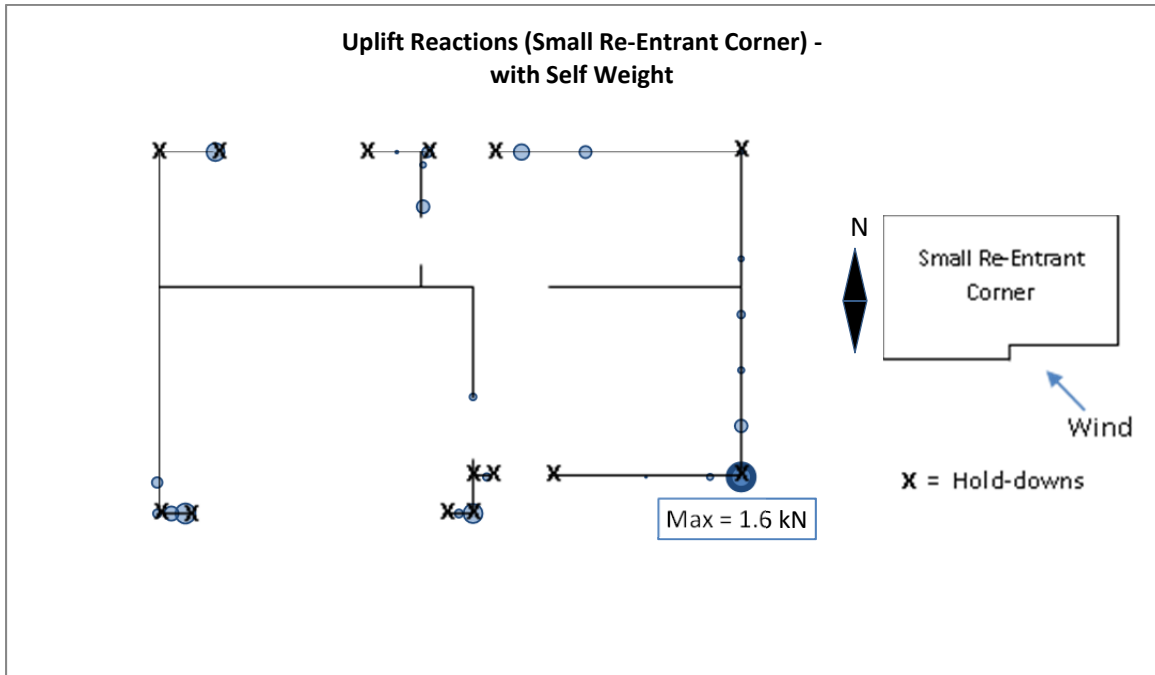


Figure L-33: Uplift Reactions for Building with Small Re-Entrant Corner under Southeast-Northwest Wind Loads (with Self Weight)

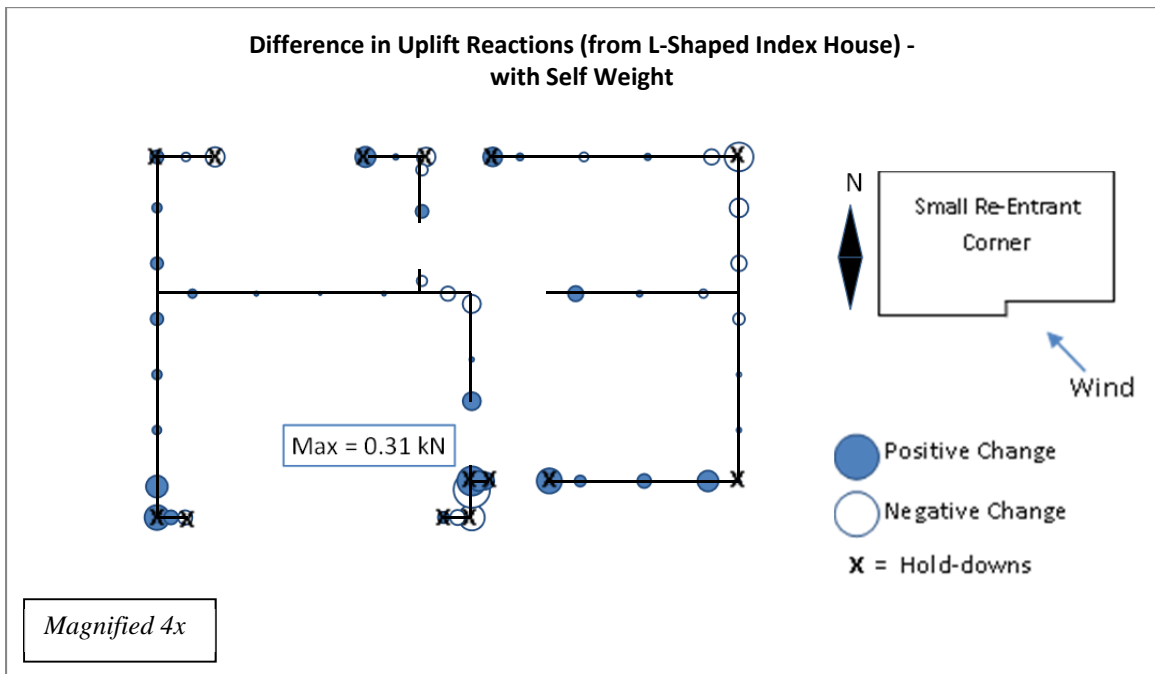


Figure L-34: Difference in Uplift Reactions between Building with Small Re-Entrant Corner and L-shaped index house under Southeast-Northwest Wind Loads (with Self Weight)

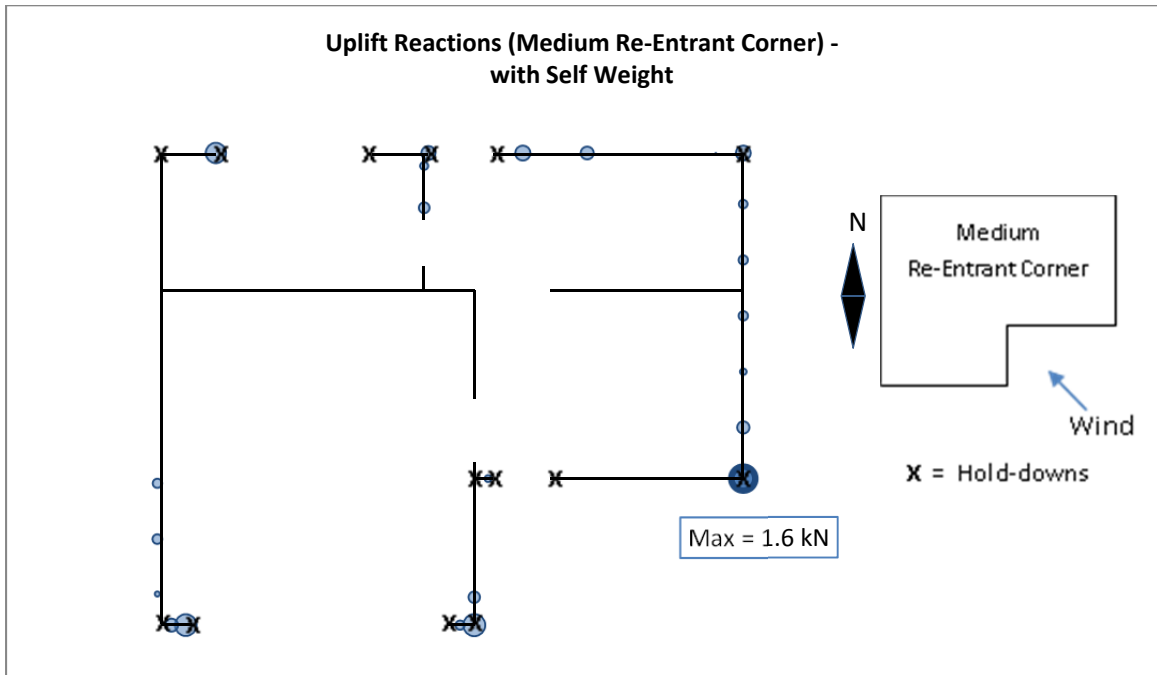


Figure L-35: Uplift Reactions for Building with Medium Re-Entrant Corner under Southeast-Northwest Wind Loads (with Self Weight)

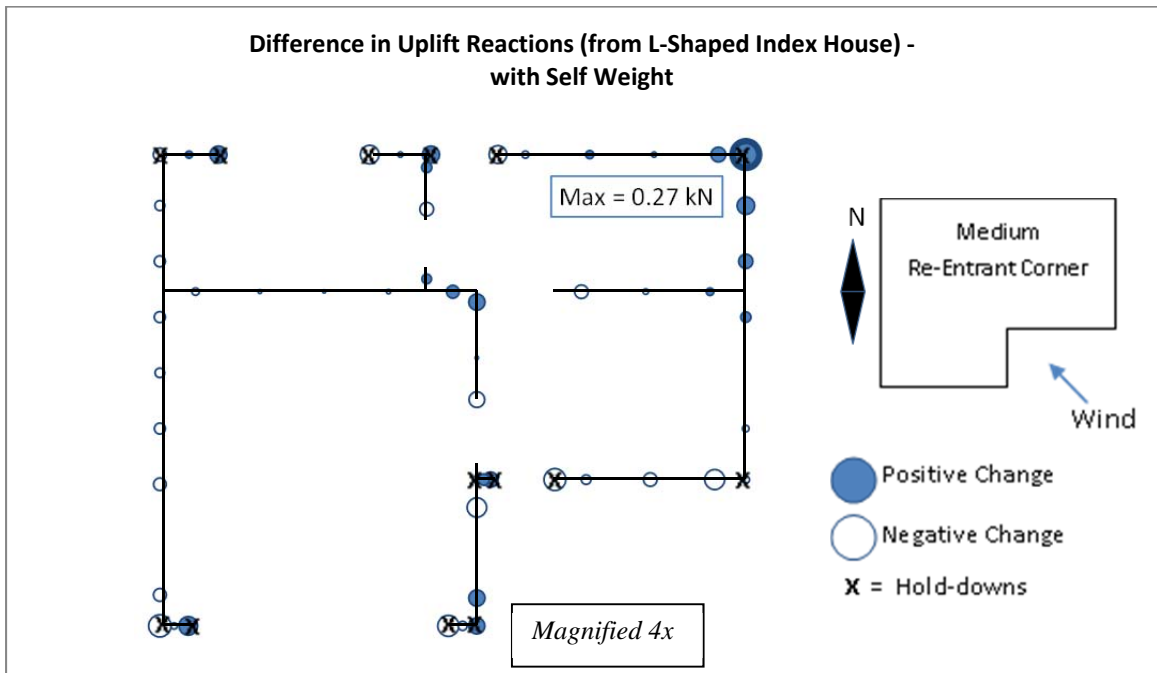


Figure L-36: Difference in Uplift Reactions between Building with Medium Re-Entrant Corner and L-shaped index house under Southeast-Northwest Wind Loads (with Self Weight)

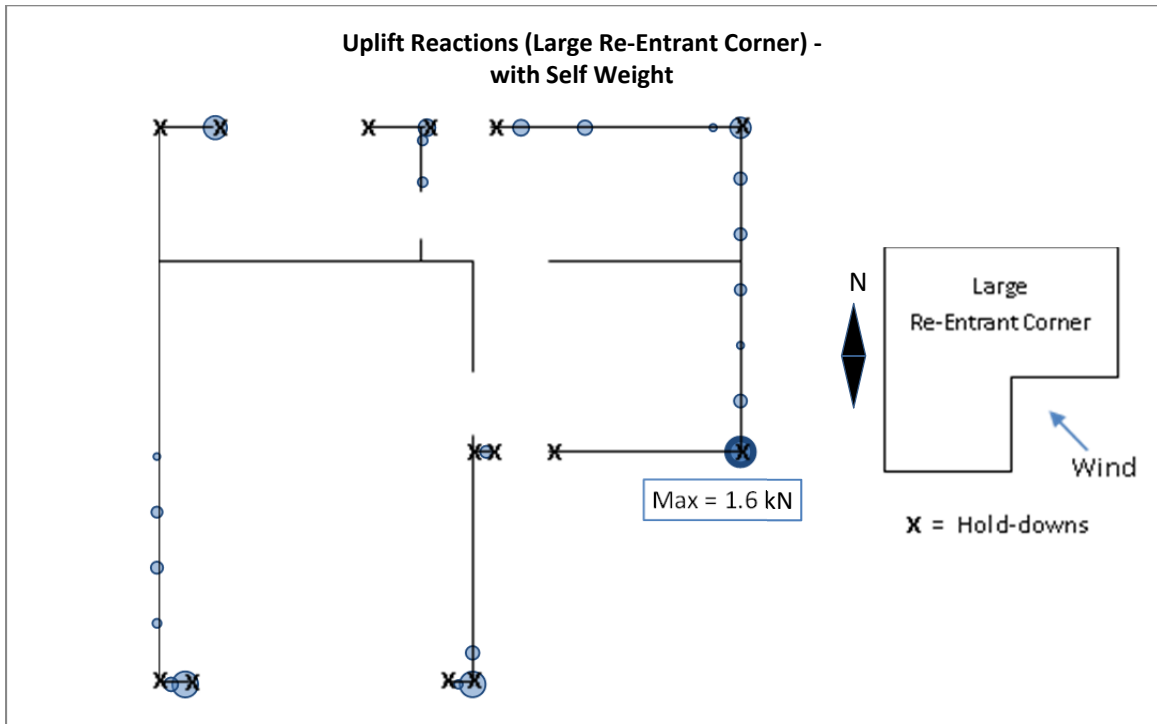


Figure L-37: Uplift Reactions for Building with Large Re-Entrant Corner under Southeast-Northwest Wind Loads (with Self Weight)

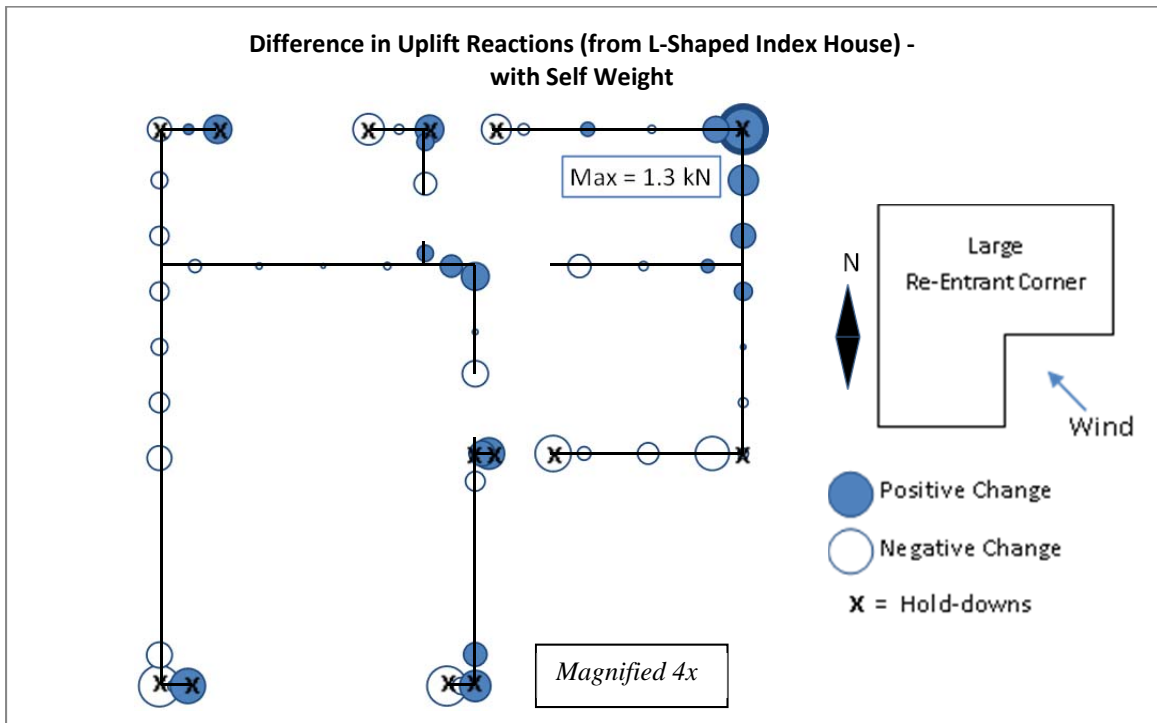


Figure L-38: Difference in Uplift Reactions between Building with Large Re-Entrant Corner and L-shaped index house under Southeast-Northwest Wind Loads (with Self Weight)

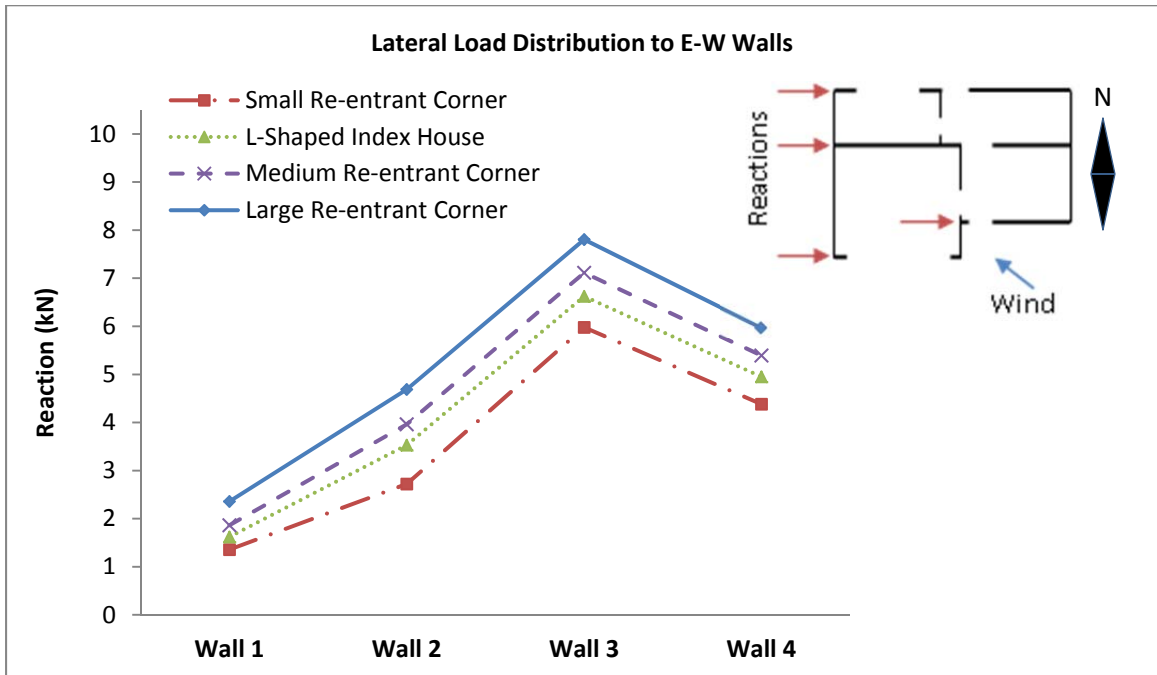


Figure L-39: Lateral Load Distribution to East-West walls under Southeast-Northwest Wind Loads (with Self Weight)

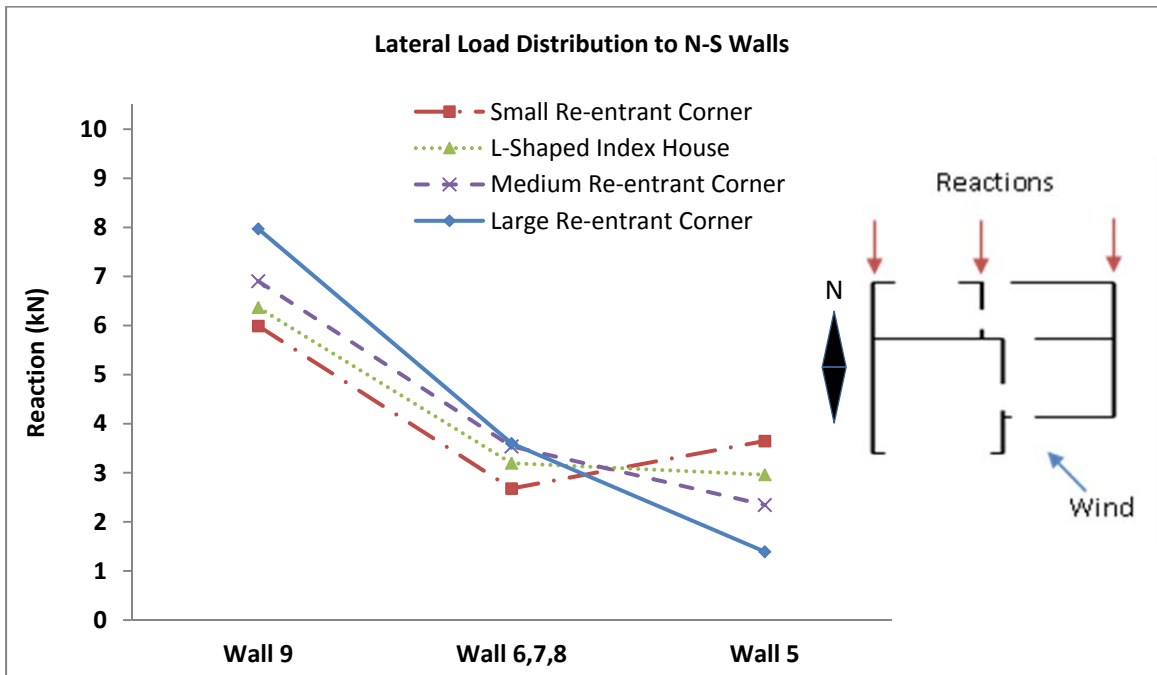


Figure L-40: Lateral Load Distribution to North-South walls under Southeast-Northwest Wind Loads (with Self Weight)

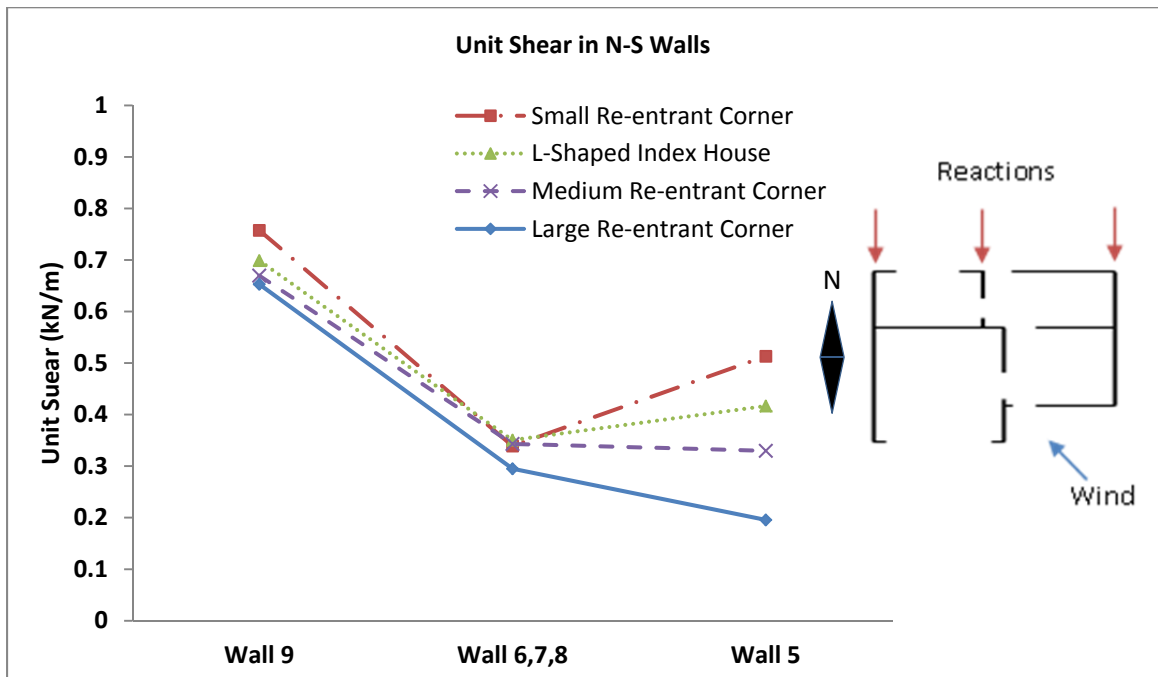


Figure L-41: Unit Shear in North-South walls under Southeast-Northwest Wind Loads (with Self Weight)